University of California San Diego

San Diego State University

Investigating the Role of Contractile Injection System Effectors in Host-Microbe Interactions

A dissertation submitted in partial satisfaction of the requirements for the degree Doctor of Philosophy

in

Biology

by

Kyle Evan Malter

Committee in charge:

San Diego State University

Professor Nicholas Shikuma, Chair
Professor Anca Segall
Professor Robert Zeller

University of California of San Diego

Professor Doug Bartlett
Professor Amy Kiger

2022

The dissertation of Kyle E Malter is approved, and it is acceptable in quality and form for publication on microfilm and electronically.

Chair

University of California San Diego

San Diego State University

2022

Dedication

I would like to dedicate this thesis to my family and thank my spouse Liberty and my two children Suki Moon, Senna Belle and my goofy giant dog Goose for their love and support throughout the journey of my Ph.D.

My mentors and partners throughout my PhD. have made this journey possible. The Shikuma lab members have been paramount to my success as a scientist and I could not have completed this journey without their assistance and incredible insight. None of this work would have been possible if it was not for; Nick Shikuma, Amanda Alker, Chip Ericson, Milagros Esmerode, Giselle Cavalcanti, Andy Fedoriouk, Carl Westin, Tiffany Dumbar, Nathalie Delherbe, Iara Rocchi, and our incredible undergraduate researchers.

I would also like to thank the members of San Diego State biology department for their enormous contributions to this work including Robert Zeller, C.J. Pickett, Ricardo Zayas, John “Jack” Allen, Anca Segall, Forrest Rower, Robert Luallen, Tuan Tran, Christopher Glembotski, Eric Blackwood, Adrian Arrieta, Marina kalyuzhnaya, David Collins, Oscar Gomez, Batool Youhenna, and so many others.

Epigraph

“Do not fear failure but rather fear not trying.”
-Roy T. Bennett

My motto throughout this body of work “It’s gonna work”

-Kyle Evan Malter

Table of contents

List of figures

Chapter 1

Chapter 2

Chapter 3

List of tables

Acknowledgements

I would like to acknowledge Professor Nicholas Shikuma for his immense aid and participation in the following works. I would also like to thank and acknowledge my committee members Dr. Robert Zeller, Anca Segal, Doug Bartlett and Amy Kiger for their constructive feedback and input throughout my project.

I would also like to acknowledge the members of the Shikuma Lab (past, and present) whose input provided major contributions, thank you to all the lab members who participated from 2016-2022.

The introduction as it appears is in-part as it appears in Annual Reviews of Microbiology 2020. G.S. Cavalcanti, A.T. Alker, N. Delherbe, K.E. Malter and N.J. Shikuma. The dissertation author is a coauthor of this manuscript and participated in the research, writing, and editing to produce this document.

Chapter 2, in full, is a reprint of the material as it appears in Cell Reports, 2019. I. Rocchi, C.F. Ericson, K. E. Malter, S. Zargar, F. Eisenstein, M. Pilhofer, S. Beyhan, N. J. Shikuma. The dissertation author is a coauthor of this manuscript. My contributions include Figure 2.3., writing, revisions, and experimental design

Chapter 3, in part, is a reprint of material as it appears in Elife, 2019. C.F. Ericson*, F. Eisenstein*, J. Medeiros, K.E. Malter, G. Cavalcanti, R.W. Zeller, D.K. Newman, M. Pilhofer and N.J. Shikuma (2019)**.** The dissertation author is a coauthor of this paper. My specific contributions include Figure 3.3. (panels B &C), Figure 3.4., Figure S3.4.1., Figure S3.4.2., input on the manuscript, methods, and revisions.

Chapter 4 has been accepted and is currently in the final stages of publishing by Developmental Biology for publication (2022). K.E. Malter, M. Esmerode, M. Damba, A.T.

Alker, E. Forsberg, and N.J. Shikuma The dissertation author is a coauthor of this manuscript. My contributions include Figure 4.1., Figure 4.2., Figure 4.3., Figure 4.4., table 4.1., tableS4.1., table S4.2., table S4.3., table S4.4., table S4.5., Figure S4.1., Figure S4.2. and writing and editing the initial drafts and all revisions.

Chapter 5 is unpublished with coauthors. K. E. Malter, C. Westin, C.F. Ericson, A.T. Alker, N. J. Shikuma (order and authorship still TBD). The dissertation author is a coauthor of this material. My contributions include Figure 5.1., Figure 5.2., Figure 5.3., Figure 5.4., Figure 5.5., Figure 5.6., table 5.1., table S5.1., Figure S5.1., supplemental Figure 5.2., table S5.2., Figure S5.3., Figure S5.4., Figure S5.5. and the initial drafts written for this document.

Vita

Education

2014 B.S., Biochemistry, University of California Los Angeles, GPA: 3.84

2022 Ph.D., Biology, San Diego State University and University of California San Diego

Publications

K Malter, M Esmerode, M Damba, E Forsberg, A Alker, and N Shikuma, Lipidomics of Tubeworm Metamorphosis in Response to Bacteria Reveals a Role of Protein Kinase C and MAPK Signaling. **Developmental Biology** (accepted, 2022)

I Rocchi*, C Ericson*, **K Malter***, S Zargar, F Eisenstein, M Pilhofer, S Beyhan and NJ Shikuma (2019**).** A Bacterial Phage Tail-like Structure Kills Eukaryotic Cells by Injecting a Nuclease Effector. Cell Reports, https://doi.org/10.1016/j.celrep.2019.06.019.

C Ericson*, F Eisenstein*, J Medeiros, **K Malter**, G Cavalcanti, RW Zeller, DK Newman, M Pilhofer and NJ Shikuma (2019**).** A Contractile Injection System Stimulates Tubeworm Metamorphosis by Translocating a Proteinaceous Effector. eLife**.** https://doi.org/10.7554/eLife.46845.

E Blackwood, L Plate, R Paxman, **K Malter,** L Wiseman, J Kelly, (2017) High-Throughput Screen Identifies Novel Small Molecule Stress Regulator That Confers Cardioprotection During Ischemia-Reperfusion Injury. **Journal of Molecular and Cellular Cardiology**, 11(112), 154.

A Alker, B Gode, A Aspiras, J Jones, S Michael, D Aguilar, A Cain, A Candib, J Cizmic, E Clark, A Cozzo, L Figueroa, P Garcia, C Heaney, A Levy, L Macknight, A McCarthy, J McNamara, K Nguyen, K Rollin, G Salcedo, J Showalter, A Sue, T Zamro, T Dunbar, **K Malter,** N Shikuma. (2021) Draft Genome Sequences of 10 Bacteria from the Marine Pseudoalteromonas Group. Microbiology resource announcements, 10(32). DOI: https://doi.org/10.1128/MRA.00404-21

G Cavalcanti, A Alker, N Delherbe, **K Malter**, NJ Shikuma. (2020) The Influence of Bacteria on Animal Metamorphosis. Annual Reviews of Microbiology. 74:*in press*. DOI: 10.1146/annurev-micro-011320-012753

Professional experience

2017-present **PhD student-** Lab of Dr. Nicholas Shikuma's microbiology laboratory, studying beneficial animal-bacterial interactions and the underlying mechanism mediating those interactions.

2016-2017 **PhD student** Lab of Dr. Christopher Glembotski's cardiac molecular biology and pharmacology laboratory, studying the adaptive endoplasmic reticulum stress response in the ischemic heart.

2015-2016 **mRNA Biologist**- Create custom designed mRNA from PCR amplified plasmid templates. Perform analytical test including, in-vitro transcription reactions, analytical high-performance liquid chromatography (HPLC) assays, Mass spectrometry (MS) and liquid chromatography followed by mass spectrometry (LCMS).

2014-2015 **UCSD laboratory volunteer researcher** – Lab of Joan Brown, responsible for executing experiments designed by lead researchers. Contribute to the designing of new research projects. Analysis of data. Preforming basic laboratory techniques such as DNA isolation, sterile cell culture, DNA cloning, gel electrophoresis, and Western blotting.

2013-2014 **UCLA undergraduate researcher-** Lab of Dr. Louis Bouchard- Research and design of novel experiments. performing cell culture techniques, transfections, and worked with multiple microscopy techniques including light, two photon, and confocal microscopy.

Honors / awards

ARCs Fellowship award, 2020

James and Mary Crouch Memorial Scholarship, 2018

American Society of Microbiology outstanding abstract award, 2017

American Society of Microbiology travel award, 2017

Graduated MAGNA CUM LAUDE, 2014, UCLA

Dean's list Fall 2012, Fall, Winter, Spring 2013, Winter 2014, UCLA

Graduated with Biochemistry departmental honors, 2014, UCLA

UCLA Academic scholarship 2012-2014, UCLA

Abstract of the dissertation

The Role of Bacterial Contractile Injection System effectors in Animal Development

by

Kyle Evan Malter

Doctor of Philosophy in Biology

San Diego State University, 2022
University of California San Diego, 2022

Professor Nicholas J. Shikuma, Chair

Bacteria-animal interactions play a widespread role in stimulating the life-cycle transitions of marine invertebrates, this interaction is critical for processes such as coral reef formation, sustaining fisheries stocks and biofouling. However, we know little about

the mechanisms mediating this beneficial bacteria-animal communication. *Pseudoalteromonas luteoviolacea* (*P. luteo*) release an array of tailocins known as metamorphosis associated contractile structures (MACs) inducing tubeworm metamorphosis. It is currently unknown how these structures induce the cellular response associated with metamorphosis. We have discovered that MACs contain at least two cargo effector proteins, Pne1 and Mif1, which are present in the MAC structure. Pne1 is a nuclease toxin effector which is responsible for MACs ability to kill mouse macrophages and SF9 insect cell lines. Mif1 is an effector loaded within the MACs inner tube complex and is critical for the inductive phenotype of MACs observed in *H. elegans* larvae. Additionally, we have shown via purified recombinant protein, this cargo is sufficient to induce metamorphosis. Through biochemical analysis we have shown Mif1 shares functionality with a class of secreted effector lipases and exhibits lipase activity. Additionally, we have identified that Mif1 stimulates the upregulation of a lipid second messenger DAG and via pharmacological characterization of metamorphosis we have determined the conserved PKC pathway to be both necessary and sufficient to induce this metamorphosis. This has provided evidence for the bacteria stimulating the PKC signal transduction pathway via lipid second messengers to directly induce animal metamorphosis. These experiments are the first to show a bacterial protein is sufficient to induce the metamorphosis of any marine animal and yields insight into how bacterial stimulate animal development.

Chapter 1

Introduction

1.1 Abstract

Microbes have been evolving on Earth for more than three billion years, setting the biological and ecological foundations for the evolution of eukaryotic life [1]. Within this context, animals evolved 400 million years ago in an environment already dominated by abundant and diverse bacteria [2,3]. Interactions with this microbial world shaped animal biology, whether in intimate symbioses or as organisms that share and modify a common habitat. Recently, the beneficial roles of microbes on animal development have gained widespread appreciation, paving the way for our realization that microbes fundamentally influence animal health, development, and evolution[4–6]. For example, bacteria direct multicellular behavior in choanoflagellates—the closest living relatives to animals, budding in hydra, light organ development in the Hawaiian bobtail squid, digestive tract development in zebrafish and immune system development and maturation in mammals. These instances of bacteria-stimulated development stand in opposition to the conventional notion that each animal's development is directed solely by its own genome. Growing attention has focused on how the host microbiome drives diverse aspects of eukaryotic development. Yet, bacteria in the microbiome are not the only bacteria influencing eukaryotic development. Although often disregarded, environmental bacteria also provide cues that regulate essential developmental processes in diverse eukaryotes. However, these widespread interactions raise the provocative and, until recently, largely unaddressed question: How do environmental bacteria shape normal animal development?

1.2 Introduction

The Influence of Bacteria on Animal Metamorphosis and Evolution

A widespread yet poorly understood example of bacteria shaping animal development is the stimulation of animal metamorphosis by bacteria. During these interactions in marine environments, surface-attached bacteria on the sea floor serve as an indicator and provide a stimulus for the swimming larvae of many animals, promoting larval settlement and triggering metamorphosis into the juvenile form (Figure 1.1.). Once induced to undergo metamorphosis by bacteria, the larval animal undergoes a dramatic developmental transition, losing larval features and taking on adult characteristics. Bacteria that promote metamorphosis are thought to serve as a critical indicator of a preferable habitat for adult animals. While this process is fundamental to the life history of diverse animals, and likely shaped their ecology and evolution, there has still been much to learn since this phenomenon was first reported in the 1930s [7].

The diversity of animals that undergo metamorphosis is enormous. Yet apart from a few animal groups, metamorphosis is poorly characterized. Most of our knowledge of animal metamorphosis is derived from only a few model organisms, notably the fruit fly (*Drosophila melanogaster*) and African Clawed Frog (e.g., *Xenopus laevis*, *Xenopus tropicalis*), which are not currently believed to undergo metamorphosis in response bacteria. Studying the metamorphosis of marine invertebrates offers valuable insight into the basis of environmental bacteria signaling in animal development in a setting where the very persistence of benthic marine ecosystems depends on it.

The complexity of settlement and metamorphosis of marine larvae invites the use of proper definitions. Here, settlement is defined as a behavioral process by which larvae that possess the ability to undergo metamorphosis (competency) reversibly bind to the substratum, while the term metamorphosis describes the transition from the attached larval stage to a sessile juvenile stage—a morphogenetic process[8]. Competency permits marine invertebrate larvae to live a planktonic life and allows some flexibility in the timing for settlement and metamorphosis in response to a suitable location based on environmental cues. The developmental change of metamorphosis is often accompanied by a corresponding change from a free-swimming to a surface-associated state [8]. Importantly, metamorphosis is an irreversible process. Therefore, making the decision of where and when to transition from a planktonic to a sessile state is critical for survival and reproduction as a surface-bound adult[9]. Here, we explore what is known and what we hope to learn about bacteria that stimulate metamorphosis, the signaling molecules present within marine biofilms, the chemical diversity of known bacterial cues, and challenges in identifying the animal sensory machinery that triggers this developmental transition.

Biofilms and their roles as settlement cues for marine invertebrate larvae

Biofilms are consortia of intimately interacting microbial cells enclosed in an extracellular matrix; biofilms cover all underwater biological, mineral or artificial surfaces [10]. Rather than being conglomerations of cells and slime, biofilms are organized communities with functional microcolonies and channels that perform complex metabolic processes[11]. The microbes within biofilms produce a matrix of extracellular polymeric

substances (EPSs), composed of polysaccharides, proteins, nucleic acids, and lipids, which provide mechanical stability, mediate adhesion to surfaces, and form a cohesive, three-dimensional polymer network that interconnects and transiently immobilizes biofilm cells[12]. EPSs are prominent components of biofilms that have been implicated in stimulating metamorphosis [13], although this has not been shown explicitly.

Natural biofilms are composed of many microbial species including bacteria, diatoms, fungi, and protozoa. Multispecies biofilms can form stable consortia, develop physiochemical gradients, and facilitate horizontal gene transfer and intense cell-cell communication; thus, these consortia represent highly competitive environments[12]. To understand the stimulation of metamorphosis by marine biofilms, several studies have characterized the microbial diversity within inductive biofilms. It has been shown that the bacterial community structure of natural biofilms varies in its response to environmental factors such as salinity, temperature [14], tidal level [15,16], dissolved oxygen [17], hypoxia[18–20], and habitat [21–23]. Natural biofilms formed under different environmental conditions vary in their attractiveness to settling larvae[14,15,21–24]. However, most factors influencing biofilm community composition, including salinity and temperature[14], or succession over time[23,25,26], did not influence settlement, whereas biofilm cell density was correlated with settlement. Importantly, denser mature biofilms support a matrix of complex molecules and morphogenic signaling compounds that are thought to contribute to larval settlement in marine invertebrates. While some studies have provided evidence that bacterial community structure might be important for settlement of marine larvae [27], the actual settlement cues associated with biofilm communities often remain unknown or poorly understood [28,29].

For most animals, the specific bacterial factors that induce metamorphosis are unknown

Animals that undergo metamorphosis represent all major branches of the animal tree of life (Figure 1.2.). Of these animal types, almost all clades possess representative species that undergo metamorphosis in response to bacteria (Figure 1.2.). Bacteria stimulate larval settlement and metamorphosis in diverse marine invertebrates, including sponges [30–33], molluscs[34–40], crabs[41], barnacles[42,43], bryozoans[15,44], annelids [45], urochordates [46], echinoderms[47,48], and ascidians [49–53]. While the cues mediating most of these interactions are unknown, the chemical compositions of a few metamorphosis cues from laboratory-developed bacterial biofilms have been partially characterized; for example, carbohydrates induce larval attachment and metamorphosis of the polychaete *Janua (Dexiospira) brasiliensis* [54]and larval attachment of the tunicate *Ciona intestinalis* [46]. Histamine isolated from algae, or the biofilm coating the algae, stimulates the metamorphosis of the sea urchin *Holopneustes purpurascens*[47,54].

In the study of bacterial factors that stimulate metamorphosis, and the animal receptors and response mechanisms, the use of simplified model systems is beginning to reveal how environmental bacteria promote animal metamorphosis. Here we review the mechanisms by which environmental bacteria influence the metamorphosis of three marine animals: (*a*) the polychaete tubeworm *Hydroides elegans* and the cnidarians, (*b*) corals, and (*c*) *Hydractinia*.

The tubeworm *Hydroides elegans* as a model animal

The marine tubeworm *Hydroides elegans* (hereafter *Hydroides*), is a powerful model organism to investigate how bacteria stimulate animal metamorphosis. In the 1990s, Hadfield et al. [55]first documented that the larvae of *Hydroides* respond to bacterial biofilms by undergoing metamorphosis. In the laboratory, *Hydroides* larvae undergo metamorphosis in response to biofilms composed of multispecies communities of microorganisms [23,45,56] and single species of bacteria[45,57,58].

Hydroides was first developed as a model organism for biofouling because it forms thick crusts of calcified tubes on submerged boat hulls, causing corrosion and higher fuel consumption when ships are underway [59]. The properties that make this tubeworm a pest also make it an effective model organism for studying how bacteria stimulate metamorphosis. Specifically, *Hydroides* is easily propagated in the lab, each female can yield thousands of eggs per spawning, and the larvae have a short development period (six days) before acquiring the ability to sense bacteria and undergo metamorphosis (i.e., become competent). To demonstrate that *Hydroides* is adapted to respond to surface-bound bacteria, Hadfield et al.[55] showed that *Hydroides* changes its swimming and settlement behavior when in direct contact with biofilms.

A valuable feature of model organisms is that they have genes and molecular pathways that are conserved among diverse animals. To further develop *Hydroides* as a model organism, we sequenced its genome[60] and found that the gene content of this tubeworm more closely resembles that of anemones, sea squirts, and humans than it does other model invertebrates such as the fruit fly (*Drosophila melanogaster*) or nematode (*Caenorhabditis elegans*). Therefore, insights into how *Hydroides* senses and responds to bacteria may be applicable to diverse animal lineages.

Diverse bacteria have been shown to induce *Hydroides* metamorphosis, including those belonging to gram-negative (*Gammaproteobacteria* and *Alphaproteobacteria* classes, *Cytophaga-Flexibacter-Bacteroides* group) and gram-positive (*Firmicutes* phylum) groups [61–64]. However, so far bacterial taxonomy has not been correlated with the induction of metamorphosis. In fact, different isolates belonging to the same genus can differ tremendously in their ability to induce metamorphosis, varying from no induction to moderate induction to very strong induction. For example, the marine bacterium *Pseudoalteromonas luteoviolacea* is a potent inducer of metamorphosis, while diverse other *Pseudoalteromonas* species show little stimulatory effect on *Hydroides* metamorphosis. *Hydroides* is well suited for the reductionist approach of studying the effect of one bacterium on one animal to identify specific bacterial factors that stimulate metamorphosis. Identifying these factors and the different mechanisms by which they stimulate metamorphosis will provide significant insight into the diversity and mechanisms of how bacteria influence animal development.

A surprisingly different way that bacteria stimulate metamorphosis

Since the 1930s discovery that bacteria stimulate animal metamorphosis[65], the prevailing model has been that animals respond to factors that are bound to the surface of bacterial cells or released nearby (Figure 1.3.). For many marine animal larvae, dissolved factors have been shown to stimulate metamorphosis[66]. However, the stimulation of *Hydroides* metamorphosis by bacteria was shown to require physical contact with a biofilm surface[55]. These findings hinted that the bacterial factors that induce metamorphosis are diverse in their biological and physical properties.

Recently, we discovered a surprisingly different way that bacteria stimulate animal metamorphosis—the first known bacterial injection system that stimulates the metamorphosis of an animal[45] (Figure 1.4. A & B). We called these structures metamorphosis-associated contractile structures (MACs) because they form syringe-like protein complexes that induce tubeworm metamorphosis. To make this discovery, a pioneering study by Huang et al.[67] used forward genetics to identify a set of 4 genes in the genome of *P. luteoviolacea* that are required to stimulate tubeworm metamorphosis. They did this by using a transposon to randomly mutagenize the bacterial genome and then screen for mutants deficient in inducing metamorphosis. We subsequently found that the 4 genes identified in this screen belong to a cluster of over 40 genes that encode the syringe-like MACs[45].

Instead of soluble or surface-bound factors produced by bacteria, MACs are complex syringe-like structures that inject protein effectors into target cells. MACs are one example of contractile injection systems (CISs), which are related to the contractile tails of some bacteriophage [the viruses of bacteria (Figure 1.4. C)]. Like other CISs, MACs are composed of a rigid inner tube surrounded by a contractile sheath, a tail spike, and a baseplate complex. Contraction of the sheath propels the inner tube and tail spike into target cells and delivers effector proteins that elicit a host response. While other CISs typically form individual syringe-like structures, MACs are the first example of a CIS forming arrays of about 100 CIS structures arranged in a star conformation (Figure 1.4. A & B).

Since the discovery of MACs, related CISs have been discovered that also form multi-CIS complexes[68]. In addition to stimulating metamorphosis, closely related

structures were found to mediate interactions between microbes and amoebae, insects, and potentially humans[68–71]. While a number of pathogenic bacteria use type VI secretion systems to inject protein toxins into target cells to cause disease[72], MACs are the first CIS to promote a beneficial microbe-animal interaction. Such a mechanism of bacteria stimulating metamorphosis is unprecedented and provides a paradigm shift in our thinking about how microbes stimulate animal development.

While we identified MACs as the structures stimulating tubeworm metamorphosis, it remained unclear how MACs influenced *Hydroides*' metamorphic transition. Recently, we used cryoelectronic tomography (cryo-ET) to directly observe a protein effector loaded within the inner tube lumen of the MAC's syringe-like needle[73]. We identified the protein effector and named it metamorphosis-inducing factor 1 (Mif1) because it is sufficient for stimulating tubeworm metamorphosis when delivered to tubeworm larvae by electroporation. Although Mif1 is the first identified bacterial protein that stimulates metamorphosis, we do not yet know its mechanism of action, and its protein sequence possesses no identifiable domains that could yield clues to its function. However, Mif1 still provides an intriguing entry point into understanding how a bacterial factor, particularly a proteinaceous factor, stimulates metamorphosis.

It is unclear how bacteria benefit from producing MACs. One clue is a second protein effector that MACs deliver to target cells in vitro[74]. Paradoxically, this second effector, which we termed *Pseudoalteromonas* nuclease effector 1 (Pne1), is toxic to insect and murine cells in vitro but had no observable effect on *Hydroides* larvae. Reciprocally, we did not observe an effect of Mif1 on the cell lines in vitro. We currently hypothesize that the two MAC effectors target different organisms to promote the *P.*

luteoviolacea lifestyle as a free-living, yet host-associated marine bacterium. A recent study exploring the distribution and diversity of MACs' structural gene homologs in the marine environment found them to be more abundant in biofilms than in the water column[75], suggesting that MACs may benefit surface-attached bacteria by facilitating their interaction with animal larvae while deterring potential biofilm-eating predators like protozoans [76].

Different bacterial factors stimulate metamorphosis in the same animal

A surprising finding derived from studying *Hydroides* is that chemically different factors from bacteria may be able to stimulate the same developmental process of metamorphosis. Diverse bacterial strains that are able to induce *Hydroides* settlement have been isolated[58,77], which shows that the inductive chemical(s) can be produced by many different bacterial families and classes. For instance, *Loktanella hongkongensis*, a marine alphaproteobacterium that induces *Hydroides* metamorphosis, does not possess genes that produce MACs [78]. Instead, it has been suggested that *L. hongkongensis* produces low-molecular-weight compounds associated with the exopolymeric matrix of the bacterial cells that are able to induce *Hydroides* metamorphosis[79].

Hydroides metamorphosis is also triggered by taxonomically distant strains of *Cellulophaga lytica* (*Flavobacteriia* class), and the gram-positive bacteria *Bacillus aquimaris* and *Staphylococcus warneri* (*Bacilli* class)[57]. Freckelton and colleagues[78] revealed that the gene assemblies for MACs are lacking in these bacteria, but they observed the presence of inductive extracellular vesicles from *C. lytica*, *B. aquimaris*, and *S. warneri*. Employing a biochemical structure-function approach, they recently showed

that lipopolysaccharide extracted from *C. lytica* cultures are able to induce *Hydroides* metamorphosis[78]. Interestingly, extracellular vesicles from both gram-positive and gram-negative species have been found to provide a mechanism for cell-to-cell interaction, including the transfer of DNA, protein, and small signaling molecules[80,81]. Thus, membrane vesicles are potentially a widespread mechanism of interaction between biofilm bacteria and invertebrate larvae.

In addition to proteinaceous MACs, small-molecule compounds have been demonstrated to stimulate *Hydroides* metamorphosis. Hung et al. [29] described two lipid moieties isolated from a mixed bacterial biofilm that also induce metamorphosis. These two compounds were a long-chain fatty acid (12-octadecenoic acid) and a hydrocarbon (6,9-heptadecadiene) that induced *Hydroides* larval settlement to a similar extent as natural biofilms. These two compounds are quite distinct from proteinaceous MACs, and it is currently unclear whether each bacterial factor stimulates metamorphosis through the same pathway. Thus, inducers that have been discovered indicate that there are a variety of modes that bacteria can use to stimulate their animal hosts, demonstrating that diverse mechanisms of interaction can promote the same developmental process.

Costs and benefits of stimulating animal metamorphosis

The interactions between bacteria and animals during bacteria-stimulated metamorphosis are not intimate, long-term symbioses. Rather, these interactions occur transiently as an animal larva searches for a location to settle and metamorphose. It is interesting to contemplate what evolutionary pressures led marine invertebrate larvae to evolve a reliance on bacterial cues for metamorphosis. While these interactions may be

circumstantial, there may be significant selective pressures that promote this interaction for one or both partners.

It is currently debated whether a biphasic (larva and adult) life history was an ancestral characteristic of the first animals or it arose multiple times among major animal clades [81–85]. Similarly, it is unknown whether the ability to undergo metamorphosis in response to bacteria was an ancestral characteristic of the first animals or whether it is a convergent trait among diverse metazoans with a biphasic life cycle. Nonetheless, the widespread nature of this phenomenon suggests that a strong selective pressure exists to evolve and maintain this microbe-animal interaction.

As bottom-dwelling and often immobile adults, marine invertebrates may benefit from using bacteria as a metamorphosis cue. Because metamorphosis is an irreversible process, the decisions of where and when to undergo metamorphosis are critical for survival of the juvenile and adult [86]. Certain bacteria may serve as proxies for specific environmental conditions and a suitable habitat, thus avoiding a switch to the benthic lifestyle in an unfavorable environment[66,87]. This response may be especially important in aquatic environments where biotic and abiotic conditions are constantly changing. Nonetheless, it is important to note that all underwater surfaces are coated with dense microbial biofilms, and thus, animal larvae must interact with biofilms to settle and metamorphose on the sea floor, i.e. to become a bottom dwelling organism. It is, therefore, reasonable to expect that larvae actively select attachment sites with certain biofilm characteristics.

It is currently unknown whether bacteria benefit or are harmed from stimulating animal metamorphosis. Many of the bacteria that induce animal metamorphosis

frequently associate with eukaryotes, for example, by accumulating on surfaces of invertebrates as epibiotic biofilms [88–90]. Surface-attached bacteria tend to be larger, with a higher proportion of cells with higher metabolic activity than free-living bacteria[91]. Because these bacteria produce exoenzymes that could help them utilize animal-derived molecules for nutrition, it is possible that inducing eukaryotic development allows specific bacteria to rapidly colonize a valuable niche, i.e., the settled animal.

Interestingly, antimicrobial metabolites are produced by many bacteria associated with marine invertebrates, for example, several members of *Pseudoalteromonas*[89,92,93]. These properties—inducing metamorphosis, producing antimicrobial metabolites, association with macroorganisms—may, in fact, be interconnected. An intriguing hypothesis is that an evolutionary arms race is imposed among sessile invertebrates: As larvae, they must locate and colonize a surface in order to metamorphose; yet as adults they must keep their own surfaces clean and ward off settlement of other larvae. The association with the bioactive bacteria might therefore offer a favorable trade-off. The bacteria that promote settlement/metamorphosis might colonize a valuable niche, the adult animal, through which they can obtain nutrients via exoenzyme production. But they also produce antimicrobials that protect their animal niche from being colonized by other bacteria. Further characterization of marine invertebrate microbiomes could help illuminate this hypothesis.

Alternatively, it is possible that the stimulation of animal metamorphosis does not directly benefit the bacterium. Because surfaces in the ocean are often limiting, the bacterial partner might be influencing marine animal metamorphosis through by-product cooperation, i.e., cooperation as an incidental consequence of selfish action[94].

Specifically, bacteria unavoidably produce publicly usable resources (e.g., toxins and antibiotics)[94,95] that become available to their local community and might be interpreted by the animal larvae as a cue to an appropriate environment for settling down. By-product mutualism might not seem like a typical form of cooperation, since the cooperative phenotype carries no cost and because the trait need not evolve in the context of the interaction[95]. Therefore, it can be difficult to resolve by-product cooperation into clear mechanisms.

Current and future challenges

The biological nature of factors inducing metamorphosis

Identifying the chemical nature of bacterial factors that stimulate animal metamorphosis is a compelling endeavor. Biofilms are abundant sources of chemical cues[87,96], and we have only scratched the surface when it comes to identifying specific metamorphosis cues, deciphering their chemical nature, and determining their ecological roles within natural biofilm communities. A few described inducers of invertebrate settlement are primary metabolites such as carbohydrates or peptides that are water-soluble[96]. For example, a soluble proteinaceous factor and amino acids were found to stimulate oyster metamorphosis[7,97]. Water-soluble primary metabolites may function as stimulatory factors, because they are also used as components of internal signal transduction systems[98]. Thus, the receptor machinery for responding to similar but externally derived signals is already present in the larval animal. Additionally, some bacteria are able to inject stimulatory factors, like Mif1, into larvae and stimulate metamorphosis[73]. The mode of delivery and chemical properties of bacterial factors that

stimulate metamorphosis are clearly diverse and likely have significant ecological implications for both microbe and animal. Our understanding of the role that bacteria and biofilms play in larval attachment and metamorphosis would be substantially enhanced if the chemical cues originating from natural biofilms were characterized.

Animal sensing and response machinery

How animals directly sense bacterial factors that stimulate metamorphosis is currently unknown for any animal. However, there are chemicals known to artificially stimulate metamorphosis, and a few eukaryotic signal transduction pathways that mediate metamorphosis have been identified. Excess concentrations of potassium or cesium ions, or perturbations of potassium channels, have been shown to induce metamorphosis in several animal species, and these ions have been used as tools to study eukaryotic pathways that mediate metamorphosis[99–103]. In comparing the metamorphosis of *Hydractinia* induced by chemical versus bacterial factors, Seipp et al.[104] showed that these processes occur in a similar manner. However, the larvae settled earlier when induced with *Pseudoalteromonas espejiana* compared to exposure of cesium ions. Moreover, the apoptotic process of the cells on the anterior end also occurs earlier in the presence of *P. espejiana* bacteria.

The protein kinase C (PKC) pathway has been heavily implicated in metamorphosis signaling in a variety of marine organisms including *H. echinata*, the sea urchin *Strongylocentrotus purpuratus*, the barnacle *Balanus amphitrite*, multiple Red Sea coral planulae (*Heteroxenia fuscescens*, *Xenia umbellata*, *Dendronephthya hemprichii*, *Litophyton arboretum, Parerythropodium fulvum fulvum*, and *Stylophora pistillata*), and the annelid *Capitella sp. 1*[105–109]. PKC was first implicated in the metamorphosis of *H.*

echinate by Leitz et al., who were able to stimulate PKC and the metamorphosis signaling cascade using diacylglycerol, and inhibit metamorphosis using kinase inhibitors acting on PKC[108]. PKC is a lipid-sensing kinase, and Leitz et al.[110,111] have additionally implicated several lipids regulating metamorphosis such as lysophosphatidylcholine and arachidonic acid, a known PKC-sensitizing lipid. While it is unclear exactly how universal the PKC pathway is in regulating metamorphosis in marine invertebrates, even the distantly related insect *Aedes aegypti* metamorphic factor juvenile hormone was demonstrated to stimulate its metamorphic induction through the PKC pathway[112].

Studies have implicated other signaling systems in addition to PKC in the induction of metamorphosis. The MAPK signaling pathway, which can be activated by various upstream signals, including PKC, has also been demonstrated to be necessary for metamorphosis through the use of pharmacological inhibitors in a sponge (*Amphimedon queenslandica*), an annelid (*Hydroides*), and an ascidian (*Ciona intestinalis*)[60,113–115]. An alternative signaling pathway has been shown in the annelid *Phragmatopoma californica* and mussel *Mytilus coruscus*, where the alterations of cAMP levels have been shown to contribute to metamorphosis induction[116,117]. Additionally, in *M. coruscus*, both inhibitors and activators of cAMP induced metamorphosis, implying that there is a delicate balance required for cAMP to regulate metamorphosis.

How multiple eukaryotic signaling systems evolved to orchestrate metamorphosis in response to bacteria is unclear. An intriguing possibility is that the ability to sense bacteria and proceed with metamorphosis is linked to innate immunity. In a few instances, larval competency is correlated with the expression of genes related to innate immunity, suggesting a possible role for Toll-like receptors or other sensing machinery of the innate

immune system[52,118]. How diverse animals evolved the ability to recognize bacterial factors and subsequently signal the induction of metamorphosis has been pondered by scientists for decades and is a clear grand challenge for future investigations.

Applied potential of studying how bacteria stimulate animal metamorphosis

Animal metamorphosis in response to bacteria has several applied implications. For example, knowledge of bacterial factors that stimulate metamorphosis can inform probiotic treatments that promote the recruitment of new animals to degraded benthic ecosystems such as coral reefs[119,120]. This knowledge could also improve the husbandry protocols for aquaculture animals for commercial use, such as oysters, that may depend on our knowledge of specific bacteria that stimulate metamorphosis in captivity[121]. In addition, knowledge of the bacterial factors that stimulate metamorphosis could inform new strategies for preventing biofouling, for example, through embedding of antifouling compounds within paints for boat hull surfaces. Finally, bacteria-stimulated metamorphosis is a widespread example of a beneficial host-microbe interaction yet is a largely unexplored space for mining of biomedical and biotechnology applications. For example, based on our discovery of MACs, we identified a new and previously undescribed family of CIS that are produced by *Bacteroidales* bacteria commonly found in the human gut[69]. Such systems inject contents into diverse animal cell types and could someday be modified as nanometer-scale devices for the delivery of specific proteins into target cells[74].

1.2 Conclusion

As we learn more about the astonishing ubiquity and diversity encompassing the microbial world and the vast range of bacteria-animal interactions, it has become clear that microbes are often essential for animal development. Although nearly all animals have stable associations with bacteria, investigating how these interactions shape animal development has been difficult, partially because of a dearth of tractable and phylogenetically relevant model systems. Only a few investigations of these interactions have unraveled the specific mechanisms by which environmental bacteria influence the life cycles of animals. Studying mechanisms by which environmental bacteria stimulate the metamorphosis of diverse animals may begin to provide explanations of why stable associations with bacteria, once considered anathema to human health, are indispensable for animals. Thus, there is still a great need to interrogate the molecular dialogue that mediates microbe-animal interactions in diverse contexts, such as the stimulation of animal metamorphosis by bacteria.

1.3 Summary points

1. Bacteria stimulate the metamorphosis of phylogenetically distant animals like corals, tubeworms, and urchins.
2. The stimulation of metamorphosis by bacteria is an example of bacteria promoting animal development.
3. Bacteria-stimulated metamorphosis is critical for coral reef formation, aquaculture, and biofouling.

4. Bacteria stimulate animal metamorphosis by producing stimulatory factors that can be biochemically very different (e.g., protein, lipid, diffusible small molecules).
5. Bacteria can stimulate metamorphosis by producing phage-tail-like structures that inject a stimulatory protein.
6. For most marine animals that undergo metamorphosis, we still do not know the identity of bacterial factors that stimulate metamorphosis, their mechanisms of action, or how the animal senses these factors.

1.4 Disclosure statement

N.J.S. has a patent application pending related to Contractile Injection Systems in the United States, Application Number: 5810.133691PCT.

1.5 Acknowledgments

This work was supported by the Office of Naval Research (N00014-17-1-2677, N.J.S. and N00014-16-1-2135, N.J.S), the Alfred P. Sloan Foundation, a Sloan Research Fellowship (N.J.S.), and the National Science Foundation (GRFP 2017232404, A.T.A.). The introduction as it appears is in-part as it appears in Annual Reviews of Microbiology 2020. G.S. Cavalcanti, A.T. Alker, N. Delherbe, K.E. Malter and N.J. Shikuma. The dissertation author is a coauthor of this manuscript and participated in the research, writing, and editing to produce this document

1.6 References

1. Knoll, A. *Life in a young planet*. (Princeton Univ. Press, 2003).

2. Pradeu, T. A Mixed Self: The Role of Symbiosis in Development. *Biol. Theory* **6**, 80–88 (2011).

3. Rosenberg, E. & Zilber-Rosenberg, I. Microbes drive evolution of animals and plants: The hologenome concept. *MBio* **7**, (2016).

4. Mazmanian, S. K., Liu, C. H., Tzianabos, A. O. & Kasper, D. L. An immunomodulatory molecule of symbiotic bacteria directs maturation of the host immune system. *Cell* **122**, 107–118 (2005).

5. Gilbert, S. F., Sapp, J. & Tauber, A. I. A symbiotic view of life: we have never been individuals. *Q. Rev. Biol.* **87**, 325–341 (2012).

6. Moran, N. A. Symbiosis. *Curr. Biol.* **16**, 866–871 (2006).

7. Zimme-Faust, R. K. & Tamburri, M. N. Chemical identity and ecological implications of a waterborne, larval settlement cue. *Limnol. Oceanogr.* **39**, 1075–1087 (1994).

8. Bishop, C. D. *et al.* What Is Metamorphosis? *Source Integr. Comp. Biol.* **46**, 655–661 (2006).

9. Siegel, D. A. *et al.* The stochastic nature of larval connectivity among nearshore marine populations. *Proc. Natl. Acad. Sci. U. S. A.* **105**, 8974–8979 (2008).

10. Flemming, H. C. & Wuertz, S. Bacteria and archaea on Earth and their abundance in biofilms. *Nat. Rev. Microbiol.* **17**, 247–260 (2019).

11. Dang, H. & Lovell, C. R. Bacterial Primary Colonization and Early Succession on Surfaces in Marine Waters as Determined by Amplified rRNA Gene Restriction Analysis and Sequence Analysis of 16S rRNA Genes Downloaded from http://aem.asm.org/ on December 5 , 2014 by TU MUENCHEN Univ. *Appl. Environ. Microbiol.* **66**, 467–475 (2000).

12. Flemming, H.-C. Eps—Then and Now. *Microorganisms* **4**, 1–18 (2016).

13. Hadfield, M. G. Biofilms and Marine Invertebrate Larvae: What Bacteria Produce That Larvae Use to Choose Settlement Sites. *Ann. Rev. Mar. Sci.* **3**, 453–470 (2011).

14. Lau, S. C. K., Thiyagarajan, V., Cheung, S. C. K. & Qian, P. Y. Roles of bacterial community composition in biofilms as a mediator for larval settlement of three marine invertebrates. *Aquat. Microb. Ecol.* **38**, 41–51 (2005).

15. Dobretsov, S. & Qian, P.-Y. Facilitation and inhibition of larval attachment of the bryozoan *Bugula neritina* in association with mono-species and multi-species biofilms. *J. Exp. Mar. Bio. Ecol.* **333**, 263–274 (2006).

16. Rahat, M. & Dimentman, C. Cultivation of bacteria-free Hydra viridis: missing budding factor in nonsymbiotic hydra. *Science (80-.).* **216**, 67–68 (1982).

17. Nocker, A., Lepo, J. E., Martin, L. L. & Snyder, R. A. Response of estuarine biofilm microbial community development to changes in dissolved oxygen and nutrient concentrations. *Microb. Ecol.* **54**, 532–542 (2007).

18. Cheung, S. G. *et al.* Effects of hypoxia on biofilms and subsequently larval settlement of benthic invertebrates. *Mar. Pollut. Bull.* **85**, 418–424 (2014).

19. Lagos, M. E., White, C. R. & Marshall, D. J. Biofilm history and oxygen availability interact to affect habitat selection in a marine invertebrate. *Biofouling* **32**, 645–655 (2016).

20. Shin, P. K. S. *et al.* Hypoxia induces abnormal larval development and affects biofilm-larval interaction in the serpulid polychaete Hydroides elegans. *Mar. Pollut. Bull.* **76**, 291–297 (2013).

21. Chiu, J. M. Y., Thiyagarajan, V., Pechenik, J. A., Hung, O. S. & Qian, P. Y. Influence of bacteria and diatoms in biofilms on metamorphosis of the marine slipper limpet Crepidula onyx. *Mar. Biol.* **151**, 1417–1431 (2007).

22. Hung, O. S., Thiyagarajan, V., Zhang, R., Wu, R. S. S. & Qian, P. Y. Attachment of Balanus amphitrite</i> to biofilms origionating from contrasting environments. **333**, 1–14 (2007).

23. Lema, K. A., Constancias, F., Rice, S. A. & Hadfield, M. G. High bacterial diversity in nearshore and oceanic biofilms and their influence on larval settlement by *Hydroides elegans* (Polychaeta). *Environ. Microbiol.* **21**, 3472–3488 (2019).

24. Campbell, A. H. *et al.* Effects of age and composition of field-produced biofilms on oyster larval setting. *Biofouling* **27**, 255–265 (2011).

25. Chung, H. C. *et al.* Bacterial community succession and chemical profiles of subtidal biofilms in relation to larval settlement of the polychaete Hydroides elegans. *ISME J.* **4**, 817–828 (2010).

26. Shikuma, N. J. J. & Hadfield, M. G. G. Temporal variation of an initial marine biofilm community and its effects on larval settlement and metamorphosis of the tubeworm Hydroides elegans. *Image (Rochester, N.Y.)* **2**, 231–238 (2006).

27. Nielsen, S. J., Harder, T. & Steinberg, P. D. Sea urchin larvae decipher the epiphytic bacterial community composition when selecting sites for attachment and metamorphosis. *FEMS Microbiol. Ecol.* **91**, 1–9 (2015).

28. Franco, Á. G., Cadavid, L. F. & Arévalo-Ferro, C. Biofilms and extracts from bacteria producing “Quorum Sensing” signaling molecules promote chemotaxis and settlement behaviors in Hydractinia Symbiolongicarpus (cnidaria: Hydrozoa) larvae. *Acta Biol. Colomb.* **24**, 150–162 (2019).

29. Hung, O. S. *et al.* Characterization of cues from natural multi-species biofilms that induce larval attachment of the polychaete Hydroides elegans. *Aquat. Biol.* **4**, 253–262 (2008).

30. Wahab, M. A. A., de Nys, R. & Whalan, S. Larval behaviour and settlement cues of a brooding coral reef sponge. *Coral Reefs* **30**, 451–460 (2011).

31. Whalan, S., Ettinger-Epstein, P., Battershill, C. & de Nys, R. Larval vertical migration and hierarchical selectivity of settlement in a brooding marine sponge. *Mar. Ecol. Ser.* **368**, 145–154 (2008).

32. Whalan, S. & Webster, N. S. Sponge larval settlement cues: The role of microbial biofilms in a warming ocean. *Sci. Rep.* **4**, 28–32 (2014).

33. Woollacott, R. M. & Hadfield, M. G. Induction of Metamorphosis in Larvae of a

Sponge. *Invertebr. Biol.* **115**, 257 (1996).

34. Wang, C. *et al.* Larval settlement and metamorphosis of the mussel *Mytilus coruscus* in response to natural biofilms. *Biofouling* **28**, 249–256 (2012).

35. Fitt, W. K. *et al.* Settlement behavior and metamorphosis of oyster larvae (*Crassostrea gigas*) in response to bacterial supernatants. *Mar. Biol.* **106**, 389–394 (1990).

36. Gribben, P. E., Wright, J. T., O'Connor, W. A. & Steinberg, P. Larval settlement preference of a native bivalve: The influence of an invasive alga versus native substrata. *Aquat. Biol.* **7**, 217–227 (2009).

37. Kaniewska, P. *et al.* Major cellular and physiological impacts of ocean acidification on a reef building coral. *PLoS One* **7**, (2012).

38. Rodriguez-Perez, A. *et al.* Conservation and restoration of a keystone species: Understanding the settlement preferences of the European oyster (*Ostrea edulis*). *Mar. Pollut. Bull.* **138**, 312–321 (2019).

39. Tamburri, M. N., Luckenbach, M. W., Breitburg, D. L. & Bonniwell, S. M. Settlement of *Crassostrea ariakensis* larvae: Effects of substrate, biofilms, sediment and adult chemical cues. *J. Shellfish Res.* **27**, 601–608 (2008).

40. Yang, J. L. *et al.* Larval settlement and metamorphosis of the mussel *Mytilus coruscus* in response to monospecific bacterial biofilms. *Biofouling* **29**, 247–259 (2013).

41. Anderson, J. A. & Epifanio, C. E. Induction of metamorphosis in the Asian shore crab Hemigrapsus sanguineus: Characterization of the cue associated with biofilm from adult habitat. *J. Exp. Mar. Bio. Ecol.* **382**, 34–39 (2009).

42. Faimali, M., Garaventa, F., Terlizzi, A., Chiantore, M. & Cattaneo-Vietti, R. The interplay of substrate nature and biofilm formation in regulating *Balanus amphitrite* Darwin, 1854 larval settlement. *J. Exp. Mar. Bio. Ecol.* **306**, 37–50 (2004).

43. Khandeparker, L., Chandrashekar Anil, A. & Raghukumar, S. Relevance of biofilm bacteria in modulating the larval metamorphosis of *Balanus amphitrite*. *FEMS Microbiol. Ecol.* **58**, 425–438 (2006).

44. Bertrand, J. F. & Woollacott, R. M. G protein-linked receptors and induction of metamorphosis in *Bugula stolonifer* (Bryozoa). *Invertebr. Biol.* **122**, 380–385 (2003).

45. Shikuma, N. J. *et al.* Marine tubeworm metamorphosis induced by arrays of bacterial phage tail-like structures. *Science (80-.).* **343**, 529–533 (2014).

46. Szewzyk, U. *et al.* Relevance of the exopolysaccharide of marine Pseudomonas sp. strain S9 for the attachment of Ciona intestinalis larvae. **75**, 259–265 (1991).

47. Swanson, R. L. *et al.* Induction of settlement of larvae of the sea urchin Holopneustes purpurascens by histamine from a host alga. *Biol. Bull.* **206**, 161–172 (2004).

48. Huggett, M. J., Williamson, J. E., de Nys, R., Kjelleberg, S. & Steinberg, P. D. Larval settlement of the common Australian sea urchin *Heliocidaris erythrogramma* in response to bacteria from the surface of coralline algae. *Oecologia* **149**, 604–619 (2006).

49. Chase, A. L., Dijkstra, J. A. & Harris, L. G. The influence of substrate material on ascidian larval settlement. *Mar. Pollut. Bull.* **106**, 35–42 (2016).

50. Karaiskou, A., Swalla, B. J., Sasakura, Y. & Chambon, J.-P. Metamorphosis in solitary ascidians. *Genesis* **53**, 34–47 (2014).

51. Hotta, K., Dauga, D. & Manni, L. The ontology of the anatomy and development of the solitary ascidian Ciona: the swimming larva and its metamorphosis. *Sci. Rep.* **10**, 1–16 (2020).

52. Roberts, B. *et al.* A complement response may activate metamorphosis in the ascidian *Boltenia villosa*. *Dev. Genes Evol.* **217**, 449–458 (2007).

53. Wieczorek, S. K. K. Inhibition and facilitation of bryozoan and ascidian settlement by natural multi-species biofilms: Effects of film age and the roles of active and passive larval attachment. *Mar. Biol.* **128**,

54. Kirchman, D., Graham, S., Reish, D. & Mitchell, R. Bacteria induce settlement and metamorphosis of *Janua (Dexiospira) brasiliensis Grube* (Polychaeta:Spirprbidae).

J. Exp. Mar. Bio. Ecol. **56**, 153–163 (1981).

55. Hadfield, M. G., Nedved, B. T., Wilbur, S. & Koehl, M. A. R. Biofilm cue for larval settlement in *Hydroides elegans* (Polychaeta): is contact necessary? *Mar. Biol.* (2014).

56. Huang, S. Y. & Hadfield, M. G. Composition and density of bacterial biofilms determine larval settlement of the polychaete Hydroides elegans. *Mar. Ecol. Ser.* **260**, 161–172 (2003).

57. Freckelton, M. L., Nedved, B. T. & Hadfield, M. G. Induction of Invertebrate Larval Settlement; Different Bacteria, Different Mechanisms? *Sci. Rep.* **7**, 42557 (2017).

58. Unabia, C. R. C. & Hadfield, M. G. Role of bacteria in larval settlement and metamorphosis of the polychaete *Hydroides elegans*. *Mar. Biol.* **133**, 55–64 (1999).

59. Nedved, B. T. & Hadfield, M. G. Hydroides elegans (Annelida: Polychaeta): A Model for Biofouling Research. *Mar. idustrial biofouling* **4**, 203–217 (2009).

60. Shikuma, N. J., Antoshechkin, I., Medeiros, J. M., Pilhofer, M. & Newman, D. K. Stepwise metamorphosis of the tubeworm *Hydroides elegans* is mediated by a bacterial inducer and MAPK signaling. *Proc. Natl. Acad. Sci.* **113**, 10097–10102 (2016).

61. Harder, T., Lau, S. C. K., Dahms, H. U. & Qian, P. Y. Isolation of bacterial metabolites as natural inducers for larval settlement in the marine polychaete *Hydroides elegans* (HASWELL). *J. Chem. Ecol.* **28**, 2029–2043 (2002).

62. Asahina, A. Y. & Hadfield, M. G. Draft Genome Sequence of *Pseudoalteromonas luteoviolacea* HI1, Determined Using Roche 454 and PacBio Single-Molecule Real-Time Hybrid Sequencing. *Genome Announc.* **3**, (2015).

63. Peng, L. H., Liang, X., Xu, J. K., Dobretsov, S. & Yang, J. L. Monospecific Biofilms of <i>Pseudoalteromonas Promote Larval Settlement and Metamorphosis of Mytilus coruscus. *Sci. Rep.* **10**, 1–12 (2020).

64. Lau, S. C. K. *et al. Loktanella hongkongensis sp.* nov., a novel member of the α-Proteobacteria originating from marine biofilms in Hong Kong waters. *Int. J. Syst. Evol. Microbiol.* **54**, 2281–2284 (2004).

65. Zobell, C. E. & Allen, E. C. The Significance of Marine Bacteria in the Fouling of Submerged Surfaces. *J. Bacteriol.* **29**, 239–51 (1934).

66. Hadfield, M. G. Biofilms and Marine Invertebrate Larvae: What Bacteria Produce That Larvae Use to Choose Settlement Sites. *Annu. Rev. Mar. Sci* **3**, 453–470 (2011).

67. Huang, Y., Callahan, S. & Hadfield, M. G. Recruitment in the sea : bacterial genes required for inducing larval settlement in a polychaete worm. (2012). doi:10.1038/srep00228

68. Böck, D. *et al.* In situ architecture, function, and evolution of a contractile injection system. *Science (80-.).* **357**, 713–717 (2017).

69. Rojas, M. I. *et al.* A Distinct Contractile Injection System Gene Cluster Found in a Majority of Healthy Adult Human Microbiomes. *mSystems* **5**, (2020).

70. Vlisidou, I. *et al.* The photorhabdus asymbiotica virulence cassettes deliver protein effectors directly into target eukaryotic cells. *Elife* **8**, 1–24 (2019).

71. Yang, G., Dowling, A. J., Gerike, U., Ffrench-Constant, R. H. & Waterfield, N. R. Photorhabdus virulence cassettes confer injectable insecticidal activity against the wax moth. *J. Bacteriol.* **188**, 2254–2261 (2006).

72. Logan, S. L. *et al.* The *Vibrio cholerae* type VI secretion system can modulate host intestinal mechanics to displace gut bacterial symbionts. *Proc. Natl. Acad. Sci. U. S. A.* **115**, E3779--E3787 (2018).

73. Ericson, C. F. *et al.* A contractile injection system stimulates tubeworm metamorphosis by translocating a proteinaceous effector. *Elife* **8**, 1–19 (2019).

74. Rocchi, I. *et al.* A Bacterial Phage Tail-like Structure Kills Eukaryotic Cells by Injecting a Nuclease Effector. *Cell Rep.* **28**, (2019).

75. Ding, W. *et al.* Distribution, diversity and functional dissociation of the mac genes in marine biofilms. *Biofouling* **35**, 230–243 (2019).

76. Matz, C. *et al.* Marine biofilm bacteria evade eukaryotic predation by targeted chemical defense. *PLoS One* **3**, 1–7 (2008).

77. Kroiher, M. & Berking, S. On natural metamorphosis inducers of the cnidarians *Hydractinia echinata* (Hydrozoa) and *Aurelia aurita* (Scyphozoa). *Helgol. Mar. Res.* **53**, 118–121 (1999).

78. Lau, S. C. *et al.* Genome sequence of the pink-pigmented marine bacterium *Loktanella hongkongensis* type strain (UST950701-009P(T)), a representative of the Roseobacter group. *Stand. Genomic Sci.* **10**, 51 (2015).

79. Lau, S. C., Harder, T. & Qian, P.-Y. Induction of larval settlement in the serpulid polychaete Hydroides elegans (Haswell): role of bacterial extracellular polymers. *Biofouling* **19**, 197–204 (2003).

80. J., B. S. *et al.* Bacterial Vesicles in Marine Ecosystems. *Science (80-.).* **343**, 183–186 (2014).

81. Deatherage, B. L. & Cookson, B. T. Membrane vesicle release in bacteria, eukaryotes, and archaea: a conserved yet underappreciated aspect of microbial life. *Infect. Immun.* **80**, 1948–1957 (2012).

82. Laudet, V. The origins and evolution of vertebrate metamorphosis. *Current Biology* **21**, R726--37 (2011).

83. Nielsen, C. Life cycle evolution: was the eumetazoan ancestor a holopelagic, planktotrophic gastraea? *BMC Evol. Biol.* **13**, 171 (2013).

84. Pechenik, J. A. On the advantages and disadvantages of larval stages in benthic marine invertebrate life cycles. *Mar. Ecol. Prog. Ser.* **177**, 269–297 (1999).

85. Strathmann, R. R. Hypotheses on the Origins of Marine Larvae. *Annu. Rev. Ecol. Syst.* **24**, 89–117 (1993).

86. Jackson, D. *et al.* Ecological regulation of development: induction of marine invertebrate metamorphosis. *Int. J. Dev. Biol.* **46**, 679–686 (2002).

87. Antunes, J., Leão, P. & Vasconcelos, V. Marine biofilms: diversity of communities

and of chemical cues. *Environ. Microbiol. Rep.* **11**, 287–305 (2019).

88. Egan, S., Thomas, T. & Kjelleberg, S. Unlocking the diversity and biotechnological potential of marine surface associated microbial communities. *Curr. Opin. Microbiol.* **11**, 219–225 (2008).

89. Holmström, C. & Kjelleberg, S. Marine *Pseudoalteromonas* species are associated with higher organisms and produce biologically active extracellular agents. *FEMS Microbiol. Ecol.* **30**, 285–293 (1999).

90. Nasrolahi, A., Stratil, S. B., Jacob, K. J. & Wahl, M. A protective coat of microorganisms on macroalgae: inhibitory effects of bacterial biofilms and epibiotic microbial assemblages on barnacle attachment. *FEMS Microbiol. Ecol.* **81**, 583–595 (2012).

91. Dang, H. & Lovell, C. R. Microbial Surface Colonization and Biofilm Development in Marine Environments. *Microbiol. Mol. Biol. Rev.* **80**, 91–138 (2016).

92. Bowman, J. P. Bioactive compound synthetic capacity and ecological significance of marine bacterial genus *Pseudoalteromonas*. *Mar. Drugs* **5**, 220–241 (2007).

93. Offret, C. *et al.* Spotlight on Antimicrobial Metabolites from the Marine Bacteria Pseudoalteromonas: Chemodiversity and Ecological Significance. *Mar. Drugs* **14**, 129 (2016).

94. Robert, A. & D., H. W. The Evolution of Cooperation. *Science (80-.).* **211**, 1390–1396 (1981).

95. Sachs, J. L. & Skophammer, R. G. Evolutionary transitions in bacterial symbiosis. in *Proceedings of the …* (2011).

96. Steinberg, P. D., De Nys, R. & Kjelleberg, S. Chemical cues for surface colonization. *J. Chem. Ecol.* **28**, 1935–1951 (2002).

97. RITTSCHOF, D. A. N. Body Odors and Neutral-basic Peptide Mimics: A Review of Responses by Marine Organisms. *Am. Zool.* **33**, 487–493 (1993).

98. Rittschof, D. Peptide-mediated behaviors in marine organisms Evidence for a

common theme. *J. Chem. Ecol.* **16**, 261–272 (1990).

99. Spindler, K.-D. & Müller, W. A. Induction of metamorphosis by bacteria and by a lithium-pulse in the larvae of *Hydractinia echinata* (Hydrozoa). *Wilhelm Roux. Arch. Entwickl. Mech. Org.* **169**, 271–280 (1972).

100. Fuchs, B. *et al.* Regulation of Polyp-to-Jellyfish Transition in Aurelia aurita. *Curr. Biol.* **24**, 263–273 (2014).

101. Müller, W. A. & Leitz, T. Metamorphosis in the Cnidaria. *Can. J. Zool.* **80**, 1755–1771 (2002).

102. Pearce, C. M. & Scheibling, R. E. Induction of metamorphosis of larval echinoids (*Strongylocentrotus droebachiensis* and *Echinarachnius parma*) by potassium chloride (KCl). *Invertebr. Reprod. Dev.* **26**, 213–220 (1994).

103. Yool, A. J. *et al.* Excess Potassium Induces Larval Metamorphosis in Four Marine Invertebrate Species. *Biol. Bull.* **170**, 255–266 (1986).

104. Seipp, S., Schmich, J., Kehrwald, T. & Leitz, T. Metamorphosis of Hydractinia echinata—natural versus artificial induction and developmental plasticity. *Dev. Genes Evol.* **217**, 385–394 (2007).

105. Amador-Cano, G., Carpizo-Ituarte, E. & Cristino-Jorge, D. Role of protein kinase C, G-protein coupled receptors, and calcium flux during metamorphosis of the sea urchin Strongylocentrotus purpuratus. *Biol. Bull.* **210**, 121–131 (2006).

106. Biggers, W. J. & Laufer, H. Settlement and Metamorphosis of *Capitella* Larvae Induced by Juvenile Hormone-Active Compounds Is Mediated by Protein Kinase C and Ion Channels. *Biol. Bull.* **196**, 187–198 (1999).

107. Henning, G., Hofmann, D. K. & Benayahu, Y. The phorbol ester TPA induces metamorphosis in Red Sea coral planulae (Cnidaria: Anthozoa). *Experientia* **52**, 744–749 (1996).

108. Leitz, T. & Klingmann, G. Metamorphosis in *Hydractinia* : Studies with activators and inhibitors aiming at protein kinase C and potassium channels. *Roux's Arch. Dev. Biol.* **199**, 107–113 (1990).

109. Yamamoto, H., Tachibana, A., Matsumura, K. & Fusetani, N. Protein Kinase C (PKC) Signal Transduction System Involved in Larval Metamorphosis of the Barnacle, *Balanus amphitrite* . *Zoological Science* **12**, 391–396 (1995).

110. Leitz, T., Morand, K. & Mann, M. Metamorphosin A: a novel peptide controlling development of the lower metazoan Hydractinia echinata (Coelenterata, Hydrozoa). *Dev. Biol.* **163**, 440–446 (1994).

111. Leitz, T. & Müller, U. Stimulation of metamorphosis in Hydractinia echinata involves generation of lysophosphatidylcholine. *Roux's Arch. Dev. Biol.* **200**, 249–255 (1991).

112. Liu, P., Peng, H.-J. & Zhu, J. Juvenile hormone-activated phospholipase C pathway enhances transcriptional activation by the methoprene-tolerant protein. *Proc. Natl. Acad. Sci.* **112**, E1871--E1879 (2015).

113. Chambon, J. P., Nakayama, A., Takamura, K., McDougall, A. & Satoh, N. ERK- and JNK-signalling regulate gene networks that stimulate metamorphosis and apoptosis in tail tissue of *ascidian* tadpoles. *Development* **134**, 1203–1219 (2007).

114. Ueda, N. *et al.* An ancient role for nitric oxide in regulating the animal pelagobenthic life cycle: evidence from a marine sponge. *Sci. Rep.* **6**, 37546 (2016).

115. Wang, H. & Qian, P. Y. Involvement of a novel p38 mitogen-activated protein kinase in larval metamorphosis of the polychaete Hydroides elegans (Haswell). *J. Exp. Zool. Part B Mol. Dev. Evol.* **314 B**, 390–402 (2010).

116. Jensen, R. A. & Morse, D. E. Chemically induced metamorphosis of polychaete larvae in both the laboratory and ocean environment. *J. Chem. Ecol.* **16**, 911–930 (1990).

117. Liang, X. *et al.* Effects on larval metamorphosis in the mussel *Mytilus coruscus* of compounds that act on downstream effectors of G-protein-coupled receptors. *J. Mar. Biol. Assoc. United Kingdom* **98**, 333–339 (2018).

118. Davidson, B. & Swalla, B. J. A molecular analysis of ascidian metamorphosis reveals activation of an innate immune response. *Development* **129**, 4739–4751 (2002).

119. Heyward, A. J., Smith, L. D. & Rees, M. Enhancement of coral recruitment by in situ mass culture of coral larvae . *Mar. Ecol. Prog. Ser.* **230**, 113–118 (2002).

120. Peixoto, R. S., Rosado, P. M., Leite, D. C. de A., Rosado, A. S. & Bourne, D. G. Beneficial microorganisms for corals (BMC): Proposed mechanisms for coral health and resilience. *Front. Microbiol.* **8**, 1–16 (2017).

121. Prado, S., Romalde, J. L. & Barja, J. L. Review of probiotics for use in bivalve hatcheries. *Vet. Microbiol.* **145**, 187–197 (2010).

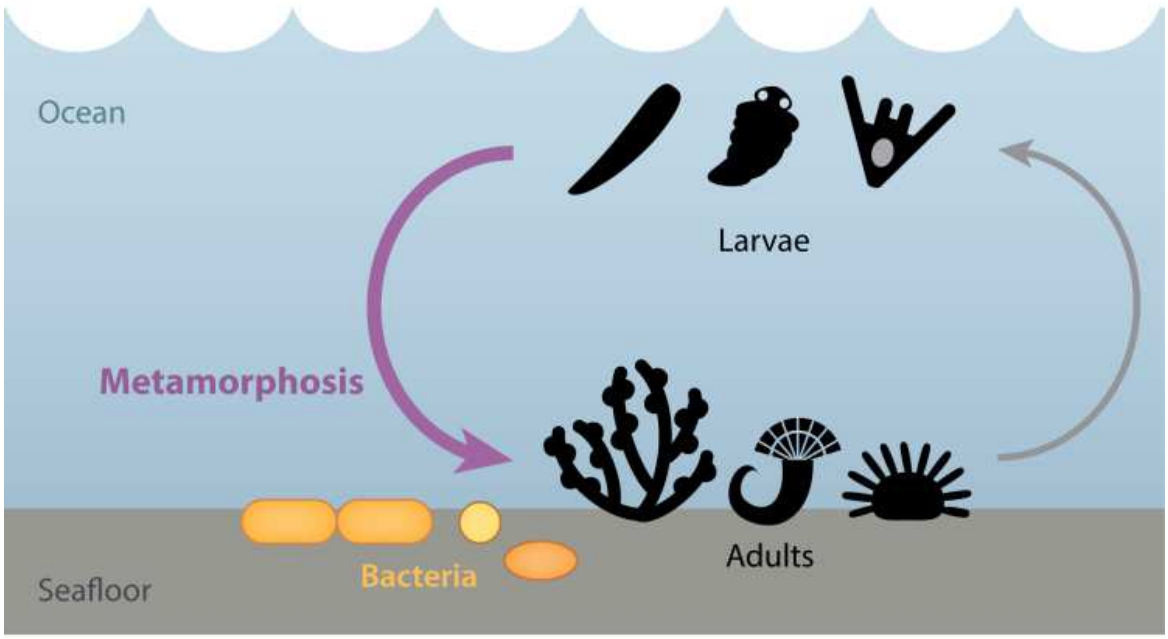

Cavalcanti GS, et al. 2020.
Annu. Rev. Microbiol. 74:137–58

Figure 1.1. Model of the stimulation of animal metamorphosis by bacteria. The swimming larvae of diverse marine animals (e.g., corals, tubeworms, and urchins) are stimulated to undergo settlement and metamorphosis by the presence of bacteria bound to the seafloor.

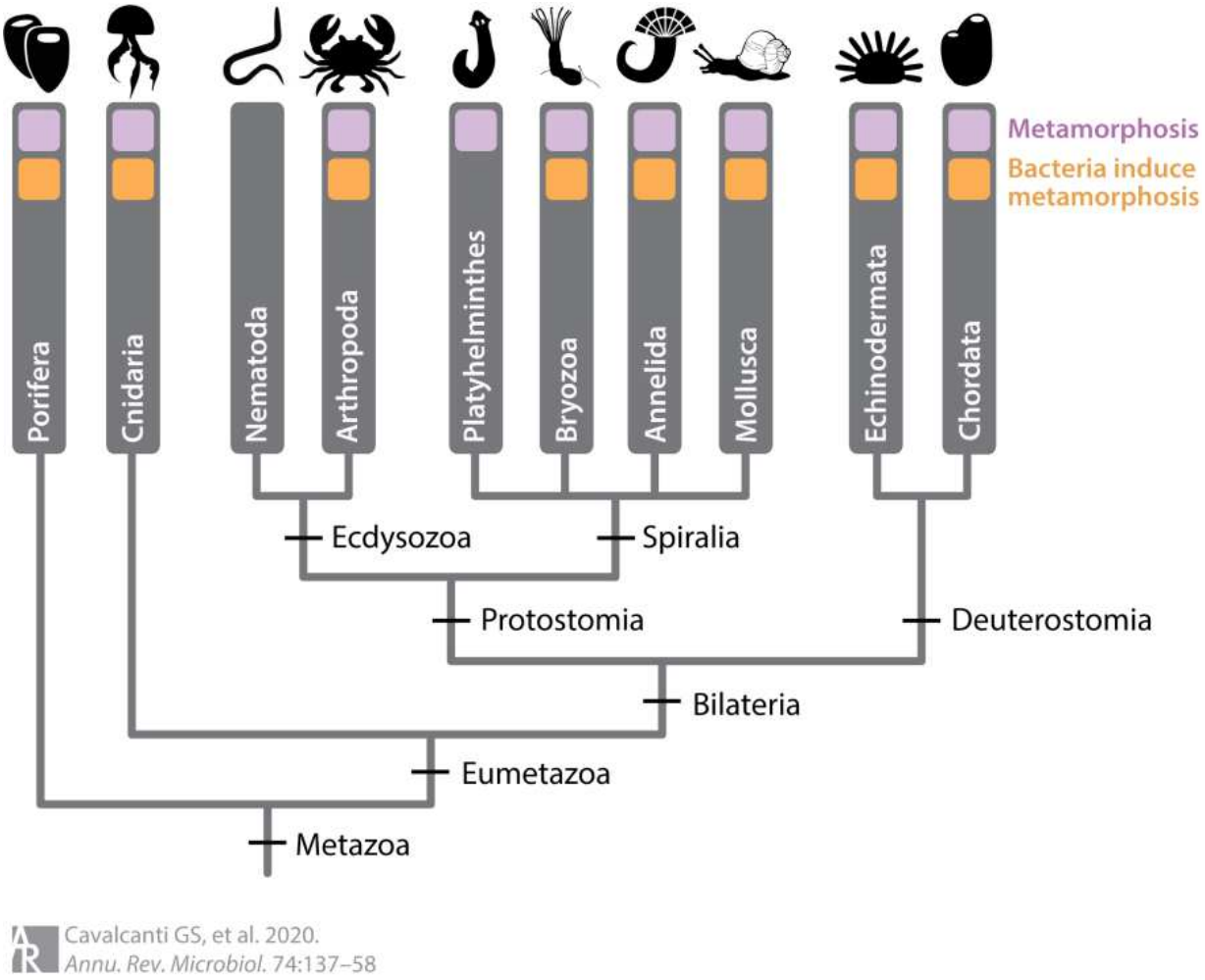

Figure 1.2. Bacteria-stimulated metamorphosis is widespread among diverse animal taxa. Shown is a representation of the animal tree of life. Taxa that undergo metamorphosis are indicated in blue. Taxa that undergo metamorphosis in response to bacteria are indicated in yellow. Adapted from Shikuma et al. 2016[60].

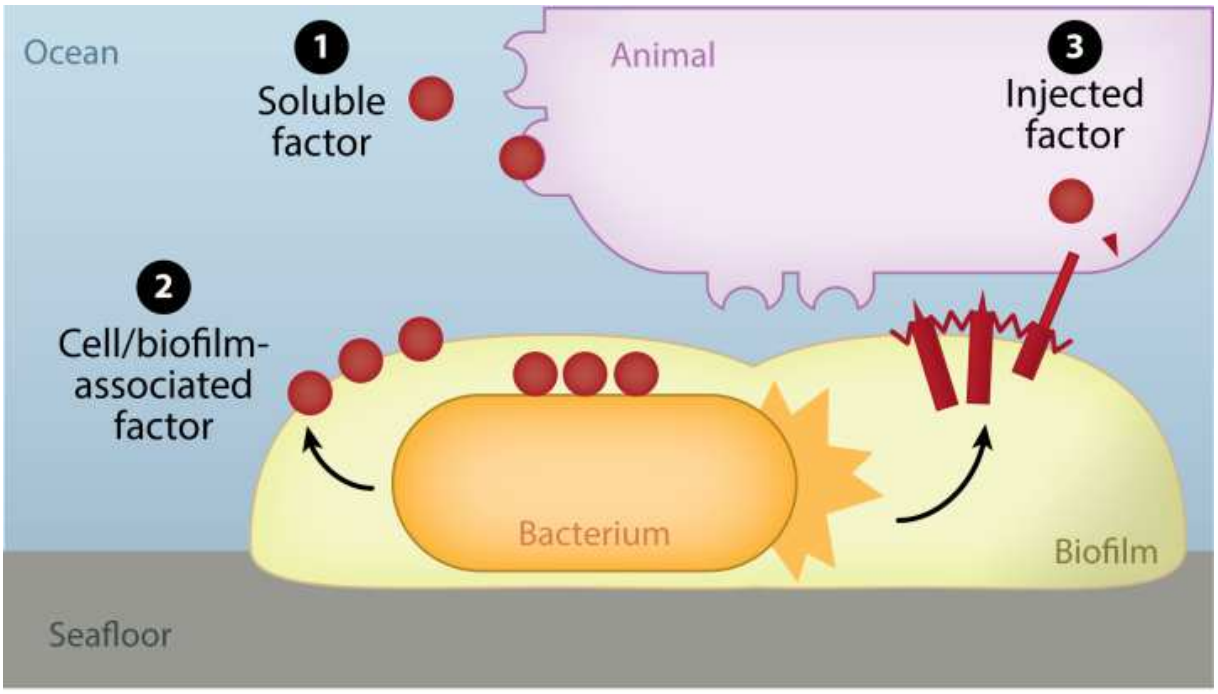

Cavalcanti GS, et al. 2020.
Annu. Rev. Microbiol. 74:137–58

Figure 1.3. Model of types of bacterial factors that stimulate animal metamorphosis. Stimulatory factors from bacteria can be (*a*) soluble, (*b*) bound to the bacterial cell or biofilm surface, or (*c*) injected into host cells.

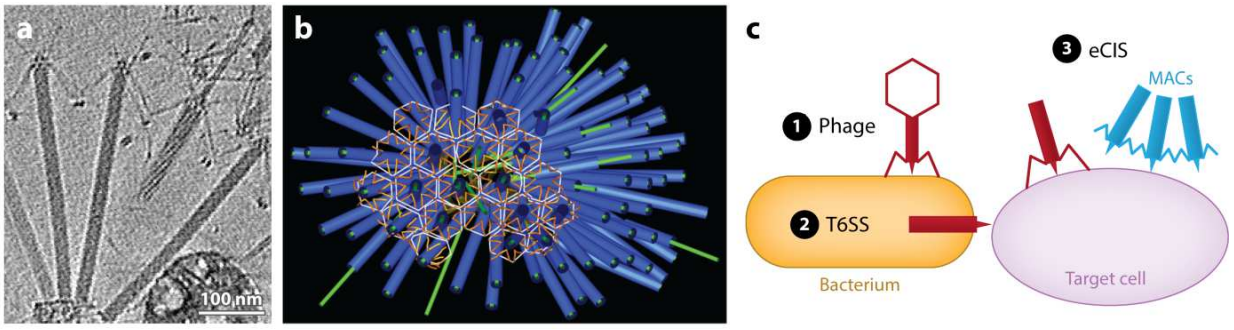

Cavalcanti GS, et al. 2020.
Annu. Rev. Microbiol. 74:137–58

Figure 1.4. MACs are an example of a CIS that often injects protein effectors into target cells. Panels *a* and *b* show a side view of MACs in extended and contracted states and a segmented model of the array, respectively. (*c*) CISs are related to the contractile tails of bacteriophage (viruses of bacteria, *i*). T6SSs (*ii*) act from within a bacterial cell, while eCISs (*iii*) are released by bacterial cell lysis and autonomously bind to target cells. MACs are one example of an eCIS. Abbreviations: CIS, contractile injection system; eCIS, extracellular CIS; MAC, metamorphosis-associated contractile structure; T6SS, type VI secretion system. Panels *a* and *b* adapted from Reference[45]. Reprinted with permission from AAAS.

Chapter 2

Bacterial Phage Tail-like Structure Kills Eukaryotic Cells by Injecting a Nuclease Effector

2.1 Abstract

Many bacteria interact with target organisms using syringe-like structures called Contractile Injection Systems (CIS). CIS structurally resemble headless bacteriophages and share evolutionarily related proteins such as the tail tube, sheath, and baseplate complex. In many cases, CIS mediate trans-kingdom interactions between bacteria and eukaryotes by delivering effectors to target cells. However, the specific effectors and their modes of action are often unknown. Here, we establish an *ex vivo* model to study an extracellular CIS (eCIS) called Metamorphosis Associated Contractile structures (MACs) that target eukaryotic cells. MACs kill two eukaryotic cell lines, Fall Armyworm Sf9 cells and J774A.1 murine macrophage cells, by translocating an effector termed Pne1. Before the identification of Pne1, no CIS effector exhibiting nuclease activity against eukaryotic cells had been described. Our results define a new mechanism of CIS-mediated bacteria-eukaryote interaction and are a step toward developing CIS as novel delivery systems for eukaryotic hosts.

2.2 Introduction

Bacteria interact with eukaryotic organisms with outcomes ranging from pathogenic to beneficial. One mechanism used by bacteria to interact with eukaryotes is through Contractile Injection Systems (CIS) [1]. CIS are evolutionarily related to the tails of bacteriophages (bacterial viruses) and are composed of an inner tube surrounded by a contractile sheath, capped with a tail spike and a baseplate complex. CIS can be classified into two types: Type 6 Secretion Systems (T6SS) and extracellular CIS (eCIS), also known as phage tail-like bacteriocins or tailocins. While T6SS reside within the

bacterial cytoplasm and are anchored to the inner membrane of Gram-negative bacteria [2,3], eCIS are released extracellularly by bacterial cell lysis and bind their target cell surface [4–6]. It has been speculated that eCIS may be an evolutionary intermediate between bacteriophage and T6SS [7].

In both eCIS and T6SS, contraction of the sheath drives the inner tube and tail spike through the target cell membrane, and both often deliver effectors to host cells. For example, an eCIS called *Photorhabdus* Virulence Cassettes (PVC) injects an effector causing deamidation and transglutamination of the cell cytoskeleton [4,8]. In T6SS, a number of effectors are described that specifically target eukaryotic cells [9]. The modes of action of these T6SS effectors include actin cross-linking in macrophages [10], interaction with microtubules for invasion of epithelial cells [11], and disruption of the actin cytoskeleton of HeLa cells [12]. However, to our knowledge and until the present work, no CIS effectors (T6SS or eCIS) targeting eukaryotic cells are yet described that possess nuclease activity.

One group of evolutionarily related CIS have been shown to mediate interactions with diverse eukaryotic organisms including amoeba, grass grubs, wax moths and wasps [2,4,13–16]. We recently described a related eCIS mediating the beneficial relationship between the Gram-negative bacterium *Pseudoalteromonas luteoviolacea* and a marine tubeworm, *Hydroides elegans*, hereafter *Hydroides* [6,17,18]. We called this eCIS from *P. luteoviolacea* MACs for Metamorphosis Associated Contractile structures, because they stimulate the metamorphosis of *Hydroides* [6]. MACs are the first CIS discovered to form

arrays of phage tail-like structures composed of about 100 tails and often measure about 1 μm in diameter. While MACs provide another example of CIS-eukaryote interactions, the range of hosts targeted by eCIS like MACs as well as the identity and mode of action of effectors that mediate these interactions remain poorly understood.

To study the interaction between MACs and eukaryotic cells, we establish an *ex vivo* CIS-cell line interaction model with insect and mammalian cell types. Using these systems, we identify a new MAC effector with nuclease activity that is responsible for cytotoxicity in both cell types that we call Pne1 for *Pseudoalteromonas* nuclease effector 1. Our results indicate that MACs can interact with a range of host cells and a specific effector mediates killing of eukaryotic cells.

2.3 Results

MACs kill insect cell lines *ex vivo*. To study MACs from *P. luteoviolacea* and test their effect on eukaryotic cells, we focused on an insect cell line from the Fall Armyworm *Spodoptera frugiperda* (Sf9), the closest relative to *Hydroides* where established cell lines are commercially available. Upon co-incubation of purified MACs, we observed the lysis of Sf9 cells within 48 hours (Figure 2.1. A). As a control, we included cell-free purifications from a strain lacking the MAC baseplate gene *macB*, which is unable to produce intact phage tail-like structures and multi-tailed arrays [6]. When Sf9 cells were co-incubated with purifications from a Δ*macB* strain or extraction buffer alone, the cells remained viable (Figure 2.1. B & C). We quantified the activity of MACs against Sf9 cells by staining dead cells using a colorimetric stain, trypan blue, or by a fluorescent dual

stain, fluorescein diacetate (FDA) and propidium iodide (PI), which stains live and dead cells, respectively. Using both methods, we observed cell death when cells were exposed to wild-type MACs, while death was not observed with purifications from a Δ*macB* strain or the extraction buffer (Figure 2.1. D-H). Filtering extract from wild-type cells through a 0.45-μm filter abolished the cell killing effect (Figure 2.1. I), consistent with the observation that MACs form >0.45μm arrays [6]. Our results suggest that MACs are capable of targeting and killing insect cells.

Identification of a MAC effector required for killing of insect cells. We previously showed that a locus containing six genes (JF50_12590-JF50_12615) within the *P. luteoviolacea* genome is required for MACs to stimulate the metamorphosis of the tubeworm *Hydroides*, yet a mutant lacking all 6 genes is still able to produce intact MAC structures [17]. To determine whether MACs require this same locus for killing of insect cell lines, we tested whether *P. luteoviolacea* mutants lacking each of the six genes were deficient in MAC-mediated insect cell killing. Among those six genes, only a ΔJF50_12610 mutant was unable to cause cell death upon co-incubation with insect cells (Figure 2.2. A-G). These results were quantified and confirmed using trypan blue or FDA/PI staining (Figure 2.2. K & L). When JF50_12610 was introduced back into its native chromosomal locus, the killing effect of MACs was restored (Figure 2.2. H). Intriguingly, when we tested MACs from the ΔJF50_12610 mutant against larvae from *Hydroides elegans* we found that this strain was capable of stimulating metamorphosis at levels comparable to that of wild-type MACs (Figure 2.2. M), suggesting functional MAC structures are still present.

To determine whether the ΔJF50_12610 strain produces intact MAC structures, we employed electron cryo-tomography (ECT). Upon inspection, MACs from wild type and ΔJF50_12610 were indistinguishable, forming intact phage tail-like structures in both extended and contracted conformations (Figure 2.2. N & O). In order to confirm that JF50_12610 is part of the MAC complex, we utilized protein identification by mass spectrometry on purified MAC extracts from WT *P. luteoviolacea.* In two independent experiments, we detected JF50_12610 which indicated that the protein is associated with the MAC complex (Figure S2.1. A). To determine whether the ΔJF50_12610 phenotype was due to the differential production of MACs, we quantified MACs tagged with super folder GFP by fluorescent microscopy and found no difference in quantity between wild-type and ΔJF50_12610 strains grown under identical conditions (Figure S2.1. B). Our results show that JF50_12610 is required for MACs to kill insect cell lines yet does not affect the ability of MACs to stimulate tubeworm metamorphosis or the production of functional MACs. The genes within the JF50_12590-JF50_12615 locus required for tubeworm metamorphosis, and not insect cell killing, are the subject of a separate work.

The JF50_12610 protein possesses nuclease activity *in vitro* and this activity is necessary for insect cell death. To determine the function of JF50_12610, we searched the 496 amino acid long protein for conserved domains and homologous proteins. We found that JF50_12610 contains a DNA/RNA non-specific nuclease domain (Pfam: PF13930). Analysis with the Phyre2 protein prediction program [19] showed that residues 258-348 of JF50_12610 bear 20% identity to the nuclease Spd1 from *Streptococcus pyogenes* [20], and residues 267-348 bear 30% identity to the nuclease

Sda1 also from *S. pyogenes* [21] (Figure 2.3. A). Through these partial alignments, we identified a conserved glutamic acid at residue 328 corresponding to Glu164 of Spd1 and Glu225 of Sda1 that coordinate water molecules hydrating the magnesium in the enzyme's active site [20,21]. Consistent with its predicted function as a toxic effector against eukaryotic cells, JF50_12610 protein is predicted to contain a nuclear localization signal [NLStradamus program [22]], which typically targets proteins to the nucleus of eukaryotic cells. Based on the predicted function of JF50_12610 and the results below, we named this effector Pne1 for *Pseudoalteromonas* nuclease effector 1.

To determine whether Pne1 possesses nuclease activity, we cloned the wild type *pne1* gene and a *pne1*-Glu328Ala mutant into an IPTG-inducible vector system with N-terminal 6xHis tag and purified both proteins by nickel affinity chromatography (Figure 2.3. B). When co-incubated with circular DNA, linear DNA or RNA, Pne1 and Pne1-Glu328Ala both exhibited nuclease activity (Figure 2.3. C, D & E), whereas a control protein, green fluorescence protein (GFP), cloned and purified under the same conditions, did not exhibit nuclease activity. Our data suggest that Pne1 is an RNA/DNA endonuclease. Based on similarities between Pne1 and magnesium-dependent homologous proteins Spd1 and Sda1, we tested the nuclease activity of Pne1 protein in the presence of the divalent cation chelator, EDTA. Interestingly, Pne1 and the Pne1-Glu328Ala proteins were still functional in the presence of EDTA (Figure 2.3. C, D & E).

To test whether Pne1 requires its nuclear localization signal or the conserved Glu328 for killing insect cells, we created *P. luteoviolacea* mutants lacking the predicted

nuclear localization signal (residues 19-52) *pne1*-ΔNLS or with the *pne1*-Glu328Ala point mutation in their native chromosomal loci. Upon exposure to insect cells, MACs from the *pne1*-ΔNLS strain partially abolished the killing effect and MACs from the *pne1*-Glu328Ala strain were unable to kill insect cells when compared to wild-type MACs (Figure 2.3. F, H, I & L). Our results show that Pne1 possesses nuclease activity *in vitro* and its nuclear localization signal may be partially responsible for the killing effect. While the Glu328Ala is not required for nuclease activity *in vitro*, this residue is necessary for MACs to kill insect cells. We are currently investigating how the Glu328Ala residue contributes to insect cell killing.

MACs possess a broad host range, killing J774A.1 murine macrophage cell line *ex vivo*. To determine whether MACs are capable of targeting a broader range of eukaryotic cells, we tested the ability of MACs to kill mammalian cells. We chose the commonly used murine macrophage cell line J774A.1 as these immune cells often encounter microbial pathogens and their effectors. Upon exposure of J774A.1 cells to wild-type MACs, we observed cell death within 24 hours (Figure 2.4. A). In contrast, MACs from a Δ*pne1* and Δ*macB*, or buffer alone did not exhibit cell killing (Figure 2.4. B-D). Quantification of cytotoxicity by lactate dehydrogenase (LDH) release assays confirmed the observed killing upon exposure to wild-type MACs and lack of killing upon exposure to MACs from the Δ*pne1* (Figure 2.4. E). Taken together, our results show that MACs are capable of targeting and killing mammalian cells and the cell killing phenotype is dependent on the presence of Pne1.

2.4 Discussion

In this work, we establish an *ex vivo* interaction model between an eCIS and two eukaryotic cell lines. With this system, we determined that the bacterial protein, Pne1, is a novel eCIS effector and possesses RNA/DNA endonuclease activity. To our knowledge, our work is the first to identify a CIS with broad eukaryotic host range and identify the first eukaryotic-targeting CIS effector with nuclease activity.

Here, we show Pne1-dependent cell death of insect and mammalian cell lines, yet we have also previously observed that MACs stimulate metamorphosis in the tubeworm *Hydroides* [6]. While it is unclear why MACs possess an effector that kills eukaryotic cells, some symbiotic bacteria have been shown to use CIS to modulate their host range. For example, the nitrogen-fixing plant symbiont *Rhizobium leguminosarum* limits its host range to plants in the clover family by secreting proteins through a T6SS, while mutation of the *imp* gene cluster (encoding components of the T6SS) allowed the bacterium to form functional root nodules on pea plants, normally outside of its host range [23]. In the environment, *Pseudoalteromonas* species are found in association with many marine invertebrates [24], and might utilize MACs and Pne1 to antagonize specific eukaryotes, like bacterivorous ciliates, while also stimulating the metamorphosis of other eukaryotes like *Hydroides*. Several CIS nuclease effectors have been identified targeting bacterial cells, including Tde1 from the soil bacterium *Agrobacterium tumefaciens* [25], RhsA from *Dickeya dandantii* [26], RhsP from *Vibrio parahaemolyticus* [27] and Tse7 from *Pseudomonas*

aeruginosa [28]. However, Pne1 is the first CIS nuclease effector to our knowledge that targets eukaryotic organisms. Interestingly, the eukaryotic nuclear localization signal at the N-terminus of Pne1 had a partial effect on its ability to kill insect cells, further suggesting its evolved role in targeting eukaryotic hosts.

Our results show that Glu328 is not required for Pne1 nuclease activity *in vitro*. However, this residue is necessary for MACs to kill insect cells. Two hypotheses that might explain these results are that (1) the Pne1-Glu328Ala mutant is not loaded into MACs and/or not translocated into insect cell lines properly or (2) Pne1-Glu328Ala is translocated but the mutation renders it non-toxic. We will direct future experiments to determine the loading into MACs and/or translocation of Pne1 and Pne1-Glu328Ala to address these possibilities. While we show that Pne1 possesses DNA/RNA endonuclease activity, we currently do not know whether *P. luteoviolacea* protects itself from Pne1's activity by means of an immunity protein. However, MACs differ from T6SS in that they are released by cell lysis extracellularly. Therefore, *P. luteoviolacea* may not require an immunity protein if, upon production of Pne1, they are programmed to lyse and release MACs.

The host range of eukaryotic-targeting eCISs are currently poorly understood and we are currently examining how MACs have different effects on other cell types and organisms. Intriguingly, work on related CIS show that many of them target eukaryotic organisms from diverse lineages, for example Grass Grubs, Wax moth, Wasps, and Amoeba [2,4,13,15,]. While the ability of related eCIS, the Anti-feeding prophage (Afp) and

Photorhabdus Virulence Cassettes (PVC), to target eukaryotic cells has been attributed to tail fibers that resemble receptor-binding proteins from adenovirus [4,13], we detected no protein homology in MAC structures. We report here that MACs are capable of targeting multiple *ex vivo* cell lines from insect and mammalian lineages. By further studying how eCIS, like MACs, have evolved from bacteriophage origins to target eukaryotic cells, we can begin to determine the underlying mechanisms associated with these diverse interactions.

In addition to expanding our basic understanding of CIS, our work opens the door for potentially using eCIS for biotechnology purposes. eCIS that target bacterial pathogens are already under development as narrow host-range antimicrobial agents [29], for example against the gastrointestinal pathogen, *Clostridium difficile* [30]. As syringe-like structures that deliver proteinaceous cargo to eukaryotic cells, we are currently working to develop MACs as potential delivery systems for biotechnology applications. While the mechanism of any eCIS-eukaryotic cell attachment has yet to be determined, it is tantalizing to imagine using genetically-modified CIS to deliver peptides of interest to specific eukaryotic cell types. The *ex vivo* system described in this work will significantly facilitate the realization of these efforts.

2.5 Methods

Macrophage Cell Culture

To test the effect of *P. luteoviolacea* MACs on eukaryotic cells, we tested their effect on murine macrophages J774A.1. Macrophage cells were cultured in DMEM (Dulbecco's Modified Eagle's Medium, Gibco #10566-016), which was prepared with the addition of 10% of heat-inactivated fetal bovine serum (FBS) and 1% sodium pyruvate. Frozen cell line stocks were taken from nitrogen tank and thawed quickly at 37°C in a water bath. Thawed cells (~1mL) were added to a 50mL conical centrifuge tube containing 5mL of pre-warmed DMEM. Cells were then centrifuged at 500 g at room temperature for 4 minutes. The supernatant was carefully discarded, and cells were resuspended in 7.5mL of pre-warmed DMEM. This step assured complete removal of DMSO from frozen cell stocks. Resuspended cells were transferred from the 50mL conical centrifuge tube into a 25cm^2 tissue culture flask and incubated at 37°C with 5% CO_2. Cell lines were maintained by passaging every 2-3 days using routine cell culture techniques.

Insect Cell Culture

To test the effect of *P. luteoviolacea* MACs interaction with eukaryotic insect cell lines, we used Sf9 cells (Novagen #71104-3). Cells were cultured in ESF 921 Insect Cell Culture Medium (Expression systems #96-001-01). Frozen cell line stocks were taken from -80°C freezer and thawed quickly at 27°C in a water bath. Thawed cells (~1mL) were added to a 125mL flask containing 10mL of room temperature ESF 921. Cells were then placed in a 27°C incubator shaker, shaking at 130 rpm, in the dark. Cell lines were maintained by passaging every 2-3 days using routine cell culture techniques.

Metamorphosis assay

To determine the effect of *P. luteoviolacea* MACs nuclease knockout strain mutant on the induction of metamorphosis previously described in *Hydroides elegans* (Shikuma et. al., 2014). Specimens of *H. elegans* were obtained from Mission bay, CA, and maintained in culture at San Diego State Univ. Gametes were spawned and embryos maintained in Instant Ocean artificial seawater (ASW) (35.95 g/L). The larvae water and container were changed daily by straining the larvae with a 41 micron mesh sieve. *Isochrysis galbana*, Tahitian strain, was provided as food for adults and larvae. Assays for induction of metamorphosis by various strains of bacteria were performed by growing bacterial strains overnight aerobically in ASWT or NSWT media. Cells were pelleted at 4000 g for 2 min, washed with sterile ASW, and cell density was adjusted to approximately 107 -108 cells/ml. Cell suspensions were aliquoted into 24-well or 96-well plates and incubated for 1 hour to allow bacterial surface attachment. After incubation, unattached bacteria were removed by gently rinsing the wells three times with sterile ASW. Approximately 30-50 competent (6 to 7-day-old) larvae of *H. elegans* were added to each well and incubated at room temperature for 24 h. After incubation, the total numbers of larvae and metamorphosed juveniles were counted and a percent metamorphosis was calculated. At least 4 technical replicates of each treatment were used in all assays performed and at least three biological replicates were performed on separate occasions.

Bacterial Strains and Plasmid Constructions

All the strains and primers used throughout the experiments reported can be seen in tables below (Table 2.1., 2.2.). All deletion and fusion strains were created according to previously published protocols [60,125]. Plasmid insert sequences were verified by DNA

sequencing. Deletion and insert strains were confirmed by PCR. All *E.coli* strains were grown in Luria-Bertani (LB) media at 37°C shaking at 200 revolutions per minute (RPM). All *P. luteoviolacea* cultures were grown in seawater tryptone (SWT) media (35.9 g/L Instant Ocean, 2.5g/L tryptone, 1.5 g/L yeast extract, 1.5 mL/L glycerol) at 25°C shaking at 200 RPM. Media that containing antibiotics were at a concentration of 100 mg/mL unless otherwise stated.

MAC Purifications

MACs are produced by the marine bacteria *Pseudoalteromonas luteoviolacea* as described previously [125]. Briefly, cells were struck out from frozen stock on SWT agar and grown at 25˚C or room temperature for 1-2 days. Cells were inoculated into 5 mL SWT broth and grown for 24 hours, 25˚C at 200 rpm. Cultures were inoculated 0.5 mL into 50 mL SWT in a 250 mL flask and grown for 16 hours, 25˚C at 200 rpm. Cultures were transferred to a 50 mL conical centrifuge tubes and centrifuged at 4000 g for 20 minutes at 4˚C. Cultures were kept on ice after this step. Subsequently, the supernatant was discarded, and the pellet was resuspended in 5mL of cold extraction buffer (20mM Tris Base, 1M NaCl, 1L of deionized water, adjust the pH to 7.5 with HCl). The resuspension mixture was then transferred to a 15mL centrifuge tube and placed in the centrifuge for another 20 minutes at 4000g at 4°C. This time, the supernatant was transferred to another 15mL tube and spun down one last time with the same above conditions. After this final spin, the supernatant (now called MAC extract) was carefully poured to another clean 15mL tube and kept at 4°C until it was ready to be used for cell infections. Indicated in (Figure 2.1. I), MAC extract was first filtered through a 0.45µm syringe filter before use.

MAC Quantification

The quantification of MACs followed the same protocols and methods from with the following modifications [148]. As MACs do not contain nucleic acids, no SYBR staining was performed. Using a 0.22μm anodisc to filter clusters, the anodisc was placed on a vacuum stage. Then, the glass column and clamp were secured on top of it and washed with 2mL of 1XPBS. After the PBS wash, 100μL of MAC extract was added to 900μL of 1XPBS and ran through the filter. Once all the liquid passed through the anodisc, The anodisc was removed, placed on a kimwipe and allowed it to dry completely. Once dried, a slide was made using 10μL of the microscope mount (10% ascorbic acid 1XPBS with 50% glycerol, filter sterilize mount with 0.02μm filter) "sandwiching" the anodisc. A ZEISS microscope was used to quantify MACs tagged with sf-GFP. Quantification of the MACs was performed using column diameter, field of view and volume which was then extrapolated to determine total number of MACs per 100uL. The values represented in (Figure S2.1. B), indicate 3 independent experiments and the average ± SD is shown. (NS, not significant).

Insect Cell Co-incubation with MACs

Prior to treatment with MACs, Sf9 cells were passaged five to twenty times and seeded into 24-well tissue culture plates at a density of $4x10^5$ cells/mL a few hours before infection. MACs that were extracted no more than a week prior to cell infections were added to each well of the 24-well plates with cells at a 1:50 ratio (10μL of the extracts into 500μL of cells). Infected cells were incubated at 27°C, adherently. At 48 hours, trypan

blue or PI/FDA was added to each well of the 24-well infection plates and microscopic images were taken of each well to visualize and quantify cell viability.

Protein Purification

The JF50_12610 wild type, JF50_12610-Glu328Ala and Green Fluorescence Protein (GFP) were cloned into a pET15b vector with N-terminal 6xHis tag. The protein was overexpressed in 500mL of LB medium growing at 37ºC until 0.9OD_{600} and induced using 1.0mM IPTG at 25ºC for 4 hours, followed by a centrifugation step of 4000g for 20min at 4ºC. The cell pellet was resuspended using a native lysis buffer (0.5M NaCl, 20mM Tris-HCl, 20mM imidazole, pH 8). The resuspended cell lysate was then submitted to a French press 2X, which was followed by sonication on high (10 seconds sonication, repeated twice, done on ice). Following cell sonication, the supernatant was purified by a bulk Ni-NTA beads, washed with 20mL lysis buffer on column, and eluted using elution buffer (0.5M NaCl, 20mM Tris-HCl, 250mM imidazole, pH 8) where protein fractions were collected. Eluted protein was buffer exchanged using pierce protein concentrators (thermos fisher cat# 88513) into (0.15M NaCl, 20mM Tris-HCl, pH 8) Collected protein fractions were then quantified using a Thermo-Fisher Pre-diluted protein standards kit (catalog# 23208), and subsequently read on a Biotek plate reader (catalog# 49984). Proteins were then normalized to equal concentrations prior to nuclease assay.

Nuclease Assay

In order to test the bioinformatically predicted nuclease activity found in JF50_12610, a DNase assay was developed. The wild type JF50_12610, JF50_12610-

E328A and Green Fluorescence Protein (GFP) were purified simultaneously and identically prior to assay. After protein purification, protein concentrations were normalized to 0.5µg/µL, including a positive control commercially available DNase I (BioBasic #DD0099-1). All normalized proteins were then incubated for 30 mins at 37ºC with a linear or plasmid DNA fragment of known concentration, or dsRNA, and either 10uM MgCl2 or 20mM EDTA. A reaction total volume of 20µL consisted of 12µL of protein (0.5ug/uL), 6µL of DNA or RNA diluted in MilliQ H2O and 2µL of either 100uM MgCl2 or 200mM EDTA. After 30 minutes of incubation, all reactions and their replicates were resolved in an 1% agarose gel stained with EtBr in 1XTBE (Tris-Borate EDTA, BioBasic #A00265) at 110 volts for about 45 minutes. Gel products were then visualized in a BioRad gel imaging machine (Gel Doc™ EZ System #1708270) appropriately.

Gentle MAC extraction and mass spectrometry

P. luteoviolacea was grown in 50mL Marine Broth (MB) media in 250mL flasks at 30˚C for 6 hours or overnight (12-14 hours). Cells were centrifuged for 30 minutes at 7000 g and 4˚C and resuspended in 5mL cold extraction buffer (20 mM Tris, pH 7.5, 1M NaCl). The resuspensions were centrifuged for 30 minutes at 4000 g and 4˚C and the supernatant was isolated and centrifuged for 30 minutes at 7000 g and 4˚C. The pellet was resuspended in 20-100µL cold extraction buffer and stored at 4°C for further use. All mass spectrometry was done by the Functional Genomics Center Zurich (FGCZ). To prep the MAC extracts for mass spectrometry, the extracts were precipitated by mixing 30µL of sample with 70µl water and 100µl 20% TCA. The samples were then washed twice with cold acetone. The dry pellets were dissolved in 45µl buffer (10mM Tris/2mM $CaCl_2$,

pH 8.2) and 5µl trypsin (100ng/µL in 10mM HCl). They were then microwaved for 30 minutes at 60˚C. The samples were dried, then dissolved in 20µL 0.1% formic acid and transferred to autosampler vials for LC/MS/MS. 1µL was injected.

Electron cryo-tomography of MAC arrays

For ECT imaging of MAC arrays, *P. luteoviolacea* WT and ΔJF50_12610 were cultured for 5-6 hours at 30°C and subsequently centrifuged for 30 minutes at ~7000 g. The pellet was resuspended in 5mL of extraction buffer and centrifuged for 30 minutes at 4000 g to separate intact cells from MAC arrays. The supernatant was carefully transferred into a new tube and centrifuged for 30 minutes at 7000 g. The pellet was resuspended in about 50 µL of extraction buffer and mixed with Protein A-conjugated 10-nm colloidal gold (Cytodiagnostics Inc.) before plunge freezing. Plunge freezing and ECT imaging were performed according to Weiss et al. [149]. 4 µL of sample was applied to glow-discharged EM grids (R2/1 copper, Quantifoil), blotted twice from the back for 3.5 s and vitrified in liquid ethane–propane using a Vitrobot Mark IV (ThermoFisher). ECT data were collected on a Titan Krios (ThermoFisher) transmission electron microscope equipped with a Quantum LS imaging filter (Gatan, slit with 20 eV) and K2 Summit direct electron detector (Gatan). Tilt series were acquired with the software SerialEM[33] using a bidirectional tilt scheme. The angular range was −60° to +60° and the angular increment was 2°. The total electron dose was between 60–100 electrons per $Å^2$ and the pixel size at specimen level was 2.72 Å. Images were recorded in focus with a Volta phaseplate (ThermoFisher) for WT and without phaseplate at 5 µm under-focus for ΔJF50_12610. Tilt series were aligned using gold fiducials and three-dimensional reconstructions were

calculated by weighted back projection using IMOD[34]. Visualization was done in IMOD. Contrast enhancement of the ΔJF50_12610 tomogram was done using the tom_deconv deconvolution filter (https://github.com/dtegunov/tom_deconv).

Macrophage Cell Co-incubation with MACs

Prior to exposure to MACs, J774A.1 cells were passaged two to five times and seeded into 24-well tissue culture plates at a density of $4x10^5$ cells/mL the night before the treatment. MACs that were extracted no more than a week prior to cell treatment were added to each well of the 24-well plates with cells at a 1:50 ratio (10μL of the extracts into 500μl of cells). Treated cells were incubated at 37°C with 5% CO_2. Culture supernatants were collected at between 1- and 24-hours post-infection. At each time point, the plate was first spun down at 400 g for 2 minutes, then 100μL of the supernatant was transferred into a 96-well plate in duplicate. For t=0 time point, remaining supernatants were removed, and cells were lysed with PBS+ 1% tritonX-100. 100 μL of the cell lysates was also transferred to 96-well plates. Microscopic images were taken of each well to visualize and record the cells viability, using a phase-contrast microscopy.

LDH Assay

To assess cell lysis, we quantified the release of lactate dehydrogenase (LDH) using Takara LDH Cytotoxicity Detection Kit (#MK401). The LDH reaction mix was made per manufacturer's instructions and kept away from the light. Cell supernatants were diluted 1:10 in PBS and diluted supernatants were mixed 1:1 with the LDH reaction mix. After the addition of the reaction mix, plates were incubated for 30 minutes at room

temperature away from the light and absorbance was measured at 492nm using a plate reader. Total LDH level at t=0 was calculated by adding LDH levels of t=0 supernatants and lysates. LDH release 24 hours post-treatment was calculated as a fraction of total LDH available at the time of infection (t=0).

Quantification and statistical analysis

All graphs are representative of three independent experiments and show the mean with the error bars representing SD; n= number of replicates assays with average of technical replicates. Sf9 live/dead cell quantification was obtained by taking one image per well of the live/dead staining and by manually counting 300 total cells and recording if the cells stained live or dead. Statistical analysis for cell viability counts, LDH assay, and Metamorphosis assay, were performed using a one-way ANOVA with multiple comparisons or by student's t-test (Figure 2.1. - 2.4.). Quantification of MACs were performed using column diameter, field of view and volume, (Figure S2.1. B). In all figures: *, p-value < 0.05; **, p-value < 0.01; ***, p-value < 0.001; ****, P-value <0.0001.

Data and software availability. Electron cryotomograms were deposited in the Electron Microscopy Data Bank (accession numbers WT: EMD-4947; Δ*pne1*: EMD-4948).

2.6 Acknowledgements

We thank Shari Wu and Tom Huxford for kindly providing us with insect cell lines and culturing technique guidance. We also thank Saori Amaike Campen and Nicole Yee from JCVI for their help in the maintenance of J774A.1 macrophage cell lines. We acknowledge the imaging facility ScopeM for instrument access at ETH Zürich. This work was supported by the funds provided by Office of Naval Research (N00014-17-1-2677 to N.J.S. and S.B.), Office of Naval Research (N00014-16-1-2135 to N.J.S), Alfred P. Sloan Foundation, Sloan Research Fellowship (to N.J.S), San Diego State University (to N.J.S), J. Craig Venter Institute (to S.B.), European Research Council (to M.P.), Swiss National Science Foundation (to M.P.) and Gebert Rüf Foundation (to M.P.).

Chapter 2, in full, is a reprint of the material as it appears in Cell Reports, 2019. I. Rocchi, C.F. Ericson, K. E. Malter, S. Zargar, F. Eisenstein, M. Pilhofer, S. Beyhan, N. J. Shikuma. The dissertation author is a coauthor of this manuscript. My specific contributions include (Figure 2.3.), writing, revisions, and experimental design.

2.7 References

1. Taylor, N. M. I., van Raaij, M. J. & Leiman, P. G. Contractile injection systems of bacteriophages and related systems. *Mol. Microbiol.* (2018). doi:10.1111/mmi.13921

2. Böck, D. *et al.* In situ architecture, function, and evolution of a contractile injection system. *Science (80-.).* **357**, 713–717 (2017).

3. Ho, B. T., Dong, T. G. & Mekalanos, J. J. A view to a kill: the bacterial type 6 secretion system. *Cell Host Microbe* **15**, 9–21 (2014).

4. Yang, G., Dowling, A. J., Gerike, U., Ffrench-Constant, R. H. & Waterfield, N. R. Photorhabdus virulence cassettes confer injectable insecticidal activity against the wax moth. *J. Bacteriol.* **188**, 2254–2261 (2006).

5. Hurst, M. R. H., Glare, T. R. & Jackson, T. A. Cloning *Serratia entomophila* antifeeding genes--a putative defective prophage active against the grass grub *Costelytra zealandica*. *J. Bacteriol.* **186**, 5116–28 (2004).

6. Shikuma, N. J. *et al.* Marine Tubeworm Metamorphosis Induced by Arrays of Bacterial Phage Tail–Like Structures. *Science (80-.).* **343**, 529–534 (2014).

7. Büttner, C. R., Wu, Y., Maxwell, K. L. & Davidson, A. R. Baseplate assembly of phage Mu: Defining the conserved core components of contractile-tailed phages and related bacterial systems. *Proc. Natl. Acad. Sci. U. S. A.* **113**, 10174–10179 (2016).

8. Vlisidou, I. *et al. Photorhabdus* Virulence Cassettes: extracellular multi-protein needle complexes for delivery of small protein effectors into host cells. *bioRxiv* 549964 (2019). doi:10.1101/549964

9. Lien, Y.-W. & Lai, E.-M. Type VI Secretion Effectors: Methodologies and Biology. *Front. Cell. Infect. Microbiol.* **7**, 254 (2017).

10. Pukatzki, S., Ma, A. T., Revel, A. T., Sturtevant, D. & Mekalanos, J. J. Type VI secretion system translocates a phage tail spike-like protein into target cells where it cross-links actin. *Proc. Natl. Acad. Sci. U. S. A.* **104**, 15508–13 (2007).

11. Sana, T. G. *et al.* Internalization of. *MBio* **6**, (2015).

12. Suarez, G. *et al.* A Type VI Secretion System Effector Protein, VgrG1, from Aeromonas hydrophila That Induces Host Cell Toxicity by ADP Ribosylation of Actin. *J. Bacteriol.* **192**, 155–168 (2010).

13. Hurst, M. R. H., Beard, S. S., Jackson, T. A. & Jones, S. M. Isolation and characterization of the *Serratia entomophila* antifeeding prophage. *FEMS Microbiol. Lett.* **270**, 42–48 (2007).

14. Sarris, P. F., Ladoukakis, E. D., Panopoulos, N. J. & Scoulica, E. V. A Phage Tail-Derived Element with Wide Distribution among Both Prokaryotic Domains: A Comparative Genomic and Phylogenetic Study. *Genome Biol. Evol.* **6**, 1739–1747 (2014).

15. Penz, T., Horn, M. & Schmitz-Esser, S. The genome of the amoeba symbiont '*Candidatus Amoebophilus asiaticus*' encodes an afp-like prophage possibly used for protein secretion. *Virulence* **1**, 541–545 (2010).

16. Penz, T. *et al.* Comparative genomics suggests an independent origin of cytoplasmic incompatibility in Cardinium hertigii. *PLoS Genet.* **8**, e1003012 (2012).

17. Shikuma, N. J., Antoshechkin, I., Medeiros, J. M., Pilhofer, M. & Newman, D. K. Stepwise metamorphosis of the tubeworm *Hydroides elegans* is mediated by a bacterial inducer and MAPK signaling. *Proc. Natl. Acad. Sci.* **113**, 10097–10102 (2016).

18. Huang, Y., Callahan, S. & Hadfield, M. G. Recruitment in the sea: bacterial genes required for inducing larval settlement in a polychaete worm. *Sci. Rep.* **2**, (2012).

19. Mezulis, S., Yates, C. M., Wass, M. N., E Sternberg, M. J. & Kelley, L. A. The Phyre2 web portal for protein modeling, prediction and analysis. *Nat. Protoc.* **10**, 845–858 (2015).

20. Korczynska, J. E., Turkenburg, J. P. & Taylor, E. J. The structural characterization of a prophage-encoded extracellular DNase from *Streptococcus pyogenes*. *Nucleic Acids Res.* **40**, 928–38 (2012).

21. Moon, A. F., Krahn, J. M., Lu, X., Cuneo, M. J. & Pedersen, L. C. Structural characterization of the virulence factor Sda1 nuclease from Streptococcus pyogenes. *Nucleic Acids Res.* **44**, 3946–3957 (2016).

22. Nguyen Ba, A. N., Pogoutse, A., Provart, N. & Moses, A. M. NLStradamus: a simple Hidden Markov Model for nuclear localization signal prediction. *BMC Bioinformatics* **10**, 202 (2009).

23. Bladergroen, M. R., Badelt, K. & Spaink, H. P. Infection-blocking genes of a symbiotic Rhizobium leguminosarum strain that are involved in temperature-dependent protein secretion. *Mol. Plant. Microbe. Interact.* **16**, 53–64 (2003).

24. Holmström, C. & Kjelleberg, S. Marine *Pseudoalteromonas* species are associated with higher organisms and produce biologically active extracellular agents. *FEMS*

Microbiol. Ecol. **30**, 285–293 (1999).

25. Ma, L. S., Hachani, A., Lin, J. S., Filloux, A. & Lai, E. M. Agrobacterium tumefaciens deploys a superfamily of type VI secretion DNase effectors as weapons for interbacterial competition in planta. *Cell Host Microbe* **16**, 94–104 (2014).

26. Koskiniemi, S. *et al.* Rhs proteins from diverse bacteria mediate intercellular competition. *Proc. Natl. Acad. Sci.* **110**, 7032–7037 (2013).

27. Jiang, N. *et al.* Vibrio parahaemolyticus RhsP represents a widespread group of pro-effectors for type VI secretion systems. *Nat. Commun.* **9**, 3899 (2018).

28. Pissaridou, P. *et al.* The *Pseudomonas aeruginosa* T6SS-VgrG1b spike is topped by a PAAR protein eliciting DNA damage to bacterial competitors. *Proc. Natl. Acad. Sci. U. S. A.* **115**, 12519–12524 (2018).

29. Scholl, D. Phage Tail–Like Bacteriocins. (2017). doi:10.1146/annurev-virology

30. Gebhart, D. *et al.* A Modified R-Type Bacteriocin Specifically Targeting Clostridium difficile Prevents Colonization of Mice without Affecting Gut Microbiota Diversity. *MBio* **6**, e02368--14 (2015).

31. Thurber, R. V, Haynes, M., Breitbart, M., Wegley, L. & Rohwer, F. Laboratory procedures to generate viral metagenomes. *Nat. Protoc.* **4**, 470–483 (2009).

32. Weiss, G. L., Medeiros, J. M. & M., P. Bacterial Protein Secretion Systems. in *Bacterial Protein Secretion Systems* (eds. Journet, L. & Cascales, E.) 353–375 (2017).

33. Mastronarde, D. N. Automated electron microscope tomography using robust prediction of specimen movements. *J. Struct. Biol.* **152**, 36–51 (2005).

34. Mastronarde, D. N. Dual-Axis Tomography: An Approach with Alignment Methods That Preserve Resolution. *J. Struct. Biol.* **120**, 343–352 (1997).

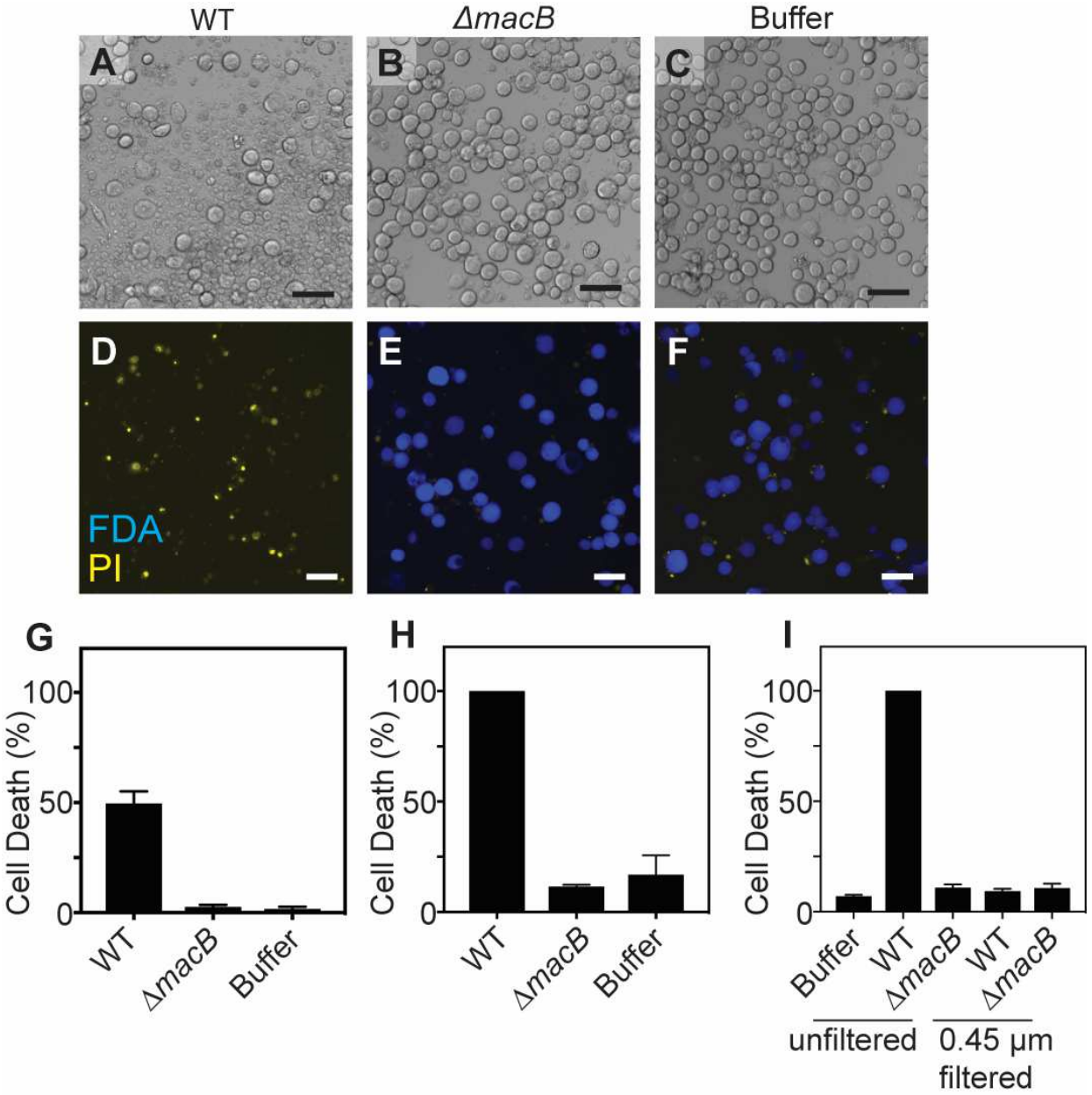

Figure 2.1. MACs cause cytotoxicity in Sf9 insect cells. (**A-C)** Sf9 cells after 48 hours incubation with MACs from wild-type *P. luteoviolacea* (WT), Δ*macB* mutant strain, or extraction buffer. **(D-F)** Live/dead staining with fluorescein diacetate (FDA) (live cells) and propidium iodide (PI) (dead cells). Scale bar is 50 μm. Quantification of cell death (%) utilizing (**G**) trypan blue and (**H**) FDA/PI live-dead stain. (**I**) Cell death of Sf9 cells exposed to MAC extract unfiltered and filtered through a 0.45 μm filter. Data are expressed as the mean ± SD of 300 cells across three independent experiments; Significance represents WT vs all other conditions by one-way ANOVA with multiple comparisons for graphs H and I or by student's t-test for panel G. (**** $p < 0.0001$)

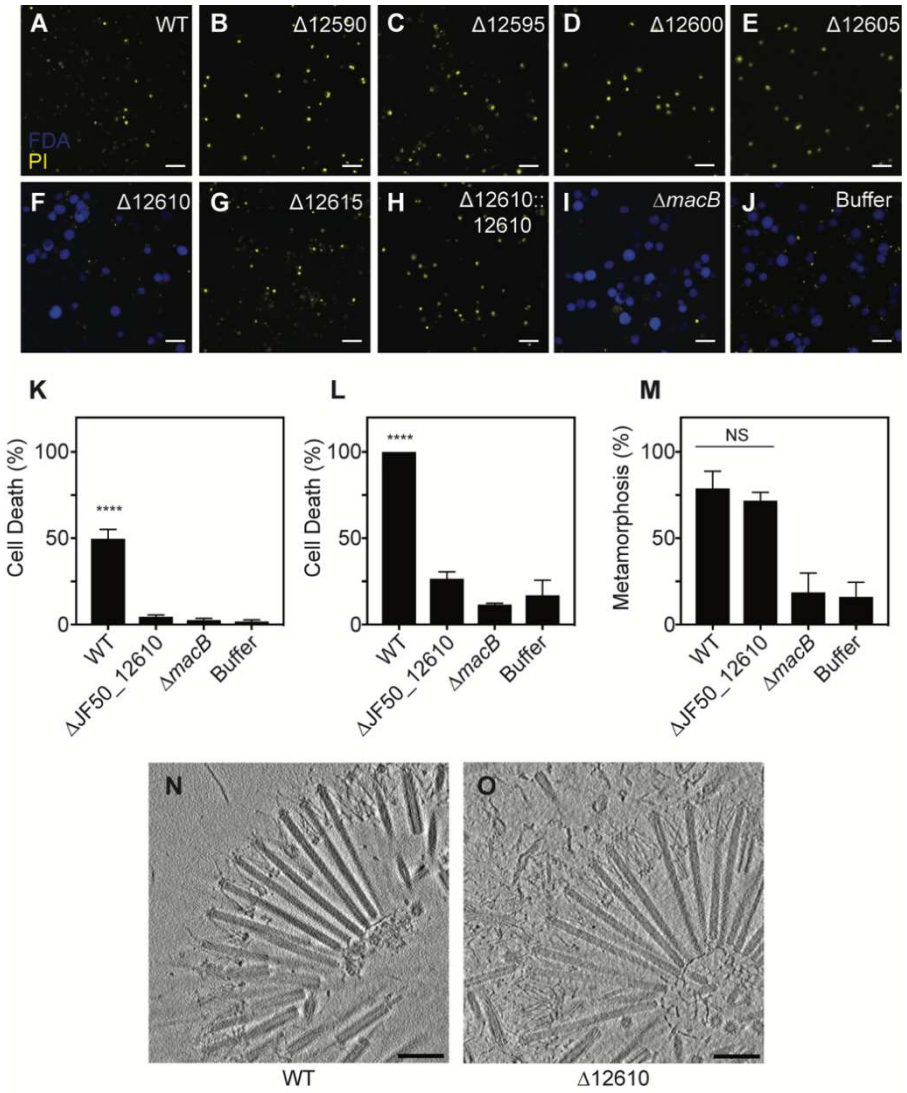

Figure 2.2. MACs require JF50_12610 to kill insect cells. (**A-J**) Sf9 cells after 48h incubation with MACs from WT, ΔJF50_12590, ΔJF50_12595, ΔJF50_12600, ΔJF50_12605, ΔJF50_12610 (Δ*pne1*), ΔJF50_12615, ΔJF50_12610::JF50_12610, Δ*macB* strains, and extraction buffer. Scale bar is 50 μm. (**K and L**) Quantification of cell death (%) by trypan blue and FDA/PI live-dead staining. Data are expressed as the mean ± SD of n=300 cells across three independent experiments; Significance represents WT vs ΔJF50_12610 by student's t-test. (**** P < 0.0001) (**M)** Metamorphosis (%) of *Hydroides* larvae in response to MACs from WT, Δ*macB* or ΔJF50_12610 strains. Metamorphosis data are represented as the mean ± SD of n=3 independent biological replicates, where 4 technical replicates were first averaged. Significance is indicated as a comparison between the two conditions indicated by the line above by one-way ANOVA with multiple comparisons (NS, not significant). Electron cryo-tomography images of MACs from (**N**) wild type and (**O**) ΔJF50_12610 strains showing an ordered structure with extended and contracted tubes connected by a meshwork of tail fibers. No structural differences between WT and ΔJF50_12610 arrays were observed. Shown are projections of 1.1 nm thick slices of cryotomograms. Scale bars are 100 nm.

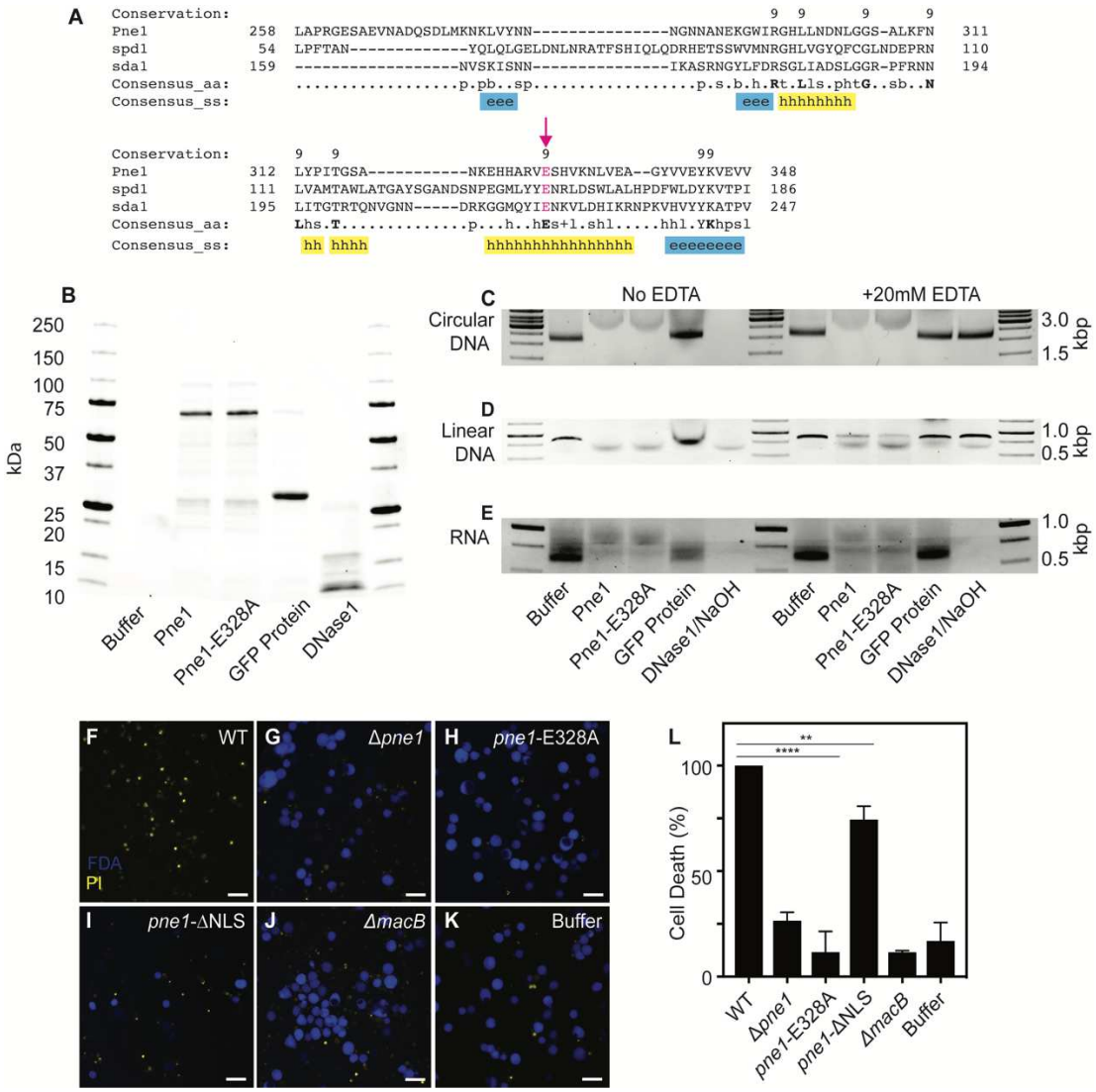

Figure 2.3. JF50_12610 (Pne1) contains a functional nuclease domain that is required for insect cell killing. (**A**) Protein alignment of Pne1 (JF50_12610), Spd1 and Sda1. Numbers indicate amino acid residues of each protein. Conserved amino acid residues indicated in bold. Consensus secondary structure (ss) alpha-helix (h, yellow) and beta-strand (e, blue). A conserved glutamic acid 328 is indicated by an arrow and highlighted in magenta. (**B**) SDS PAGE of purified wild type Pne1, Pne1-Glu328Ala, GFP, and DNase1. Representative 1% agarose gel of DNA co-incubated with Pne1, Pne1-Glu328Ala and GFP at 37°C for 30 minutes with **(C)** circular DNA, 2.25 Kbp **(D)** linear DNA, 0.8 Kbp or **(E)** RNA, 0.6 Kbp in the presence or absence of 20mM EDTA. Live/Dead images of Sf9 insect cells after 48 hours incubation with MACs from (**F**) WT, (**G**) Δ*pne1*, (**H**) *pne1*-Glu328A, (**I**) *pne1*-ΔNLS, (**J**) Δ*macB*, and (**K**) MAC extraction buffer. Scale bar is 50 µm. (**L**) Quantification of cell death (%) by FDA/PI live-dead stain. Data are represented as the mean ± SD of n=300 cells counted across 3 independent biological replicates. Significance is indicated as a comparison between the two conditions indicated by the line above (**** $p < 0.0001$, ** $p < 0.01$).

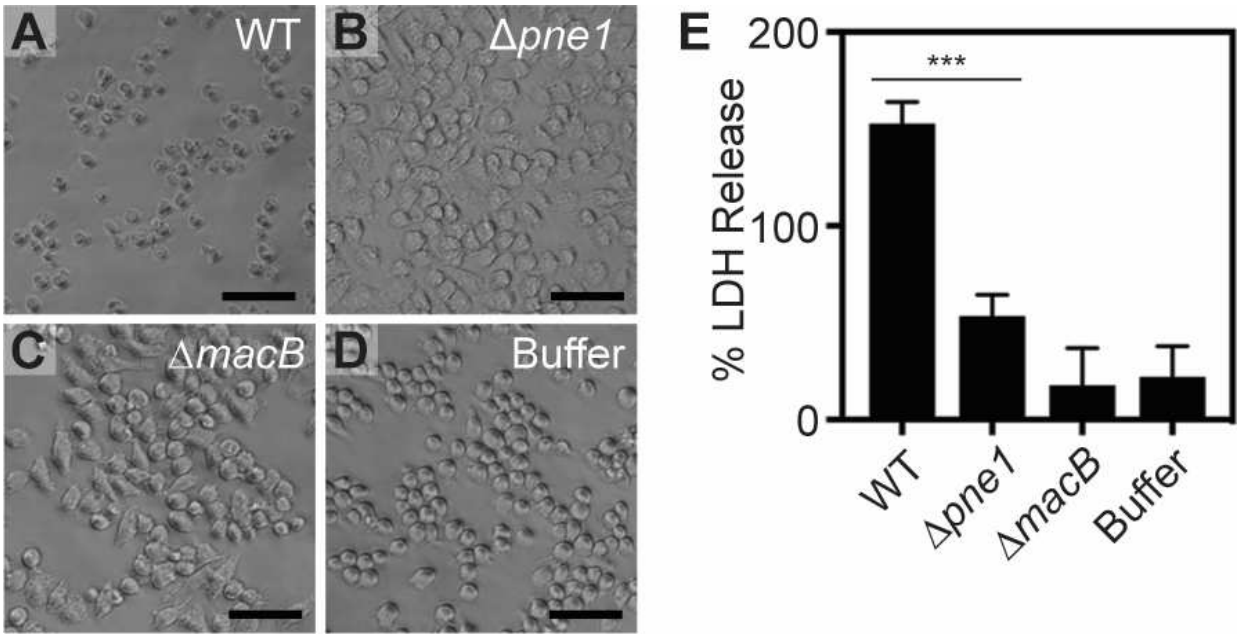

Figure 2.4. MACs kill J774A.1 murine macrophages and killing is dependent on *pne1*. (**A-D**) J774A.1 cells after incubation with MACs from WT, Δ*pne1*, Δ*macB* or extraction buffer. Scale bar is 50 µm. (**E**) Cell death was quantified by Lactate Dehydrogenase (LDH) release assay at 24 hours. Data are represented as the mean ± SD of n=3 independent biological replicates, where 4 technical replicates were first averaged. Significance is indicated as a comparison between the two conditions indicated by the line above by student's t-test (*** $p < 0.001$).

Chapter 3

A Contractile Injection System Stimulates Tubeworm Metamorphosis by Translocating a Proteinaceous Effector

3.1 Abstract

The swimming larvae of many marine animals identify a location on the sea floor to undergo metamorphosis based on the presence of specific bacteria. Although this microbe-animal interaction is critical for the life cycles of diverse marine animals, what types of biochemical cues from bacteria that induce metamorphosis has been a mystery. Metamorphosis of larvae of the tubeworm *Hydroides elegans* is induced by arrays of phage tail-like contractile injection systems, which are released by the bacterium *Pseudoalteromonas luteoviolacea*. Here we identify the novel effector protein Mif1. By cryo-electron tomography imaging and functional assays, we observe Mif1 as cargo inside the tube lumen of the contractile injection system and show that the *mif1* gene is required for inducing metamorphosis. Purified Mif1 is sufficient for triggering metamorphosis when electroporated into tubeworm larvae. Our results indicate that the delivery of protein effectors by contractile injection systems may orchestrate microbe-animal interactions in diverse contexts.

3.2 Introduction

Bacteria can have profound effects on the normal development of diverse animal taxa [1]. One of the most pervasive examples of bacteria-stimulating development is the induction of animal metamorphosis by bacteria [2]. During these interactions in marine environments, surface-bound bacteria often serve as environmental triggers that induce mobile animal larvae to settle on a surface and undergo metamorphosis. Although the stimulation of metamorphosis by bacteria is critical for diverse animal-mediated processes such as coral reef formation [3,4], the recruitment of stocks for marine fisheries

[5,6] and the fouling of submerged surfaces like the hulls of ships (i.e. biofouling) [7,8], we know little about the mechanisms that govern this microbe-animal interaction.

Despite the fact that the link between bacteria and animal metamorphosis was first discovered in the 1930s [9], few bacterial products have been described that stimulate this developmental transition. To date, identified bacterial cues can all be classified as small molecules. Two examples are the small bacterial metabolite tetrabromopyrrole, which induces partial or complete metamorphosis of corals [10,11] and the polar molecule histamine from algae or associated microbes, which induces urchin metamorphosis [12]. To our knowledge, however, no proteinaceous bacterial cues have yet been identified that stimulate animal metamorphosis.

To investigate how bacteria induce animal metamorphosis, we have previously studied the interaction between the tubeworm *Hydroides elegans* (hereafter *Hydroides*) and the bacterium *Pseudoalteromonas luteoviolacea* [8,13–15]. We found that *P. luteoviolacea* produces arrays of Metamorphosis Associated Contractile structures (MACs) that induce the metamorphosis of *Hydroides* larvae (Huang et al., 2012; Shikuma et al., 2014). MACs are an example of a Contractile Injection System (CIS); macromolecular machines that are specialized to puncture membranes and often deliver proteinaceous effectors into target cells [18,19]. Like other CISs, MACs are evolutionarily related to the contractile tails of bacteriophages (bacterial viruses) and are composed of an inner tube protein (homologous to gp19 from phage T4 and Hcp from type 6 secretion systems) surrounded by a contractile sheath, a tail-spike, and a baseplate complex

(Shikuma et al., 2014). The conserved mechanism is driven by contraction of the sheath, which propels the inner tube/spike into the target cell.

Different ways of loading effectors onto a CIS have been suggested. Translocation mechanisms of effectors via the spike complex of a CIS have been well characterized [20,21]. The presence of an alternative pathway of loading effectors into the inner tube lumen has been speculated but is only poorly understood. For example, an amorphous density inside the inner tube of the Antifeeding prophage (Afp) was attributed to either the toxin payload or a tape-measuring protein [22]. Other classes of effectors were found to interact with the inner tube protein (hcp) and are likely released post-firing by tube dissociation in the target cytoplasm [23,24].

In this study, we set out to identify a potential metamorphosis-inducing effector that MACs inject into *Hydroides* larvae, as well as the loading of such an effector into MACs. We show that a previously identified genomic region in *P. luteoviolacea* [14] encodes a bacterial protein that localizes to the inner tube lumen of the MAC structure and is necessary for inducing the metamorphosis of *Hydroides* larvae. Our results identify a proteinaceous effector stimulating animal metamorphosis and provide a direct visualization of an effector in the tube lumen of an assembled CIS.

3.3 Results

Two bacterial genes are responsible for densities within the inner tube lumen of MACs and are involved in metamorphosis induction. We previously identified a genomic locus in *P. luteoviolacea* encoding six genes (gene numbers JF50_12590, JF50_12595, JF50_12600, JF50_12605, JF50_12610 and JF50_12615) that are essential for inducing the larvae of *Hydroides* to undergo metamorphosis [14]. Here we analyzed biofilms of strains with in-frame deletions of each of the six genes and tested their ability to induce *Hydroides* metamorphosis. The ΔJF50_12605 and ΔJF50_12615 mutants exhibited a reduced ability to induce metamorphosis (less than 20%, Figure 3.1. A), while mutation of the other four genes had no observable effect. When JF50_12605 and JF50_12615 were replaced back into their native chromosomal loci, metamorphosis induction was restored (Figure 3.1. B). We confirmed the effect of MACs on *Hydroides* metamorphosis by producing cell-free MAC array preparations. While larvae exposed to MACs from a ΔJF50_12615 mutant did not induce metamorphosis (even at high concentrations), MACs from a ΔJF50_12605 mutant induced metamorphosis when added at higher doses (Figure S3.1.1. A & B). Our results suggest that JF50_12615 was essential for the induction of metamorphosis, while JF50_12605 contributed but was dispensable. Based on our results here and below, we name the protein encoded by JF50_12615 as “Mif1” for Metamorphosis-Inducing Factor 1.

To search for structural differences between MACs from wildtype *P. luteoviolacea* and the specific gene deletion mutants, we employed cryo-electron tomography (cryoET)

imaging. Deletion of the full JF50_12590–JF50_12615 locus (Figure S3.1.2.), or each of the six genes individually (Figure S3.1.3.), did not impair the formation of ordered arrays of MACs, featuring both extended and contracted conformations. Upon detailed analyses, we observed that extended MACs from both ΔJF50_12605 and Δ*mif1* strains exhibited a central lumen with very low density. By contrast, MACs from wildtype and the other deletion mutants possessed a density distribution that was homogeneous and a lumen was not discernable (Figure 3.1. C-G and Figure S3.1.3.). We refer to these structural phenotypes as “empty” and “filled” respectively. Strikingly, quantitative analyses showed that the empty phenotype in ΔJF50_12605 and Δ*mif1* MACs correlated with the inability to induce metamorphosis (Figure 3.1. A & H). The replacement of *mif1* and JF50_12605 back into their native chromosomal loci reverted the empty phenotype back to filled (Figure S3.1.4.).

The density within the MAC tube lumen represents a cargo protein. To investigate whether the structural differences between wildtype and Δ*mif1*/ΔJF50_12605 MACs represented potential cargo, we performed sub-tomogram averaging of the extended sheath-tube complex (resolution estimation in Figure S3.2.1.). The resulting MAC structures for both wildtype and Δ*mif1* revealed densities corresponding to the sheath and the inner tube (Figure 3.2. A-F), similar to the structures of homologous CISs [25]. While the Δ*mif1* structure lacked any discernible density inside the ~4 nm-wide tube lumen (Figure 3.2. E & F), the wildtype structure exhibited repeating packets of density inside the tube (Figure 3.2. A-D), suggesting the presence of a potential cargo. The densities in the tube lumen reinforced less strongly compared to the sheath-tube complex,

which could be caused by one or a combination of the following factors: 1) during averaging, the alignment of the cargo was affected by the strong densities from the sheath-tube, 2) the cargo was not structured or flexible, and/or 3) the cargo was present at a sub-stoichiometric amount compared to tube subunits or tube-rings. In any case, it is likely that the packet-like shape of the cargo density was caused by alignment artifacts. This is supported by a difference map between the wildtype and ∆Mif1 structure, which shows a continuous density filling the inner tube lumen (Figure 3.2. G & H). It is important to note, however, that the cargo and tube densities were separated by a low-density region (arrowheads in Figure 3.2. B). Furthermore, any expelled tubes from triggered MACs always showed an “empty” phenotype in cryotomography images (Figure S3.2.2.). These results together could indicate weak or entirely absent interactions between cargo and tube, possibly facilitating rapid release of the cargo from the tube upon contraction.

To test whether JF50_12605 and/or Mif1 were present within the MAC complex and represented the cargo within the tube lumen, we performed protein identification by mass spectrometry of purified MACs. In two independent experiments, we detected Mif1 but not JF50_12605 in wildtype MAC samples (Figure 3.3. A). MACs from the ΔJF50_12605 mutant exhibited considerably fewer spectral counts for the Mif1 protein. In contrast, JF50_12605 was not detected within the wild-type MAC complex (Figure 3.3. A). These results are consistent with the “empty” phenotype observed by cryoET imaging of the ΔJF50_12605 strain (Figure 3.1D and Figure S3.1.3. E). To further corroborate the association of Mif1 with MAC arrays, we tagged Mif1 with a FLAG-tag in its native chromosomal locus in three different locations. After purifying MACs, we detected Mif1

strongly associated with MACs from two Mif1-FLAG-tagged strains and one at a reduced level by dot-blot and an anti-FLAG antibody (Figure 3.3. B).

Because JF50_12605 is important for localizing Mif1 within the MAC complex, we analyzed protein-protein interactions between JF50_12605 and Mif1. To this end, we performed a reciprocal pull down of S-tagged JF50_12605 and 6xHis-tagged Mif1. We detected JF50_12605 when pulling down Mif1 by nickel chromatography, and we detected Mif1 when pulling down JF50_12605 with S-tag antibodies (Figure 3.3. C). To determine whether Mif1 or JF50_12605 associated with other components of the MAC complex, we utilized a bacterial two-hybrid system based on the interaction-mediated reconstruction of a cyclic AMP (cAMP) signaling cascade [26]. When JF50_12605, Mif1 and MacT1 (JF50_12680, tube) were screened for interactions, we found a significant interaction between JF50_12605 and Mif1 as well as JF50_12605 with itself (Figure 3.3. D-F). However, neither JF50_12605, nor Mif1 interacted with MacT1 (JF50_12680, tube). Together, these data indicate that Mif1 is present within the MAC structure and represents the densities seen in the tube lumen, while JF50_12605 might act as a chaperone that helps to localize Mif1 inside the MAC tube. Mif1, however, could also associate with MACs independently of JF50_12605 in an inefficient manner. This is shown by 1) the residual presence of Mif1 in MACs from a ΔJF50_12605 mutant as detected by mass spectrometry (Figure 3.3. A), and (Figure 3.2.) the fact that high concentrations of a cell-free ΔJF50_12605 MAC extract can induce metamorphosis (Figure S3.1.1.).

Purified and electroporated Mif1 protein induces tubeworm metamorphosis. Because our results suggested that Mif1 was loaded into the MAC tube lumen, we next tested whether Mif1 was sufficient for stimulating metamorphosis when delivered to *Hydroides* larvae. We therefore purified N-terminally His-tagged Mif1 by nickel chromatography (Figure 3.4. A) and verified its identity by western blot with a Mif1-specific antibody (Figure 3.4. B). As controls, we purified JF50_12605 and GFP under the same conditions. Mif1 protein provided exogenously to competent larvae of *Hydroides* at concentrations of up to 250 ng/µl did not stimulate metamorphosis (Figure S3.4.1.). We reasoned, however, that the Mif1 protein might require intracellular delivery into host cells to initiate metamorphosis of *Hydroides*. To this end, we utilized a custom electroporator that was previously successfully used for other marine invertebrates [27,28]. Successful translocation of protein was confirmed by anti-GFP western blotting of larval lysate after electroporation (Figure S3.4.2.). When we delivered Mif1 into competent *Hydroides* larvae, a significant percentage of the larvae underwent metamorphosis (Figure 3.4. C). In contrast, neither JF50_12605 nor GFP stimulated metamorphosis when electroporated under the same conditions. Our results suggest that Mif1 was sufficient to stimulate *Hydroides* metamorphosis when delivered by electroporation.

3.5 Discussion

In conclusion, our data indicate that the bacterium *P. luteoviolacea* induces metamorphosis of animal larvae by delivering the effector protein Mif1 via the tube lumen of an extracellular contractile injection system (MACs). These insights are significant for different fields of research as discussed below.

First, previously reported bacterial cues for animal metamorphosis are all classified as small molecules [10–12]. The identification of a protein (Mif1) that stimulates tubeworm metamorphosis requires us to expand the scope of possible biomolecules and mechanisms by which bacteria stimulate animal development. Our findings suggest that rather than MACs stimulating metamorphosis solely by physical puncturing and depolarization of larval membranes, the delivered Mif1 protein could have an enzymatic activity. This challenges previous hypotheses on metamorphosis induction [29,30], however, it would be in line with many studies on other eukaryote-targeting CIS effectors with enzymatic activities [31–33]. Future investigations will shed light on the molecular mechanism by which Mif1 triggers animal metamorphosis, which is a challenging task, given that Mif1 does not feature any recognizable conserved protein domains.

Second, our results directly showed the previously hypothesized possibility of effector delivery via the tube lumen of a CIS [21–24]. Interestingly, the comparison of MACs with a different class of CIS, namely the Type Six Secretion System (T6SS), reveals significant differences. The T6SS effectors that are thought to be delivered by the T6SS tube lumen show protein-protein interactions between the T6SS effector and the T6SS tube protein (Hcp) [23,24]. By contrast, we did not detect such interactions between Mif1 and MAC tube protein. One possible explanation could be that the biophysical characteristics of the T6SS tube and the MAC tube are different. While the T6SS tube is inherently unstable and disassembles soon after contraction [34], inner tubes of MACs and other extracellular CISs (and contractile phages) can be readily detected by electron

microscopy and therefore seem to be much more stable. Given our observation that expelled MAC tubes were always empty (e.g. Figure S3.2.2.), this poses the question of how the effectors exit such a stable tube after contraction. We hypothesize that this could be the very reason for weak or entirely absent interactions between Mif1 and MAC tube, as well as for the low-density region that was seen in subtomogram averages separating Mif1 and MAC tube (Figure 3.2. B). Another mechanistic consequence of low affinity between Mif1 and tube could be the requirement of an assembly factor, i.e. JF50_12605, that allows for efficient targeting of Mif1 to the tube.

Third, our insights into MAC function could be significant to re-engineer the system for future medical and biotechnological applications. As micron-scale, syringe-like structures, MACs have potential for being developed as delivery systems targeting eukaryotic cells. Extracellular CISs such as MACs are of particular interest, because they are released from the producing bacterial cell and autonomously bind to the target cell's surface. Extracellular CISs that target bacterial pathogens are already under development as narrow host-range antimicrobial agents [35]. The identification of effectors carried by MACs provides the basis for loading MACs with a cargo of choice. We recently reported a second effector that MACs deliver to eukaryotic cells [36], expanding the number of MAC effectors that could be engineered. Intriguingly, A cryotomogram of the Δ*pne1* (JF50_12610) mutant shows that the tube has a filled phenotype (Figure S3.1.3.). The filled phenotype suggests that Pne1 is not found within the inner tube, but instead could be loaded in a different location (e.g. spike) within the MACs complex. Understanding

tube lumen-delivered effectors could be particularly helpful, based on the potential of a higher payload per CIS, as compared to spike-bound effectors.

Fourth, the identification of Mif1 and its delivery mechanism will facilitate the investigation of how bacterial factors trigger animal signaling systems, leading to metamorphosis. This could have potential practical applications for preventing biofouling, improving aquaculture husbandry, restoring degraded ecosystems like coral reefs, and as a biotechnology platform.

The fact that bacteria are known to stimulate metamorphosis in every major group of animals alive today [2], combined with the detection of MAC-like gene clusters in microbes from diverse environments including the ocean, terrestrial environments and even the human gut [25,37], underscores the huge diversity of bacterium-animal interactions that remains to be explored.

3.6 Materials and Methods

Metamorphosis assays. Bioassays were conducted with specimens of *Hydroides elegans* obtained from Quivira Basin, San Diego, California. Embryos were obtained and maintained as previously described [8,14]. Competent larvae were exposed to biofilms of *P. luteoviolacea* wild type, as a positive control, to *P. luteoviolacea* mutants, and to *P. luteoviolacea* strains unable to produce MAC structures (Δ*macB*), as well as to artificial seawater (-). The percent of larvae that underwent metamorphosis was scored 24 hours

after the induction of metamorphosis. Metamorphosis was scored visually by observing the number of individuals that formed branchial radioles, and a primary and secondary tube. Four biological replicates of approximately 30 larvae each were performed for each treatment on three separate occasions with larvae spawned from different adults.

Bacterial Strains, Plasmid Construction and Culture conditions. All bacterial strains, plasmids and primer sequences used are listed in the supplemental tables S2.1. and S2. All deletion and fusion strains were created according to previously published protocols [14,17,36]. Plasmid insert sequences were verified by DNA sequencing. Deletion and insert strains were confirmed by PCR. All *E.coli* strains were grown in Luria-Bertani (LB) media at 37°C shaking at 200 revolutions per minute (RPM). All *P. luteoviolacea* cultures were grown in seawater tryptone (SWT) media (35.9 g/L Instant Ocean, 2.5g/L tryptone, 1.5 g/L yeast extract, 1.5 ml/L glycerol) at 25°C shaking at 200 RPM. Media that contained antibiotics were at a concentration of 100 mg/ml unless otherwise stated.

Gentle MAC extraction. *P. luteoviolacea* was grown in 50 ml SWT media in 250 ml flasks at 30˚C for 6 hours or overnight (12-14 h). Cells were centrifuged for 30 minutes at 4000 g and 4˚C and resuspended in 5 ml cold extraction buffer (20 mM Tris, pH 7.5, 1M NaCl). Cultures were centrifuged for 30 minutes at 4000 g and 4˚C and the supernatant was isolated and centrifuged for 30 minutes at 7000 g and 4˚C. The pellet was resuspended in 20-100 µl cold extraction buffer and stored at 4°C for further use.

Plunge freezing of MACs. Plunge freezing was performed as implemented in Weiss et al.[38]. In essence, gentle MAC extractions were seeded with 10 nm BSA-coated colloidal gold particles (1:4 v/v, Sigma) and 4 µl of the mixture was applied to a glow-discharged holey-carbon copper EM grid (R2/1, Quantifoil). The grid was backside blotted in a Vitrobot (FEI Company) by using a Teflon sheet on the front pad and plunge-frozen in a liquid ethane-propane mixture (37 %/63 %) cooled by a liquid nitrogen bath. Frozen grids were stored in liquid nitrogen.

Cryo-electron tomography. The gentle MAC extractions were imaged by cryo-electron tomography (cryoET) [38]. Images were recorded on a Titan Krios TEM (FEI) equipped with a Quantum LS imaging filter operated at a 20 eV slit width and K2 Summit (Gatan). Pixel sizes ranged from 2.14 Å for the first batch of data in the Super Resolution (SR) mode to 2.72 Å for the remaining sessions. Tilt series were collected using a bidirectional tilt-scheme from -30° to +60° and -32° to -60° in 2° increments. Total dose was ~90 e-/Å^2 and defocus was kept at -5 to -6 µm. Some tilt series were recorded in focus using a Volta phase plate [39]. Tilt series were acquired using SerialEM [40] and reconstructed and segmented using the IMOD program suite [41]. Density plots to determine filled and empty phenotypes were done using Fiji [42]. Contrast enhancement of some tomograms was done using the tom_deconv deconvolution filter (https://github.com/dtegunov/tom_deconv).

Sub-tomogram averaging. Tomograms used for structure identification and picking were binned by a factor of 4. Defocus was estimated using Gctf [43] and CTF correction, exposure filtering and backprojection was done using IMOD. SR data was binned by a factor of 2 resulting in a pixel size of 4.29 Å/px. The discrete extended MAC structures were identified visually in individual tomograms and their longitudinal axes were modeled with open contours in 3dmod [44]. Individual model points were added at defined intervals of about 12 nm along the contours using the addModPts program from the PEET package [45] resulting in 24'721 initial particles for filled tubes and 37'024 initial particles for empty tubes. Models were imported into Dynamo [46], particles were extracted, the azimuth angle was randomized and all particles were averaged to obtain an initial reference. Four times binned subtomograms (17.14 Å/px) were used for four iterations of initial alignment with the reference low-pass filtered to about 50 Å. No symmetry was applied, but rotational search was limited to +/- 30°. Before unbinning, subtomograms were cleaned by distance and cross correlation coefficient leaving 20'358 filled and 20'782 empty tube particles. 2 times binned subtomograms (8.57 Å/px) were extracted using the refined coordinates and the dataset was split in two half sets. Half sets were aligned independently for 5 iterations. Unbinned subvolumes (4.29 Å/px) were extracted using the refined coordinates and aligned for 8 more iterations. Subvolumes were cleaned by cross correlation coefficient and final averages were generated using 13'039 particles and 13'425 particles for filled and empty tubes, respectively. UCSF Chimera [47] was used for visualization of the 3D models and to generate the difference map between wildtype and ΔMif1 structure.

Bacterial Two-Hybrid Analysis. Bacterial Two-Hybrid Analysis was performed following the protocols detailed previously [26]. Briefly, proteins of interest were cloned into one of four Bacterial Two Hybrid (BTH) plasmids pUT18, pUT18C, pKT25, and pKNT25. These produced individual N- or C-terminal fusions between the proteins of interest and the T18 and T25 subunits on of the adenylate cyclase (*CyaA*) protein. All plasmid sequences were confirmed by PCR. Plasmid combinations containing the genes of interest were then electroporated into BTH101 electrocompetent cells that lacked a native *CyaA* gene. The BTH101 cells were grown on LB agar containing ampicillin (100 mg/ml), kanamycin (100 mg/ml) and 1% glucose. Glucose was used to suppress the expression of proteins before performing the assay. Protein-protein interactions were quantified by performing a β-galactosidase assay with cells being grown overnight at 37°C and shaking at 200 RPM. Protein expression was induced with 1.0 mM IPTG. The cultures were incubated at 25°C shaking at 200 RPM for 6 hours before being mixed with a one-step "β-gal" mix [48]. A plate reader was then used to measure the absorbance at 420 nm and 600 nm. The optical densities were used to calculate Miller Units as previously described [49].

Protein Purification and Electroporation. To purify JF50_12615, JF50_12605 and GFP proteins, genes of interest were cloned into the pET15b plasmid and grown in *E.coli* BL21 pLysE. Bacteria were struck out on LB agar plates with ampicillin (100 µg/ul) and grown at 37°C for 24 hours. A single colony was inoculated into 5 ml LB with ampicillin (100 µg/ul) and grown at 37ºC shaking at 200 RPM for 14-16 hours. The overnight culture was diluted 1:500 into 500 ml LB with ampicillin (100 µg/ul), grown at

37°C shaking at 200 RPM until the culture reached an OD_{600} of 0.95. Protein expression was induced with 0.1 mM IPTG and grown for 25°C for 16 hours. The culture was centrifuged at 4000 g for 20 minutes and the supernatant was removed. The pellet was then resuspended in lysis buffer (20 mM imidazole, 25 mM tris-HCl, 500 mM NaCl, pH 8) with a protease inhibitor cocktail (100 µM leupeptin, 1 µM pepstatin and 5 µM bestatin). The culture was French pressed twice (1000 psi) and sonicated 3 times for 10-30 seconds each time. The lysed culture was then spun down at 12,000 g for 20 minutes and the supernatant was discarded. Inclusion bodies were purified from the pellet by first washing the pellet twice with 20 mM tris pH 8, 2 M urea, 2% triton X-100, 500 mM NaCl. The remaining pellet was resuspended using 5 ml 6M guanidinium HCl, 5 mM imidazole, 20 mM tris pH 8, 500 mM NaCl. The 6XHIS tagged proteins were then bound to Ni-agarose beads which had been pre-equilibrated to the resuspension buffer. The proteins were refolded by adding 1ml/min of 5 mM imidazole, 20 mM tris pH 8, 500 mM NaCl up to a total of 50 ml. After refolding, the beads were loaded onto a vacuum column and washed twice with 10 ml of refolding buffer. The protein was then eluted using 250 mM imidazole, 20 mM tris pH 8, 500 mM NaCl. Fractions containing the protein were buffer exchanged into a storage buffer (25 mM tris, 250 mM NaCl, pH 7.6) and stored at -80°C. A Bradford protein assay (BioRad) was done in order to quantify the amount of protein present. An antibody produced against the Mif1-specific peptide sequence CERSKGEFTEGKPKP (Genscript) was used to confirm expression and purification.

Western Blot. Protein samples and lysates were first normalized using Bradford protein assay to quantify protein concentrations. Equal concentrations of protein were

loaded onto BioRad stain-Free SDS-PAGE gels 4-20% (catalog no. 4568093) and imaged prior to transfer to confirm equal loading using BioRad gel doc ez system and stain free tray. The protein gel was then used to transfer protein to a PVDF membrane via semi-dry transfer system. The membranes were blocked in 5% milk-TBST (50 mM Tris-Cl, pH 7.6; 150 mM NaCl, 0.1% tween-20) for 30 mins. The primary antibody was added at 1:1000 dilution (unless otherwise stated) to 5% milk-TBST and rocked overnight at 4°C. The membrane was washed 3 times for 10 mins each in TBST. Secondary antibody was added at 1:20,000 to TBST and rocked for 1 hour at room temperature. The membrane was washed 3 more times for 15 min each before chemiluminescent substrate was added and visualized using BioRad XRS imaging cabinet. Antibodies include a custom Mif1 antibody (Genscript), S-Tag antibody (GenScript catalog no. A00625, RRID:AB_915085), DYKDDDDK antibody (Thermo Fisher Scientific catalog no. 701629, RRID:AB_2532497), GFP antibody (Thermo Fisher Scientific catalog no. G10362, RRID:AB_2536526) and Goat anti-Rabbit IgG (H+L) secondary antibody, HRP (Thermo Fisher Scientific Catalog no. 31460, RRID:AB_228341).

Electroporation. The method for electroporation of *Hydroides* larvae was adapted from those established for ascidian embryos [27,28]. Specifically, 50 µl of 0.77 M mannitol, 20 µl of concentrated larvae (approximately 30 larvae), and 10 µl of purified protein (1.25-12.5 µg, 15.6-156 ng/µl final concentration based on protein recovery from inclusion bodies) were mixed and added to a 2 mm electroporation cuvette. The mixture was then electroporated with 30 V (150 V/cm) at 10 ohms and 3000 µF using a custom electroporation apparatus as previously described [27]. After electroporation, the mixture

was immediately removed from the cuvette and mixed with 1 ml filtered artificial sea water and transferred into a 24-well plate. The larvae were then observed for metamorphosis 24 to 72 hours later (dependent on WT MACs positive control). Purification of proteins was performed on three separate occasions and each purification was electroporated twice, for a total of six independent biological replicates, each yielding similar outcomes.

Quantification of electroporation. To test whether purified protein is transferred to tubeworm larvae by electroporation, larvae were concentrated to 30 larvae/µl. Final GFP concentration used was 0.625 µg/µl (50 µg total per electroporation). 20 µl of larvae were either electroporated by adding them to 50 µl 0.77 M mannitol and 10 µl of 5 µg/µl purified GFP, then electroporated at 30 V (150 V/cm) at 10 ohms and 3000 µF or not electroporated. Larvae were recovered from the electroporation cuvette by adding 1 ml instant ocean and moved to microcentrifuge tubes. Larvae were then washed 5 times with 1 ml instant ocean by first spinning down at 4000 g for 30 seconds and removing all but 50 µl of liquid. After the five washes larvae were then spun down at 4000 for 2 minutes and the sea water was removed. On ice, the larvae were then lysed in 100 µl 50 mM tris pH 8, 150 mM NaCl, 1% Triton X-100, and vortexed three times for 30 seconds each. Cell debris was pelleted by centrifuging at 21,000 g for 10 minutes and the pellet was discarded. The lysate was then quantified by first diluting a small aliquot of lysate (5 µl) 1:10 and using a Bradford protein assay. The GFP standard curve was created by performing 2-fold serial dilutions of the original purified GFP and using densitometry of the western blot. 8.76 µg of larvae lysate was loaded onto the same gel, with both the mock zap negative control and the electroporated larvae. Recovered protein was

calculated using densitometry and the GFP standard curve. This was repeated for 4 biological replicates each with separate western blots.

Pulldown assays. *E. coli* containing a dual expression plasmid with 12605, Mif1, or both 12605 and Mif1 was grown in 50 ml of LB supplemented with chloramphenicol (100 µg/ml) until an OD_{600} 0.6 at 37°C. The *E. coli* plasmid was induced with 1 mM IPTG and the temperature was lowered to 20°C, then expression was allowed to proceed overnight (16 hours). Cells were recovered by pelleting at 4000 g for 10 minutes and media was discarded. Cells were resuspended in 25 mM tris pH 7.6, 150 mM NaCl and protease inhibitor cocktail (100 µM leupeptin, 1 µM pepstatin and 5 µM bestatin). Cells were lysed twice by French press 1000 Psi and then centrifuged at 10,000 g to remove cellular debris where the supernatant was then transferred to a new tube and the pellet was discarded. The conjugated agarose beads (Ni-NTA agarose and S-Tag binding agarose, EMD Millipore 69704-3) were equilibrated with the lysis buffer and 1 ml of agarose was added in batch to the recovered supernatant. Agarose was then recovered on a column and washed an additional two times with the lysis buffer to remove non-specific bound proteins. Proteins were eluted using either, 500 µl 3 M MgCl2, 20 mM tris pH 7.6 (S-TAG beads), or 500 µl 250 mM imidazole, 500 mM NaCl, 20 mM Tris pH 7.6 (Ni-NTA beads). 20 µg protein was loaded onto SDS-PAGE gel and then transferred onto PVDF membrane for western blot using either the endogenous Mif1 antibody or S-Tag antibody (GenScript Cat# A00625, RRID:AB_915085).

Mass spectrometry. *P. luteoviolacea* was grown in 50 ml Marine Broth (MB) media in 250 ml flasks at 30°C for 6 hours or overnight (12-14 hours). Cells were centrifuged for 30 minutes at 7000 g and 4°C and resuspended in 5 ml cold extraction buffer (20 mM Tris, pH 7.5, 1 M NaCl). The resuspensions were centrifuged for 30 minutes at 4000 g and 4°C and the supernatant was isolated and centrifuged for 30 minutes at 7000 g and 4°C. The pellet was resuspended in 20-100 µl cold extraction buffer and stored at 4°C for further use. All mass spectrometry was done by the Functional Genomics Center Zurich (FGCZ). To prep the MAC extracts for mass spectrometry, the extracts were precipitated by mixing 30 µl of sample with 70 µl water and 100 µl 20% TCA. The samples were then washed twice with cold acetone. The dry pellets were dissolved in 45 µl buffer (10 mM Tris/2 mM $CaCl_2$, pH 8.2) and 5 µl trypsin (100 ng/µl in 10 mM HCl). They were then microwaved for 30 minutes at 60°C. The samples were dried, then dissolved in 20 µl 0.1% formic acid and transferred to autosampler vials for LC/MS/MS. 1 µl was injected.

Data Availability. Subtomogram averages were deposited in the Electron Microscopy Data Bank (accession numbers EMD-4730 and EMD-4731).

3.7 Acknowledgments

We thank Dr. Anca Segall and Dr. Manal Swairjo for reagents, technical support and constructive suggestions. We thank Ms. Amanda Alker and Ms. Nathalie Delherbe for their constructive suggestions. ScopeM at ETHZ and Ohad Medalia at the University of Zürich are acknowledged for instrument access. We thank Paula Picotti and Marco Faini for discussions of mass spectrometry experiments. This work was supported by the

Harold & June Memorial Scholarship (C.F.E.), Norma Sullivan Memorial Endowed Scholarship (C.F.E.), Howard Hughes Medical Institute (DKN), NIH NIDCD (1R21DC013180-01A1, R.W.Z.), Office of Naval Research (N00014-17-1-2677, N.J.S. and S.B.), Office of Naval Research (N00014-16-1-2135, N.J.S), Office of Naval Research (N00014-14-1-0340, N.J.S and D.K.N.), Alfred P. Sloan Foundation, Sloan Research Fellowship (N.J.S.), San Diego State University (N.J.S.), European Research Council (679209, M.P.), Swiss National Science Foundation (31003A_179255, M.P.) and Gebert Rüf Foundation (M.P.).

Chapter 3, in part, is a reprint of material as it appears in Elife, 2019. C.F. Ericson*, F. Eisenstein*, J. Medeiros, K.E. Malter, G. Cavalcanti, R.W. Zeller, D.K. Newman, M. Pilhofer and N.J. Shikuma (2019)**.** The dissertation author is a coauthor of this paper. My specific contributions include Figure 3.3. (panels B &C), Figure 3.4., Figure S3.4.1., Figure S3.4.2., input on the manuscript, methods, and revisions.

3.8 References

1. McFall-Ngai, M. *et al.* Animals in a bacterial world, a new imperative for the life sciences. *Proc. Natl. Acad. Sci.* **110**, 3229–3236 (2013).

2. Hadfield, M. G. Biofilms and Marine Invertebrate Larvae: What Bacteria Produce That Larvae Use to Choose Settlement Sites. *Ann. Rev. Mar. Sci.* **3**, 453–470 (2011).

3. Whalan, S. & Webster, N. S. Sponge larval settlement cues: The role of microbial biofilms in a warming ocean. *Sci. Rep.* **4**, 28–32 (2014).

4. Webster, N. S. *et al.* Metamorphosis of a scleractinian coral in response to microbial biofilms. *Appl. Environ. Microbiol.* **70**, 1213–21 (2004).

5. Dworjanyn, S. A. & Pirozzi, I. Induction of settlement in the sea urchin *Tripneustes gratilla* by macroalgae, biofilms and conspecifics: A role for bacteria? *Aquaculture* **274**, 268–274 (2008).

6. Yu, X., He, W., Li, H., Yan, Y. & Lin, C. Larval settlement and metamorphosis of the pearl oyster *Pinctada fucata* in response to biofilms. *Aquaculture* **306**, 334–337 (2010).

7. Khandeparker, L., Chandrashekar Anil, A. & Raghukumar, S. Relevance of biofilm bacteria in modulating the larval metamorphosis of Balanus amphitrite. *FEMS Microbiol. Ecol.* **58**, 425–438 (2006).

8. Nedved, B. T. & Hadfield, M. G. *Hydroides elegans* (Annelida: Polychaeta): a model for biofouling research. (2008).

9. Zobell, C. E. & Allen, E. C. The Significance of Marine Bacteria in the Fouling of Submerged Surfaces. *J. Bacteriol.* **29**, 239–251 (1935).

10. Tebben, J. *et al.* Induction of larval metamorphosis of the coral *Acropora millepora* by tetrabromopyrrole isolated from a *Pseudoalteromonas* bacterium. *PLoS One* **6**, 1–8 (2011).

11. Sneed, J. M., Sharp, K. H., Ritchie, K. B. & Paul, V. J. The chemical cue tetrabromopyrrole from a biofilm bacterium induces settlement of multiple Caribbean corals. *Proc. R. Soc. B Biol. Sci.* **281**, 20133086–20133086 (2014).

12. Swanson, R. L., Marshall, D. J. & Steinberg, P. D. Larval desperation and histamine: how simple responses can lead to complex changes in larval behaviour. *J. Exp. Biol.* **210**, 3228–3235 (2007).

13. Hadfield, M. G., Unabia, C. C., Smith, C. M. & Michael, T. M. Settlement preferences of the ubiquitous fouler Hydroides elegans. in *Recent developments in biofouling control* 65–74 (1994).

14. Shikuma, N. J., Antoshechkin, I., Medeiros, J. M., Pilhofer, M. & Newman, D. K. Stepwise metamorphosis of the tubeworm *Hydroides elegans* is mediated by a bacterial inducer and MAPK signaling. *Proc. Natl. Acad. Sci.* **113**, 10097–10102 (2016).

15. Huang, S. Y. & Hadfield, M. G. Composition and density of bacterial biofilms determine larval settlement of the polychaete Hydroides elegans. *Mar. Ecol. Ser.* **260**, 161–172 (2003).

16. Huang, Y., Callahan, S. & Hadfield, M. G. Recruitment in the sea : bacterial genes required for inducing larval settlement in a polychaete worm. (2012). doi:10.1038/srep00228

17. Shikuma, N. J. *et al.* Marine Tubeworm Metamorphosis Induced by Arrays of Bacterial Phage Tail–Like Structures. *Science (80-.).* **343**, 529–534 (2014).

18. Taylor, N. M. I., van Raaij, M. J. & Leiman, P. G. Contractile injection systems of bacteriophages and related systems. *Mol. Microbiol.* (2018). doi:10.1111/mmi.13921

19. Brackmann, M., Nazarov, S., Wang, J. & Basler, M. Using Force to Punch Holes: Mechanics of Contractile Nanomachines. *Trends Cell Biol.* **27**, 623–632 (2017).

20. Mechanism of loading and translocation of type VI secretion system effector Tse6.

21. Shneider, M. M. *et al.* PAAR-repeat proteins sharpen and diversify the Type VI

secretion system spike. *Nature* **500**, 350–353 (2013).

22. Heymann, J. B. *et al.* Three-dimensional structure of the toxin-delivery particle antifeeding prophage of serratia entomophila. *J. Biol. Chem.* **288**, 25276–25284 (2013).

23. Sana, T. G. *et al. Salmonella* Typhimurium utilizes a T6SS-mediated antibacterial weapon to establish in the host gut. *Proc. Natl. Acad. Sci.* **113**, E5044--E5051 (2016).

24. Silverman, J. M. *et al.* Haemolysin Co-regulated Protein is an Exported Receptor and Chaperone of Type VI Secretion Substrates. *Mol. Cell* **51**, (2013).

25. Jiang, F. *et al.* Cryo-EM Structure and Assembly of an Extracellular Contractile Injection System. *Cell* **177**, 370-383.e15 (2019).

26. Karimova, G. & Ullmann, A. [5] A bacterial two-hybrid system that exploits a cAMP signaling cascade in Escherichia coli. *Methods Enzymol.* (2000).

27. Zeller, R. W., Virata, M. J. & Cone, A. C. Predictable mosaic transgene expression in ascidian embryos produced with a simple electroporation device. *Dev. Dyn.* **235**, 1921–1932 (2006).

28. Zeller, R. W. Electroporation in Ascidians: History, Theory and Protocols. in *Transgenic Ascidians* **1029**, 37–48 (Springer International Publishing AG, 2018).

29. Yool, A. J. *et al.* Excess Potassium Induces Larval Metamorphosis In Four Marine Invertebrate Species. *Biol. Bull.* **170**, 255–266 (1986).

30. Carpizo-Ituarte, E. & Hadfield, M. G. Stimulation of Metamorphosis in the Polychaete *Hydroides elegans* Haswell (Serpulidae). *Biol. Bull.* **194**, 14–24 (1998).

31. Ma, A. T. & Mekalanos, J. J. In vivo actin cross-linking induced by Vibrio cholerae type VI secretion system is associated with intestinal inflammation. *Proc. Natl. Acad. Sci. U. S. A.* **107**, 4365–70 (2010).

32. Jiang, F. *et al.* The Pseudomonas aeruginosa Type VI Secretion PGAP1-like

Effector Induces Host Autophagy by Activating Endoplasmic Reticulum Stress. *Cell Rep.* **16**, 1502–1509 (2016).

33. Vlisidou, I. *et al. Photorhabdus* Virulence Cassettes: extracellular multi-protein needle complexes for delivery of small protein effectors into host cells. *bioRxiv* 549964 (2019). doi:10.1101/549964

34. Szwedziak, P. & Pilhofer, M. Bidirectional contraction of a type six secretion system. *Nat. Commun.* **10**, 1565 (2019).

35. Scholl, D. Phage Tail–Like Bacteriocins. (2017). doi:10.1146/annurev-virology

36. Rocchi, I. *et al.* A Bacterial Phage Tail-like Structure Kills Eukaryotic Cells by Injecting a Nuclease Effector. *Cell Rep.* **28**, 295-301.e4 (2019).

37. Böck, D. *et al.* In situ architecture, function, and evolution of a contractile injection system. *Science (80-.).* **357**, 713–717 (2017).

38. Weiss, G. L., Medeiros, J. M. & Pilhofer, M. In Situ Imaging of Bacterial Secretion Systems by Electron Cryotomography. in *Methods in molecular biology (Clifton, N.J.)* **1615**, 353–375 (2017).

39. Danev, R., Buijsse, B., Khoshouei, M., Plitzko, J. M. & Baumeister, W. Volta potential phase plate for in-focus phase contrast transmission electron microscopy. *Proc. Natl. Acad. Sci.* **111**, 15635–15640 (2014).

40. Mastronarde, D. N. Automated electron microscope tomography using robust prediction of specimen movements. *J. Struct. Biol.* **152**, 36–51 (2005).

41. Kremer, J. R., Mastronarde, D. N. & McIntosh, J. R. Computer Visualization of Three-Dimensional Image Data Using IMOD. *J. Struct. Biol.* **116**, 71–76 (1996).

42. Schindelin, J. *et al.* Fiji: an open-source platform for biological-image analysis. *Nat. Methods* **9**, 676–82 (2012).

43. Zhang, K. Gctf: Real-time CTF determination and correction. *J. Struct. Biol.* **193**, 1–12 (2016).

44. Mastronarde, D. N. Correction for non-perpendicularity of beam and tilt axis in tomographic reconstructions with the IMOD package. *J. Microsc.* **230**, 212–217 (2008).

45. Heumann, J. M., Hoenger, A. & Mastronarde, D. N. Clustering and variance maps for cryo-electron tomography using wedge-masked differences. *J. Struct. Biol.* **175**, 288–299 (2011).

46. Castaño-Díez, D., Kudryashev, M., Arheit, M. & Stahlberg, H. Dynamo: A flexible, user-friendly development tool for subtomogram averaging of cryo-EM data in high-performance computing environments. *J. Struct. Biol.* **178**, 139–151 (2012).

47. Pettersen, E. F. *et al.* UCSF Chimera - A visualization system for exploratory research and analysis. *J. Comput. Chem.* **25**, 1605–1612 (2004).

48. Schaefer, J., Jovanovic, G., Kotta-Loizou, I. & Buck, M. A data comparison between a traditional and the single-step β-galactosidase assay. *Data Br.* **8**, 350–352 (2016).

49. Miller, J. H. *Experiments in molecular genetics*. (Cold Spring Harbor Laboratory, 1972).

Figure 3.1. Two bacterial genes are important for inducing *Hydroides* metamorphosis and deletions of these genes produce MACs with an "empty" phenotype. (**A**) Metamorphosis (%) assay of *Hydroides* larvae in response to biofilms of *P. luteoviolacea* wildtype (WT) and different gene deletion strains. Deletion of JF50_12605 or *mif1* (JF50_12615) showed a significant loss in the ability to induce metamorphosis when compared to wildtype. (**B**) Restoration of JF50_12605 and *mif1* (JF50_12615) into their native chromosomal loci restored function. Graphs in (A/B) show an average of biological replicates, where each point represents one biological replicate. *p-value ≤ 0.05, ns = not significant. (**C-E**) Representative cryotomographic images of the "filled" phenotype from wildtype MACs (**C**), and "empty" phenotype from ΔJF50_12605 (**D**), and Δ*mif1* (**E**) MACs. Scale bar, 100 nm. (**F/G**) Shown are representative MAC structures (on left; taken from **C/E**) and their density plots. The wildtype "filled" phenotype shows a relatively homogeneous density profile across the diameter of the MAC. The Δ*mif1* "empty" phenotype shows a low-density region in the center of the MAC (arrowhead indicates low-density region in empty structure). (**H**) Shown is the fraction of empty structures for different deletion mutants as observed by cryoET imaging. Note that the "empty" phenotype correlates with the inability to induce metamorphosis (**A**).

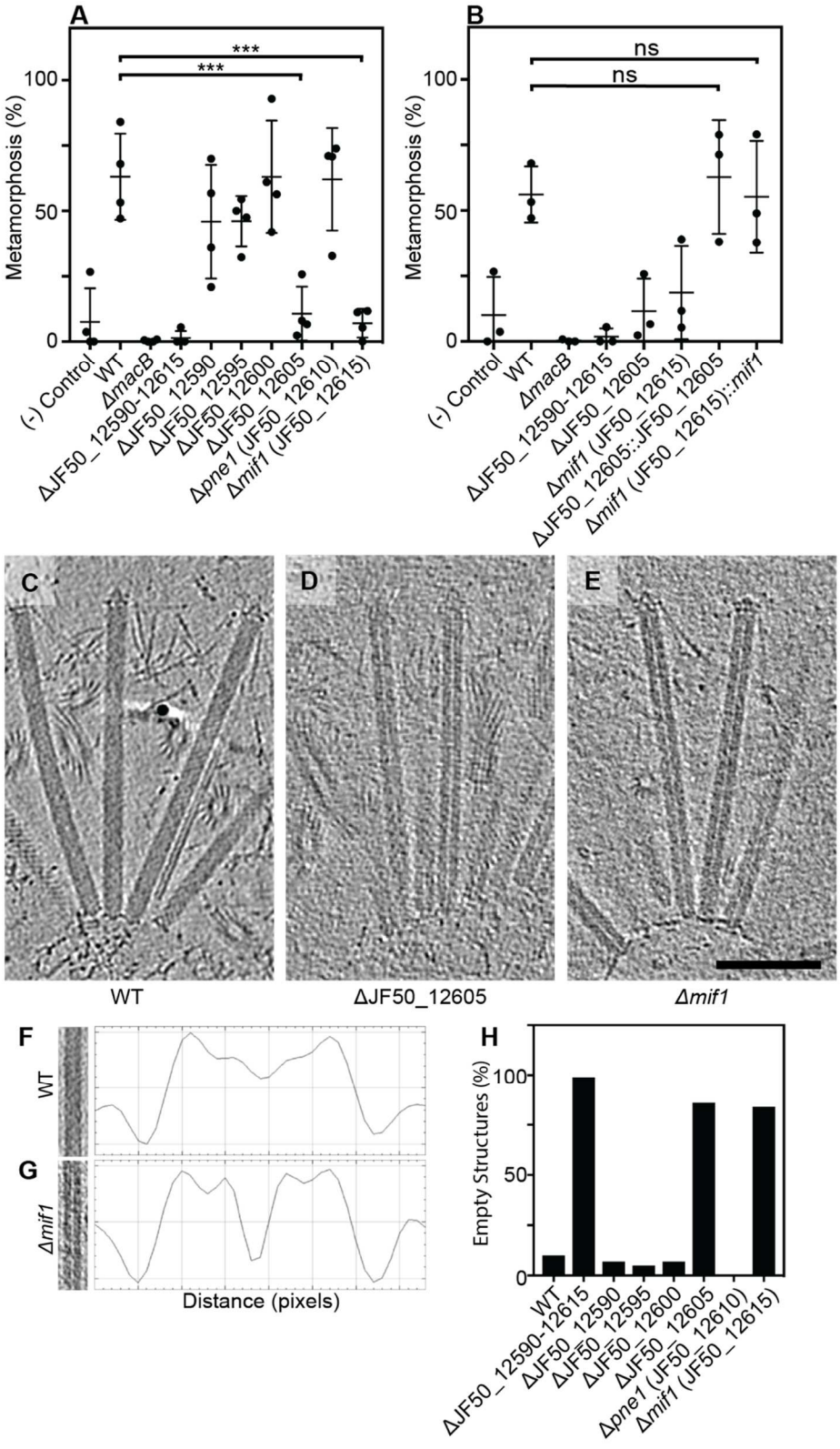
A
B
Metamorphosis (%)
100
50
0
***
***
ns
ns
(-) Control
WT
ΔmacB
ΔJF50_12590-12615
ΔJF50_12590
ΔJF50_12595
ΔJF50_12600
ΔJF50_12605
Δpne1 (JF50_12610)
Δmif1 (JF50_12615)
ΔJF50_12605::JF50_12605
Δmif1 (JF50_12615)::mif1
C
D
E
WT
ΔJF50_12605
Δmif1
F
G
WT
Δmif1
Distance (pixels)
H
Empty Structures (%)

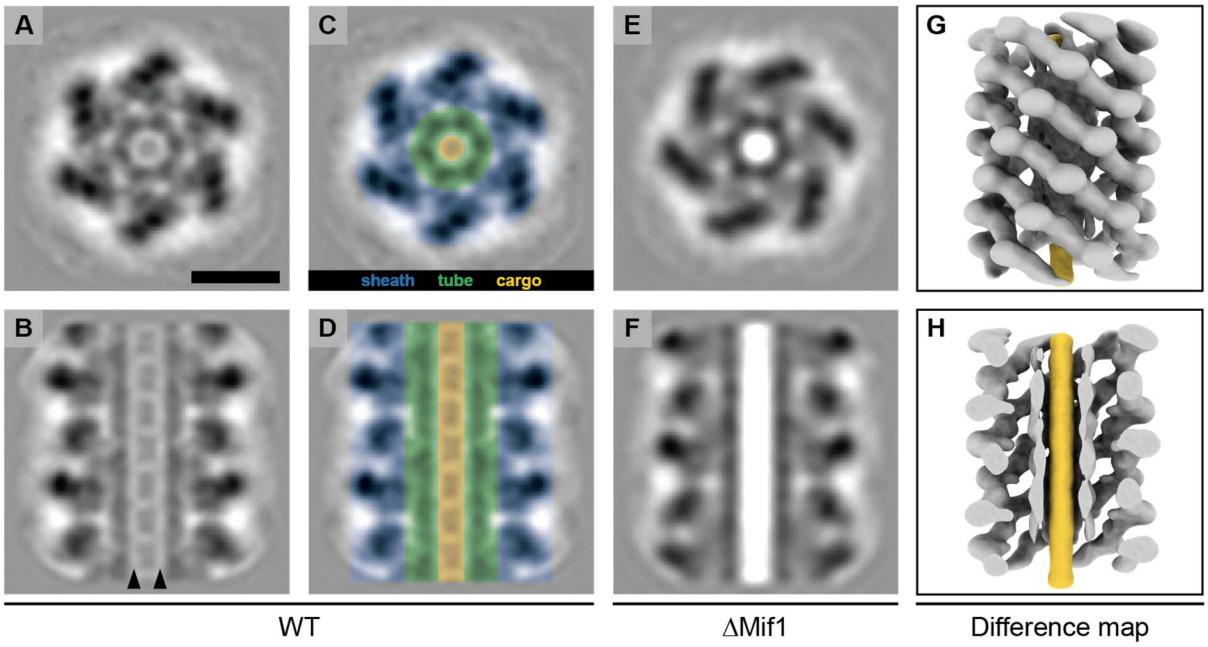

Figure 3.2. MACs from a Δ*mif1* mutant lack electron density in the tube lumen. (**A-F**) Cross sectional (**A/C/E**) and longitudinal (**B/D/F**) slices through subtomogram averages of the MAC sheath-tube complex from wildtype (WT; **A-D**) and ΔMif1 (**E-F**). The hexameric sheath and tube modules could be clearly discerned (indicated in **C/D**). The inner tube lumen displayed clear differences in density between WT and ΔMif1. The wildtype tube lumen was filled with densities that likely represent cargo (**A-D**, indicated in yellow), which was not present in the ΔMif1 lumen (**E/F**). Note the low-density region that separates the tube and cargo (indicated by arrowheads in B). **(G/H)** Shown are isosurfaces of the ΔMif1 structure (grey) and of a difference map (yellow; calculated from the wildtype and ΔMif1 structure), highlighting the additional density in the wildtype tube lumen. Scale bar, 10 nm.

Figure 3.3. Mif1 is present in MAC complexes and JF50_12605 is required for Mif1's association with the MAC complex. (**A**) Mass spectrometry of wildtype MAC arrays detected Mif1 but not JF50_12605. Spectral counts for Mif1 were low for MACs purified from the ΔJF50_12605 mutant, indicating a possible chaperone-like function for JF50_12605. (**B**) Dot blot of purified MACs from wildtype or strains with Mif1 tagged at amino acid positions 943 [C-terminus] (Mif1-FLAG-943), 555 (Mif1-FLAG-555), and 190 (Mif1-FLAG-190) were probed with anti-FLAG antibody. The signal indicates association of Mif1 with MAC arrays. (**C**) Co-expression, reciprocal pull-down and western blotting of S-tagged JF50_12605 and 6xHis-tagged Mif1 indicate an interaction between both proteins. Strains in which only one component was tagged were used as controls. (**D-F**) Quantification of Bacterial Two Hybrid experiments were used to analyze possible interactions between JF50_12605, Mif1 and tube (MacT1) proteins. Briefly, the two fragments of CyaA (T18/T25) were fused to the respective target proteins with the CyaA activity only being restored by interaction between target proteins. JF50_12605 showed a strong interaction with itself and with Mif1.

A

		WT		ΔJF50_12605	
Mif1 (JF50_12615)	Spectral count	14	12	2	1
	Coverage	20%	16%	1.9%	1.6%
JF50_12605	Spectral count	-	-	-	-
	Coverage	-	-	-	-
MacT1 (JF50_12680, tube)	Spectral count	35	49	47	38
	Coverage	93%	97%	92%	93%

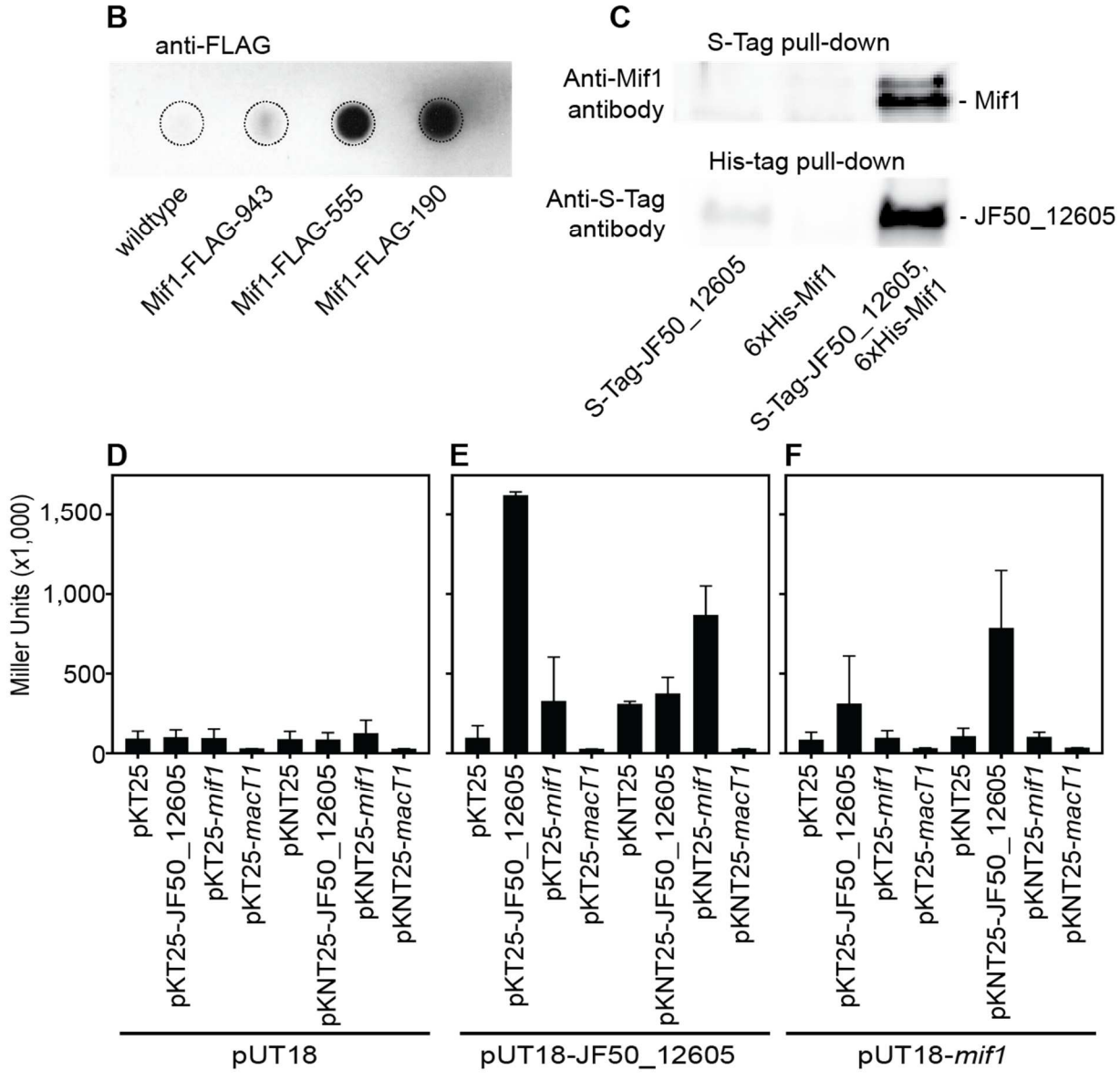

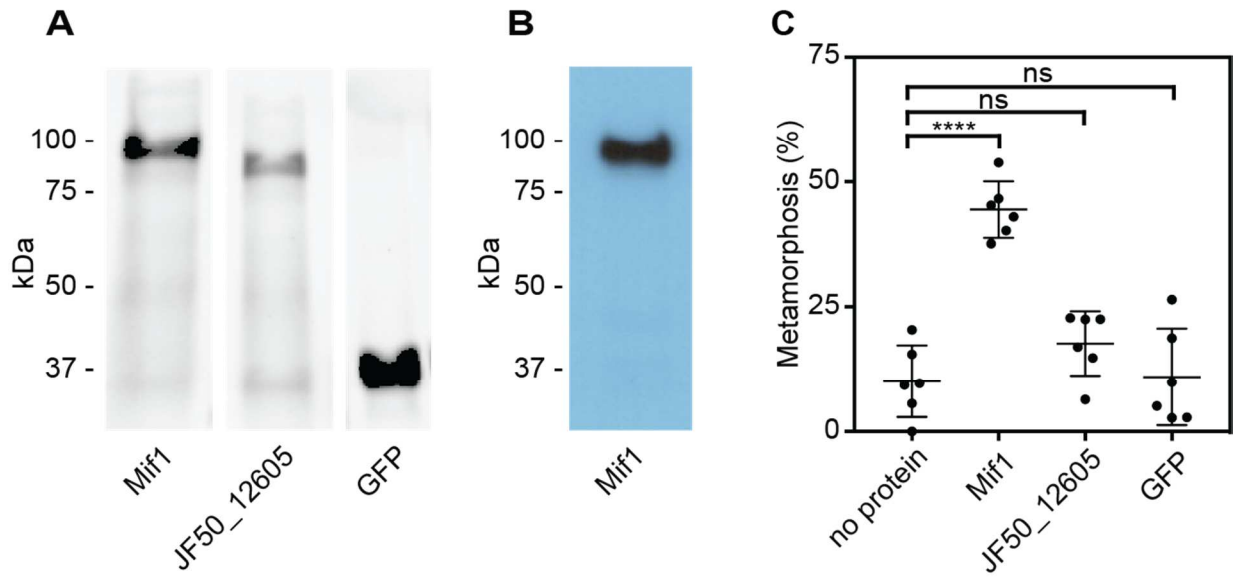

Figure 3.4. Mif1 is sufficient for stimulating metamorphosis when delivered by electroporation. (A) Shown is an SDS page gel of purified Mif1, JF50_12605 and GFP. (**B**) Western blot of purified Mif1 protein probed with a C-terminal anti-Mif1 peptide antibody confirms Mif1 identity. (**C**) Metamorphosis (%) of *Hydroides* larvae 24 hours after electroporation with purified Mif1, JF50_12605 or GFP protein, shows induction of metamorphosis by electroporated Mif1. Graph shows an average of biological replicates, where each point represents one biological replicate. ****p-value ≤ 0.0001 by t-test, ns = not significant.

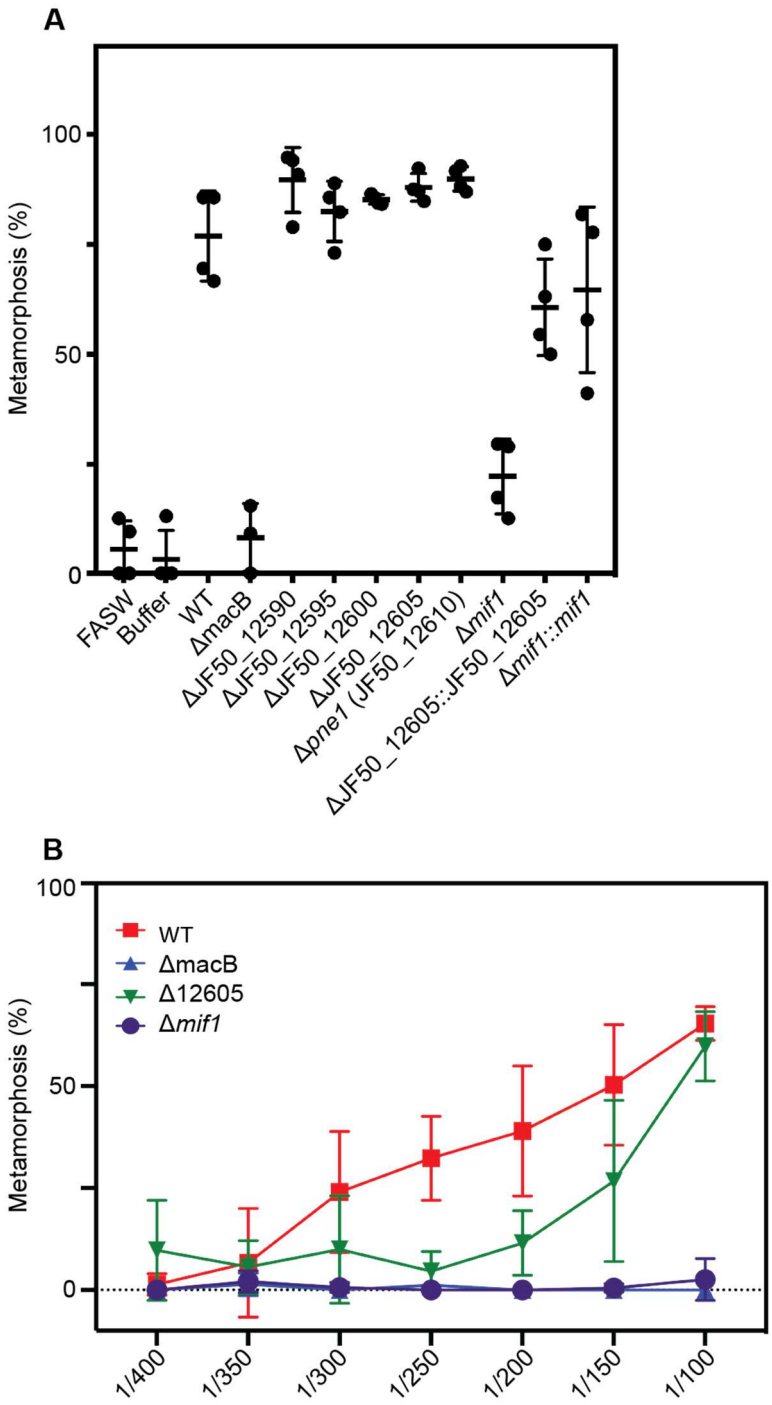

Figure S3.1.1. Metamorphic response of *Hydroides* larvae to cell-free MAC extracts from wild type *P. luteoviolacea* and individual gene mutants. (**A**) Metamorphosis (%) of *Hydroides* larvae 24 hours after exposure to extracted MACs from *P. luteoviolacea* wildtype (WT) and mutants. MAC extracts were diluted 1:100 before being mixed with larvae. (**B**) Dose response curve of MAC extracts from WT (red), ΔmacB (blue), ΔJF50_12605 (green), and Δ*mif1* (purple) mutants.

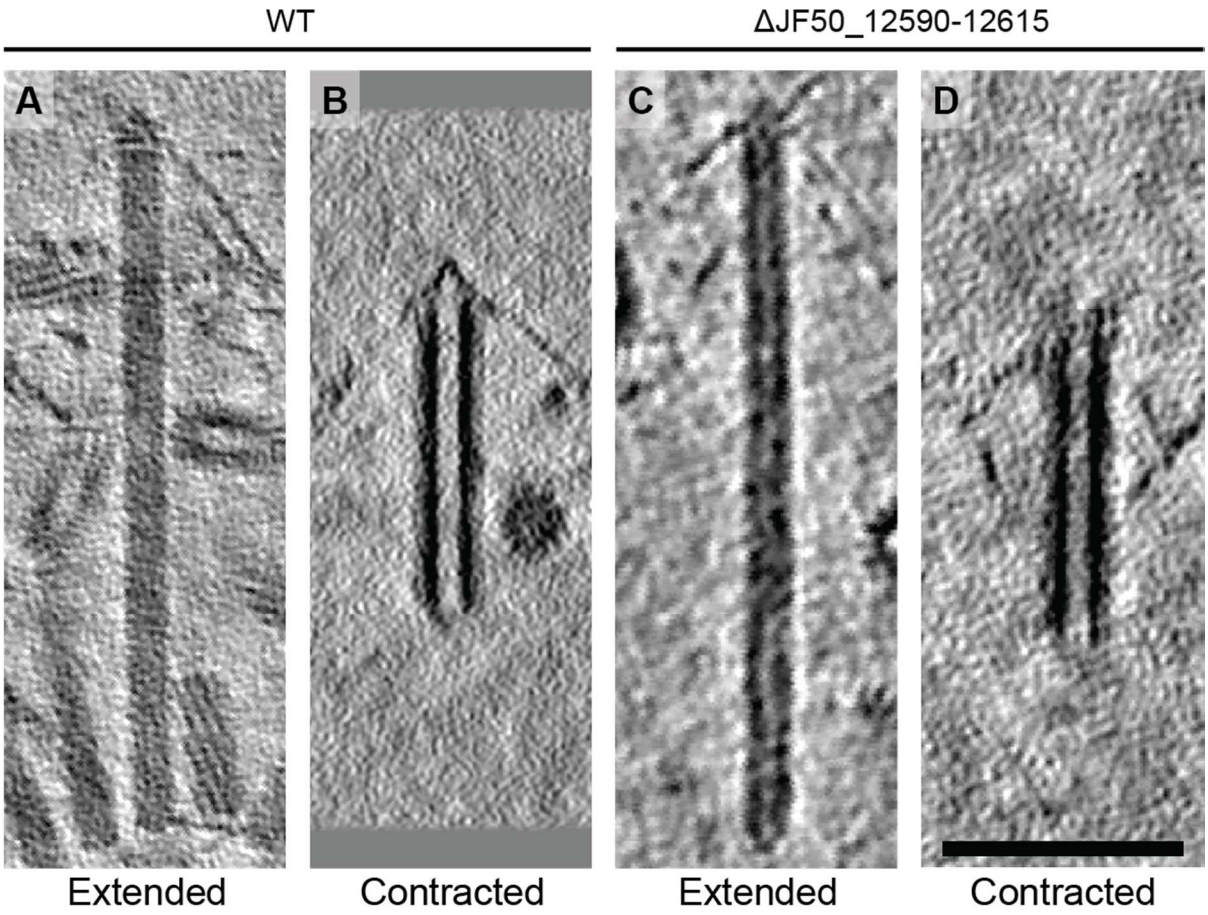

Figure S3.1.2. Wildtype and ΔJF50_12590-12615 have structurally similar arrays. (**A-D**) MAC arrays were present in (**A/B**) wildtype (WT) and (**C/D**) ΔJF50_12590-12615 MAC extracts. Both strains showed arrays that comprised individual contractile structures in extended and contracted conformations. Shown are cryotomographic slices. Scale bar, 100 nm.

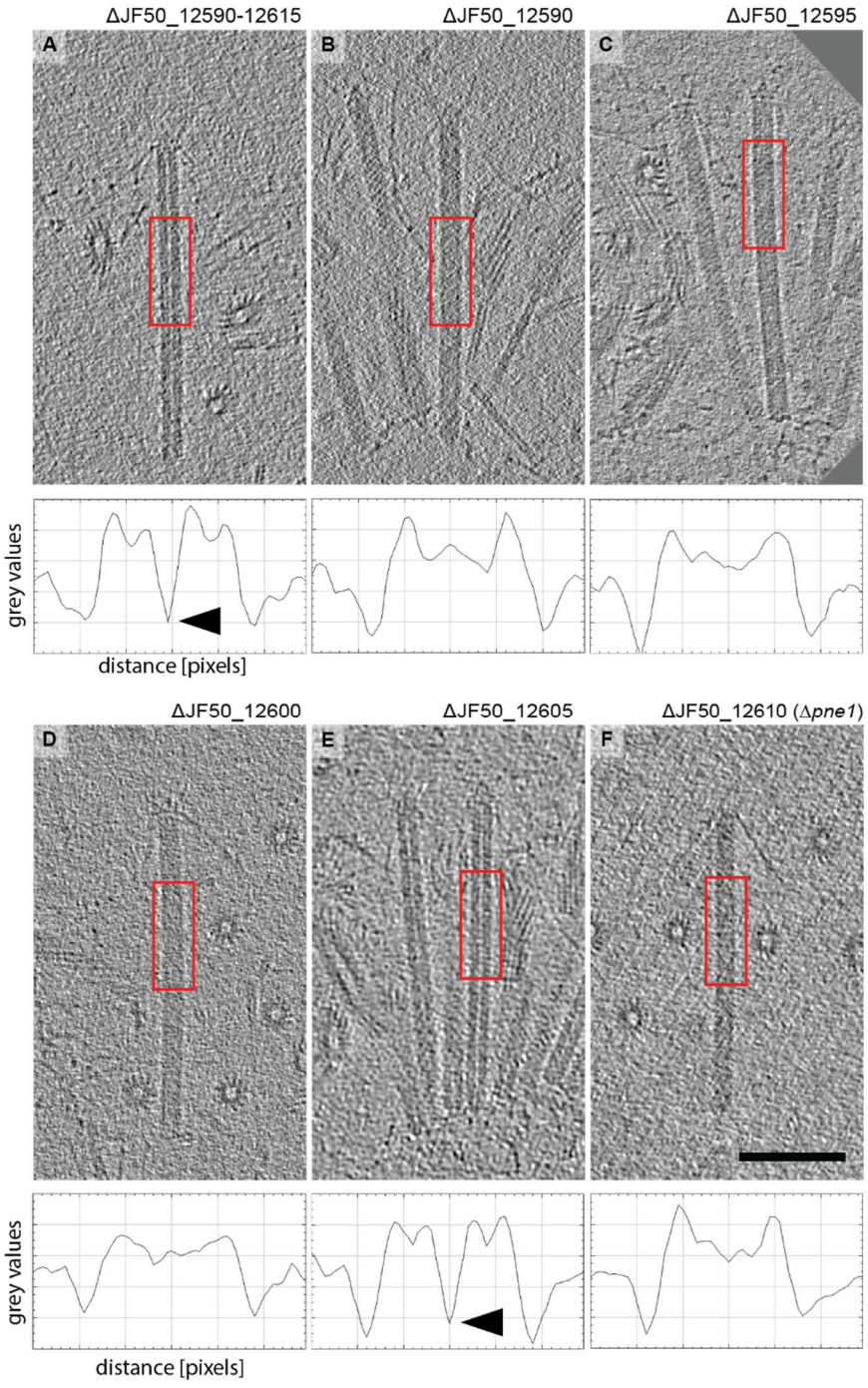

Figure S3.1.3. "Filled" and "empty" phenotypes in all studied gene mutant strains. (**A-F**) Shown are cryotomographic slices of representative extended MACs for different strains and the corresponding density plots (plots were calculated from the boxed image region). "Empty" and "filled" phenotypes are characterized by differences in densities in the MAC center (arrowheads indicate low-density region in empty structures). Scale bar, 100 nm.

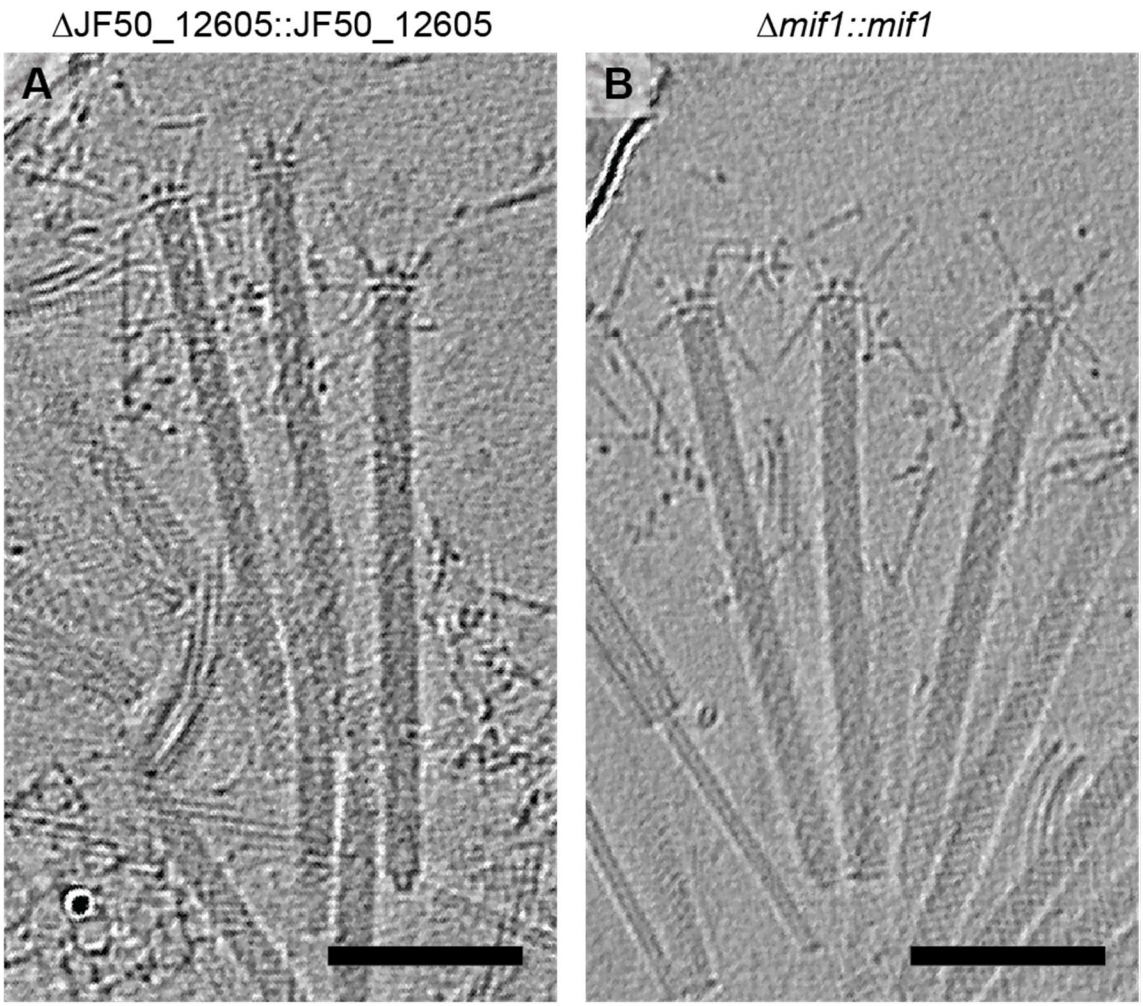

Figure S3.1.4. Replacing JF50_12605 and *mif1* into their native chromosomal loci generates MACs with filled tubes. (**A-B**) When complemented into the native chromosomal loci, (**A**) JF50_12605 and (**B**) *mif1* assemble wildtype-like MACs with a filled phenotype**.** Scale bar, 100 nm.

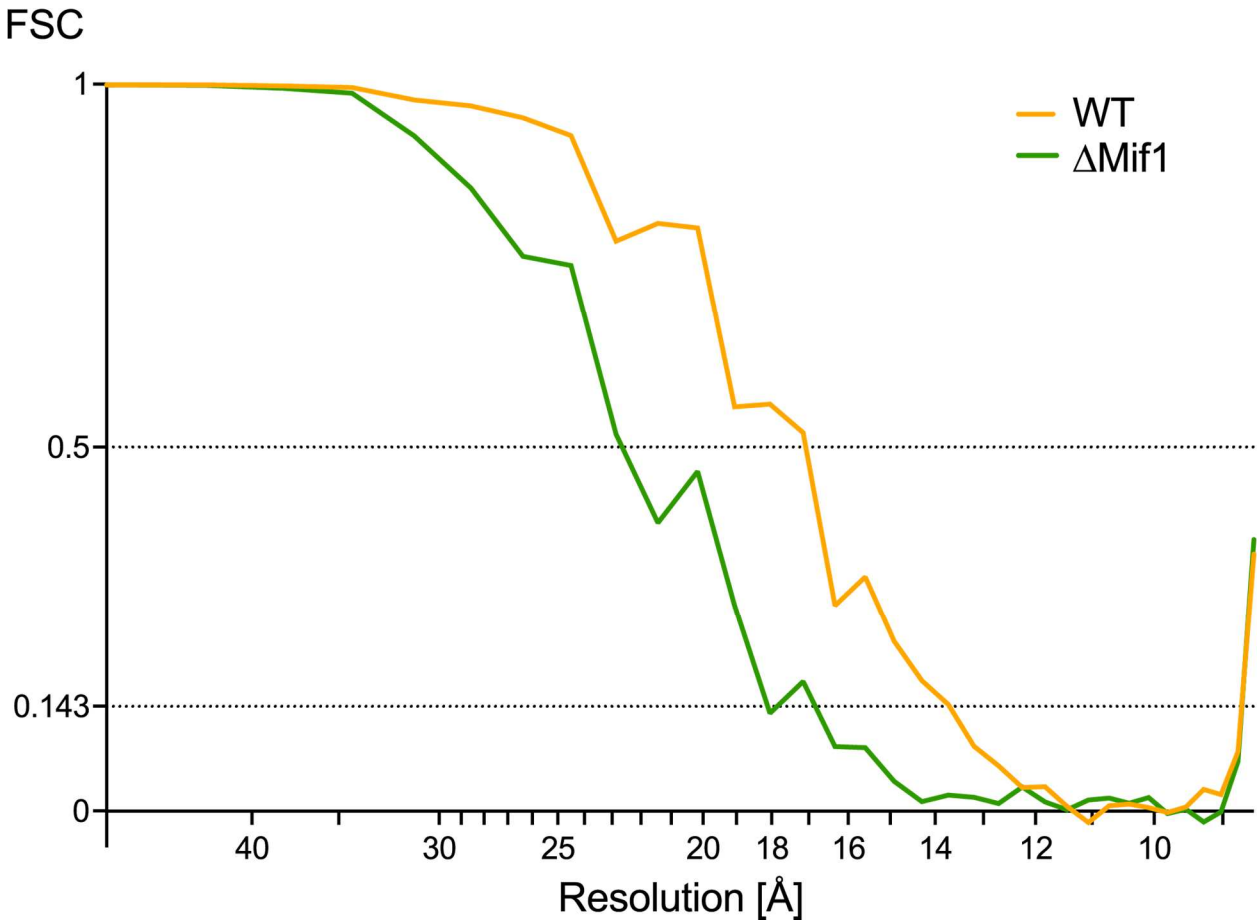

Figure S3.2.1. Fourier shell correlations. Fourier shell correlation (FSC) between the two independently aligned and averaged half-datasets for the wildtype (yellow graph, WT) and the ΔMif1 (green graph) MAC subtomogram averages. Resolution estimates are ~17 Å and ~23 Å at the 0.5 threshold for wildtype and ΔMif1, respectively, and ~14 Å and ~18 Å at the 0.143 threshold.

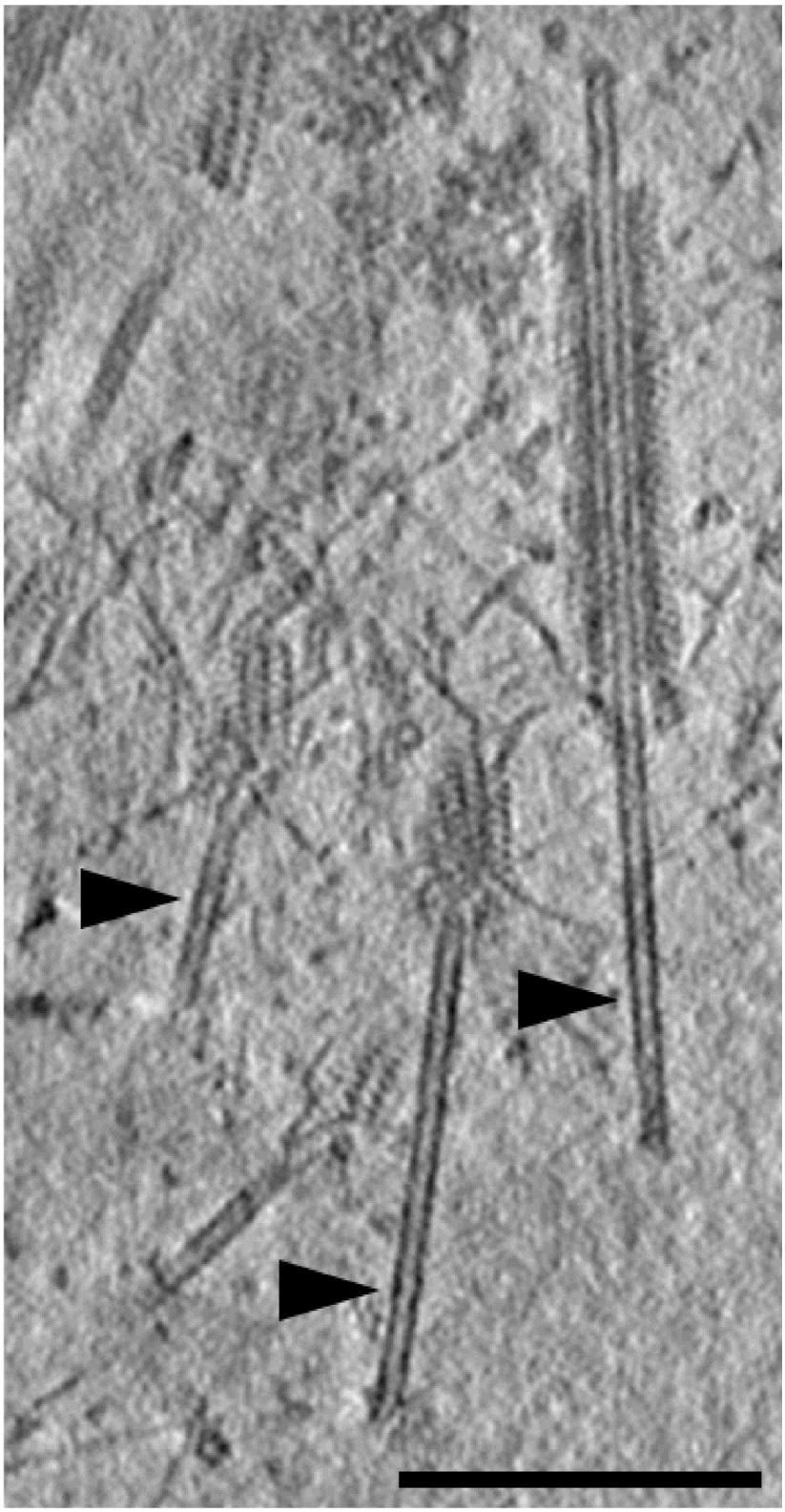

Figure S3.2.2. Triggered MAC tubes show "empty" phenotype. Shown is a representative cryotomographic slices of WT MACs. Arrowheads indicate expelled tubes with "empty" phenotype.

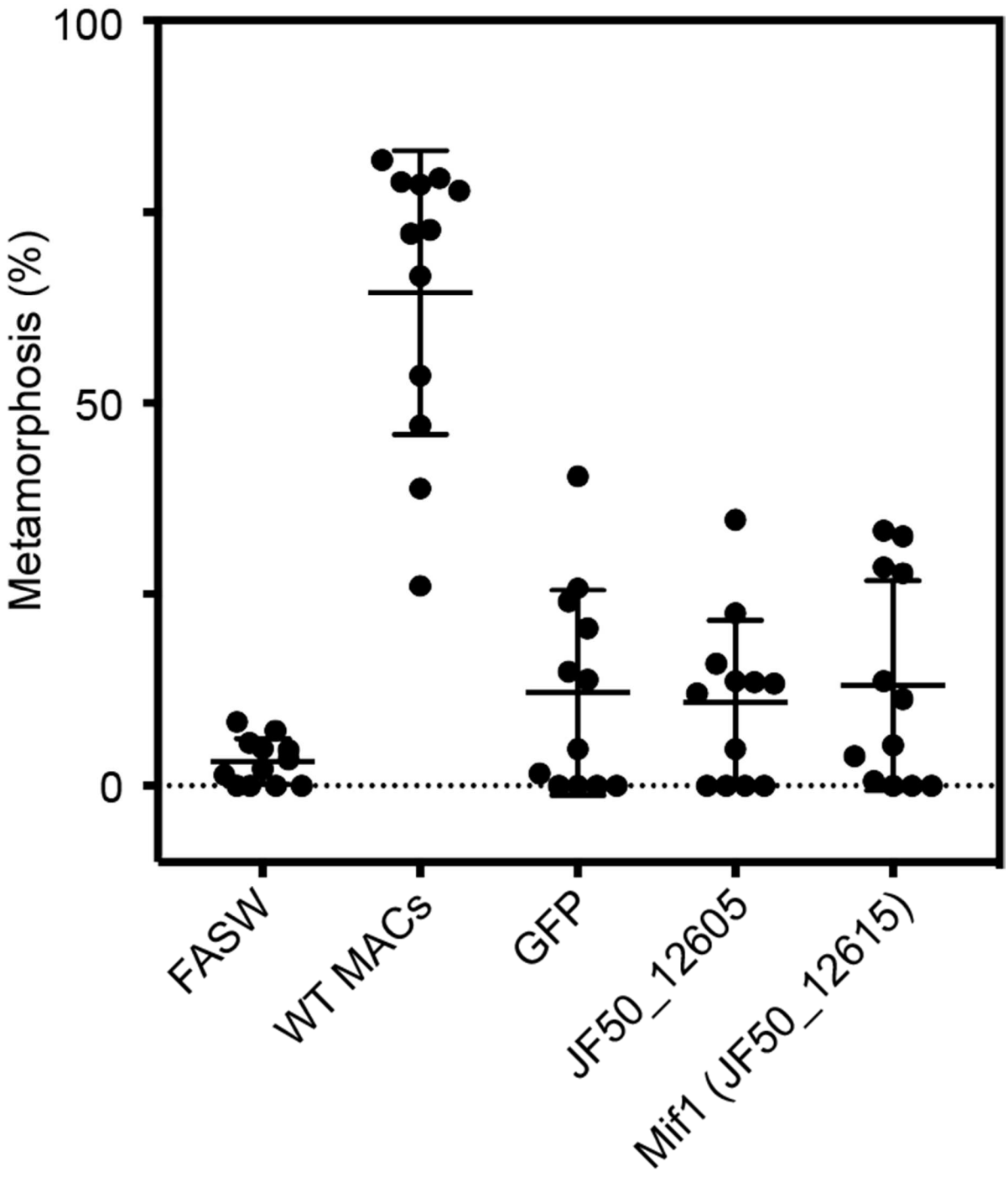

Figure S3.4.1. Purified Mif1 is unable to induce metamorphosis when added exogenously. Metamorphosis (%) of *Hydroides* larvae after being soaked in 250 ng/µl of purified GFP, JF50_12605, and JF50_12615 protein for 24 hours. Wildtype (WT) MACs diluted 1:100 were used as a positive control for larval competence.

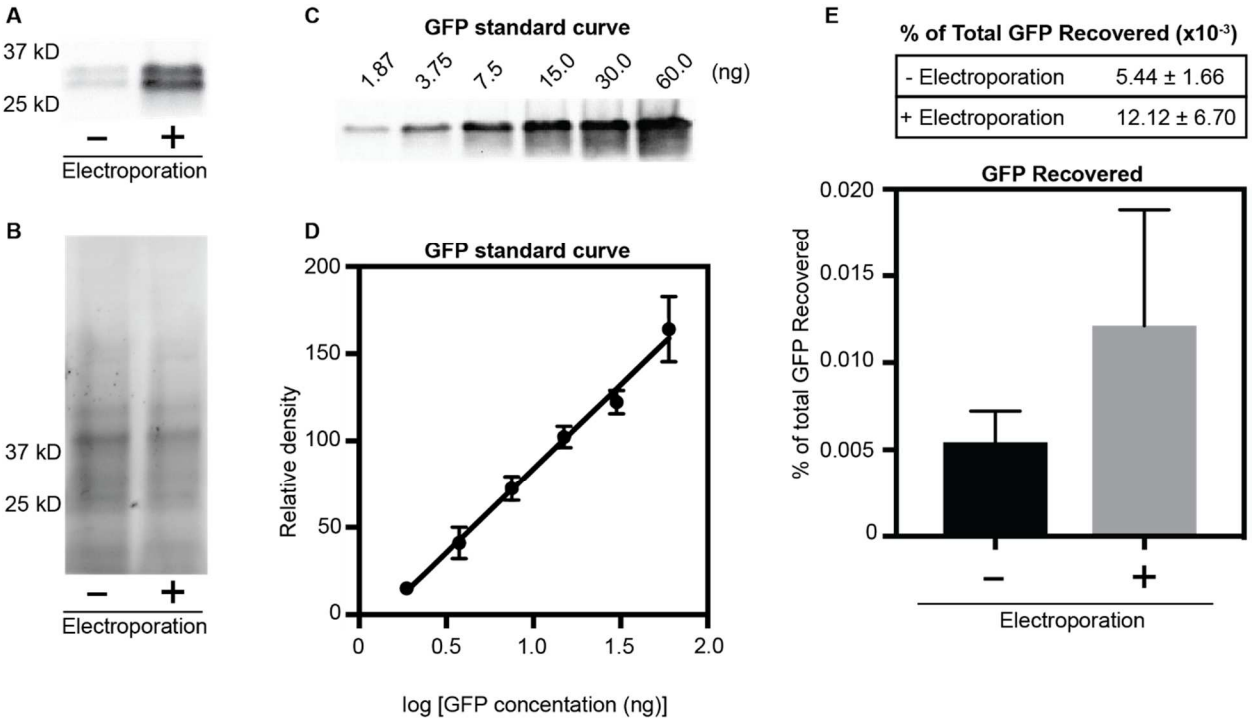

Figure S3.4.2. Quantification of GFP protein associated with larvae after electroporation. We tested if electroporation results in a higher abundance of protein within tubeworm larvae. To this end, tubeworm larvae were mixed with purified GFP protein (0.625 µg/µl**,** 50 µg total**)** and electroporated at 30 V (150 V/cm) at 10 ohms and 3000 µF**.** As a control, a second treatment of tubeworm larvae mixed with GFP without electroporation was performed. After electroporation, larvae were washed 5 times to remove unassociated GFP protein. (**A**) Western blot analysis of larval lysate with and without electroporation resulted in higher recovery of GFP in electroporated larvae (+) when compared to un-electroporated control (-). (**B**) To normalize protein loading, we visualized the stain-free SDS-PAGE gel. (**C/D**) To quantify the amount of protein recovered after electroporation, a GFP standard curve was created by performing a Western blot on known GFP concentrations (n=3). (**E**) To determine the amount of GFP associated with tubeworm larvae, we quantified GFP with (+) and without (-) electroporation. Values are a mean percent of total GFP electroporated (n=4 biological replicates, ± SD).

Table S3.1. Strains and plasmids used in this work.

Strain no.		Genotype	Source or Reference
	Strain		
NJS5	HI1 Str^R	*P. luteoviolacea* HI1, Str^R	[16]
NJS23	Δ*macB*	*P. luteoviolacea* HI1, Str^R Δ*macB*	[17]
NJS235	ΔJF50_12590-F50_12615	*P. luteoviolacea* HI1, Str^R ΔR4	[14]
NJS289	ΔJF50_12590	*P. luteoviolacea* HI1, Str^R ΔJF50_12590	This Study
NJS287	ΔJF50_12595	*P. luteoviolacea* HI1, Str^R ΔJF50_12595	This Study
NJS285	ΔJF50_12600	*P. luteoviolacea* HI1, Str^R ΔJF50_12600	This Study
NJS283	ΔJF50_12605	*P. luteoviolacea* HI1, Str^R ΔJF50_12605	This Study
NJS281	ΔJF50_12610	*P. luteoviolacea* HI1, Str^R ΔJF50_12610	This Study
NJS279	ΔJF50_12615	*P. luteoviolacea* HI1, Str^R ΔJF50_12615	This Study
NJS294	ΔJF50_12605::12605	*P. luteoviolacea* HI1, Str^R ΔJF50_12605::JF50_12605	This Study
NJS295	ΔJF50_12615::12615	*P. luteoviolacea* HI1, Str^R ΔJF50_12615::JF50_12615	This Study
	Plasmid		
pNJS007	pCVD443	Amp^R, Km^R, sacB, pGP704 derivative	[16]
pNJS266	pCVD443_Δ12590	pCVD443::Δ12590 Amp^R , Km^R	This Study
pNJS265	pCVD443_Δ12595	pCVD443::Δ12595 Amp^R , Km^R	This Study
pNJS264	pCVD443_Δ12600	pCVD443::Δ12600 Amp^R , Km^R	This Study
pNJS263	pCVD443_Δ12605	pCVD443::Δ12605 Amp^R , Km^R	This Study
pNJS262	pCVD443_Δ12610	pCVD443::Δ12610 Amp^R , Km^R	This Study
pNJS261	pCVD443_Δ12615	pCVD443::Δ12615 Amp^R , Km^R	This Study
pNJS256	pCVD443_12590-615 complement	Amp^R, Km^R	[14]
pNJS282	pCVD443_12605 complement	Amp^R, Km^R	This Study
pNJS074	pCVD443_Δ12585	Amp^R, Km^R	This Study
pNJS267	pUT18	Amp^R	[26]
pNJS268	pUT18C	Amp^R	[26]
pNJS269	pKT25	Km^R	[26]
pNJS270	pKNT25	Km^R	[26]

Table S3.1. Strains and plasmids used in this work. Continued.

pNJS283	pUT18_12605	Amp^R	This Study
pNJS299	pUT18_12615	Amp^R	This Study
pNJS527	pUT18_12680	Amp^R	This Study
pNJS284	pKT25_12605	Km^R	This Study
pNJS285	pKT25_12615	Km^R	This Study
pNJS529	pKT25_12680	Km^R	This Study
pNJS286	pKNT25_12605	Km^R	This Study
pNJS300	pKNT25_12615	Km^R	This Study
pNJS530	pKNT25_12680	Km^R	This Study
pNJS393	pET15b_12605	Amp^R	This Study
pNJS395	pET15b_12615	Amp^R	This Study
pNJS397	pET15b_GFP	Amp^R	This Study

Table S3.2. Primers used in this work.

Primer	Sequence
1556_dA	TGATGGGTTAAAAAGGATCGATCCTCTAGATTGGAGCAATAAACGGGTTC
1556_dB	GTTCATAATTAAACTGCGATCGCAGCCATAAGGCCTCCTTGATA
1556_dC	TATCAAGGAGGCCTTATGGCTGCGATCGCAGTTTAATTATGAAC
1556_dD	TTTTGAGACACAACGTGAATTCAAAGGGAGAGCTCCGCTTTGGGTACTGG CTTTA
1556_intF	CCGAGCAAACGTTATCACAA
1556_intR	TCAGCGCTCTCATTATGTGC
1555_dA	TGATGGGTTAAAAAGGATCGATCCTCTAGACCGAGCAAACGTTATCACAA
1555_dB	CCTTGCATGAGGTTAAGAAAGTTTGACGTACCCTTCAGCCATATT
1555_dC	AATATGGCTGAAGGGTACGTCAAACTTTCTTAACCTCATGCAAGG
1555_dD	TTTTGAGACACAACGTGAATTCAAAGGGAGAGCTCGATGCGGTAACGGTT GTTCT
1555_intF	AGCGATTGATGCTGAACAAA
1555_intR	ACCATCGCATAACCCGTAAC
1554_dA	TGATGGGTTAAAAAGGATCGATCCTCTAGATACGCCGTCCAGTTAGGACT
1554_dB	GTTTGTTAACGTCACGGCAGCTGCATTGCCATTTAAACTCC
1554_dC	GGAGTTTAAATGGCAATGCAGCTGCCGTGACGTTAACAAAC
1554_dD	TTTTGAGACACAACGTGAATTCAAAGGGAGAGCTCATTGATTGGAAGCGC GATAG
1554_intF	TTTATGAGGCACCAACGACA
1554_intR	GCCTGTGCCGTTTTATCTGT
1553_dA	TGATGGGTTAAAAAGGATCGATCCTCTAGAGGCGATCAGTGGAGTGAAGT
1553_dB	AATACTTCTTGCTCAGCCCCGCGTGCTTCTTCTGTCATGT
1553_dC	ACATGACAGAAGAAGCACGCGGGGCTGAGCAAGAAGTATT
1553_dD	TTTTGAGACACAACGTGAATTCAAAGGGAGAGCTCTCAGAACCAGCAGTCT CACG
1553_intF	CGGGCCTAGAAATCACTCAA
1553_intR	TCGACGTCAAATCAGTCGAG
1552_dA	TGATGGGTTAAAAAGGATCGATCCTCTAGAGAGAGCAAGAAGTGGCGAGT
1552_dB	TAGCCTTTTAGTGCCGCTTTTGAGGCGTCCATATCTGACA
1552_dC	TGTCAGATATGGACGCCTCAAAAGCGGCACTAAAAGGCTA
1552_dD	TTTTGAGACACAACGTGAATTCAAAGGGAGAGCTCTGCTGACCAAGCAGAT TGAC
1552_intF	GGGCAATTGTTGTGGATTTT
1552_intR	TGATCCCAAACCACTTGTGA
1551_dA	TGATGGGTTAAAAAGGATCGATCCTCTAGAGACTGCTGGTTCTGATTCGAT
1551_dB	AACAGATCATTACATTAAAATGAGCCTCTGTTCTTGTTGTTGCATTTCA
1551_dC	TGAAATGCAACAACAAGAACAGAGGCTCATTTTAATGTAATGATCTGTT
1551_dD	TTTTGAGACACAACGTGAATTCAAAGGGAGAGCTCCTTCTCCATTTTCGCC TTTG
1551_intF	CGTTTTCAGTGACCATCACG
1551_intR	CGGTGGGCAAAAAGGTATAA
pUT18_605_F1	CAGCTATGACCATGATTACGCCAAGCTTGCATGCCATGACAGAAGAAGCA CGCGAAAAAA

Table S3.2. Primers used in this work. Continued.

	CTGGCGGCTGAATTCGAGCTCGGTACCCGGGGATCATTCACAA
pUT18_605_R1	GTGCTAATTGATAAAAT
	CAGCTATGACCATGATTACGCCAAGCTTGCATGCCATGCAACAA
pUT18_615_F1	CAAGAACAGGAGCAAG
	CTGGCGGCTGAATTCGAGCTCGGTACCCGGGGATCCATTAAAA
pUT18_615_R1	TGAGCCTTTCTTTTTCA
	CATGATTACGCCAAGCTTGCATGCCATGGCTACTACTAAAGCAG
pUT18_680_F	ATATCG
	AATTCGAGCTCGGTACCCGGGGATCATGGAACTCAATCTTGATG
pUT18_680_R	TCATCT
	CCGATTACCTGGCGCGCACGCGGCGGGCTGCAGGGATGACAG
pKT_605_F1	AAGAAGCACGCGAAAAAA
	AACGACGGCCGAATTCTTAGTTACTTAGGTACCCGCTAATTCAC
pKT_605_R1	AAGTGCTAATTGATAA
	CCGATTACCTGGCGCGCACGCGGCGGGCTGCAGGGATGCAAC
pKT_615_F1	AACAAGAACAGGAGCAAG
	AACGACGGCCGAATTCTTAGTTACTTAGGTACCCGTTACATTAA
pKT_615_R1	AATGAGCCTTTCTTTT
	CCTGGCGCGCACGCGGCGGGCTGCAATGGCTACTACTAAAGCA
pKT_680_F1	GATATCG
pKT_680_R1	GCCGAATTCTTAGTTACTTAGGTACTTAATGGAACTCAATCTTGA
	CAGCTATGACCATGATTACGCCAAGCTTGCATGCCATGACAGAA
pKNT_605_F1	GCGAAAAAA
	TGATGCGATTGCTGCATGGTCATTGAATTCGAGCTATTCACAAG
pKNT_605_R1	GATAAAAT
	CAGCTATGACCATGATTACGCCAAGCTTGCATGCCATGCAACAA
pKNT_615_F1	AGGAGCAAG
	TGATGCGATTGCTGCATGGTCATTGAATTCGAGCTCATTAAAATC
pKNT_615_R1	CTTTTTCA
pKNT_615_F2	CATGATTACGCCAAGCTTGCATGCCATGCAACAACAAGAACAGG
pKNT25-680_F	CATGATTACGCCAAGCTTGCATGCCATGGCTACTACTAAAGCAG
pKNT25-680_R	GCTGCATGGTCATTGAATTCGAGCTATGGAACTCAATCTTGATG
pET15b_605_F1	TGCCGCGCGGCAGCCATATGATGACAGAAGAAGCACGCG
pET15b_605_R1	GCTTTGTTAGCAGCCGGATCCCTAATTCACAAGTGCTAATT

Chapter 4

Diacylglycerol, PKC and MAPK Signaling Initiate Tubeworm Metamorphosis in Response to Bacteria

4.1 Abstract

External environmental cues can have significant impacts on the timing and outcomes of animal development. For the swimming larvae of many marine invertebrates, the presence of specific surface-bound bacteria are important cues that help larvae identify a suitable location on the sea floor for metamorphosis and adult life. While metamorphosis in response to bacteria occurs in diverse animals from across the animal tree of life, we know little about the signal transduction cascades stimulated at the onset of metamorphosis upon their interaction with bacteria. The metamorphosis of a model tubeworm, *Hydroides elegans*, is triggered by the bacterium *Pseudoalteromonas luteoviolacea* which produces a stimulatory protein called Mif1. In this work, we define three key nodes in a signaling cascade promoting *Hydroides* metamorphosis in response to Mif1. Using metabolomic profiling, we find that the stimulation of *Hydroides* larvae by *P. luteoviolacea* leads to an increase in diacylglycerol during the initiation of metamorphosis, and that Mif1 is necessary for this upregulation. Genomic and pharmacological examination suggests that diacylglycerol triggers a phosphotransferase signaling cascade involving Protein Kinase C (PKC) and Mitogen-Activated Protein Kinase (MAPK), to induce *Hydroides* metamorphosis. Additionally, Mif1 activates the expression of two nuclear hormone receptors, HeNHR1 and HeNHR2 in the cerebral ganglia of *Hydroides* larvae. Our results define a post-translational signal transduction pathway mediating bacteria-stimulated metamorphosis in a model invertebrate animal.

4.2 Introduction

How a single-celled zygote develops into a multicellular organism has fascinated scientists for centuries. While animal development was once thought to occur in isolation of the environment, it is now becoming clear that an animal's environmental context can dictate when, where, and how an animal develops [1]. A striking example of this phenomenon is the induction of animal metamorphosis by bacteria [2,3], wherein the free-swimming larvae of many bottom-dwelling marine invertebrates use environmental bacteria as an indicator of a preferable habitat before attaching to the sea floor and undergoing metamorphosis [4]. Although the induction of metamorphosis by bacteria was first described in the 1930s [5], it remains unclear how animal larvae sense and respond to bacterial cues to undergo this essential life history transition.

Metamorphosis has been studied in detail in amphibians and insects, where internal hormonal cues signal through nuclear hormone receptor (NHR) transcription factors to orchestrate a prolonged, stage-specific, developmental program based on a cascade of gene expression [6–9]. In contrast, the free-swimming larvae of many bottom-dwelling marine animals reach a metamorphic competence stage, where they possess the developmental ability to undergo a rapid metamorphosis in response to external cues [4]. This rapid metamorphic transition in response to external cues is thought to help the swimming animal larvae identify a suitable location on the sea floor and transition quickly for survival, growth and reproduction as a juvenile and adult [10].

Evidence suggests that the rapid metamorphic response of marine animal larvae is initiated through posttranslational signaling mechanisms. In the tubeworm *Hydroides elegans* and the Bryozoan *Bugula neritina*, metamorphosis can begin even in the presence of transcription and translation inhibitors [11,12]. Comparative proteomics in *B. neritina* during metamorphosis identified a downregulation of two phosphorylated proteins: the mitochondrial processing peptidase beta subunit, and the calcium-dependent actin binding protein Severin, which suggests a role for protein phosphorylation and not *de novo* protein synthesis during metamorphosis initiation [13]. These studies suggest that the machinery required for the initiation of metamorphosis is present once the larvae reach competency.

A number of conserved post-translational signaling systems have been shown to be involved in orchestrating metamorphosis in marine invertebrates. These systems include the cyclic adenosine monophosphate (cAMP) second messengers [14–16], the neurotransmitters serotonin and nitric oxide (NO) [17,18], alterations in membrane potential [19–23], Mitogen Activated Protein Kinase (MAPK) signaling [24,25], and the Protein Kinase C (PKC) signaling pathway [20,22,26–28]. The PKC pathway has been identified within representatives of many major animal phyla, including *Hyractinia echinata*, *Mitrocomella polydiademata* and Red Sea coral planulae (*Cnidaria*), *Capitella* sp. 1 (*Annelida*), the barnacle *Balanus Amphitrite* (*Arthropoda*) and the sea urchin *Strongylocentrotus purpuratus* (*Echinodermata*) [20,22,26–29]. Of the above-mentioned signaling systems, PKC was activated in response to bacteria in the hydrozoans *Hydractinia echinata* and *Phialidium gregarium* [30,31], while serotonin, membrane potential and MAPK have been

implicated in mediating metamorphosis in response to bacteria in the annelid, *Hydroides elegans* [23,24,32].

To investigate the animal signaling systems mediating metamorphosis in response to bacteria, we study the metamorphosis of the marine biofouling tubeworm *Hydroides elegans* (hereafter, *Hydroides*) [33]. *Hydroides* was shown previously to undergo metamorphosis in response to a marine bacterium *Pseudoalteromonas luteoviolacea*, providing a model system to better understand the modes by which bacteria promote animal development [34–36]. To induce *Hydroides* metamorphosis, *P. luteoviolacea* produces an array of bacteriophage tail-like particles called Metamorphosis Associated Contractile structures (MACs) that are necessary for the bacterium to stimulate metamorphosis [24,37]. MACs carry a protein effector called Metamorphosis inducing factor 1 (Mif1) that is required for MACs to induce *Hydroides* metamorphosis [38]. Upon stimulation by MACs, we found previously that the inhibition of either the p38 Mitogen Activated Protein Kinase (p38 MAPK) or c-Jun N-terminal Kinase (JNK) MAPK pathways are critical for *Hydroides* metamorphosis [24]. However, the other signal transduction events that occur upon the stimulation of *Hydroides* metamorphosis by MACs and the effector Mif1 remain mysterious.

In this study, we hypothesized that post-translational signal transduction contributes to the orchestration of metamorphosis of *Hydroides* in response to the bacterial protein Mif1. We therefore leverage comparative metabolomics to identify metabolites that are differentially produced during bacteria-stimulated metamorphosis.

Our approach utilized mutants of *P. luteoviolacea* that lack an essential component of MACs or the effector Mif1 to identify changes in lipid second messengers. From these analyses, we demonstrate that MACs and Mif1 stimulate three key nodes of posttranslational signaling. Mif1 promotes diacylglycerol (DAG) production in *Hydroides,* and we demonstrate that DAG alone is sufficient to induce metamorphosis. Mif1 promotes PKC and MAPK signaling, which upregulates the production of two nuclear hormone receptor genes.

4.3 Results and discussion

***P. luteoviolacea* Mif1 promotes broad changes in the lipid profile of tubeworm larvae, including the production of diacylglycerol**. To identify the signaling pathways in *Hydroides* that are initiated by MACs and Mif1, tubeworm larvae were exposed to MACs extracts from *P. luteoviolacea* wild type or mutants for one hour to induce a response, as observed previously [37]. We employed a previously developed protocol to isolate MACs from *P. luteoviolacea* cells, which has been shown to strongly induce *Hydroides* metamorphosis [37,38]. Larvae were then subjected to total lipid extraction; samples were analyzed by high performance reverse phase liquid chromatography-quadrupole time of flight mass spectrometry (LC-QTOF-MS) and data were analyzed by comparative metabolomics using XCMS (Figure 4.1. A). To determine the effect of MACs and Mif1 on the *Hydroides* larvae, we compared the total lipid profile of *Hydroides* larvae when exposed to (1) MACs extraction buffer alone, (2) MACs extract from wild type *P. luteoviolacea*, or MACs extract from two mutant *P. luteoviolacea* strains: (3) a strain Δ*macB* that lacks the baseplate gene and does not form functional MACs or (4) a strain Δ*mif1* that forms intact MACs but lacks the Mif1 effector required for metamorphosis [37,38]. From these analyses, we identified a total of 7683 unique metabolic features identified by *m/z* ratio.

When we performed comparative metabolomics in a multiple group comparison of all four treatments, we identified 41 differentially regulated lipid products (plotted based on retention time, intensity and sorted by significance (p-value)). XCMS analysis is a

preprocessing method that sorts molecules based on a univariate analysis of variance by one-way ANOVA based on relative intensities to identify differentially regulated metabolites vs the baseline mean, and then sorts them based on p-value [39]. Forty one significantly dysregulated lipids (p-value <0.01) were visualized as a cloud plot based on their retention time (relative hydrophobicity), intensity (relative abundance), m/z value (mass to charge ratio) and p-value (significant difference) (Figure 4.1. B and Table S4.1.). Many significantly dysregulated products were identified as small hydrophobic peptides (e.g. Asp, Ile, Asn, and Pro) with a short retention time, eluting before the more hydrophobic lipid products (Table S4.1.). Additionally, we found compounds which had both *m/z* and retention times consistent with the general membrane components including phosphatidylcholine (PC), phosphatidyl serine (PS), and phosphatidyl ethanolamine (PE). While PC, PS and PE were identified as dysregulated, these components only increased in the Δ*mif1* mutant, perhaps in response to sensing the bacterial products. Although this was intriguing, we did not attribute these changes to the signaling required to induce metamorphosis, as MACs lacking Mif1 (Δ*mif1*) do not induce metamorphosis [38]. We did, however, identify an increase of compounds consistent with the class of lipids phosphatidylcholine (PC) and phosphatidylethanolamine (PE) in the wild type condition. It is unclear whether these lipids play a role in the signaling of metamorphosis induction or are perhaps upregulated to support membrane breakdown and/or restructuring during metamorphosis.

Two species of diacylglycerol (DAG, m/z 654.5051 & m/z 639.4936) were identified in the multigroup comparison based on the m/z ratio and a retention time and were of

particular interest because of their known role as signaling lipids in eukaryotes (Figure 4.1. B, b inset, C). The identified diacylglycerols were upregulated when wild type MACs were added to *Hydroides* larvae and metamorphosis had been initiated compared to treatments where extraction buffer, or MACs from Δ*macB* or Δ*mif1* were added to larvae and they did not undergo metamorphosis.

Diacylglycerols have previously been characterized as signaling lipids and can be found in all eukaryotes. DAG is responsible for recruiting the cysteine rich C1 domain containing proteins to the membrane and can subsequently activate specific enzymatic functions [40]. DAG is canonically produced when a phospholipase C type lipase binds to the membrane and cleaves between the phosphate and the headgroup, leaving behind the glycerol backbone with the two acyl chains [41]. Consistent with our observation, previous studies in the Cnidarian, *H. echinata*, showed that DAG was sufficient to stimulate metamorphosis [42,43]. The C1 binding domain was first discovered in PKC isoforms and has since been identified in many other proteins such as Chimerins, DAG kinases, PKD, RasGRPs and Munc13s [44]. PKC has been shown to be important for mediating signal transduction during metamorphosis in other marine invertebrates such as *H. echinata* and the Annelid *Capitella* sp. 1 [22,45]. Based on our observation that m/z 654.5051 and m/z 639.4936 DAG concentrations were greater in larvae treated with MACs from WT when compared to other treatments and the prior literature connecting DAG with metamorphosis in other animals, we investigated the role of the PKC pathway and its importance for bacteria-stimulated metamorphosis in *Hydroides*.

The lipid second messenger diacylglycerol stimulates *Hydroides* metamorphosis.

To further ascertain the potential role of DAG in the metamorphosis signaling pathway, we tested whether DAG alone is sufficient to induce metamorphosis by exogenously adding 1,2-dioctanoyl-sn-glycerol (a putative PKC activator) to *Hydroides* larvae. We chose a form of DAG possessing short 8 carbon acyl chains to promote its solubility in seawater. Adding 1,2-dioctanoyl-sn-glycerol to competent *Hydroides* larvae was sufficient to induce metamorphosis when compared to the solvent controls (Figure 4.1. D). To determine the sensitivity of larvae to 1,2-dioctanoyl-sn-glycerol a dose-response curve showed that *Hydroides* responds to 1,2-dioctanoyl-sn-glycerol with an EC50 of 3.156 μM ($\log(3.156 \times 10^{-6}) = -5.501$) (Figure 4.1. E). These data show that DAG stimulates metamorphosis in *Hydroides* at comparable levels to *P. luteoviolacea* MACs and Mif1. Our results are congruent with previous finding in *H. echinata* where DAG has been shown to stimulate metamorphosis with similar effective concentrations ranging from 5 μM to 100 μM [42].

***Hydroides* possesses a conserved PKC signaling pathway.** DAG signals through several proteins with DAG-binding C1 domains, including PKC. Because PKC signaling has been shown to be important for mediating the metamorphosis in diverse marine animals, we focused our investigation on the stimulation of PKC by DAG in *Hydroides*. In humans, PKC signaling output is heavily determined by cell type and cell lineage, and different cell types are capable of divergent downstream signaling resultant from the same initial stimulus. There are ten isoforms of PKC in humans (nine not

including splice variants), each thought to regulate some distinct, and some overlapping signals [46].

To identify PKC isoforms in *Hydroides* and their expression prior to metamorphosis, we searched the sequenced *Hydroides* genome [24] with each of the known human PKC isoforms. Using PSI-BLAST, we identified seven genes encoding proteins with a PKC kinase domain (Figure 4.2. and Table 4.1.). We used a hidden Markov model domain search (HMMER) to identify the following domains within each putative PKC ortholog; the C2 Ca^{2+} binding domain, the PB1 domain, the C1 DAG/phorbol ester binding domain, a ser/thr protein kinase domain, and the PKC terminal domain [47] (Figure 4.2. and Table S4.2.). A maximum likelihood phylogenetic analysis showed that three *Hydroides* PKC genes cluster with the Ca^{2+}-independent novel human PKC isoforms (Figure 4.2.). Of the *Hydroides* genes that cluster with PKC isoforms, XLOC_080992 (hereafter HePKC1) clusters with the novel PKC genes theta and delta isoforms, while XLOC_012419 (hereafter HePKC2) and XLOC_026127/XLOC_043332 (hereafter HePKC3) cluster with the novel PKC genes eta and epsilon isoforms. Four of the *Hydroides* genes clustered separately from the human PKC isoforms, potentially indicating they are paralogs and may possess an alternative function not relating to PKC. None of the *Hydroides* genes cluster with the conventional PKC genes and, even though the HePKC1 gene possesses the C2 Ca^{2+} binding domain, the architecture of the gene is more similar to that of the Ca^{2+} independent PKC types theta and delta isoforms. When we searched the *Hydroides* transcriptome during the competent stage and a timepoint 30-minutes after the stimulation of metamorphosis by MACs [24], we found that all isoforms

were expressed in the competent larvae (Table 4.1.). Three isoforms increased their expression post induction and four decreased their expression.

Two PKC inhibitors abrogate *Hydroides* metamorphosis in response to MACs and Mif1. Classical and novel PKC proteins are in the cell cytosol and recruited to the membrane by the presence of DAG. Once activated, they release their pseudo-substrate, a portion of the protein which blocks the active site, and then phosphorylate downstream signaling molecules via ATP cleavage [43]. To test whether PKC is important in bacteria-stimulated metamorphosis, we examined the ability of two PKC inhibitors to block *Hydroides* metamorphosis in response to *P. luteoviolacea* MACs and Mif1. The first, Ro 32-0432 is a potent active site competitive inhibitor that is highly selective for PKC type kinases and with low affinity for non-PKC kinases [48]. Ro 32-0432 exhibits a IC50 of 9-37nM and 108nM for conventional PKCs and PKC epsilon, respectively [49,50]. Although less potent, the second inhibitor bisindolylmaleimide IV (Bis IV) is an allosteric uncompetitive inhibitor that shows a high selectivity for PKC over other kinases (IC50 of 0.55μM) [48,51].

To test Ro 32-0432 and Bis IV on PKC in *Hydroides*, we pre-incubated competent larvae with each inhibitor for 60 minutes and subsequently exposed the larvae to MACs extracts from *P. luteoviolacea*. We found that Ro 32-0432 inhibited metamorphosis in the presence of MACs in a dose-dependent manner with an IC50 of 235 nM ($\log(2.35 \times 10^{-7}) = -6.627$) (Figure 4.3. A & B) and Bis IV inhibited with an IC50 concentration of 1.259 μM ($\log(1.259 \times 10^{-6}) = -5.900$) (Figure 4.3. A & C). We also tested whether each inhibitor

blocked metamorphosis in the presence of DAG as the initiator of metamorphosis. We found that both Ro 32-0432 and Bis IV were capable of inhibiting metamorphosis stimulated by either DAG or MACs (Figure 4.3. A & D). While it is unclear whether Ro 32-0432 and Bis IV PKC inhibitors block metamorphosis strictly by inhibiting PKC activity, our data show that metamorphosis stimulated by either DAG or MACs is blocked by Ro 32-0432 and Bis IV PKC inhibitors.

We cannot rule out the possibility that Ro 32-0432 and/or Bis IV inhibit other proteins or processes besides the PKC pathway, leading to the inhibition of *Hydroides* metamorphosis in response to Mif1. In a screen of 300 kinases, Ro 32-0432 and Bis IV inhibited 9 and 4 non-PKC kinases by more than 80%, respectively [52]. In addition to PKCs, Bis IV also inhibits Protein Kinase A at a higher concentration (IC50 of 11.8μM) [51]. Both Ro 32-0432 and Bis IV strongly inhibit Ribosomal protein S6 Kinase alpha-2 (RSK3) and Ro 32-0432 also inhibits other genes in the RSK family, likely because the N-terminal kinase domain is part of the AGC family of kinases, which include PKC's kinase domain [52]. RSK kinases are downstream of ERK1/2 and p38 [53], and because ERK1/2 and p38 MAPKs are implicated in *Hydroides* metamorphosis [24], it is plausible that Ro 32-0432 and/or Bis IV inhibits metamorphosis through RSK. Other kinases that are inhibited by both Bis IV and Ro 32-0432 are the Glycogen Synthase Kinase-3 (GSK-3) α and β isoforms [52]. GSK-3 is known to modulate diverse processes including growth, differentiation and apoptosis in human cells [54]. These processes are all critical for metamorphosis, although it is unknown whether and/or how inhibition of GSK-3 could block metamorphosis in *Hydroides*. In humans the inhibitor Ro 32-0432 and Bis VIII (the

same class of compounds as Bis IV) have been shown to promote the phosphorylation of p38 and JNK MAPK proteins [55,56] and commercial phospho-antibodies to p38 and JNK MAPK cross-react with *Hydroides* homologs [24]. When *Hydroides* larvae were exposed to Bis IV we observed that p38 and JNK total protein and protein phosphorylation increased (Figure S4.1. A), while exposure to Ro 32-0432 marginally increased p38 phosphorylation (Figure S4.1. B). These results are consistent with the effects of Ro 32-0432 and Bis VIII on p38 and JNK MAPK phosphorylation responses in human cell lines.

Our observation that PKC inhibitors block *Hydroides* metamorphosis are consistent with other studies implicating PKC in the metamorphosis of other marine invertebrates. Larvae of the Annelid, *Capitella sp. 1*, undergo metamorphosis in response to arachidonic acid and the known morphogen, juvenile hormone (JH), a hormone which stimulates the PKC pathway in insects [22,57,58]. Additionally, diacylglycerol promotes the metamorphosis of the Cnidarian, *Hydractinia echinata*, and metamorphosis is inhibited by a kinase inhibitor, staurosporine, which inactivates the PKC pathway [20]. In the Cnidarian, *Cassiopea andromeda*, Thieme et al. use the inhibitor Ro 32-0432 to implicate PKC in head morphogenesis from larvae-like buds [59]. Metamorphosis in insects, which are not known to require an external cue to undergo metamorphosis, also utilize PKC signaling in regulating metamorphosis. The mosquito *Aedes aegypti* utilizes the metamorphosis regulating chemical juvenile hormone-III to stimulate PKC via the phospholipase C pathway [58]. With the addition of the data presented here, we can hypothesize that PKC has been adapted by *Hydroides* as a signaling pathway used to respond to bacteria and stimulate metamorphosis.

MACs stimulate the expression and localization of two nuclear hormone receptor genes. Nuclear hormone receptors play key roles in regulating gene expression in response to hormonal signals during metamorphosis in insects and amphibians, and PKC has been shown previously to regulate nuclear hormone receptor activity and/or expression during metamorphosis [60,61]. For example, in the insects *Helicoverpa armigera* and *Drosophila melanogaster*, PKC phosphorylates the ecdysone receptor (EcR), modulating EcR activity during metamorphosis [62,63]. Additionally, EcR expression has been shown to be localized to the brain during silk moth metamorphosis [64]. We therefore hypothesized that *Hydroides* possesses one or more nuclear hormone receptors that are regulated by PKC in the larval brain, and that Ro 32-0432 and Bis IV would inhibit this regulation.

We identified two putative nuclear hormone receptors in *Hydroides* located on different genomic contigs (hereafter, HeNHR1 and HeNHR2) that were upregulated 4.09 fold and 4.15 fold 30-minutes after bacteria-stimulated metamorphosis, respectively (Table 4.1.) [24]. Both HeNHR1 and HeNHR2 contain the putative Zinc finger C4 type domain (e-value 7.5e-26 and 7.5e-26, respectively) and the ligand binding domain of nuclear hormone receptors (e-value 1.8e-15 and 1.8e-15, respectively) (Figure 4.4. A), and both domains together are indicative of nuclear hormone receptor transcription factors.

To observe the expression and localization of HeNHR1 and HeNHR2 transcripts within *Hydroides* larvae with or without MACs and PKC inhibitors Ro 32-0432 and Bis IV, we performed Whole Mount *In Situ* Hybridization (WMISH). To this end, seven-day old larvae were treated for one hour with 1μM Ro 32-0432, 10μM Bis IV or DMSO solvent control and then subjected to WT MACs or buffer for one hour prior to fixation. WMISH using HeNHR1 and HeNHR2-specific probes were stained for an equivalent time between compared groups (Buffer, MACs, MACs with Ro 32-0432, and MACs with Bisindolylmaleimide IV). In larvae treated with MACs, HeNHR1 and HeNHR2 staining occurred in the larval cerebral ganglia (Figure 4.4. C & G and Figure S4.2. C & D), while buffer-treated larvae did not show localization or high expression of either nuclear hormone receptor in the same anatomical location (Figure 4.4. B & F and Figure S4.2. A & B). When the larvae were treated with either Ro 32-0432 or Bis IV before subjection to MACs, the larvae did not show localization or upregulation of HeNHR1 and HeNHR2 to the cerebral ganglia (Figure 4.4. D, E, H, I, and Figure S4.2. E-H). Our results show that *Hydroides* upregulates two nuclear hormone receptors in the cerebral ganglia during metamorphosis, resembling the regulation of EcR during insect metamorphosis. Further, results show that Ro 32-0432 and Bis IV inhibitors block HeNHR1 and HeNHR2 localization or upregulation. The full characterization of HeNHR1 and HeNHR2 and their role of in *Hydroides* metamorphosis will be the subject of a future work.

PKC has been proposed previously to act as a node in a multi-step signal transduction process during bacteria-stimulated metamorphosis in the hydrozoan *Phialidium gregarium* [31]. In the proposed model, serotonin (5-HT) is released by

producing cells, which binds nearby cells causing membrane depolarization and Ca2+ influx, activating PKC signaling and subsequent metamorphic events. The proposed model of 5-HT action was suggested to be different in *Hydroides* [32], in part, because the known PKC activator, 12-O-Tetradecanoylphorbol-13-Acetate (TPA), a phorbol ester, was insufficient to stimulate *Hydroides* metamorphosis [65]. It is unclear why 1,2-dioctanoyl-sn-glycerol stimulates metamorphosis in *Hydroides* (Figure 4.1. D), while TPA does not. However, it has been proposed that the activation of PKC by DAG and TPA is not equivalent [66], and the pathways stimulated by TPA in *Hydroides* might differ from those of activated by DAG, as seen by our data. Our observation that HeNHR1/2 are expressed in the larval cerebral ganglia is consistent with a model where 5-HT positive cells activate PKC and HeNHR1/2 expression during *Hydroides* metamorphosis.

MACs and Mif1 activate *Hydroides* metamorphosis through DAG production, PKC and MAPK. We previously reported that the p38 and JNK MAPKs are required for the stimulation of *Hydroides* metamorphosis by MACs [24]. To further define the signaling pathway involving DAG during the metamorphosis of *Hydroides*, we pre-exposed larvae to the p38 inhibitor SB203580 or the JNK inhibitor SP600125, at the same effective concentrations established previously, 10μM and 2.5μM, respectively [24], and stimulated metamorphosis using DAG (Figure 4.3. D). We found that that DAG is unable to stimulate metamorphosis when larvae are exposed to either SB203580 or SP600125 MAPK inhibitors. These data suggest that MAPK signaling is downstream of DAG signaling during *Hydroides* metamorphosis and suggest that both the PKC and MAPK pathways are required for metamorphosis.

There are discernable parallels between bacteria-stimulated metamorphosis in *Hydroides* and other PKC-, MAPK- and nuclear hormone receptor-mediated host-microbe interactions in other model organisms. For example, PKC delta and p38 MAPK were shown previously to regulate innate immunity in the roundworm *Caenorhabditis elegans*, by mediating the production of antimicrobial peptides in response to a fungal pathogen [67]. These innate immune responses allowed for non-redundant signaling of another PKC isozyme and release of an antimicrobial peptide. PKC control of the MAPK pathway has very dramatic implications for the response of the cell to a given stimulus from simple heat shock response in *Saccharomyces cerevisiae*, and to the control of mechanosensory response in *C. elegans* [68,69]. In *C. elegans*, the nuclear hormone receptor NHR-86 and p38 MAPK drive immune effector gene expression that provide protection against *Pseudomonas aeruginosa* [70]. In *Drosophila*, juvenile hormone and the ecdysone receptor (EcR), which play key roles in metamorphosis, have also been shown to induce and potentiate antimicrobial peptide gene expression [71]. Our future work into the function(s) of Mif1 that stimulate metamorphosis may provide insight into how *P. luteoviolacea* stimulates DAG production, and PKC/MAPK/NHR signal transduction. Understanding the cell signaling pathways that are regulated by *P. luteoviolacea* and its Mif1 effector informs our growing understanding of how bacteria can promote development in eukaryotic organisms.

4.4 Conclusion

Diacylglycerol, PKC and MAPK are highly conserved signaling systems found in diverse metazoans. The present work defines a working model of how *P. luteoviolacea* stimulates *Hydroides* metamorphosis. In this model pathway, MACs and Mif1 produced by bacteria stimulate an increase in DAG. DAG then signals the downstream pathways of PKC and MAPK signaling and activates the expression of two nuclear hormone receptors, HeNHR1 and HeNHR2 to promote metamorphosis (Figure S4.3.). Defining these cascades are important for understanding bacteria-stimulated metamorphosis in *Hydroides* and provides a step toward our broader understanding of how bacteria promote animal development. Defining the signaling systems responsible for metamorphosis in *Hydroides* provides insight that may inform efforts to promote ecosystem remediation or antifouling technologies.

4.5 Materials and methods

***Hydroides* Collection and Maintenance.** Specimens of *Hydroides elegans* were collected from Quivira Basin, San Diego, CA and propagated as described previously [37]. Briefly, gametes were harvested from adult animals. Fertilized embryos were mixed and moved to a 1 L beaker containing 0.45 µm filtered artificial seawater with *Isochrysis* algae (6×10^4 cells/mL). On the second day, larvae were diluted to 5 larvae/mL. Water changes were performed, and new algae was added daily until reaching competence (6-8 days).

Production of MACs Extract. Purification of MACs was carried out as previously described [72]. Briefly, from frozen stock, *Pseudoalteromonas luteoviolacea* HI1 and genetic derivatives were struck out to single colonies on to Sea Water Tryptone (SWT) media (35.9 g/L Instant Ocean, 2.5 g/L tryptone, 1.5 g/L yeast extract, 1.5 mL/L glycerol, 15 g/L agar for solid media) and grown overnight at 30˚C. A single colony was inoculated into 5 mL SWT culture and grown overnight at 30˚C, 200 rpm. The overnight culture was inoculated at 1:100 into a 50 mL flask and grown for 10 hr at 30˚C, 200 rpm. The 50 mL overnight culture was then centrifuged at 4,800 rcf for 20 min at 4˚C. The supernatant was removed, and the pellet was gently suspended in 5 mL of extraction buffer (20 mM Tris Base, 1 M NaCl, pH 7.5) with aid of a serological pipette. The suspended pellet was then centrifuged again at 4,800 rcf for 20 mins at 4˚C. The supernatant was then removed and again centrifuged at 4,800 rcf for 20 mins at 4˚C to remove any remaining cells. After

centrifugation only the top 3 mL of supernatant was removed. MAC extract up to 2 days old was used for metamorphosis assays.

Metamorphic induction of larvae and extraction of total lipids. Larvae were grown for 7 days until reaching competency, as described above. Larvae were then exposed to extraction buffer (20mM Tris, 1M NaCl, pH 7.5), or extracted MACs from *P. luteoviolacea* wild type, Δ*macB* or Δ*mif1*. The larvae were incubated with the MACs or buffer control at a 1:50 concentration for 1 hour. After incubation, larvae were then subjected to lipid extraction following the previously established Bligh Dyer protocol [73]. In brief, ASW was removed and the larvae were resuspended in 300 µL of 1:2 mixture of chloroform:methanol and vortexed vigorously for 2 mins. An additional 100 µL of chloroform was added and the sample vortexed for another 30 sec. 100 µL of water was then added to separate the organic and aqueous layers and briefly vortexed. The sample was then centrifuged at >10,000 G for 10 mins to further clarify the layers. The aqueous phase was then subject to UV 280 nm protein concentration analysis to determine relative quantities of larval protein extract and to normalize the total lipid concentrations. The chloroform phase was removed and dried under nitrogen stream. Samples were resuspended with 100% acetonitrile normalized by protein concentration to a total concentration of 4.94 mg/mL. The sample was resuspended via repeated water bath sonication for 5 mins and vortexing for 30 sec totaling 5 times.

Metabolomics analyses of *Hydroides* larvae exposed to MACs. Untargeted LCMS analyses were performed on the tubeworm extracts using a Bruker Elute UHPLC

coupled with an Impact II QTOF mass spectrometer. The first analysis was performed on a 2 mm Dacapo DX-C18 column (Imtakt, Portland OR, USA) in reverse phase. A gradient elution was used from 40% channel A (0.1% formic acid in 98% water and 2% acetonitrile) to 100% channel B (0.1% formic acid in 98% acetonitrile and 2% water) over 22 minutes with a hold of 100% channel B over 10 minutes using a flow rate of 200 µL/min and a 5 µL injection volume. The mass spectrometer was operated in positive mode using a mass range of 50 - 1000 *m/z* at a scan rate of 8 Hz. The end plate offset was set to 500V, the capillary voltage was set to 4200 V with nebulizer gas pressure set at 1.0 bar, the dry gas flow rate at 5.0 L/min and the dry gas temperature at 250ºC. Ion funnels 1 and 2 were set to 200 and 400 V respectively. The hexapole was set to 90 V. The quadrupole ion energy was set to 3.0 eV and low mass set to 50 m/z. The collision cell collision energy was set to 7 eV, and a pre-pulse storage time of 7.5 µs. Stepping was used with the mode on basic, the always collision RF went from 900.0 to 2500.0 V with a transfer time from 27.0 to 90.0 µs and timing from 10 to 90%. The MS/MS only collision energy went from 50 to 125% and the timing went from 50 to 50%. The Scan mode was on MRM with the number of precursors as 5. The threshold absolute threshold (per 1000 sum.) was 31 cts. Smart Exclusion with 5x. Active exclusion excluded after 3 Spectra, released after 1.00 min, with a Reconsidered Precursor, if the current intensity/previous intensity is at 5.0. Untargeted data was analyzed using XCMS Online [39], using a multigroup job to identify lipid metabolites significantly different ($p < 0.01$, fold change > 0.05) between larvae extracts exposed to buffer, MACs extracted from *P. luteoviolacea*, wild type, Δ*macB* and Δ*mif1*. The data are publicly available at XCMS

(https://xcmsonline.scripps.edu/landing_page.php?pgcontent=listPublicShares) public job id #1502723.

Identification of PKC homologs in the *Hydroides* genome. Seven *Hydroides* PKC genes and gene homologs were found by BLASTn using the ten known human PKC isoforms as queries against the translated genome of *Hydroides elegans* [24]. Once identified, the selected genes and isoforms of those genes were then searched against the NCBI non-redundant database using a PSI-BLAST and performing 5 iterations with a E-value cutoff of 0.05 and 500 sequences per iteration [74]. PKC proteins were searched for known domains by HMMER biosequence analysis using hidden Markov models [47], where significant hits to Pfam or Gene3d were identified (Table S4.2.). A maximum likelihood phylogeny was generated using the human PKC isoforms and the seven identified *Hydroides* PKC genes. An alignment was first performed using Mafft e-ins-i alignment with default parameters [75]. Aligned amino acid sequences were used to generate a maximum likelihood tree using PhyML through the ATGC Montpellier Bioinformatics Platform [76]. The Smart Model Selection [77,78] option was used to calculate the best substitution model for the data, in which LG+G+I+F was selected. The branches are supported by 100 resamples. A previously published transcriptome of *Hydroides* (Shikuma et al., 2016) was mined to identify expression levels of larval transcripts at 6 d and at 30 mins post exposure to MACs (Table 4.1.).

***Hydroides* metamorphosis assays**. Competent *Hydroides* larvae were concentrated to 40 larvae/mL and incubated for one hour with penicillin and streptomycin.

The larvae and antibiotics were then transferred into 24-well plates at 1 mL per well for a final concentration of ~40 larvae/well. Inhibitors and activators used in this work include Ro 32-0432 hydrochloride, Tocris Bioscience, Cat# 1587. 1,2-Dioctanoyl-sn-glycerol, Cayman Chemical, Cat# 62225. Bisindolylmaleimide IV, Cayman Chemical, Cat # 13299. SB 203580 hydrochloride, Tocris Bioscience, Cat# 1402. SP 600125, Sigma-Aldrich, Cat# w5567. Inhibitors were dissolved in acetonitrile, or DMSO according to manufacturer recommendation. All assays included the appropriate solvent controls for the given inhibitor tested, solvent volume was equal across all inhibitor concentrations and control wells. Inhibitors were added 1 hr prior to addition of either MACs or candidate inducers. The range of the concentration tested was determined by larval sensitivity and toxicity, ranging from 100 nM to 100 μM. Larval metamorphosis was scored visually 24 hours after addition of MACs extracts or DAG. Metamorphosis was scored as positive for larvae observed to possess an elongated body, loss of cilia, formation of branchial rudiments and the formation of a calcareous tube. Assays were performed with at least 3 biological replicates (n=3), where larvae were derived from different male and female individuals.

Pretreatment of larvae for western blot and whole mount in situ hybridization. Larvae were first grown for 7 days following the collection and maintenance protocols. 1,000 larvae were then separated and concentrated into 2 mL of artificial sea water. Larvae were then treated with penicillin 100 ug/mL and streptomycin 100 ug/mL for 1 hour. Inhibitors Ro-32-0432 1μM and Bis IV 10μM and solvent controls (ACN/DMSO) were then added to the larvae for another hour. MACs 1:75 dilution or 1,2-dioctanoyl-sn-glycerol was added to the larvae for a final hour before takedown.

Whole mount *in situ* hybridization. The WMISH procedure was modified from methods by Seaver and Kaneshige [79]. Sequences for HeNHR1 and HeNHR2 (Table S4.4.) were identified from a previously performed *Hydroides elegans* transcriptome analysis [24]. WMISH RNA probes were generated using the protocol outlined in [80]. In short, total RNA was isolated from treated larvae via TRIzol (Thermo fisher CAT#15596018) and cDNA was created using oligo d(T)23VN primers (New England Biolabs CAT#E6300s). From the cDNA the 1st PCR product was produced and validated for size (Table S4.5.). A second PCR with T7 RNA polymerase engineered reverse primers were used to make the template for the probes and were validated by sanger sequencing (Table S4.5.). Probes were made using T7 RNA polymerase (Lucigen CAT#30223-1) with dioxigenin-UTP (Sigma Aldrich CAT#11209256910). The negative control probe was made using ascidian cDNA for a gene which is not present on the *Hydroides genome*. WMISH was performed by first relaxing larvae by adding 1 volume of 6.5% MgCl for 2 minutes. The larvae were fixed in 4% paraformaldehyde in 0.5M NaCl, 0.1M MOPS pH 7.5 overnight at 4˚C. The larvae were then dehydrated by washing in 25% EtOH in 1xPBS tween (1.86mM NaH_2PO_4 8.41mM Na_2HPO_4 175mM NaCl pH 7.4 0.1% tween-20), 50% EtOH PBS tween, and 75% EtOH PBS tween before storing them in 100% EtOH at -80˚C. The larvae were rehydrated by subsequent washes in 75%, 50%, 25%, 0% EtOH in PBS tween. Larvae were then digested with proteinase K 0.01mg/mL in PBS tween for 5 mins. The reaction was stopped with 3 washes in PBS tween plus 2mg/mL glycine. The larvae were then washed in 1% triethanolamine with 1.5µL/500µL acetic anhydride twice. Then washed twice in PBS tween. The larvae were then refixed in 4% paraformaldehyde in

PBS tween for 1 hour at room temperature followed by five washes in PBS tween. To kill endogenous alkaline phosphatase the larvae were heated to 80˚C for 10 minutes in PBS tween. The larvae were then washed in hybridization buffer (50% formamide, 0.075 Na citrate, 750mM NaCl, 50µg/mL heparin sodium (Selleck chemicals CAT#70288-86-7), 0.1% tween, 1% SDS, 50µg/mL herring sperm DNA, pH 4.5), and after the first wash was left in the hybridization buffer overnight at 60˚C. The probes were diluted to 3.0ng/µL in hybridization buffer and boiled at 80˚C before being added to the larvae where they were allowed to hybridize for at least 48 hours at 60˚C. The probe was removed, and the larvae were washed with 75% hybridization buffer and 25% 2X SSC (20x SSC 0.3M Na citrate and 3M NaCl). Followed by 50% hybridization buffer and 50% 2X SSC, then 25% hybridization buffer and 75% 2X SSC, finally by two washes with 2x SSC buffer. The larvae were then exchanged into PBS tween by washing with 0.05X SSC twice followed by, 75% 0.05X SSC and 25% PBS tween, then, 50% 0.05X SSC and 50% PBS tween, 25% 0.05X SSC and 75% PBS tween, finally by washing with 100% PBS tween five more times. The larvae were then blocked in 0.5% Roche blocking solution (Sigma Aldrich CAT#9000-7-1-9) in 0.1M Tris pH 7.5, 0.15M NaCl for one hour. The blocking solution was washed and then the anti-DIG antibody (Sigma CAT# 11093274910) was added to the blocking buffer at 1:5000 dilution and the larvae were incubated at 4˚C overnight. The larvae were then washed 5 times in PBT (1xPBS, 0.2% triton x-100 and 0.1% BSA, Thermo fisher CAT# AAJ6465522). The larvae were then washed in the alkaline phosphatase reaction buffer without MgCl, AP buffer (100mM NaCl, 50mM MgCl, 100mM Tris pH 9.5, 0.5% tween-20). Then washed twice with the AP buffer to equilibrate the pH and prevent precipitation. The larvae were developed in AP buffer plus 200uL/10mL

NBT/BCIP stock solution (Millapore sigma CAT# 11681451001) in the dark until purple staining appeared (1hr for Beta tubulin prove, 2 hours for HeNHR1, HeNHR2 and scramble probe). NBT/BCIP incubation was performed for the same amount of time for treatments exposed to each HeNHR1 or HeNHR2 probe. Larvae were then washed 5 times in PBS tween before mounting on slides in 80% glycerol.

Western blot. Protein was recovered on ice by first centrifuging larvae at 4000rpm for 5min and removing ~1950µL of sea water and resuspending by vortexing larvae in a lysis solution of 50mM tris pH 7.6, 1% triton X-100, 150mM NaCl. Larvae were then frozen at -80˚C to aid in lysis. After thawing, the sample was centrifuged at 21,000g for 20min and the pellet was discarded. Protein was quantified by Bio-Rad protein assay (CAT #5000001). 15ug of protein was loaded onto a 4-12% SDS-polyacrylamide gel and run for 60 min at 110V. The protein was then transferred onto a PVDF membrane. The membrane was dried and recharged with methanol. Membrane was washed with TBS tween 1% (TBST), 3 times and primary antibodies were added at a 1:1000 dilution and rocked in a 10% BSA TBST solution overnight (Cell Signaling Technologies CAT #s 9212, 9252, 9912, 9913). Membrane was washed 3x with TBST for 10 mins each and incubated with secondary-HRP (Novus Biological CAT#BP1-75306) conjugated antibody at 1:10,000 for 1 hour. 3x final washes with TBST for 15 min were performed before final visualization with West Femto substrate (Thermo Fisher CAT#34095) on a Bio-Rad Gel Doc XR.

4.6 Acknowledgements

We would like to thank Dr. Giselle Cavalcanti, Dr. Tiffany Dunbar, and Mr. Andriy Fedoriouk for their valuable feedback on the manuscript. This work was supported in part by the National Science Foundation (1942251, N.J.S.; 2017232404, A.T.A.), the Office of Naval Research (N00014-17-1-2677 and N00014-20-1-2120 N.J.S.), the Gordon and Betty Moore Foundation (GBMF9344, https://doi.org/10.37807/GBMF9344), the Alfred P. Sloan Foundation, Sloan Research Fellowship (N.J.S.) and the ARCS Foundation (K.E.M., A.T.A.).

Chapter 4 has been accepted and is currently in the final stages of publishing by Developmental Biology for publication (2022). K.E. Malter, M. Esmerode, M. Damba, A.T. Alker, E. Forsberg, and N.J. Shikuma The dissertation author is a coauthor of this manuscript. My specific contributions include Figure 4.1., Figure 4.2., Figure 4.3., Figure 4.4., table 4.1., tableS4.1., table S4.2., table S4.3., table S4.4., table S4.5., Figure S4.1., Figure S4.2. and writing and editing the initial drafts and all revisions.

4.7 References

1. Gilbert, S. F., Bosch, T. C. G. & Ledón-Rettig, C. Eco-Evo-Devo: developmental symbiosis and developmental plasticity as evolutionary agents. *Nat. Rev. Genet.* **16**, 611–622 (2015).

2. Cavalcanti, G., Alker, A., Delherbe, N., Malter, K. E. & Shikuma, N. J. The Influence of Bacteria on Animal Metamorphosis. *Annu. Rev. Microbiol.* **74**, in press (2020).

3. Hadfield, M. G. Biofilms and Marine Invertebrate Larvae: What Bacteria Produce That Larvae Use to Choose Settlement Sites. *Ann. Rev. Mar. Sci.* **3**, 453–470 (2011).

4. Hadfield, M. G., Carpizo-Ituarte, E. J., Carmen, K. Del & Nedved, B. T. Metamorphic competence, a major adaptive convergence in marine invertebrate larvae. *Am. Zool.* **41**, 1123–1131 (2001).

5. Zobell, C. E. & Allen, E. C. The Significance of Marine Bacteria in the Fouling of Submerged Surfaces. *J. Bacteriol.* **29**, 239–51 (1934).

6. Tata, J. R. *Hormonal Signaling and Postembryonic Development (Molecular Biology Intelligence Unit)*. (1998).

7. Lawrence, I. G., Jamshed, R. T. & Burr, G. A. *Metamorphosis Postembryonic Reprogramming of Gene Expression in Amphibian and Insect Cells*. (Academic press, 1996). doi:https://doi.org/10.1016/B978-0-12-283245-1.50023-3.

8. Brown, D. D. & Cai, L. Amphibian metamorphosis. *Dev. Biol.* **306**, 20–33 (2007).

9. Hill, R. J., Billas, I. M. L., Bonneton, F., Graham, L. D. & Lawrence, M. C. Ecdysone receptors: From the ashburner model to structural biology. *Annu. Rev. Entomol.* **58**, 251–271 (2013).

10. Hadfield, M. G. Why and how marine-invertebrate larvae metamorphose so fast. *Semin. Cell Dev. Biol.* **11**, 437–443 (2000).

11. Carpizo-ituarte, E. & Hadfield, M. G. Transcription and Translation Inhibitors Permit Metamorphosis up to Radiole Formation in the Serpulid Polychaete *Hydroides elegans* Haswell. *Mar. Biol. Lab.* **204**, 114–125 (2003).

12. Thiyagarajan, V., Wong, T. & Qian, P. Y. 2D gel-based proteome and phosphoproteome analysis during larval metamorphosis in two major marine biofouling invertebrates. *J. Proteome Res.* **8**, 2708–2719 (2009).

13. Wong, Y. H., Arellano, S. M., Zhang, H., Ravasi, T. & Qian, P. Y. Dependency on

de novo protein synthesis and proteomic changes during metamorphosis of the marine bryozoan *Bugula neritina* . *Proteome Sci.* **8**, 1–14 (2010).

14. Strader, M. E., Aglyamova, G. V. & Matz, M. V. Molecular characterization of larval development from fertilization to metamorphosis in a reef-building coral. *BMC Genomics* **19**, 1–17 (2018).

15. Liang, X. *et al.* Effects on larval metamorphosis in the mussel *Mytilus coruscus* of compounds that act on downstream effectors of G-protein-coupled receptors. *J. Mar. Biol. Assoc. United Kingdom* **98**, 333–339 (2018).

16. Bryan, P. J., Qian, P., Kreider, J. L. & Chia, F. Induction of larval settlement and metamorphosis by pharmacological and conspecific associated compounds in the serpulid polychaete *Hydroides elegans* . *Mar. Ecol. Prog. Ser.* **146**, 81–90 (1997).

17. Li, Z. The Relationship of Protein Kinase C and Nitric Oxide Signaling in Metamorphosis of Marine Gastropod Larvae, Crepidula fornicata. 1–22 (2011).

18. Leise, E. M., Thavaradhara, K., Durham, N. R. & Turner, B. E. Serotonin and Nitric Oxide Regulate Metamorphosis in the Marine Snail *Ilyanassa obsoleta* . *Am. Zool.* **41**, 258–267 (2001).

19. Yool, A. J. *et al.* Excess Potassium Induces Larval Metamorphosis in Four Marine Invertebrate Species. *Biol. Bull.* **170**, 255–266 (1986).

20. Leitz, T. & Klingmann, G. Metamorphosis in *Hydractinia* : Studies with activators and inhibitors aiming at protein kinase C and potassium channels. *Roux's Arch. Dev. Biol.* **199**, 107–113 (1990).

21. Pearce, C. M. & Scheibling, R. E. Induction of metamorphosis of larval echinoids (*Strongylocentrotus droebachiensis* and *Echinarachnius parma*) by potassium chloride (KCl). *Invertebr. Reprod. Dev.* **26**, 213–220 (1994).

22. Biggers, W. J. & Laufer, H. Settlement and metamorphosis of *Capitella* larvae induced by juvenile hormone-active compounds is mediated by protein kinase C and ion channels. *Biol. Bull.* **196**, 187–198 (1999).

23. Carpizo-Ituarte, E. & Hadfield, M. G. Stimulation of Metamorphosis in the Polychaete Hydroides elegans Haswell (Serpulidae). *Biol. Bull.* **194**, 14–24 (1998).

24. Shikuma, N. J., Antoshechkin, I., Medeiros, J. M., Pilhofer, M. & Newman, D. K. Stepwise metamorphosis of the tubeworm *Hydroides elegans* is mediated by a bacterial inducer and MAPK signaling. *Proc. Natl. Acad. Sci.* **113**, 10097–10102 (2016).

25. Chambon, J. P., Nakayama, A., Takamura, K., McDougall, A. & Satoh, N. ERK-

and JNK-signalling regulate gene networks that stimulate metamorphosis and apoptosis in tail tissue of *ascidian* tadpoles. *Development* **134**, 1203–1219 (2007).

26. Amador-Cano, G., Carpizo-Ituarte, E. & Cristino-Jorge, D. Role of protein kinase C, G-protein coupled receptors, and calcium flux during metamorphosis of the sea urchin *Strongylocentrotus purpuratus*. *Biol. Bull.* **210**, 121–131 (2006).

27. Yamamoto, H., Tachibana, A., Matsumura, K. & Fusetani, N. Protein Kinase C (PKC) Signal Transduction System Involved in Larval Metamorphosis of the Barnacle, *Balanus amphitrite* . *Zoological Science* **12**, 391–396 (1995).

28. Henningi, G., Hofmann, D. K. & Yahu, Y. B. Metamorphic processes in the soft corals *heteroxenia fuscescens* and *xenia umbellata* : The effect of protein kinase c activators and inhibitors. *Invertebr. Reprod. Dev.* **34**, 35–45 (1998).

29. Freeman, G. & Ridgway, E. B. Cellular and intracellular pathways mediating the metamorphic stimulus in hydrozoan planulae. *Roux's Arch. Dev. Biol.* **199**, 63–79 (1990).

30. Schneider, T. & Leitz, T. Protein kinase C in hydrozoans: involvement in metamorphosis of *Hydractinia* and in pattern formation of *Hydra* . *Roux's Arch. Dev. Biol.* **203**, 422–428 (1994).

31. McCauley, D. W. Serotonin plays an early role in the metamorphosis of the hydrozoan *Phialidium gregarium*. *Dev. Biol.* **190**, 229–240 (1997).

32. Nedved, B. T. Neuromuscular Development and Metamorphosis In the Serpulid Polychaete Hydroides Elegans. (UNIVERSITY OF HAWAIʻI AT MANOĀ, 2010).

33. Nedved, B. T. & Hadfield, M. G. Hydroides elegans (Annelida: Polychaeta): A Model for Biofouling Research. *Mar. idustrial biofouling* **4**, 203–217 (2009).

34. Huang, Y., Callahan, S. & Hadfield, M. G. Recruitment in the sea : bacterial genes required for inducing larval settlement in a polychaete worm. (2012). doi:10.1038/srep00228

35. Huang, S. Y. & Hadfield, M. G. Composition and density of bacterial biofilms determine larval settlement of the polychaete Hydroides elegans. *Mar. Ecol. Ser.* **260**, 161–172 (2003).

36. Shikuma, N. J. Bacteria-Stimulated Metamorphosis: an Ocean of Insights from Investigating a Transient Host-Microbe Interaction. *mSystems* **6**, 1–5 (2021).

37. Shikuma, N. J. *et al.* Marine tubeworm metamorphosis induced by arrays of bacterial phage tail-like structures. *Science (80-.).* **343**, 529–33 (2014).

38. Ericson, C. F. *et al.* A contractile injection system stimulates tubeworm metamorphosis by translocating a proteinaceous effector. *Elife* **8**, 1–19 (2019).

39. Gowda, H. *et al.* Interactive XCMS online: Simplifying advanced metabolomic data processing and subsequent statistical analyses. *Anal. Chem.* **86**, 6931–6939 (2014).

40. Nishizuka, Y. Intracellular Signaling by Hydrolysis of Phospholipids and Activation of Protein Kinase C. *Science (80-.).* **258**, 607–614 (1992).

41. Titball, R. W. Bacterial Phospholipases C. *Microbiol. Rev.* **57**, 347–366 (1993).

42. Leitz, T. & Müller, W. A. Evidence for the involvement of PI-signaling and diacylglycerol second messengers in the initiation of metamorphosis in the hydroid Hydractinia echinata Fleming. *Dev. Biol.* **121**, 82–89 (1987).

43. Nishizuka, Y. Protein kinase C and lipid signaling for sustained cellular responses. *FASEB* **9**, 484–496 (1995).

44. Brose, N. & Rosenmund, C. Move over protein kinase C, you've got company: alternative cellular effectors of diacylglycerol and phorbol esters. *J. Cell Sci.* **115**, 4399–4411 (2002).

45. Leitz, T. & Wagner, T. The marine bacterium *Alteromonas espejiana* induces metamorphosis of the hydroid *Hydractinia echinata* . *Mar. Biol.* **115**, 173–178 (1993).

46. Black, A. R. & Black, J. D. Protein kinase C signaling and cell cycle regulation. *Front. Immunol.* **3**, 1–18 (2012).

47. Finn, R. D., Clements, J. & Eddy, S. R. HMMER web server: interactive sequence similarity searching. *Nucleic Acids Res.* **39**, W29-37 (2011).

48. Wu-Zhang, A. X. & Newton, A. C. Protein kinase C pharmacology: refining the toolbox. *Biochem. Journals* **452**, 195–209 (2013).

49. Wilkinson, S. E., Parker, P. J. & Nixon, J. S. Isoenzyme specificity of bisindolylmaleimides, selective inhibitors of protein kinase C. *Biochem. J.* **294**, (1993).

50. Fabre, S., Prudhomme, M. & Rapp, M. Protein kinase C inhibitors; Structure—activity relationships in K252c-related compounds. *Bioorg. Med. Chem.* **1**, 193–196 (1993).

51. Davis, P. D. *et al.* Inhibitors of Protein Kinase C. 1. 2,3-Bisarylmaleimides. *J. Med. Chem.* **35**, 177–184 (1992).

52. Anastassiadis, T., Deacon, S. W., Devarajan, K., Ma, H. & Peterson, J. R. Comprehensive assay of kinase catalytic activity reveals features of kinase inhibitor selectivity. *Nat. Biotechnol.* **29**, 1039–1045 (2011).

53. Anjum, R. & Blenis, J. The RSK family of kinases: Emerging roles in cellular signalling. *Nat. Rev. Mol. Cell Biol.* **9**, 747–758 (2008).

54. Patel, P. & Woodgett, J. R. Glycogen Synthase Kinase 3: A Kinase for All Pathways? *Curr. Top. Dev. Biol.* **123**, 277–302 (2017).

55. Ohtsuka, T. & Zhou, T. Bisindolylmaleimide VIII enhances DR5-mediated apoptosis through the MKK4/JNK/p38 kinase and the mitochondrial pathways. *J. Biol. Chem.* **277**, 29294–29303 (2002).

56. Kamiguti, A. S. *et al.* Regulation of hairy-cell survival through constitutive activation of mitogen-activated protein kinase pathways. *Oncogene* **22**, 2272–2284 (2003).

57. Biggers, W. J. & Laufer, H. Detection of Juvenile Hormone-Active Compounds by Larvae of the Marine Annelid *Capitella* sp. I. *Arch. Insect Biochem. Physiol.* **32**, 475–484 (1996).

58. Liu, P., Peng, H.-J. & Zhu, J. Juvenile hormone-activated phospholipase C pathway enhances transcriptional activation by the methoprene-tolerant protein. *Proc. Natl. Acad. Sci.* **112**, E1871–E1879 (2015).

59. Thieme, C. & Hofmann, D. K. Control of head morphogenesis in an invertebrate asexually produced larva-like bud (Cassiopea andromeda; Cnidaria: Scyphozoa). *Dev. Genes Evol.* **213**, 127–133 (2003).

60. Laudet, V. The origins and evolution of vertebrate metamorphosis. *Curr. Biol.* **21**, R726–R737 (2011).

61. Riddiford, L. M., Hiruma, K., Zhou, X. & Nelson, C. A. Insights into the molecular basis of the hormonal control of molting and metamorphosis from *Manduca sexta* and *Drosophila melanogaster*. *Insect Biochem. Mol. Biol.* **33**, 1327–1338 (2003).

62. Chen, C. H. *et al.* Protein kinase C delta phosphorylates ecdysone receptor B1 to promote gene expression and apoptosis under 20-hydroxyecdysone regulation. *Proc. Natl. Acad. Sci. U. S. A.* **114**, E7121–E7130 (2017).

63. Sun, Y., An, S., Henrich, V. C., Sun, X. & Song, Q. Proteomic identification of PKC-mediated expression of 20E-induced protein in drosophila melanogaster. *J. Proteome Res.* **6**, 4478–4488 (2007).

64. Hossain, M., Shimizu, S., Fujiwara, H., Sakurai, S. & Iwami, M. EcR expression in

the prothoracicotropic hormone-producing neurosecretory cells of the *Bombyx mori* brain: An indication of the master cells of insect metamorphosis. *FEBS Journal* **273**, 3861–3868 (2006).

65. Holm, E. R., Nedved, B. T., Carpizo-Ituarte, E. & Hadfield, M. G. Metamorphic-Signal Transduction in Hydroides elegans (Polychaeta: Serpulidae) Is Not Mediated by a G Protein. *Biol. Bull.* **195**, 21–29 (1998).

66. Slater, S. J. *et al.* Protein kinase Cα contains two activator binding sites that bind phorbol esters and diacylglycerols with opposite affinities. *J. Biol. Chem.* **271**, 4627–4631 (1996).

67. Ziegler, K. *et al.* Antifungal Innate Immunity in *C. elegans* : PKC d Links G Protein Signaling and a Conserved p38 MAPK Cascade. *Cell Host Microbe* **5**, 341–352 (2009).

68. Kamada, Y., Jung, U. S., Piotrowski, J. & Levin, D. E. The protein kinase C-activated MAP kinase pathway of *Saccharomyces cerevisiae* mediates a novel aspect of the heat shock response. *genes Dev.* **9**, 1559–1571 (1995).

69. Hyde, R., Corkins, M. E., Somers, G. A. & Hart, A. C. PKC-1 acts with the ERK MAPK signaling pathway to regulate *C. elegans* mechanosensory response. *Genes Brain Behav.* **10**, 286–298 (2011).

70. Peterson, N. D. *et al.* The nuclear hormone receptor NHR-86 controls anti-pathogen responses in *C. elegans*. *PLoS Genet.* **15**, 1–19 (2019).

71. Flatt, T. *et al.* Hormonal Regulation of the Humoral Innate Immune Response in Drosophila melanogaster. *J. Exp. Biol.* **211**, 2712–2724 (2008).

72. Rocchi, I. *et al.* A Bacterial Phage Tail-like Structure Kills Eukaryotic Cells by Injecting a Nuclease Effector. *Cell Rep.* **28**, 295-301.e4 (2019).

73. Bligh, E. G. & Dyer, W. J. A Rapid Method of Total Lipid Extraction and Purification. *Can. J. Biochem. Physiol.* **37**, 911–917 (1959).

74. Schäffer, A. A. *et al.* Improving the accuracy of PSI-BLAST protein database searches with composition-based statistics and other refinements. *Nucleic Acids Res.* **29**, 2994–3005 (2001).

75. Katoh, K. & Standley, D. M. MAFFT Multiple Sequence Alignment Software Version 7: Improvements in Performance and Usability. *Mol. Biol. Evol.* **30**, 772–780 (2013).

76. Guindon, S. & Gascuel, O. A Simple, Fast, and Accurate Algorithm to Estimate Large Phylogenies by Maximum Likelihood. *Syst. Biol.* **52**, 696–704 (2003).

77. Guindon, S. *et al.* New Algorithms and Methods to Estimate Maximim-Likelihood Phylogenies Assessing the Performance of PhyML 3.0. *Syst. Biol.* **59**, 307–321 (2010).

78. Lefort, V., Longueville, J.-E. & Gascuel, O. SMS: Smart Model Selection in PhyML. *Mol. Biol. Evol.* **34**, 2422–2424 (2017).

79. Seaver, E. C. & Kaneshige, L. M. Expression of 'segmentation' genes during larval and juvenile development in the polychaetes *Capitella sp. I* and *H. elegans*. *Dev. Biol.* **289**, 179–194 (2006).

80. Hua, R., Yu, S., Liu, M. & Li, H. A PCR-based method for RNA probes and applications in neuroscience. *Front. Neurosci.* **12**, 1–11 (2018).

Table 4.1. Homology and expression of *Hydroides* PKC and NHR proteins. Genes identified as PKC or NHR gene isoforms or homologs were identified using PSI-BLAST to identify the closest human or animal homolog or until convergence in which case the top hit is represented. RNA seq Fragments Per Kilobase of transcript per Million mapped reads (FPKM) was identified for larvae at competency (6 days post fertilization) or larvae 30 min post-induction of metamorphosis with *P. luteoviolacea* from previously published data [24].

GENE ID	PSI-BLAST GENE IDENTIFICATION	SPECIES NAME	QUERY COVER	E-VALUE	% IDENTITY	COMPETENT LARVAE FPKM	30 MINS POST-INDUCTION FPKM
XLOC_080992 HEPKC1	Protein Kinase C delta a isoform X2	*Megalops cyprinoides*	99%	0	51.65 %	1.37262	1.51084
XLOC_012419 HEPKC2	Protein Kinase C epsilon type	*Homo sapiens*	56%	0	77.22 %	1.20571	1.12477
XLOC_026127/XLOC_043332 HEPKC3	Protein Kinase C epsilon type	*Homo sapiens*	74%	0	62.89 %	4.17854	4.9028
XLOC_064437	Protein Kinase C epsilon type	*Homo sapiens*	73%	0	22.72 %	0.0518709	0.0313017
XLOC_091043	Protein Kinase C delta-type	*Homo sapiens*	77%	0	23.81 %	2.04218	1.6393
XLOC_083546/XLOC_137410	Protein Kinase C delta-type	*Homo sapiens*	53%	2.00 E-48	33.77 %	0.0620922	0.0159114
XLOC_037648	Protein Kinase C delta type	*Myripristis murdjan*	94%	0	27.91 %	1.29021	1.43314
XLOC_089429 HENHR1	Ecdysone-induced protein	*Photinus pyralis*	75%	0	21.63 %	5.4852	22.6351
XLOC_109682 HENHR2	Peroxisome proliferator-activated receptor	*Thunnus maccovii*	73%	0	22.83 %	4.59586	17.6312

Figure 4.1. Lipidomics of *Hydroides elegans* metamorphosis in response to MACs and the role of DAG in metamorphosis initiation. (**A**) Experimental design showing *Hydroides* larvae treated with extraction buffer, wild type MACs extract, Δ*macB* MACs extract or Δ*mif1* MACs extract for 1 hour before total lipids were removed by chloroform/methanol extraction, lipidomic analyses and data analyses using XCMS. (**B**) A cloud plot shows all significant features identified by univariate t-test ($p<0.01$), with more significant features in darker blue and relative intensity indicated by circle size. (**b**) The inset represents the relative intensity of two DAG molecules across the varying conditions as displayed on the cloud plot. The y-axis represents mass to charge of individually identified compounds, and x-axis represents relative hydrophobicity as the retention time. (**C**) Relative intensity of signal from two diacylglycerols (m/z = 639.4936) and (m/z = 654.5051) after treatment with extraction buffer, wild type MACs extract, Δ*macB* MACs extract or Δ*mif1* MACs extract. Metabolomics data are represented as the mean signal intensity ± SD of n=6 biological replicates. P-values by one-way ANOVA and Tukey's multiple comparison test between WT MACs and buffer, Δ*macB*, or Δ*mif1* were p-value=0.0705, 0.0626, and 0.1629 respectively for DAG m/z = 639.4936 and p-value of 0.0006, 0.0004, and 0.0004 for DAG m/z 654.5051. (**D**) Metamorphosis assay with *Hydroides* larvae in Artificial Seawater (ASW), 1:1,000 acetonitrile solvent control, 100 µM 1,2-dioctanoyl-sn-glycerol (DAG), or 1:50 dilution of MACs extract. Data are represented as the mean ± SD of 4 biological replicates. (**E**) Metamorphosis assay with competent larvae soaked in increasing concentrations of 1,2-dioctanoyl-sn-glycerol

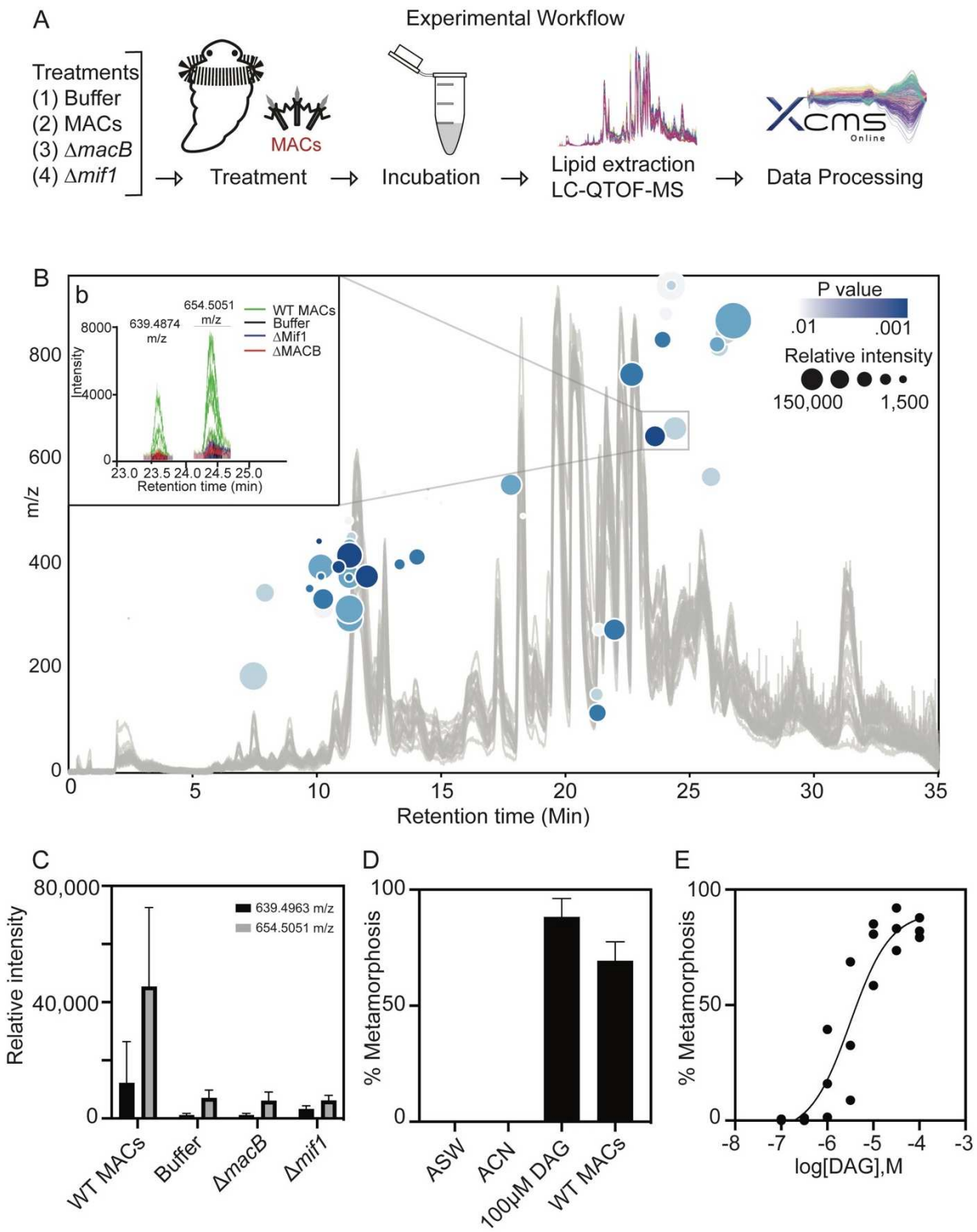
A
Experimental Workflow
Treatments
(1) Buffer
(2) MACs
(3) ΔmacB
(4) Δmif1
MACs
Treatment
Incubation
Lipid extraction
LC-QTOF-MS
Data Processing
B
b
654.5051 m/z
639.4874 m/z
WT MACs
Buffer
ΔMif1
ΔMACB
Intensity
Retention time (min)
P value
.01
.001
Relative intensity
150,000
1,500
m/z
Retention time (Min)
C
Relative intensity
639.4963 m/z
654.5051 m/z
WT MACs
Buffer
ΔmacB
Δmif1
D
% Metamorphosis
ASW
ACN
100μM DAG
WT MACs
E
% Metamorphosis
log[DAG],M

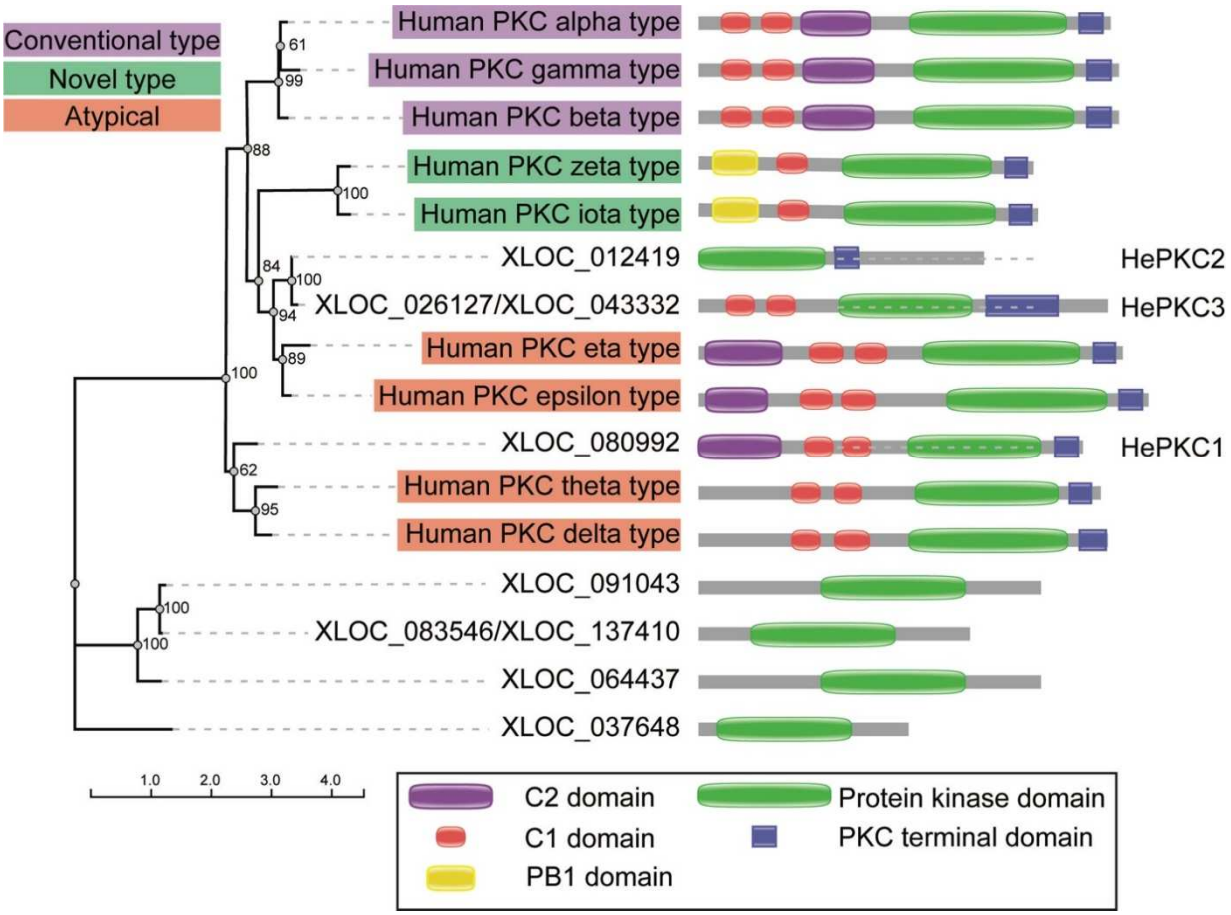

Figure 4.2. The *Hydroides* genome possesses 3 PKC isoforms or homologs. Seven *Hydroides* PKC isoforms or homologs are represented by a maximum likelihood phylogeny created using a Mafft e-ins-i alignment and PhyML and supported with 100 bootstraps, with nine human PKC isoforms: sp|Q02156|KPCE_HUMAN, sp|Q05513|KPCZ_HUMAN, sp|P41743|KPCI_HUMAN, sp|P24723|KPCL_HUMAN, sp|P17252|KPCA_HUMAN, sp|P05129|KPCG_HUMAN, sp|P05771|KPCB_HUMAN, sp|Q04759|KPCT_HUMAN, sp|Q05655|KPCD_HUMAN. The human PKC genes are color coordinated based on class (conventional, novel, or atypical). All PKC-associated protein domains identified by Pfam and/or Gene3d are displayed beside each branch and color coordinated with accordance to the legend. Three *Hydroides* homologs cluster with human PKC isoforms: HePKC1, HePKC2 and HePKC3.

Figure 4.3. *Hydroides* requires PKC and MAPK signaling to undergo metamorphosis in response to Mif1 and DAG. (**A**) Treatment combinations and representative images of larvae after 24 hours of treatment with each condition, the IC50 was used for inhibitors and 100uM DAG was used to strongly stimulate metamorphosis. (**B and C**) *Hydroides* metamorphosis in response to MACs, with a 1-hour pre-treatment of increasing concentrations of the PKC inhibitors Ro 32-0432 IC50 = 235 nM (**B**), or bisindolylmaleimide IV (Bis IV) IC50 = 1.259 μM (**C**). Data points indicate individual biological replicates (n=3). Each biological replicate plotted is the average of 4 technical replicates, where larvae from each replicate were derived from different male and female individuals. (**D**) Metamorphosis assay with wild type MACs or 1,2-dioctanoyl-sn-glycerol (DAG) as the larvae inducer and 1-hour pre-treatment with PKC inhibitors. (**E**) Metamorphosis assay with MAPK inhibitors in the presence of 1,2-dioctanoyl-sn-glycerol. Data are presented as mean of 3 biological replicates, where larvae from each replicate were derived from different male and female individuals, with error bars indicating standard deviation. Significance was determined by a one-way ANOVA with Tukey's multiple comparisons test. Comparisons are indicated by the line above compared conditions and **** represents p-values <0.0001.

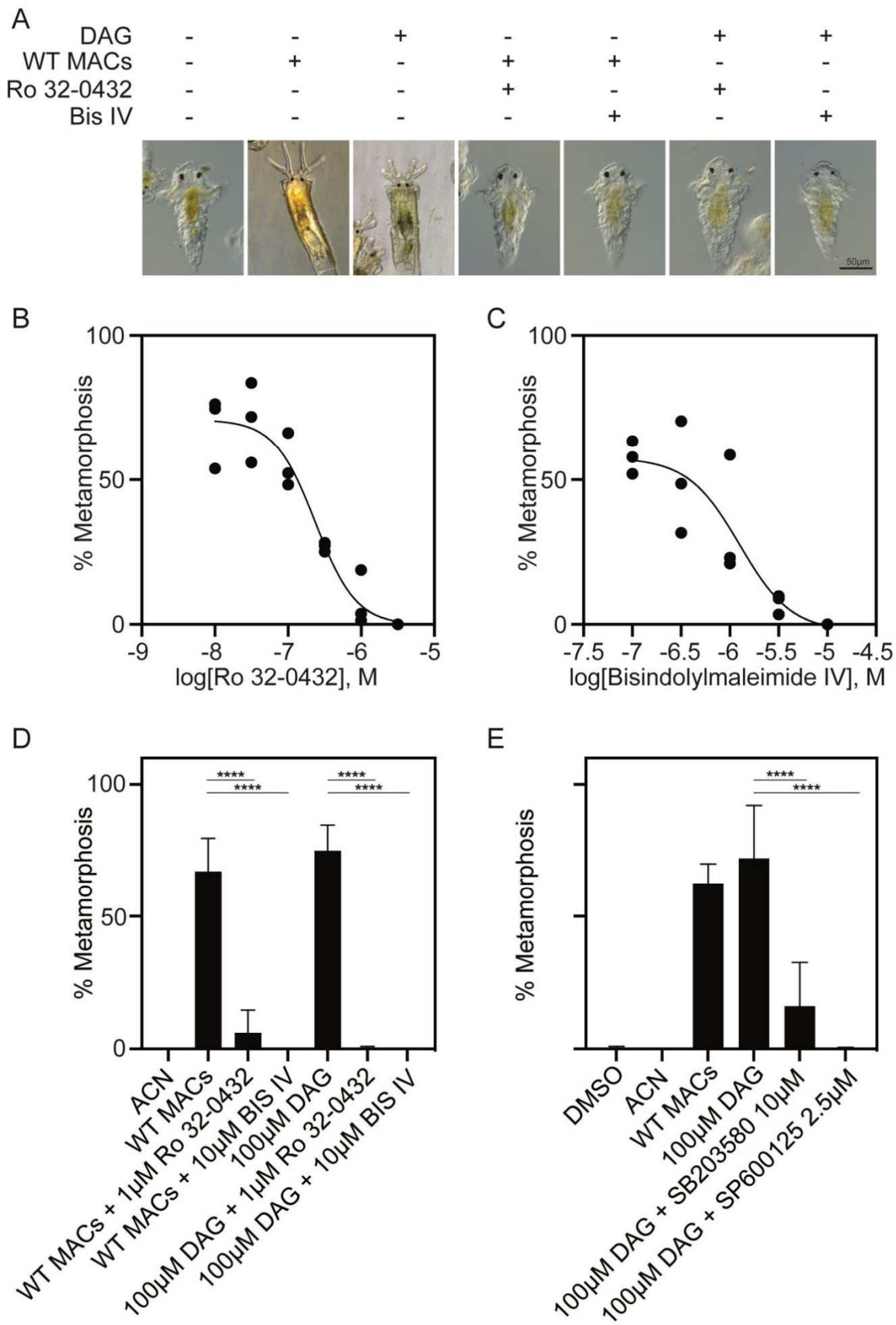
A
DAG - - + - - + +
WT MACs - + - + + - -
Ro 32-0432 - - - + - + -
Bis IV - - - - + - +
50µm
B
% Metamorphosis
100
50
0
-9 -8 -7 -6 -5
log[Ro 32-0432], M
C
% Metamorphosis
100
50
0
-7.5 -7 -6.5 -6 -5.5 -5 -4.5
log[Bisindolylmaleimide IV], M
D
% Metamorphosis
100
50
0
****
****
****
****
ACN
WT MACs
WT MACs + 1µM Ro 32-0432
WT MACs + 10µM BIS IV
100µM DAG
100µM DAG + 1µM Ro 32-0432
100µM DAG + 10µM BIS IV
E
% Metamorphosis
****
****
DMSO
ACN
WT MACs
100µM DAG
100µM DAG + SB203580 10µM
100µM DAG + SP600125 2.5µM

Figure 4.4. Mif1 induces HeNHR1 and HeNHR2 expression through PKC signaling. (**A-J**) Competent larvae were pretreated for 1 hour with 1μM Ro 32-0432 or 10uM bisindolylmaleimide IV or solvent, and then subsequently exposed to WT MACs to induce metamorphosis for an additional hour. The larvae were then probed with Digoxigenin-11-UTP labeled RNA for nuclear hormone receptors HeNHR1 (**B-E**) and HeNHR2 (**F-I**), beta tubulin (**J**) or a negative control (**K**) and visualized by NBT/BCIP staining. Anatomical structures indicated, (ASO) apical sensory organ, (CG) cerebral ganglia, and (Pro) prototroch. An image of a live larvae is shown for reference **(L).** Representative images are shown from three biological replicates (See **Figure S4.2.** for representative images from each biological replicate).

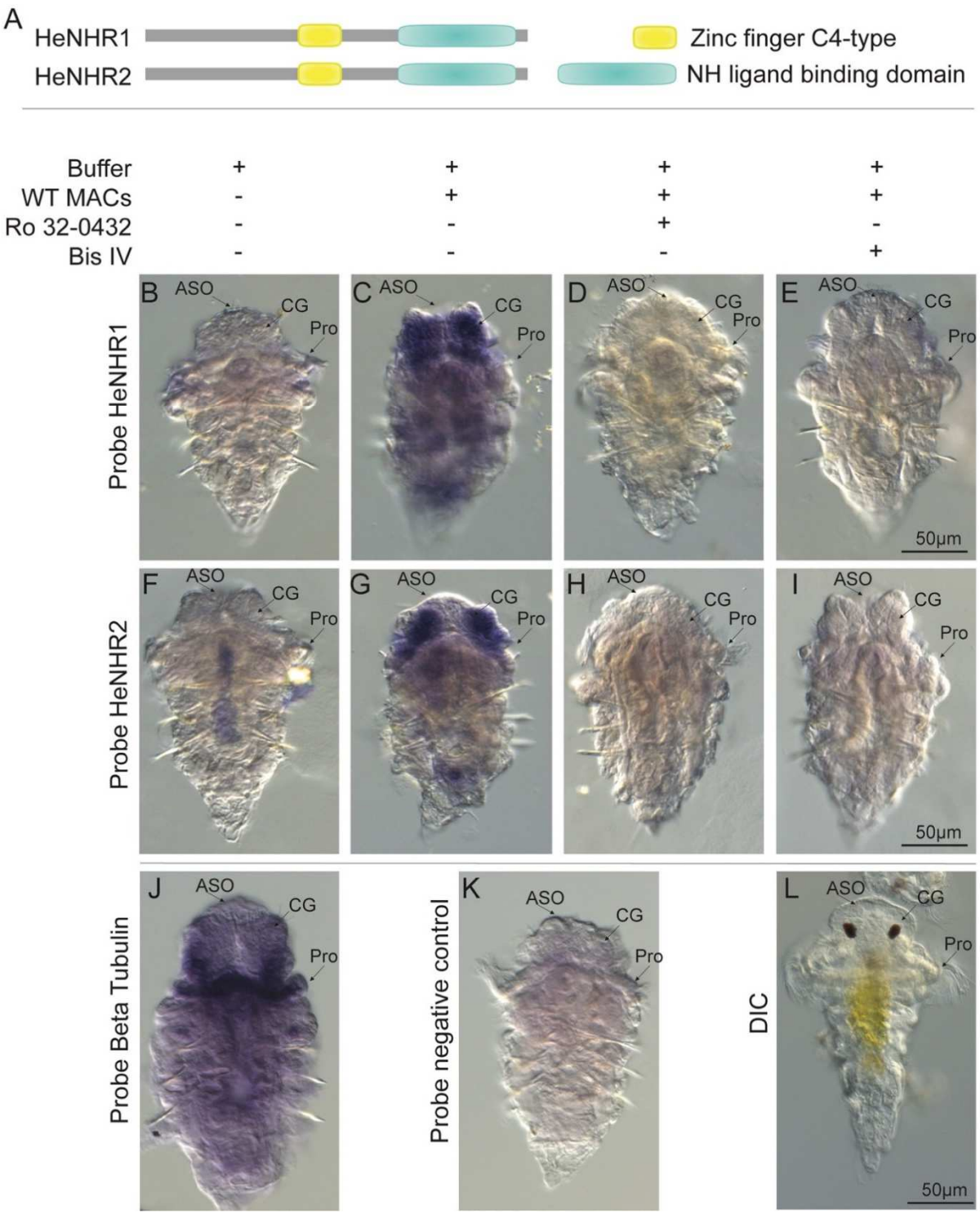
A
HeNHR1
HeNHR2
Zinc finger C4-type
NH ligand binding domain
Buffer + + + +
WT MACs - + + +
Ro 32-0432 - - + -
Bis IV - - - +
Probe HeNHR1
Probe HeNHR2
Probe Beta Tubulin
Probe negative control
DIC
B C D E F G H I J K L
ASO
CG
Pro
50µm

Table S4.1. Differentially regulated lipids identified by LCMS. Multigroup comparison of 7 day old Larvae treated with buffer, MACs, Δ*macB*, or Δ*mif1*. Lipids were extracted, subjected to reverse phase liquid chromatography followed by mass spectrometry. Identified lipids were sorted by p-value significance after a multigroup comparison. The mass to charge (MZMED), retention time (RTMED), and max intensity (MAXINT) aided in further identification of the compounds. The top predicted compound and metlin identifier denotes a potential compound or class of compounds.

Feat id	pvalue	mzmed	rtmed	maxint	metlin ID	compound
1	0.000695673	639.4935573	23.605375	4488	4371	DG(18:2(9Z,12Z)/18:2(9Z,12Z)/0:0)
2	0.000920345	607.3209645	7.325366667	1712	42546	1,25-Dihydroxy-20S-21-(3-hydroxy-3-methylbutyl)-23-yne-26,27-hexafluorovitamin D3
3	0.001123328	373.2913994	12.01208333	6126	2099	3,5,3',5'-Tetra-tert-butyldiphenoquinone
4	0.001177623	391.3024526	10.877725	2420	42249	(22E,24E)-1α,25-dihydroxy-22,23,24,24a-tetradehydro-24a-homovitamin D3 / (22E,24E)-1α,25-dihydroxy-22,23,24,24a-tetradehydro-24a-homocholecalciferol
5	0.001339688	440.2145658	10.089325	4198	122512	Asp Ile Asn Pro
6	0.0017772	413.285086	11.31121667	18834	42024	1α-fluoro-25-hydroxy-16,17,23,23,24,24-hexadehydrovitamin D3 / 1α-fluoro-25-hydroxy-16,17,23,23,24,24-hexadehydrocholecalciferol
7	0.002118198	272.2203847	21.9739	2622	71808	Kikkanol A
8	0.002171939	758.5513014	22.6696	2324	59406	PC(15:0/22:5(4Z,7Z,10Z,13Z,16Z))
9	0.002334092	824.5747108	23.9099	5586	8663	PS(O-16:0/22:2(13Z,16Z))
10	0.002356108	373.2908044	10.167975	2684	2099	3,5,3',5'-Tetra-tert-butyldiphenoquinone
11	0.002772148	350.2958716	9.70915	5804	none	none
12	0.003044479	114.0904449	21.28931667	1950	985971	5,5-Dimethyl-1-pyrroline-N-oxide
13	0.003102045	410.3108023	14.02935833	4946	75481	N-oleoyl tyrosine
14	0.003121472	396.3077041	13.32931667	3052	64689	15(S)-15-methyl PGF2α ethyl amide
15	0.003536341	330.2699695	10.25628333	4748	none	none
16	0.00395616	371.2763907	11.29546667	117436	none	none
17	0.004055955	311.2559582	11.304225	39992	44012	METHOPRENE (S)
18	0.004210339	293.2455037	11.314425	29266	263520	Pentadecanoic acid, 14-methyl-, methyl ester
19	0.004289698	431.2965135	11.31183333	147902	44017	PRISTIMEROL
20	0.004934001	391.3021151	10.16018333	3388	23359	Val Lys Lys
21	0.005137348	860.611306	26.75505	62316	39555	PC(18:0/22:4(7Z,10Z,13Z,16Z))[U]
22	0.005315871	372.2800315	11.306925	28152	none	none
23	0.005500528	547.2647504	17.807625	3156	106859	Ala Lys Lys Tyr
24	0.005569237	815.7399841	26.10166667	2992	none	none
25	0.005816469	414.2901951	11.33495	4812	985900	SNC80

Table S4.1. Differentially regulated lipids identified by LCMS. Continued.

26	0.006227071	654.5050814	24.412325	8074	4496	DG(18:3(9Z,12Z,15Z)/20:5(5Z,8Z,11Z,14Z,17Z)/0:0)[iso2]
27	0.006227071	836.6083253	26.45525	20970	39381	PC(16:0/22:2(13Z,16Z))[U]
28	0.006304746	149.1313413	21.2653	4196	71487	Ectocarpen
29	0.006304746	448.3230211	11.38563333	58554	146856	Gly Lys Lys Val
30	0.006645689	927.6697109	24.25925	1164	80690	PI(21:0/22:1(11Z))
31	0.006791317	184.0744161	7.4473	2756	3318	Phosphocholine
32	0.007927305	562.4584646	25.858125	7106	none	none
33	0.007951841	810.5887127	26.17525833	56494	103136	PI-Cer(d18:0/18:0)
34	0.007976453	342.2614129	7.909566667	5012	45720	CAY10580
35	0.00827772	272.2201944	21.3405	2012	71808	Kikkanol A
36	0.008329012	479.275033	11.26885	3702	1752	Pentazocine glucuronide
37	0.008329012	840.6280051	26.25495	5158	39117	PC(21:0/22:6(4Z,7Z,10Z,13Z,16Z,19Z))
38	0.008750805	873.5784311	24.04226667	3768	80997	PI(O-16:0/20:1(11Z))
39	0.00896954	312.2592537	10.26261667	5662	none	none
40	0.00896954	392.2767871	9.696975	1688	36677	N-arachidonoyl D-serine
41	0.009193669	926.6654981	24.24390833	1710	80309	PI(18:0/21:0)

Table S4.2. *Hydroides* PKC domain identification using HMMR or gene3d analyses.

XLOC_080992	FAMILY ID	FAMILY ACCESSION	ALI. START	ALI. END	MODEL START	MODEL END	BIT SCORE	IND. E-VALUE	COND. E-VALUE
	\	PF00069.25	400	646	2	258	209.32	6.30E-62	3.50E-65
	Pkinase_Tyr	PF07714.17	400	644	2	253	130.03	9.00E-38	5.00E-41
	C1_1	PF00130.22	200	251	1	52	57.94	6.60E-16	3.70E-19
	C1_1	PF00130.22	272	323	1	52	61.52	5.00E-17	2.80E-20
	Pkinase_C	PF00433.24	678	719	1	46	35.22	1.50E-08	8.20E-12
	FTA2	PF13095.6	387	431	14	54	10.86	0.26	0.00015
	FTA2	PF13095.6	507	530	181	204	3.48	48	0.027
	Gene3D			Domain E-values					
	Fam	Accession	end	ind.	cond.				
	2enjA00-i2	2.60.40.150	132	7.30E-43	1.00E-44				
XLOC_012419	Family id	Family Accession	Ali. Start	Ali. End	Model Start	Model End	Bit Score	Ind. E-value	Cond. E-value
	Pkinase	PF00069.25	4	232	19	257	200.41	3.30E-59	1.50E-62
	Pkinase_Tyr	PF07714.17	5	227	24	249	112.77	1.70E-32	7.40E-36
	Pkinase_C	PF00433.24	268	308	1	45	36.9	4.40E-09	2.00E-12
	Kinase-like	PF14531.6	99	190	158	255	17.19	0.0025	1.10E-06
	APH	PF01636.23	46	133	101	197	17.6	0.0028	1.30E-06
XLOC_026127/ XLOC_043332	Family id	Family Accession	Ali. Start	Ali. End	Model Start	Model End	Bit Score	Ind. E-value	Cond. E-value
	Pkinase	PF00069.25	270	515	2	257	221.29	1.40E-65	3.10E-69
	Pkinase_Tyr	PF07714.17	270	510	2	249	129.29	1.50E-37	3.40E-41
	C1_1	PF00130.22	55	106	1	51	59.95	1.60E-16	3.50E-20
	C1_1	PF00130.22	131	182	1	52	55.66	3.40E-15	7.60E-19
	Pkinase_C	PF00433.24	551	577	1	27	26.11	1.00E-05	2.30E-09
XLOC_064437	Family id	Family Accession	Ali. Start	Ali. End	Model Start	Model End	Bit Score	Ind. E-value	Cond. E-value
	Pkinase	PF00069.25	228	490	2	256	173.74	4.50E-51	1.30E-54
	Pkinase_Tyr	PF07714.17	227	486	1	249	100.52	9.10E-29	2.50E-32
	Pkinase_fungal	PF17667.1	359	415	322	386	26.39	2.80E-06	7.70E-10
	APH	PF01636.23	362	391	166	197	23.43	4.70E-05	1.30E-08
XLOC_091043	Family id	Family Accession	Ali. Start	Ali. End	Model Start	Model End	Bit Score	Ind. E-value	Cond. E-value
	Pkinase	PF00069.25	234	494	3	255	173.28	6.20E-51	1.40E-54
	Pkinase_Tyr	PF07714.17	232	480	1	238	94.2	7.70E-27	1.70E-30
	Pkinase_fungal	PF17667.1	364	421	322	387	29.62	2.90E-07	6.50E-11
	APH	PF01636.23	366	395	165	196	24.41	2.30E-05	5.20E-09
XLOC_083546/ XLOC_137410	Family id	Family Accession	Ali. Start	Ali. End	Model Start	Model End	Bit Score	Ind. E-value	Cond. E-value
	Pkinase	PF00069.25	89	349	3	255	173.49	5.40E-51	1.50E-54
	Pkinase_Tyr	PF07714.17	87	346	1	249	99.22	2.30E-28	6.30E-32
	Pkinase_fungal	PF17667.1	213	276	316	387	30.19	1.90E-07	5.40E-11
	APH	PF01636.23	222	250	166	196	23.56	4.30E-05	1.20E-08
XLOC_037648	Family id	Family Accession	Ali. Start	Ali. End	Model Start	Model End	Bit Score	Ind. E-value	Cond. E-value
	Pkinase	PF00069.25	30	287	3	254	167.33	4.10E-49	6.80E-53
	Pkinase_Tyr	PF07714.17	28	250	1	213	96.89	1.20E-27	2.00E-31
	Kinase-like	PF14531.6	123	285	124	288	27.34	2.00E-06	3.40E-10
XLOC_028442	Family id	Family Accession	Ali. Start	Ali. End	Model Start	Model End	Bit Score	Ind. E-value	Cond. E-value
	C1_1	PF00130.22	169	220	1	51	61.21	6.30E-17	7.00E-21
	C1_1	PF00130.22	245	296	1	52	56.92	1.40E-15	1.50E-19
	C2	PF00168.30	9	118	1	103	54.51	1.10E-14	1.30E-18

Table S4.3. *Hydroides* PKC isoform and homologous protein sequences.

>XLOC_064437
MVPVTIYYVPNLPNLISSGIAKIPLLDAVYSTWSTDNYAQQQNLLEYAWESIYPVFSPWFPMGFGDFNTRKGTNIVVRNESENTGFFKIPVW
NMTTALAIYYPKENQWFSAGICLLLFYVTACIGCAVAIHSMHATNPQNQIATTNSPTTSNPDATEDIVTDSEHSAPRDYFEALPTQEPSTSAA
GEPDRIEISNTSSEETTAEIVASVVTEMDALAVAETDTSAELKVLHKIGRGGFACVYKAEMQMRGDVEARHIALKQMSKRFMLARDQVKYAS
TAVLDFDNCEQVLKELDMLKAVRNGPFVNKILLAFQTREHVWFGLEYCGGQSLSALVTTGKRFEENAIQFYARELICGISFIHSKGIVHRDLS
LNNIMLTMEGHICIIDFGLADNDVRDDTELQDVVGTPEFIAPEVYAEKPYNKACDWWSMGVCMYYLVHGHAPFQAPDKATLARKVMHDEV
VFSITTVSYELIDFIYGLLDKDARTRLGSARCPDGPIREHPFVKDVDWSDVVAQRIKTPVVTPREERRTHVSTEEEPLAAISISRDSSPPGVAD
GSSFDSDASSPLARATSVQLRDHQYLFRGFEFGPQAILLDGRVIRRRGSMSSFGSIRSDASSVWEIRPGDISLTAFDEGSRNFGVIPSDAS
W

>XLOC_091043
MHATNPTYPIVTTNPIATTNSGPPIIEIRPDSTSASDQSEALPSQDPATSAETVELDSNSDETTDDSAEPESCEKNDKHISSPEETETESKVPE
ETGENATDDAKSPSAETETNKASSKETSTETMAPVVADADNALAITSAGIDDALAIMSADTDALPTTSTETDDALAITSANTDDALAITSAGTD
DALAIMSADTDALPTTSTETDALPTTSTETDALAIANMDTDAELKMLQKIGRGGFARVYKAEMRMRGDVEARHIALKQMSKRFMLERDQVK
YASMAVLDFDNCEQALKELEMLKTVRNGPFISQLLLAFQTREHVWFGLEFCGGQSLSALIYNETKFKENTIQFYARELICGISFIHAKGIVHRD
MSLNNIMLTGDGHICIIDFGLAENNVNDDTELHDLVGTREFIAPEIYAGRPYNKAVDWWSMGVGMFYLVHGHAPFQDSDKNTLARKVMFDV
LRFSSTKVSCDLIDFIYCLLNKDARTRLGSPGCRDGPIREHPFVKDVNWTHVEQGRIGTPVVTQAREEERRLHSGSTEEDAEGGTKAISVSF
SVIVAGSSCDSDASISVDRTTSEQLRDHQYLFHGFEFGPQAILLDGTMIRRRGSMSSFGSKRSDASSVWDIKPGDISLTRFDEGSRNFGVIP
SDASW

>XLOC_083546/XLOC_137410
MSADTDALPTTSTESDALATSSTETDALPTTSTETDALPTTSAETDALPTTSTETDALPTTSTETDALPTTKTDALAIADMDTDAELKMLQKIG
RGGFARVYKAEMRMRGDVEARHIALKQMSKRFMLERDQVKYASMAVLDFDNCEQALKELQMLKTVRSGPFLSQIILAFQTREHVWFGLEF
CGGQSLSALVNNETKFKESVIQFYARELICGLSFIHSKGIVHRDMSLNNIMLTTEGHICIIDFGLAENNVNDDTELHDLVGTREFIAPEMYAGR
PYNKAVDWWSFGVGMFYLVHGHAPFQDSDKNTLARKVMFDVLRFSSTKVSCDLIDFIYCLLNKDAKTRLGSPGCPDGPIREHPFVKDVNW
THVEAGRIETPVDSSPRVEERRPHSGSTEEGAKGGVKAISVSFSVIVAGSSCDSDASSYVDRTTSEQLRDHQYLFHGFEYGPEAILLDGMEI
RRRGSMSSFGSKRSDTSSVWDIKPGDISLTRFDEGSRNFGVIPSDASWLASILNEPVDIKRQCARGSGRGTENRDNKMTEPDKIKVALNAI
VKDDLKAVQYRDSISTALSSAAENR

>XLOC_037648
MIYCIRLLWTYQKRESTEVIPVVPEKEIELGRKIGKGGYGQVYMARIVNADGTYEFCAVKCISKRYMMAKDDLHLRERRPAGPLLHSMLAKR
EMEIMKCVRDGPFICRLILAFQTKEFLWISMEHCRRSLKEVLRTDRRLNYRDIQFYTRELICGVQYMHNQGVIHRDLNLSNLMLAQNGHLRII
DFGLAVDNVTENTQLWEMAGTASYVAPEIWKELPYNKSADWWSVGICIYTLIHGYTPFNGEARCDIPYLTKFKHIRFDFSFDTRLARFLRGL
LDRNPRMRLGHPMSRFGPIRGQDFVAGINWDDVENEQLEPPDWATSDEDALFLGRGTGPISFDYRRRRAIQHINEIDLDGHQYLFQGFQF
GPTCSLGDLSESVPTADTERSRKGRARIA
>XLOC_026127/XLOC_043332 (HePKC3)
MIDLEPNGKVRVKIELNGSTSEEPPKETRAFKENKGALKQRRAAIRRRVHQVNDHKFMATYLRQPTFCSTCSDFIWGLLSPQGYQCQVCTL
VVHKRCHEAVVTRCPGVKDATAATQTAAGSGKRFGINVPHRFKVHSYKRFTFCDHCGSLLYGIIKQGLQCEACKINIHKRCEKNVAPDCGIN
KRDMAQVMKELGISGDKLVNKGRKKTSICGGSSGTSLDSSSPNRPISAPISAISEEAGDPMASLLGRRGSSLKRERRTHRFGLKDFQFIKVL
GKGSFGKVMLAEKKGTEEVYAVKVLKKEVIIQDDDVECTMTEKRILDLSARHPFLTALHSCFQTKDRLFFVMEYVNGGDLMFQIQRARKFDE
PRARFYAAEVTLALMFLHRHGIIYRDLKLDNILLDAEGHCKIADFGMCKEGMTPGKLTTTFCGTPDYIAPEILQELDYSTSVDWWALGVLMYE
MMAGQPPFEAENEDDLFESILHDDVLYPVWLSKEAVAILKAFMTKKPAKRLGCVAAHGFESAILIHPFFHQKIDWEALEERKVKPPFKPKIKS
RTDANNFDKDFTQEAPRLTPVEDDIIKAIXXXXXXXXXXXXXXXXXXXXXXXXXXXXXXXXXXXXXXXXXXXXXXXXXXXXXXXXXXXXX
XXXXAGAEQQKQQQQDVVANSSSGGNSGSSDKSTVASAAAAKATTTQNEQKRLSGEGGGGGDVGGGTHKANAPPSNMAAKGGGVAM
NEEKSRNKSGGAVVDRIIAKCDVTIAGSQPEKPVTESYHTNHGHCAFMTS*
>XLOC_080992 (HePKC1)
MPAGFIRVKLLQCERGEYSVAAGDTFDPFVAVNVKEAQNTPGRGVQLIQRKKTIYPEWNTCFDAHLYDGRVIQLIVMQRPNLFVADANIGA
QHLADKCKDGGVANVKLDLKPSGKLIIQVRHFTESEEMSAKQSRTSNGRPQSSSVEVKVAAPHGTPINNKYQQKQMPEKNGDEKFDTGT
MGLKRRVAIKHQKIHEVMGHHFIAKFFRQPVFCSYCTEFMWGLNKQGYQCQDCNCTVHKRCHDKVIARCPGNAMDSMETKKLTERFNINV
PHRFKVNNYTSPTFCDHCGSLLWGLFRQGLKCQECGVNCHKKCEKNMPNLCGVNQKILAEAIQKINKTKVSSSKTTTRNADAAKSRSTEE
AGDSNADNYELLMKFESARRADGLPVKEFKGKKYSPSDFNFLKVLGKGSFGKVMLAELKGNNEYYAIKALKKDVVLEDDDVECTMIERRVL
ELGCQHPYMTHLHSTFQSDSHLFFVMEYLNGGDLMFHIQQSGRFDLERSRFYGAEIVCGLQFMHKRGIVYRDLKLDNVLLDRDGHIKIADF
GMCKENIAGENRATTFCGTPDYIAPEILKGNKYNASVDWWSFGVLLYEMLIGQSPFHGDDEDDLFHSICHDTPHYPRWLSKDAAACLSLLF
ERIPDERLGMQNCPQGGIREQAFFAPLDWQKLENRRLEPPFKPKIKSASDVSNFDTDFTMERAALTPPDKELLKTMDQGVFLGFSFTNPD
MTKL*

>XLOC_012419 (HePKC2)
MLAEKKGTEEVYAVKVLKKEVIIQDDDVECTMTEKRILDLSARHPFLTALHSCFQTKDRLFFVMEYVNGGDLMFQIQRARKFDEPRARFYAA
EVTLALMFLHRHGIIYRDLKLDNILLDAEGHCKIADFGMCKEGMTPGKLTTTFCGTPDYIAPEILQELDYSTSVDWWALGVLMYEMMAGQPP
FEAENEDDLFESILHDDVLYPVWLSKEAVAILKAFMTKKPAKRLGCVAAHGFESAILIHPFFHQKIDWEALEERKVKPPFKPKIKSRTDANNFD
KDFTQEAPRLTPVEDDIIKAINQDEFAGFSHVNDEFGKMYQLGYGNCGPAGAEQQKAQQQQKDVVANSSSGGNSGSSDKSTVASATAAK
TTTQNEQKRLSGESGGGGDVGGGTHKANAPPSSGAAKGGGVAMNEEKSRNKSGGAVVDRFDNTTSDNVVNTKKLNNPASSSSSTSGG
STAGIPTSPKTPPVLSSPKTKNAFLDIPAFNANQKNSSSCSEGNKKTATATTTAANQSCTSTMPLMTSESSQSVTSQSQAVSPKSPSPKATT
PTTVTAHL*

>XLOC_028442
MQNMVFFNGTLKLKIYEAVDLRPTEFATRHSLKDTPFMLDPYISLDIDDVPLGKTTTKLKTLKPQWEEDFVTEVHNGQNLVLTVFHDAAIPPD
EFVAMCTIALEDLSGKDSSEIWIDLEPNGKVRVKIELNGSTSEEPPKETRAFKENKGALKQRRAAIRRRVHQVNDHKFMATYLRQPTFCSTC
SDFIWGLLSPQGYQCQVCTLVVHKRCHEAVVTRCPGVKDATAATQTAAGSGKRFGINVPHRFKVHSYKRFTFCDHCGSLLYGIIKQGLQCE
ACKINIHKRCEKNVAPDCGINKRDMAQVMKELGISGDKLVNKGRKKTSICGGSSGTSLDSSSPNRPISAPISAISEEAGDPMASLLGRRGSS
LKRERRTHRFGLKDFQFIKVLGKGSFGK

Table S4.4. *Hydroides* HeNHR1 and HeNHR2 gene sequences

>HeNHR1 (XLOC_089428)
ATGCTTGATCATACCAAGGTCGCGTTACCACCTGGGAACCATCATCAACTCGATG
GCACTTTCGAGAAGAGCCTCTTGGATATCGGAAACACGGCCGCGCTGGATGAAA
TAGACTCTATTTTATCATCGGCTGCTTCCACTATGGAGGAGTCTTCCCTTGTGCC
ATTCGCCAGTCTGCTCAATGATCCGCAACTGACCTTGACCGGGGACATGCCGCT
GGATGACAGTACATCGGAGGTGAGCTCCGATACCGACAGTGGTTTCCAGGAGTC
TCCGCCGGCCTGGACCGACGATAGCCTGGATGCCTGGCTGACTAAGAGTGTGG
CCAGTTCGCAAATGGGACAGGCACTGCCCTCGATTGACTCGATCATGTCGACCC
CGCAGCTGCCTCAGAAGGTAATGACGACCACTGAGCAAAGCTTTACTTTAGACA
ATTCAATTGAATTCCAGCAAAACGCGACGGCGGCTGCTGATTTGATGCTGCTTAC
GCCTCCGACGACGCCGTGCATTGCAAGTCCCATCGAAAACAGCGTGCAGATCAA
AACCGAGCCCCTGGATTCGACCACGTGCCTGGATATGAACAACCTGCACGCTGC
AGCTGCATCGCCGCTCACCGTGCAAAACGTGCTCGCTGCAACCAGCGCCGCAG
CTCAACAGAATCAAGGGGTCAACGAACTCTTGCAGCAGCAAAATCCAGGGGTCA
ACAATGTTATGCAACATAACCAAGGCATGGGAGAGCTAATGCAGAGATCACCGG
TGAAAACGGAAGCGGCCAGCGCAGAGGAGTTGTTCAGACTCAAGTTCAGTCCAC
ATGTGCTGCCACCTTGTCGGGTCTGTGGCGCACAGGCGACGGGTTACCACTAT
GGAGCGAACACCTGCGAGCCTTGCAAGGGCTTTTATCATCGTATGACGAAACGT
ATGGATAAGAACCTGGCCTGTCTCAAGCAAAACAACTGCGTCATCACGGCCAAA
AACCGCGGCGCCTGTCCTGCCTGTCGCTACCAAAAATGCATCAAAGCGGGCATG
TGCAAGAACAATATCAAAACCGGACGTTATAGTTACTCCAAGCGATCACGTGATA
TCATCGAACTGCAGAACAGCATCTCAGAACGAAAACAGCAGCAGCAGCGCGACG
CCTATGAACTGGCGCTGCAGGCCCATTCTGCGCTTGCGCAAACCGCTGCCGCC
CCCACTCGCCAGGTGGCGCAGCAAGAGACACTTCCGGTTGAAGCGGATGTGAC
GTCACAATGTATTATTACGGCTCTCAAGGCAGCAAGAGAAAAGATCATGGGCAA
GATGATGCAAACGGGTTGCGATCTGTCGGCCGAACAACAAACCGCCATTCATGT
ATTTAGTCAGCATTTAGAAAACGGACAGCGATCTTTAGCATATGAATCTTTCCTGC
AGTGGGTCAATTTGAGTTTCAAGCACAATCACTGGTCAAGCTTTGTCAAGGCCAT
TCCGGGCTTCAAGACGCTGCCCATGCAAGACCAGATCGCCATTATCAAAAAGTG
CTTCATGGACTTTTGGGCCGTGACGCGGCATCGTCTCTTCGATGTCAGCTCGGG
CATGTTCTACACATTCGGTGGCATCACGATTCCGATCAACGATATTATCGGCGAT
GAGCCCTGTAGTGATTTGATGAAGGCTGTCAAGCGACTTCAGAGCCTGAGTCTA
TCGTCTGACGAGTGTTGTACCCTCTCGGCCTTCGTAGCAGTTAACGCAGAATCG
ACCGGTATGACCGACATCGCCGGTGTAGAGCAGATCAAACAGAACCTGTTGGAC
GCTCTCATGTACGCCCTGCGCCAAAACAGAGCCCGTCCCGAACTTACTTTCGCT
CAAATCATCTCTGCCCTCACTCAACTGAAGAGCGCCGTTCACGCCTTTCCGCGT
CAGATGACCAAGTTCCACGAGACCGTCACACCACCCCTGTTTCACGAGATTGTT
CTGGCTAATCTCGATAGTTAA

Table S4.4. *Hydroides* HeNHR1 and HeNHR2 gene sequences. Continued.

>HeNHR2 (XLOC_109682)
ATGCTTGATCATACTAAAGTAGCGTTACCACCGGGGAATCATCATCAACTCGATG
GCACTTTCGAGAAGAGCCTCTTGGATATCGGAAACACGGCCGCGCTGGATGAAA
TAGACTCTATTTTGTCATCGGCTGCTTCCACGATGGAGGAGTCTTCCCTTGTGCC
ATTCGCCAGTCTGCTCAATGACCCACAACTGACCTTGACCGGGGACATGCCGCT
GGATGACAGTACTTCGGAGGTGAGCTCCGATACCGACAGTGGCTTCCAGGAGT
CTCCGCCGGCCTGGGCCGACGATAGCCTGGATGCCTGGCTTACGAAGAGTGTG
GCCAGCTCGCAGATGGGACAGGCACTGCCCTCGATTGACTCGATCATGTCTAAC
CCTCAGCTGCCATCGAAGGTAATGACGACCACTGAGCAAAGCTTTACTTTAGACA
ATTCAATTGAATTCCAGCAAAACGCGACGGCGGCTGCTGATTTGATGCTGCTTAC
GCCTCCAACGACGCCGTGCATTTCAAGCCCAATCGAAACCAGCGTGCAGATCAA
AACTGAGCCCCTGGATTCAACCACGTGCCTGGATATGAACAACCTGCATGCTGC
AGCTGCATCGCCGCTCACCGTGCAAAACGTGCTCGCTGCAACCAGCGCCGCAG
CTCAACAGAATCAAGGGGTCAACGAACTCTTGCAGCAGCAAATTCCAGGGGTCA
ACAGTGTTATGCAACAAAGCCAAGGGATGGGAGAGCTAATGCAGAGGTCACCG
GTGAAGACAGAAGCGGCCAGCGCAGAGGAGTTGTTCAGACTCAAGTTCAGTCCA
CATGTACTGCCACCGTGCCGAGTCTGCGGCGCCCAGGCGACGGGCTACCACTA
TGGGGCGAACACCTGCGAACCTTGCAAGGGCTTTTATCATCGTATGACGAAACG
TATGGATAAGAACCTGGCATGTCTCAAGCAAAACAACTGTGTCATCACCGCCAAA
AACCGCGGCGCCTGCCCTGCGTGTCGCTACCAAAAATGCATCAAAGCCGGCAT
GTGCAAGAACAATATCAAAACCGGACGTTATAGTTACTCCAAGCGATCACGTGAT
ATCATCGAACTGCAGAACAGCATCTCAGAACGGAAACAGCAGCAACAGCGCGAC
GCCTATGAACTGGCGCTGCAGGCCCATTCTGCGCTTGCGCAAACCGCTGCTGC
CGCCCCCACTCGCCAGGTGGTGCAGCAAGAGACACTTCCGGTTGAAACGGATG
TGACGTCACAATGTATTATTACGGCTCTCAAGGCAGCAAGAGAAAAGATCATGG
GCAAGATGATGCAAACGGGTTGCGATCTGTCGGCCGAGCAACAAACCGCCATTC
ATGTATTTAGTCAGCATTTAGAAAACGGACAGCGATCTTTAGCGTATGAATCTTTC
CTGCAGTGGGTCAATTTGAGTTTCAAGCACAATCACTGGTCAAGCTTTGTCAAGG
CCATTCCTGGCTTCAAGACGCTGCCCATGCAAGACCAAATCGCCATTATCAAAAA
GTGCTTCATGGACTTTTGGGCAGTGACGCGGCATCGCCTCTTCGATGTCAGCTC
GGGCATGTTCTACACATTCGGTGGCATCACGATTCCGATCAACGATATAATAGGC
GATGAGCCCTGTAGCGATTTGATGAAGGCTGTCAAGCGACTTCAGAGCCTGAGT
CTATCGTCTGACGAGTGTTGTACCCTCTCGGCCTTCGTAGCAGTTAACGCAGAAT
CGACCGGTATGACCGACATCGCCGGCGTAGAGCAGATCAAACAGAACCTGTTG
GATGCCCTCATGTACGCCCTGCGCCAAAACAGAGCCCGTCCCGAACTTACTTTC
GCTCAAATCATCTCTGCCCTCACGCAACTGAAGAGCGCCGTTCACGCCTTTCCG
CGTCAGATGACGAAGTTCCATGAGACCGTCACACCGCCCCTGTTTCACGAGATT
GTTCTGGCTAATCTCGATAGCTAA

Table S4.5. Primers for WMISH probe generation.

1st PCR, Primers for probes amplified from cDNA	
HeNHR1 TCONS_00112171_insitu_F1	TACCACCTGGGAACCATCAT
HeNHR1 TCONS_00112171_insitu_R1	GCGTAAGCAGCATCAAATCA
HeNHR2 TCONS_00137921_insitu_F1	CTGGCATGTCTCAAGCAAAA
HeNHR2 TCONS_00137921_insitu_R1	ATTGACCCACTGCAGGAAAG
BetaTub_insitu_F1	CCTCCAGTTGGAGAGGATCA
BetaTub_insitu_R1	ACCAACTGATGGACGGAGAG
2nd PCR, T7 promotor on reverse primer	
HeNHR1 TCONS_00112171_insitu_EX+T7+R1	CAGTGAATTGTAATACGACTCACTATAGGGAGA GCGTAAGCAGCATCAAATCA
HeNHR2 TCONS_00137921_insitu_EX+T7+R1	CAGTGAATTGTAATACGACTCACTATAGGGAGA ATTGACCCACTGCAGGAAAG
BetaTub_insitu__EX+T7+R1	CAGTGAATTGTAATACGACTCACTATAGGGAGA ACCAACTGATGGACGGAGAG

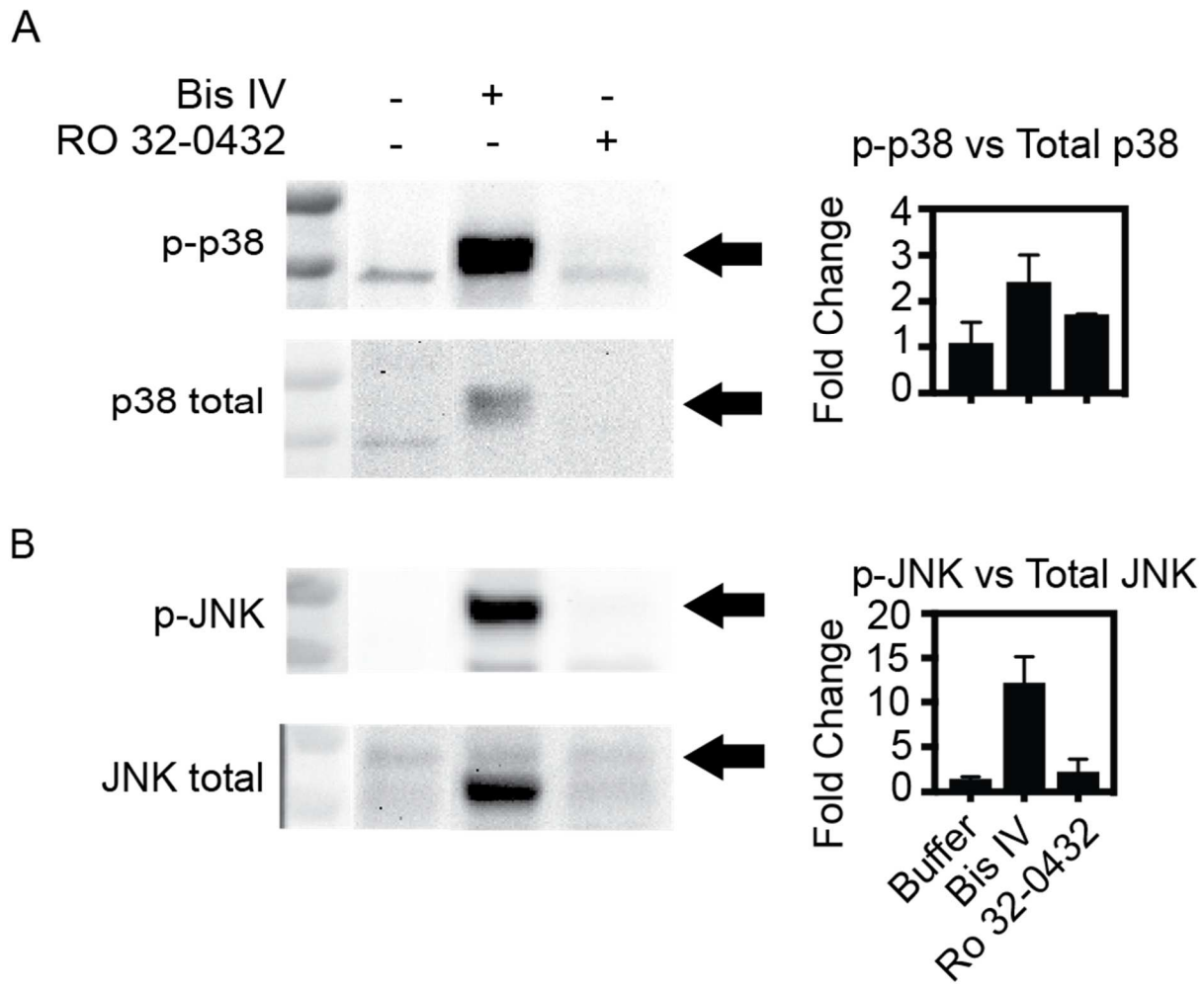

Figure S4.1. Phosphorylation of p38 and JNK MAPK in response to PKC inhibitors, MACs or DAG. Seven day old competent *Hydroides* larvae were incubated with Bis IV, Ro 32-0432 PKC inhibitors, MACs and/or DAG for 1 hour prior to protein extraction. 15µg of total protein was then used to determine phosphorylation state of downstream signaling pathways post treatment. (**A, B**) Larvae were pretreated with either buffer, 10µM Bis IV, or 1µM Ro 32-0432 for 1 hour before collection of total protein. The MAPK pathway proteins p38 and JNK were probed after treatment for both their phosphorylated state and the total endogenous protein levels to determine the relative ratio of phosphorylated vs unphosphorylated protein. A total of three (n=3) biological replications were performed, where larvae were derived from different male and female individuals. Graphs show the densitometry analyses for three replicates showing the ratio of phosphorylated protein over the total endogenous protein. The fold change vs the buffer average was plotted with error bars indicating the standard deviation.

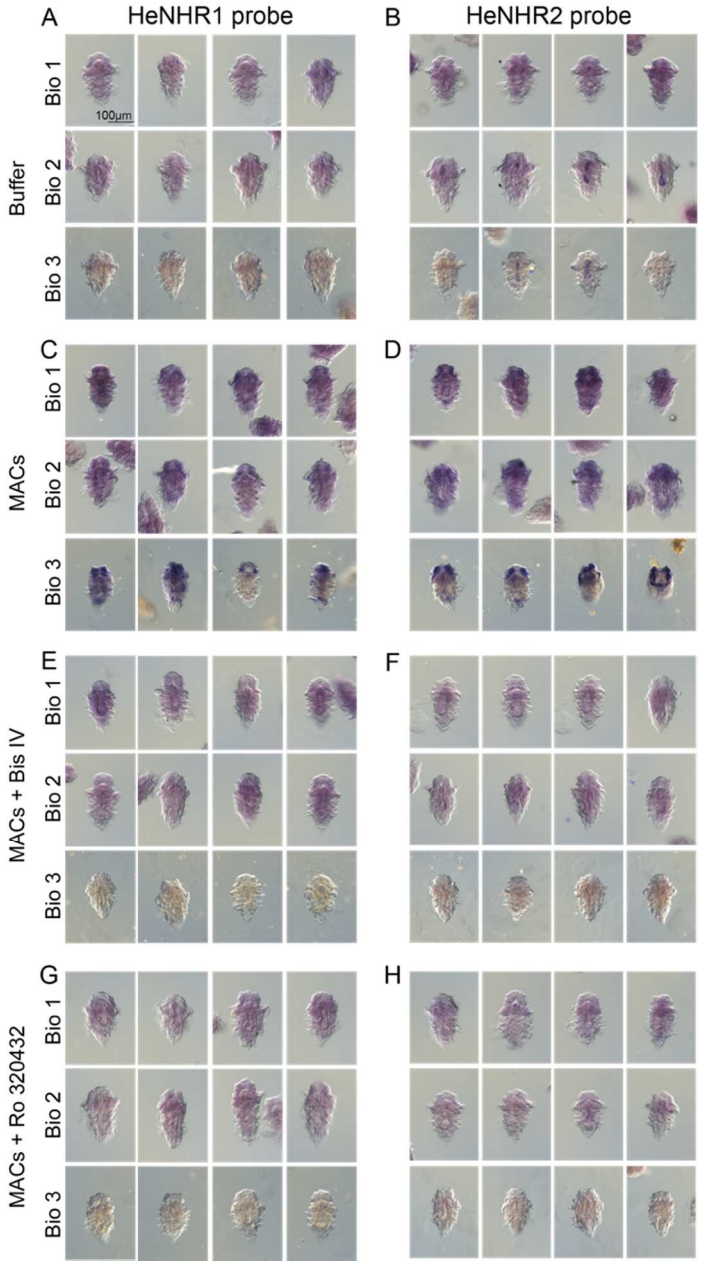

Figure S4.2. Whole mount *in situ* hybridization of 2 Nuclear Hormone Receptors during *Hydroides* metamorphosis. Larvae were pretreated with either DMSO solvent control (buffer), PKC inhibitor Ro 32-0432 (Ro 32) at 1µM or Bisindolylmaleimide IV(BISIV) 10µM for one hour prior to the addition of MACs or extraction buffer. The larvae were then fixed and probed for HeNHR1 (A,C,E,G) or HeNHR2 (B,D,F,H) expression. WMISH was performed on 3 different occasions with separate larvae spawned from different male and female *Hydroides* adults (biological replicates). Four larvae from each condition of each biological replicate (Bio 1/2/3) are shown.

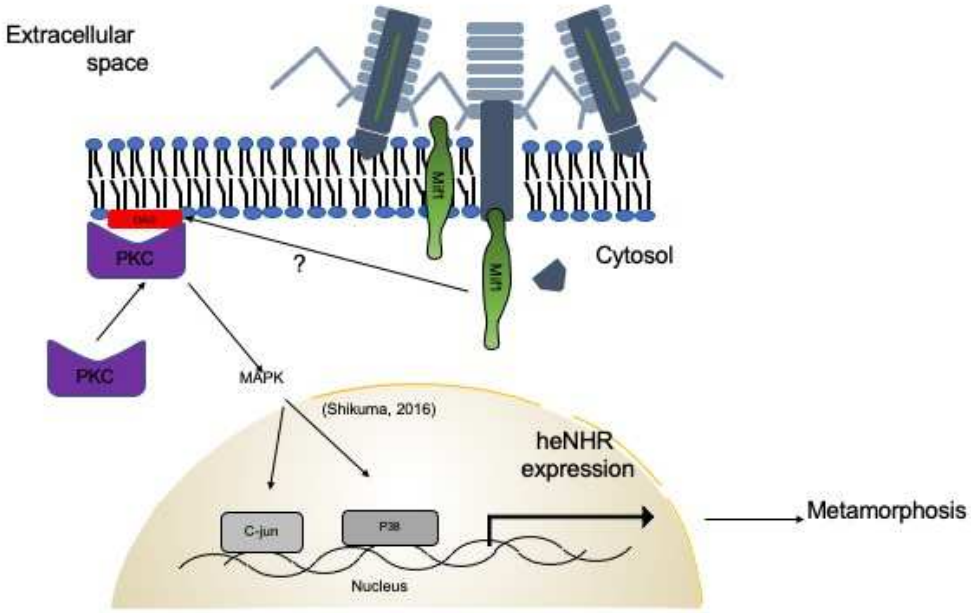

Figure S4.3. Overview of MACs signaling in *Hydroides*.

Chapter 5

Bacteria Stimulate Tubeworm Development by Injecting a Protein Toxin

5.1 Abstract

Contractile Injection Systems (CIS) are nanometer-scale syringe-like structures produced by gram-negative bacteria that often deliver protein payloads to target organisms to elicit specific cellular responses. Metamorphosis Associated Contractile structures (MACs) are one type of CIS produced by the marine bacterium *Pseudoalteromonas luteoviolacea* and are unique because they stimulate the metamorphosis of a marine tubeworm called *Hydroides elegans* by injecting a protein effector termed Metamorphosis Inducing Factor 1 (Mif1). While Mif1 is both necessary and sufficient to induce the tubeworm metamorphosis, it remains unclear how Mif1 promotes *Hydroides* metamorphosis. Here we show that Mif1 associates with eukaryotic lipid membranes and possesses phospholipase A1 and D activities. Through fragmentation analysis we identify a portion of the Mif1 protein associates with membrane lipid and this region is required for lipase activity. These data suggest a role for lipid cleavage in the initiation of tube worm metamorphosis. Understanding the role that bacteria contribute to animal development and the mechanisms by which they are capable of interacting furthers our understanding of animal-bacteria interactions and their role in animal development.

5.2 Introduction

Bacteria promote the normal development of diverse animal species. Animals evolved in a world dominated by microbes[1]. Notable examples of bacteria contributing to animal development include commensal bacteria in the host's gut that contribute to the production of many metabolites required for the gut tissue lining development and digestion[2]. Marine *Aliivibrio fisheri* bacteria stimulate the normal development of a specialized light organ in the Hawaiian bobtail squid[3]. Bacteria in the guts of zebrafish promote beta cell expansion of insulin producing cells[4]. These examples only scratch the surface of our understanding into the complexity of microbe-host interactions. While bacterial symbiosis with plants and animals are widespread, the roles that bacteria play in stimulating normal animal development remain poorly understood[5].

Bacterial secretion systems and their interaction with animals. Many bacteria interact with animal hosts by producing syringe-like structures called Contractile Injection Systems (CIS), which are related to the contractile tails of bacteriophage [6]. CIS are homologous to the contractile tails of bacteriophage but lack a DNA-filled capsid. These secretions systems often carry protein payloads. Contraction of the sheath propels the rigid inner tube through target cell membranes, delivering the protein cargo[7]. Some of these secretions systems such as the type VI secretion system (T6SS) are bound in the bacterial membrane, while others such as the antifeeding prophage (AFP), the *Photorhabdus* virulence cassette (PVC), and Metamorphosis Associated Contractile structures (MACs) are all released extracellularly from a small population of lysed bacteria similar to the release of bacteriophage during the lytic cycle[8]. CIS effector proteins have

been characterized having a wide range of functions, however, many are bacterial toxins such as lipases, nucleases, proteases, and deaminases[9–12].

CIS effectors and their roles in host cell signaling. Type 6 Secretion Systems have been shown to wield entire superfamilies of effector proteins that possess phospholipase activity; these phospholipases are known to play a role in antagonistic behavior between bacterial species[13]. Phospholipase activity is a common enzymatic function of CIS effectors and their toxicity in host cells is usually attributed to their non-specific targeting of the major lipid components in the plasma membrane. Destruction of the phospholipids leads to holes in the membrane and loss of membrane gradient within bacteria[14]. In eukaryotes lipase toxins release potent inflammation signaling molecules which signal cell apoptosis[15]. However, not all lipases target the general membrane components and lead to cell death. Some bacterial lipases exist to produce lipid second messengers such as diacylglycerol and phosphatidic acid[16]. These lipases differ from toxin lipases in their specificity for lipid membrane components. Most lipases which generate lipid second messengers bind and cleave special membrane lipids such as glycerophosphoinositol lipids. These lipids are selectively located in various membrane compartments within the cell and exist as minor membrane components, (~10%) of the total membrane lipids[17].

Bacteria stimulate the metamorphosis of diverse animal taxa. One instance in which microbes promote normal animal development is the stimulation of animal metamorphosis in response to bacteria. During these transient interactions in the sea, the free-swimming larvae of many marine invertebrates must identify a suitable location for settlement and metamorphosis on the sea floor. The location is crucial because

metamorphosis is an irreversible process, and the animal is often unable to relocate under unfavorable conditions. For many of these invertebrate larvae, bacteria have been shown to stimulate metamorphosis. However the mechanism of bacteria-stimulated metamorphosis remain unclear[18].

The animal signaling systems involved and the speed at which they undergo metamorphosis hints that second messenger signaling and neuronal signaling are critical mechanisms mediating the animal responses to bacteria when undergoing settlement and metamorphosis[19–24]. A major role for membrane perturbations has been hypothesized in the stimulation of metamorphosis, whether through second messenger signaling, such as lipid activation of Protein Kinase C (PKC), or by other mechanisms such as membrane depolarization. The PKC lipid stimulated signaling system has been previously characterized in *Hyractinia echinata*, *Mitrocomella polydiademata,* Red Sea coral planulae, *Capitella* sp. 1, *Balanus Amphitrite* and *Strongylocentrotus purpuratus,* where the lipids stimulated PKC pathway has been implicated in metamorphosis [21,25–29]. Lipid vesicles or specific lipids found in bacterial biofilms are also able to stimulate larval metamorphosis [30,31].

A model bacterium-animal interaction for studying bacteria stimulated metamorphosis. To study bacteria-stimulated metamorphosis, we study the bacterium *Pseudoalteromonas luteoviolacea* that stimulates the metamorphosis of the tubeworm *Hydroides elegans* (hereafter *Hydroides*). *Hydroides* undergoes metamorphosis in the presence of a single monospecies biofilm of the bacteria *Pseudoalteromonas luteoviolacea (P. luteo)*[32]. The use of a single animal and bacteria simplifies the complex systems which occur in nature and the simple phenotypic readout of metamorphosis can

be used to probe this interaction. *P. luteo* is amenable to genetic manipulation and through reverse genetics, the discovery of this proteinaceous injection system was found to facilitate the communication and signaling that occurs between these two organisms.

P. luteoviolacea stimulates *Hydroides* metamorphosis by producing a phage tail-like structure called Metamorphosis Associated Contractile structures (MACs). MACs are one of a class of structures called Contractile Injection Systems (CIS), which share homology to the contractile tails of bacteriophage[8]. MACs are produced by a subpopulation of *P. luteoviolacea* bacteria in an array of multiple tails, which upon interaction with a target cell contract and inject a protein payload. There are two known effectors associated with the MACs, *Pseudoalteromonas* Nuclease Effector 1 (Pne1), which is a nuclease toxin which has been shown to kill certain target cells[33], and second effector, metamorphosis inducing factor 1 (Mif1), which is both necessary and sufficient to induce the *Hydroides* metamorphosis but currently has no known associated function[34].

Previously, we have shown that the Mif1 protein effector loaded within the inner tube lumen of the MACs structure stimulates the metamorphosis of *Hydroides* larvae. Further, Mif1 stimulates and requires diacylglycerol production, as well as PKC and MAPK signaling during *Hydroides* metamorphosis. However, how Mif1 functions and stimulates metamorphosis remains unclear. In this work, we set out to determine how the protein effector Mif1 from *P. luteoviolacea* MACs stimulate the metamorphosis of *Hydroides* larvae. We found that N-terminal and C-terminal regions of the Mif1 protein are particularly important *Hydroides* metamorphosis. Further, we found that Mif1 shares homology with lipid binding proteins and that Mif1 possesses lipase activity.

5.3 Results and Discussion

Mif1 is predicted to contain three domains and associate with cell membranes. The bacterial effector protein Mif1 has been shown previously to stimulate metamorphosis of Hydroides[35]. However, how this protein is sensed and the downstream signaling associated with Mif1 stimulation of metamorphosis is still unknown. To generate hypotheses about the structure and function of Mif1, we analyzed the Mif1 amino acid sequence using several protein domain prediction programs. When we ran Mif1 through HMMR, and Phyre2, we found that the E-values of predicted protein hits were below the threshold of E-value=0.01 and confidence below 40% for all identified structures/domains, respectively, providing little confidence in these predictions of Mif1 (Figure S5.1.)[36,37]. Mif1 did, however, show some homology to a DUF (domain of unknown function) 4157 when searched via five iterations of psiBLAST, which was identified within other eCIS effector proteins[38] and is predicted to encode a metallopeptidase (Figure S5.2.)[39].

In comparison to the other protein prediction programs, when we used the protein prediction program Alphafold2[40], the analysis provided a strong prediction of the Mif1 structure with a pIDDT above 50% for most of the protein folding regions and a predicted alignment error showing confident structure across the majority of the protein and identifying at least three possible domains (Figure 5.1. A, B & C). The structure predicted by Alphafold2 showed two alpha helical globular domains at the N- and C-terminus of the proteins, with a large beta pleated sheet portion in the middle of the protein (Figure 5.1. A). We additionally divided the Mif1 protein into 3 sections (1-200, 200-760 and 760-943 amino acids) and ran each section independently through Alphafold2.

To identify proteins that possess structural homology with the Alphafold2 Mif1 structure prediction, we used 3D-Blast to search the Mif1 prediction against the protein data base (PDB) or structural classification of proteins (SCOP) database[41,42]. The N-terminal 1-200 amino acids showed homology with a known protein lipase chaperone structure (Table S5.2. B) (PDB 2ES4). For example, the top hit (e-value 2.00E-26) is to Burkholderia glumae lipase-specific foldase. The center region of Mif1 200-760 amino acids of the protein, matched with membrane associated protein complexes (Table S5.2. C). For example, the top hit is the PapC pilus translocation pore complex (e-value 8.00E-50). The C-terminal 760-943 amino acids hit significantly to a 14-3-3 zeta (PDB 1IB1), which is shown to do interact in protein-protein binding and is activated via PKC phosphorylation (Table S5.2. D). These results predict that Mif1 is a membrane associated protein and might have distinct functions associated with three different domains found within the protein.

To determine whether the Mif1 secondary structure matches the Alphafold structural prediction, we viewed purified Mif1 via negative stain transmission electron microscopy (TEM). Our data showed many proteins demonstrated similar characteristics expected for a protein with very little tertiary structure. Most the proteins were generally long and showed secondary structure that resembled a protein with lots of mobility and little structure otherwise (Figure 5.1. E & F).

We have previously shown that Mif1 is loaded within the inner tube of the MACs complex[34]. To determine whether specific segments of the Mif1 protein are required for loading of Mif1 into the MACs complex and/or responsible for inducing *Hydroides* metamorphosis, we created 5 *P. luteoviolacea* strains lacking 200 amino acid segments

of Mif1 across the 943 amino acid protein (Figure 5.2. A). After performing cryo-electron microscopy on each of the 5 strains expressing truncated variants of the Mif1 protein, we observed that mutants in the N-200aa and C-200aa portions of the Mif1 protein produced MACs that lacked electron density within the MACs inner tube, while the other 3 mutants lacking segments of Mif1 in the 200-800 amino acid region possessed an electron density within the inner tube, similar to wild type *P. luteoviolacea* MACs (Figure 5.2. B). We next tested whether the 5 strains expressing truncated forms of Mif1 would be able to stimulate the metamorphosis of *Hydroides* larvae. Upon exposure to MACs from strains expressing the truncated Mif1 proteins, we found that *the mif1*Δ0-200, *mif1*Δ200-400, *mif1*Δ400-600 and *mif1*Δ749-949 strains stimulated low rates of metamorphosis, While the *mif1*Δ600-800 mutant showed rates of metamorphosis similar to the Δ*mif1* mutant and buffer controls. Our data show that each of the 5 regions of Mif1 are required for loading of Mif1 into the MACs complex and/or stimulation of *Hydroides* metamorphosis.

Mif1 contains toxic domains located at the N-terminus and C-terminus. Many CIS effectors are protein toxins delivered to the host organism to elicit specific cellular responses. When overexpressed in *E. coli*, we noticed that certain portions of the Mif1 protein appeared to be highly toxic to the *E. coli.* To determine whether specific regions of the Mif1 protein were responsible for the observed toxicity, we cloned 5 different fragments of Mif1 into an overexpression plasmid and expressed them in *E. coli* BL21 PlysE from an IPTG-inducible T7 promoter. The fragments included the Mif1 protein divided into thirds (amino acids 1-304 304-608 and 609-943, named fragment A, B, and C, respectively) with two larger portions covering two thirds of the protein (amino acids 1-600 and 343-943, named fragment D and E, respectively) that overlapped the smaller

thirds in case the intersections are required for interaction (Figure 5.3. A). When cells expressing the Mif1 fragments or a control plasmid expressing *gfp* were plated on a media containing 0.1 mM IPTG and serial diluted we found that the E and A fragment but not the full-length protein led to an increase in cell death (Figure 5.3. B & C). Cells plated onto control media lacking IPTG did not exhibit differences in growth when compared to a strain expressing *gfp*. We further divided the A and C fragments into 3 more overlapping proteins A1-A3 (amino acids 1-150, 50-200 and 151-304) and C1-C3 (amino acids 643-793, 693-843 and 793-943). None of the A1, A2 or A3 fragments exhibited toxicity in *E. coli*. However, for the C-terminus we were able to identify the 150 aa C1 fragment as the portion of the protein found in the C-term responsible for its toxin phenotype (Figure 5.3. B & C). These results suggest that the protein may contain a toxic domain within the N- and C-termini of the protein itself.

We further confirmed these findings by looking for cell death via propidium iodide (PI) staining. Mfi1 expressing *E. coli* constructs were induced for 4 hours and then the *E.* coli was stained with the membrane impermeable nuclear stain propidium iodide to determine cellular integrity. Our results show that the Mif1 overexpression construct led to increased PI staining but overexpression of the chaperone protein 605 did not cause loss of membrane integrity (Figure S5.6. A-C). To determine if 605 might decrease the toxicity of the Mif1 protein, we co-expressed both Mif1 and 605 in the same *E. coli* from a dual expression plasmid, however there was no decrease in toxicity when co-expressed (Figure S5.6. D). Our results confirm that expression of Mif1 in *E.* coli leads to bacterial cell death.

Mif1 binds to glycerophosphoinositol membrane lipids. Because Mif1 exhibits toxicity when overexpressed in *E. coli* and the A1 and C1 regions promote disruption of the cellular membrane visualized by propidium iodide staining, we next asked whether Mif1 was capable of binding to membrane lipids. Since Mif1 I known to act in the eukaryotic membranes found in *Hydroides*, we tested whether Mif1 was able to bind to phospholipids spotted membranes and performed a western blot to identify specific Mif1-lipid binding interactions. If the protein binds to specific lipids, we can determine the relative association and preference based on spot intensity. When recombinant Mif1 protein was exposed to a commercially available membrane strips which assessed binding. The first membrane strip with a variety of lipids from triacyl glycerides to sphingomyelin and all of the common membrane associated lipids showed that Mif1 was capable of binding to Phosphatidylinositol-4-phosphate (Ptdins(4)P) with high affinity and to a lesser degree Phosphatidic acid (PA) (Figure 5.4. A). Because Mif1 appeared to bind phosphatidylinositol lipids, testing Mif1 against a second membrane with a variety of phosphatidylinositol isomers showed that Mif1 has high affinity for Ptdins(3,5)P over Ptdins(3)P or Ptdins(4)P (Figure 5.4. B). Finally, to determine the binding region of Mif1 for the various phospholipids, the first, middle, and last third of the protein (fragment A, B, and C) were tested for binding. Our results show that interestingly all fragments were able to associate with phosphatidyl serine (PS), which was not seen with the full protein, it is unclear why the fragments but not the full protein was able to associate with this membrane lipid. Fragments A and B were only shown to bind to PS, however, fragment C was able to bind to the membrane lipids, PS, Ptdins(4,5)P, Ptdins(3)P, Ptdin(3,4)P, Ptdins(4)P and Ptdins(5)P in that order of preference (Figure 5.5. C). Our results showed

that full length mif1 binds preferentially binds Ptdins(3,5)P > Ptdins(3)P > Ptdins(4)P > Ptdins(5)P > PA, in that order of preference.

The association between Mif1 and inositol phospholipids might suggest a role for Mif1 in targeting eukaryotic cell physiology. Specific inositol phospholipids are preferentially found in specific eukaryotic organelles, and our present data hints at a role for Mif1 to specific cellular processes within the eukaryotic host.

Mif1 is an esterase that cleaves the PLA1 carboxyester and PLD phosphodiester linkages found in phospholipids. The animal signaling systems involved and the speed at which they undergo metamorphosis hints that second messenger signaling and neuronal signaling are critical mechanisms mediating the animal responses to bacteria when undergoing settlement and metamorphosis[19–24]. A major role for membrane perturbations has been hypothesized in the stimulation of metamorphosis, whether through second messenger signaling, such as lipid activation of Protein Kinase C (PKC), or by other mechanisms such as membrane depolarization. The PKC lipid stimulated signaling system has been previously characterized in *Hyractinia echinata*, *Mitrocomella polydiademata,* Red Sea coral planulae, *Capitella* sp. 1, *Balanus Amphitrite* and *Strongylocentrotus purpuratus,* where the lipids stimulated PKC pathway has been implicated in metamorphosis [21,25–29]. Lipid vesicles or specific lipids found in bacterial biofilms are also able to stimulate larval metamorphosis [30,31].

Because Mif1 associates with membrane lipids, we next tested Mif1 for enzymatic activity. To this end, we tested recombinantly purified Mif1 protein for its ability to cleave acyl-ester linkages by using a synthetic lipid decanoic acid-PNPP fusion and through the cleavage of Tween-20. In these assays, we found that Mif1 possesses the ability to cleave

both tween-20 and PNPP-decanoic acid assays, which demonstrate that Mif1 possesses Phospholipase A1 (PLA1) type cleavages (Figure 5.5. A & B).

We next set out to determine whether Mif1 is one of 3 common types of phospholipases; Phospholipase A2 (PLA2), Phospholipase C (PLC), or Phospholipase D (PLD). Mif1 exhibited no activity in the PLA2-specific, or PLC-specific assays. However, we did observe that Mif1 possessed activity in a commercial PLD assay (Figure 5.5. C, D, & E). These data suggest a role for Mif1 as a phospholipase in the membrane. It is unclear whether the PLD activity or the PLA1 activity are required for metamorphosis by Mif1 and the products produced (decanoic acid and phosphatidic acid). When added exogenously, however, neither decanoic acid or phosphatidic acid alone stimulated *Hydroides* metamorphosis (Figure S5.5.). These results corroborate the lipid binding results above, which show that Mif1 binds to PIPs and PA, which is the cleavage product of a PLD.

The Mif1 protein possesses two regions that cleave membrane lipids. To determine the portion of the protein which contains the lipase activity we analyzed each of the Mif1 expression fragments for lipase activity via PNPP-decanoic acid cleavage assy. Our results show that the E and C fragment which contain the C-terminal portion of the protein possessed the most activity (Figure 5.6. A). However, we did identify some activity associated with just the A fragment of the protein. To better understand how each of the fragments contribute to the Mif1 lipase activity we combinatorial combined these fragments together. Each of the fragments were expressed in a separate *E. coli* and purified. After purification the protein concentrations were normalized and added together such that the total protein concentration was kept constant. After combining the fragments

together, the lipase assay was repeated to determine how the protein works together. Our findings show that the Mif1 protein acts cooperatively with each of the fragments contributing to the lipase function. Where the A+B+C fragment retained the most activity followed by the A+C fragment and then by the A+B and B+C, finally the C and A fragment alone possessed some activity while the B fragment alone contained no lipase activity (Figure 5.6. B). These data suggest that the Mif1 protein requires all the protein for wild-type activity and no isolated domain exists which contains the lipase activity.

Many Type 6 Secretion System effectors exert their effect on target cells via lipase activity[13]. Many of these lipases are cytotoxic lipases that are used as toxin proteins and delivered to induce cell death in the target cells usually bacteria antagonists. However, there are examples of lipases which produce very specific signaling to occur within the host cell. For example, the MARTX toxins from *Vibrio cholerae* has been shown to bind PIPs and through PLA1 cleavage inhibit endosomal trafficking and autophagy[44]. The alpha-beta hydrolase domain of the MARTX protein is not a generic toxin like phosphatidylcholine specific PLDs that completely degrade the major component of the cellular membrane, but instead act on low abundance lipids and specific signaling pathways within the cell. Mif1 likely acts through a different signal cascade than the MARTX toxin since is not toxic to *Hydroides* larvae, however, since the lipids Mif1 targets are found on endosomes and lysosomes PI(3,5)P, PI(4)P, and PI(3)P, the target lipids and subcellular localization may be shared. The protein may also be cleaved and facilitate its own activity or act as an anti-toxin within the host cell. Our data illuminates the complexity of these large effector toxins and their potential role in multiple different signaling processes.

5.3 Conclusion.

Our finding show that the Mif1 protein requires the N and C terminus for loading into the MACS complex. A systematic knock out of 200bp regions within the Mif1 protein shows that a region at 600-800 amino acids of the Mif1 protein is essential for function as a metamorphosis inducing protein. We also determine that Mif1 can bind to inositol phospholipids and phosphatidic acid and possess PLA1 and PLD type lipid linkages (Figure S5.5.). Our findings demonstrate the role of a bacterial lipase effector and its functional abilities, which furthers our understanding the complex nature of bacteria-animal signaling interactions that take place.

5.4 Materials and Methods

Bacterial toxin assays. *E. coli* BL21 Plyse Bacteria containing the pET15b IPTG inducible plasmid were grown shaking at 200rpm and 37˚C overnight. The over-night culture was then plated using 1/5 serial dilution scheme with an initial OD of 0.1 (OD600) and allowed to grow overnight at 37˚C. The plates contained either LB + 100µg/µL ampicillin + 0.1 mM IPTG or identical media lacking IPTG.

Pull down assays. BL21 bacteria containing chloramphenicol resistant pACYC plasmid (Sigma-aldrich CAT**#71147**) with Mlp1 cloned at the S-tag site and ampicillin resistant Pet15b with Hisx6-tagged Mif1, GFP, or Mif1 fragments. The bacteria were grown under dual pressure with Ampicillin 100µM and Chloramphenicol 100µM, shaking at 200rpm at 37˚C in lysogeny broth (Thermofisher CAT#DF0446-17).

Protein Purification. BL21 plysE bacteria containing the pET15b plasmid expressing the individual bacteria constructs were initially streaked out onto LB + ampicillin agar plates overnight. A single colony was inoculated into 5 mL of LB + ampicillin media culture tubes and grown overnight shaking at 200 rpm at 37˚C. The entire 5 mL overnight cultures were then added to 500 mL LB + ampicillin in beveled flasks shaking 200 rpm at 37˚C until reaching an OD of 0.4-1.0. The bacteria were then induced with IPTG 0.1 mM - 1 mM and the temperature was changed to 30˚C during protein induction. The flasks were then allowed to grow for an additional 16 hours. The cells were then spun down at 4000 g for 20 minutes and the supernatant was removed. The pellets were then resuspended in 5mL of 25mM tris pH 7.8, 500mM NaCl, 20mM imidazole, and

reversible protease inhibitors pepstatin a 20μM, bestatin 10μM, and leupeptin 100μM. The samples were then stored resuspended at -80˚C. After thawing, the samples were then lysed twice by french press with the SIm-Aminco french press and mini cell at 1000 psi. The collected lysates were then lysed by probe sonication for 30 seconds to disrupt DNA. The lysed samples were then centrifuged at >10,000g for 20 mins and the supernatant was collected and spun down for an additional 20 mins. 2mL of 70% slurry of Ni-NTA agarose beads were then equilibrated with the lysis buffer (25mM tris pH 7.8, 500mM NaCl, 20mM imidazole) and added to the collected supernatants. The samples with Ni-NTA beads were allowed to rock at 4˚C for at least 1 hour. The samples were spun down at 4000 rpm for 5 min and the unbound supernatant removed and stored. The beads were then washed three times with 50 mL of ice cold 25mM tris pH 7.8, 500mM NaCl, 20mM imidazole. The beads were then transferred to a separator column and incubated with 2mL of an elution buffer 25mM tris pH 7.4, 500mM NaCl, 250mM imidazole for 15 min. The solution was then gravity filtered into a 15mL conical tube. An additional 2mL of elution buffer was gravity washed over the column, and the beads were spun down to remove the remaining buffer. The collected elution was buffer exchanged into 25mM tris pH 7.6, 250mM NaCl and concentrated in pierce protein concentrators 10,000Da Molecular weight cutoff. Protein was then quantified by Bradford assay and stored at -80˚C.

PIP strip methods. Pip strips and membrane strips were ordered from echelon biosciences (CAT# P-6001 and P-6002). The strips were blocked with 2.5% non-fat milk, 0.125% tween-20, 1X PBS (137mM NaCl, 2.7mM KCl, 10mM Na2HPO4, 1mM CaCl2,

0.5mM MgCl2). 3-5µg of protein was added to the blocking buffer and let rock at 4˚C overnight. The strips were washed 3 times for 10 mins with 1x PBST while rocking. The Mif1 endogenous primary rb ab was added to the PBST at 1:1000 dilution and rocked at 4˚C overnight. The primary ab was washed for 10 mins with 1x PBST while rocking at room temp. Finally, the secondary goat anti-rb antibody was added at 1:10,000 in 1x PBST and allowed to rock for 1 hour at room temp. Three more washes with 1x PBST were completed for 15 mins each prior to visualization with chemiluminescence.

Lipase assay protocols.

Tween-20 assay protocol. Protocol was modified from (Tigerstrom and Stelmaschuk, 1989) The lipase assay buffer consisted of 20mM Tris-HCl pH 8.0, 1.8% Tween-20, and 3mM CaCl. The release and precipitation of the acyl chain was measured by turbidity at OD500. 20µg (1µg/µL) of protein was added to 200µL of assay buffer in a clear bottom 96 well plate and read at OD500 for X mins. Protein activity was compared to control proteins GFP and JF15605 which were purified in tandem to Mif1.

PnPP-decanoic acid assay protocol. Substrate was purchased from Sigma-Aldrich (Cat#N0252-100MG) The substrate solution was made with a final concentration of 50mM Tris-HCl pH 7.5, 1mM CaCl2, 0.3% Triton X-100, 1mM pNPP decanoic acid, 4% (v/v) isopropanol, 1%(v/v) acetonitrile, and 15µL protein at 1µg/µL in 25mM tris pH 7.6 and 250mM NaCl. The reaction mixture was read at abs OD405 for 10hr every 5 minutes.

PC-PLC assay protocol. Phospholipase C assay kit was purchased from Thermofisher scientific(CAT#E10215). The protocol and buffers used were followed per the manufacturer's protocol. 15µg of protein was used for each assay and fluorescent

excitation 485/20 and emission 528/20 filters were used to determine release of substrate. The assay was run in a clear bottom black walled 96 well plate.

PLA2 assay protocol. PLA2 assay kit was purchased from ThermoFisher (CAT#E10217). The protocol and buffers used were followed per the manufacturer's protocol. 15µg of protein was used for each assay and fluorescent excitation 485/20 and emission 528/20 filters were used to determine release of substrate. The assay was run in a clear bottom black walled 96 well plate.

PLD assay protocol. The amplex red phospholipase D assay kit was purchased from ThermoFisher (CAT# A12219). The protocol and buffers used were followed per the manufacturer's protocol. 15µg of protein was used for each assay and fluorescence excitation and emission, 535 nm and 595 nm respectively.

Expression and *E. coli* cell death assay. Bacteria were struck out onto Luria-Bertani broth agar plates with 100µg/µL Ampicillin and grown overnight at 37˚C. A single colony was inoculated into 5mL LB media with 100µg/µL Ampicillin and was shaken at 200 RPM at 37˚C overnight. The cultures were then normalized by OD and serial diluted using a ⅕ serial dilution scheme (1, ⅕, 1/25 …etc) for eight total serial dilutions. 5µL of each dilution was spotted onto both a LB media plate containing 100µg/µL ampicillin without IPTG and the same serial dilution was then plated onto a second plate containing LB+amp with 0.1mM IPTG. The cultures were grown overnight at 37˚C and imaged after 22 hours of growth.

Cloning methods. As previously described in (Ericson et. al.)[48].

Mating methods. As previously described in (Ericson et. al.)[48].

Pulldown assay. As previously described in (Ericson et. al.)[48].

Strains used in this study.

Pseudoalteromonas luteoviolacea HI1 StrR

Pseudoalteromonas luteoviolacea HI1 StrR ΔmacB

Pseudoalteromonas luteoviolacea HI1 StrR ΔJF50_12615 (HI1_01551)

Pseudoalteromonas luteoviolacea HI1 StrR JF50_12615ΔNterm-200aa

Pseudoalteromonas luteoviolacea HI1 StrR JF50_12615Δ200-400aa

Pseudoalteromonas luteoviolacea HI1 StrR JF50_12615Δ400-600aa

Pseudoalteromonas luteoviolacea HI1 StrR JF50_12615Δ600-800aa

Pseudoalteromonas luteoviolacea HI1 StrR JF50_12615ΔCterm-200aa

Plasmids used in this study:	host
pET15b-JF50_12605	BL21 plysE
pET15b-JF50_12615	BL21 plysE
pET15b_12615_Fragment A	BL21 pLysE
pET15b_12615_Fragment B	BL21 pLysE
pET15b_12615_Fragment C	BL21 pLysE
pET15b_12615_fragment_D	BL21 pLysE
pET15b_12615_fragment_E	BL21 pLysE
Pet15b_Mif1_frag_A1	BL21 plysE
Pet15b_Mif1_frag_A2	BL21 plysE
Pet15b_Mif1_frag_A3	BL21 plysE
Pet15b_Mif1_frag_C1	BL21 plysE
Pet15b_Mif1_frag_C2	BL21 plysE
Pet15b_Mif1_frag_C3	BL21 plysE
pACYCDuet_605	BL21
pACYCDuet_605+GFP	BL21
pACYCDuet_605+pet15b_Mif1	BL21
pACYCDuet_605+pet15b_Mif1_FragA	BL21
pACYCDuet_605+pet15b_Mif1_FragB	BL21
pACYCDuet_605+pet15b_Mif1_FragC	BL21
pACYCDuet_605+pet15b_Mif1_FragD	BL21
pACYCDuet_605+pet15b_Mif1_FragE	BL21
pCVD443_Mif_Δ200-400	SM10
pCVD443_Mif_Δ400-600	sm10
pCVD443_Mif_Δ600-800	sm10

pCVD443_JF50_12615ΔN200aa	SM10
pCVD443_JF50_12615ΔC200aa	SM10

5.5 Acknowledgements

Chapter 5 is unpublished with coauthors. K. E. Malter, C. Westin, C.F. Ericson, A.T. Alker, N. J. Shikuma. (Authorship and order still TBD). The dissertation author is a coauthor of this material. My specific contributions include Figure 5.1., Figure 5.2., Figure 5.3., Figure 5.4., Figure 5.5., Figure 5.6., Table 5.1., Table S5.1., Figure S5.1., Figure S5.2., Table S5.2., Figure S5.3., Figure S5.4., Figure S5.5. and the initial drafts written for this document.

5.6 References

1. Shikuma, N. J. Bacteria-Stimulated Metamorphosis: an Ocean of Insights from Investigating a Transient Host-Microbe Interaction. *mSystems* **6**, 1–5 (2021).

2. Jandhyala, S. M. *et al.* Role of the normal gut microbiota. *World J. Gastroenterol.* **21**, 8787–8803 (2015).

3. Aschtgen, M.-S., Wetzel, K., Goldman, W., McFall-Ngai, M. & Ruby, E. *Vibrio fischeri* -derived outer membrane vesicles trigger host development. *Cell. Microbiol.* **18**, 488–499 (2016).

4. Hill, J. H., Franzosa, E. A., Huttenhower, C. & Guillemin, K. A conserved bacterial protein induces pancreatic beta cell expansion during zebrafish development. *Elife* **5**, 1–18 (2016).

5. Zobell, C. E. & Allen, E. C. The Significance of Marine Bacteria in the Fouling of Submerged Surfaces. *J. Bacteriol.* **29**, 239–51 (1934).

6. Cavalcanti, G., Alker, A., Delherbe, N., Malter, K. E. & Shikuma, N. J. The Influence of Bacteria on Animal Metamorphosis. *Annu. Rev. Microbiol.* **74**, in press (2020).

7. Hadfield, M. G. Why and how marine-invertebrate larvae metamorphose so fast. *Semin. Cell Dev. Biol.* **11**, 437–443 (2000).

8. Wang, Y. & Ruby, E. G. The roles of NO in microbial symbioses. *Cell. Microbiol.* **13**, 518–526 (2011).

9. Chambon, J.-P., Nakayama, A., Takamura, K., McDougall, A. & Satoh, N. ERK- and JNK-signalling regulate gene networks that stimulate metamorphosis and apoptosis in tail tissues of ascidian tadpoles. *Development* **134**, 1203–1219 (2007).

10. Amador-Cano, G., Carpizo-Ituarte, E. & Cristino-Jorge, D. Role of Protein Kinase C, G-Protein Coupled Receptors, and Calcium Flux During Metamorphosis of the Sea Urchin *Strongylocentrotus purpuratus*. *Biol. Bull.* **210**, 121–131 (2006).

11. Wang, H. & Qian, P.-Y. Involvement of a novel p38 mitogen-activated protein kinase in larval metamorphosis of the polychaete Hydroides elegans (Haswell). *J. Exp. Zool. B. Mol. Dev. Evol.* **314**, 390–402 (2010).

12. McCauley, D. W. Serotonin plays an early role in the metamorphosis of the hydrozoan *Phialidium gregarium*. *Dev. Biol.* **190**, 229–240 (1997).

13. Moniri, N. H. & Booth, R. G. Role of PKA and PKC in histamine H1 receptor-

mediated activation of catecholamine neurotransmitter synthesis. *Neurosci. Lett.* **407**, 249–253 (2006).

14. Henningi, G., Hofmann, D. K. & Yahu, Y. B. Metamorphic processes in the soft corals *heteroxenia fuscescens* and *xenia umbellata* : The effect of protein kinase c activators and inhibitors. *Invertebr. Reprod. Dev.* **34**, 35–45 (1998).

15. Leitz, T. Biochemical and cytological bases of metamorphosis in Hydractinia echinata. *Mar. Biol. Int. J. Life Ocean. Coast. Waters* **116**, 559–564 (1993).

16. Unabia, C. R. C. & Hadfield, M. G. Role of bacteria in larval settlement and metamorphosis of the polychaete *Hydroides elegans* . *Mar. Biol.* **133**, 55–64 (1999).

17. Hadfield, M. G. Why and how marine-invertebrate larvae metamorphose so fast. *Semin. Cell Dev. Biol.* **11**, 437–443 (2000).

18. Biggers, W. J. & Laufer, H. Settlement and Metamorphosis of *Capitella* Larvae Induced by Juvenile Hormone-Active Compounds Is Mediated by Protein Kinase C and Ion Channels. *Biol. Bull.* **196**, 187–198 (1999).

19. Freeman, G. & Ridgway, E. B. Cellular and intracellular pathways mediating the metamorphic stimulus in hydrozoan planulae. *Roux's Arch. Dev. Biol.* **199**, 63–79 (1990).

20. Leitz, T. & Klingmann, G. Metamorphosis inHydractinia: Studies with activators and inhibitors aiming at protein kinase C and potassium channels. *Roux's Arch. Dev. Biol.* **199**, 107–113 (1990).

21. Yamamoto, H., Tachibana, A., Matsumura, K. & Fusetani, N. Protein Kinase C (PKC) Signal Transduction System Involved in Larval Metamorphosis of the Barnacle, *Balanus amphitrite* . *Zoological Science* **12**, 391–396 (1995).

22. Freckelton, M. L. *et al.* Bacterial lipopolysaccharide induces settlement and metamorphosis in a marine larva . *bioRxiv* (2019). doi:doi: http://dx.doi.org/10.1101/851519

23. Guo, H., Rischer, M., Westermann, M. & Beemelmanns, C. Two Distinct Bacterial Biofilm Components Trigger Metamorphosis in the Colonial Hydrozoan Hydractinia echinata. *MBio* **12**, (2021).

24. Geller, A. M. *et al.* The extracellular contractile injection system is enriched in environmental microbes and associates with numerous toxins. *Nat. Commun. 2021 121* **12**, 1–15 (2021).

25. Fraser, A. D., Plattner, M. & Leiman, P. G. Energetics of Sheath Contraction in

Contractile Injection Systems. *Biophys. J.* **112**, 334a (2017).

26. Shikuma, N. J. *et al.* Marine tubeworm metamorphosis induced by arrays of bacterial phage tail-like structures. *Science (80-.).* **343**, 529–33 (2014).

27. Flaugnatti, N. *et al.* A phospholipase A 1 antibacterial Type VI secretion effector interacts directly with the C-terminal domain of the VgrG spike protein for delivery. doi:10.1111/mmi.13292

28. Sana, T. G. *et al.* Salmonella Typhimurium utilizes a T6SS-mediated antibacterial weapon to establish in the host gut. *Proc. Natl. Acad. Sci. U. S. A.* **113**, E5044-51 (2016).

29. Aubert, D. F. *et al.* A Burkholderia Type VI Effector Deamidates Rho GTPases to Activate the Pyrin Inflammasome and Trigger Inflammation. *Cell Host Microbe* **19**, 664–674 (2016).

30. Ma, L. S., Hachani, A., Lin, J. S., Filloux, A. & Lai, E. M. Agrobacterium tumefaciens deploys a superfamily of type VI secretion DNase effectors as weapons for interbacterial competition in planta. *Cell Host Microbe* **16**, 94–104 (2014).

31. Russell, A. B. *et al.* Diverse type VI secretion phospholipases are functionally plastic antibacterial effectors. *Nature* **496**, 508–512 (2013).

32. Chatzidaki-Livanis, M., Geva-Zatorsky, N. & Comstock, L. E. Bacteroides fragilis type VI secretion systems use novel effector and immunity proteins to antagonize human gut Bacteroidales species. *Proc. Natl. Acad. Sci.* **113**, 3627–3632 (2016).

33. A., S. H. *et al.* Disruption of lipid homeostasis in the Gram-negative cell envelope activates a novel cell death pathway. *Proc. Natl. Acad. Sci.* **113**, E1565–E1574 (2016).

34. Cummings, B. S., McHowat, J. & Schnellmann, R. G. Phospholipase A(2)s in cell injury and death. *J. Pharmacol. Exp. Ther.* **294**, 793–799 (2000).

35. Bender, J. & Flieger, A. Lipases as Pathogenicity Factors of Bacterial Pathogens of Humans BT - Handbook of Hydrocarbon and Lipid Microbiology. in (ed. Timmis, K. N.) 3241–3258 (Springer Berlin Heidelberg, 2010). doi:10.1007/978-3-540-77587-4_246

36. Suh, P. G. *et al.* Multiple roles of phosphoinositide-specific phospholipase C isozymes. *J. Biochem. Mol. Biol.* **41**, 415–434 (2008).

37. Rocchi, I. *et al.* A Bacterial Phage Tail-like Structure Kills Eukaryotic Cells by Injecting a Nuclease Effector. *Cell Rep.* **28**, 295-301.e4 (2019).

38. Nicholas J. Shikuma, Beyhan, S., Pilhofer, M. & Ericson, C. Protein and peptide delivery systems and methods for making and using them. (2019).

39. Unabia, C. R. C. & Hadfield, M. G. Role of bacteria in larval settlement and metamorphosis of the polychaete *Hydroides elegans*. *Mar. Biol.* **133**, 55–64 (1999).

40. Malter, K. E. *et al.* Diacylglycerol, PKC and MAPK Signaling Initiate Tubeworm Metamorphosis in Response to Bacteria. *Dev. Biol.* (2022). doi:https://doi.org/10.1016/j.ydbio.2022.04.009

41. Jumper, J. *et al.* Highly accurate protein structure prediction with AlphaFold. *Nature* **596**, 583–589 (2021).

42. Welte, W., Nestel, U., Wacker, T. & Diederichs, K. Structure and function of the porin channel. *Kidney Int.* **48**, 930–940 (1995).

43. Carpizo-Ituarte, E. & Hadfield, M. G. Stimulation of metamorphosis in the polychaete Hydroides elegans Haswell (Serpulidae). *Biol. Bull.* **194**, 14–24 (1998).

44. Quentin, D. *et al.* Mechanism of loading and translocation of type VI secretion system effector Tse6. *Nat. Microbiol.* **3**, 1142–1152 (2018).

45. Rocchi, I. *et al.* A Bacterial Phage Tail-like Structure Kills Eukaryotic Cells by Injecting a Nuclease Effector. *Cell Rep.* **28**, 295--301.e4 (2019).

46. Ericson, C. F. *et al.* A contractile injection system stimulates tubeworm metamorphosis by translocating a proteinaceous effector. *Elife* **8**, 1–19 (2019).

47. Agarwal, S. *et al.* Autophagy and endosomal trafficking inhibition by Vibrio cholerae MARTX toxin phosphatidylinositol-3-phosphate-specific phospholipase A1 activity. *Nat. Commun.* **6**, 8745 (2015).

48. Ericson, C. F. *et al.* A contractile injection system stimulates tubeworm metamorphosis by translocating a proteinaceous effector. *Elife* **8**, 1–19 (2019).

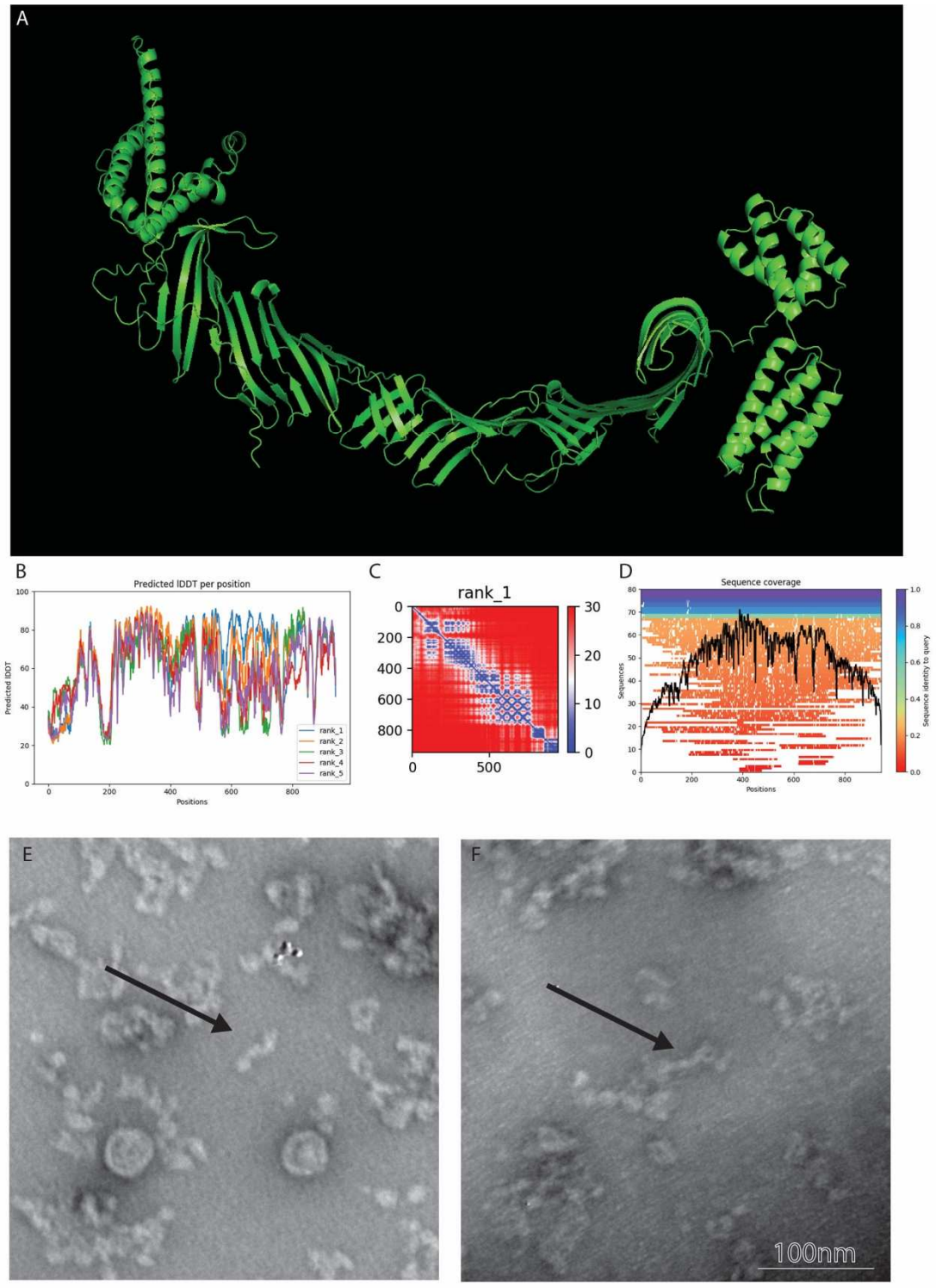

Figure 5.1. Mif1 alpha fold prediction. (A) Alphafold2 prediction of the effector protein Mif1. (B) Predicted local difference distance test (lDDT) local superposition-free score for each residue 1-943. (B) Predicted alignment error of predicted residues vs scored residues. (C) Sequence coverage of predicted residues. (E,F) Negative staining Transmission electron microscopy of purified Mif1. Scalebar = 100nm.

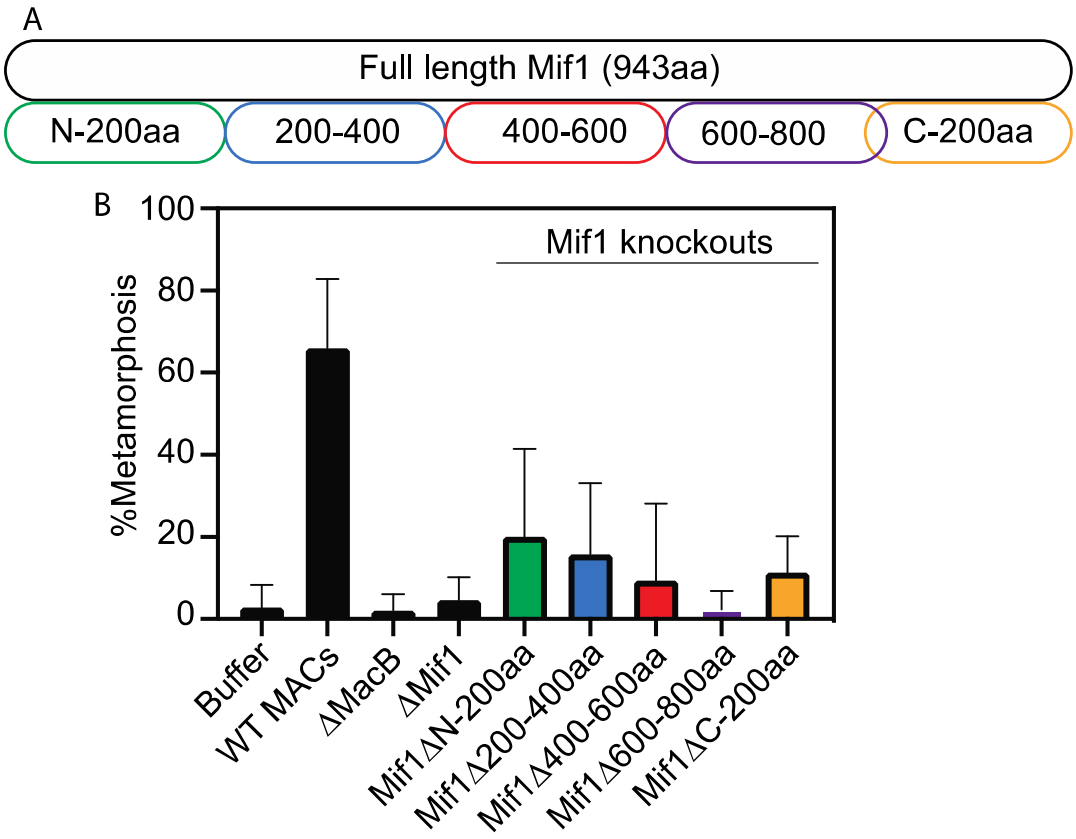

Figure 5.2. The N and C-term domains are required for protein loading into the MACs inner tube complex. (A) Two hundred amino acid residues were systematically removed from Mif1 to determine their role in Mif1 effector loading. (B) Metamorphosis assays of extracted MACs complexes with the various mutants were tested and assessed for their ability to induce metamorphosis (The average of 4 technical replicates each).

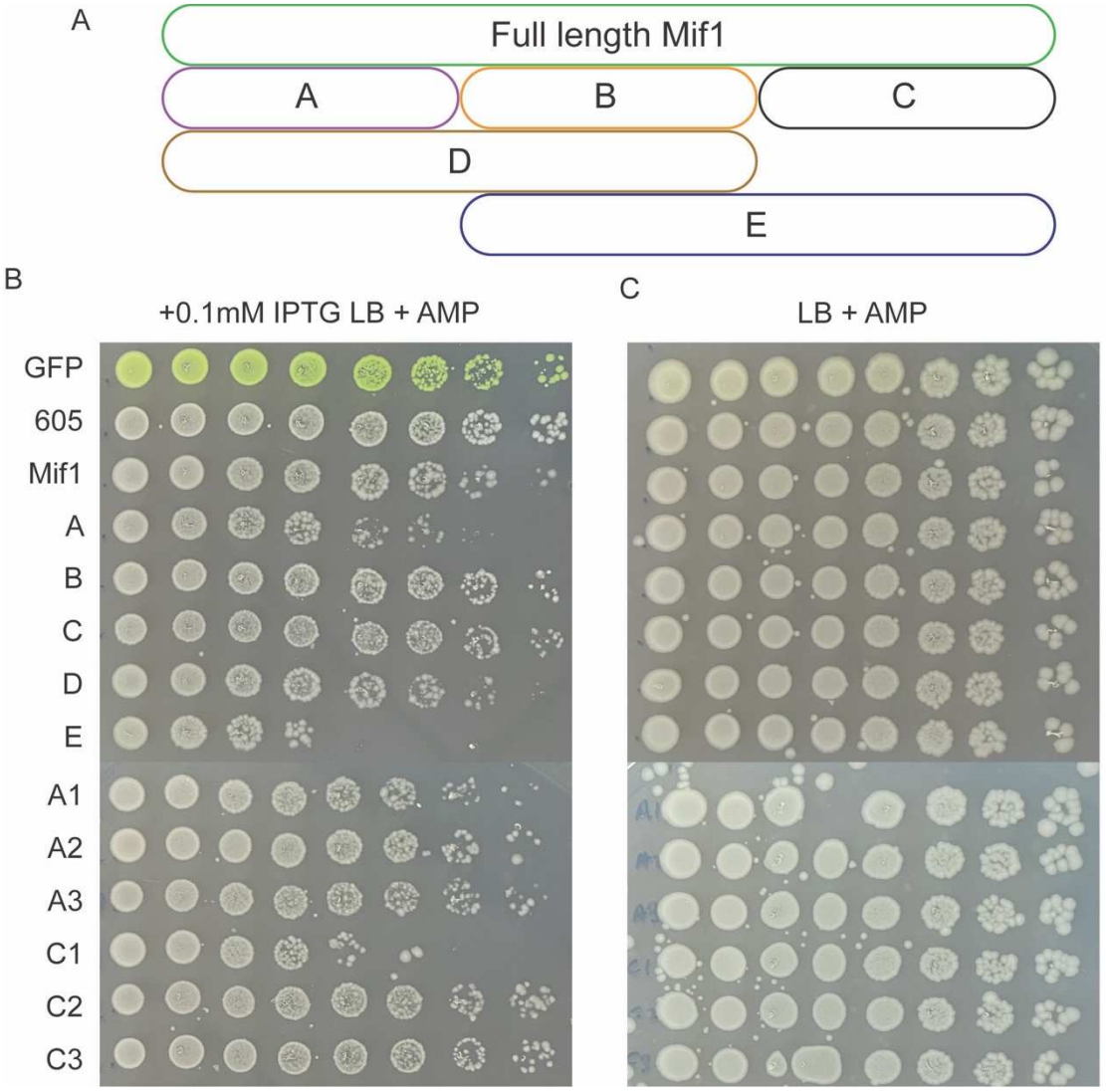

Figure 5.3. The N- and C-termini of Mif1 are toxic when overexpressed in *E. coli*. *E. coli* expressing recombinant *mif1, mif1* fragments, JF50_0605 or *gfp* genes from an IPTG inducible promoter in a pET15b vector. (A) Cartoon showing the fractions of Mif1 tested. (B) Bacteria were grown overnight and then spotted by 1/5 serial dilutions starting at OD 1.0 and induced with 0.1mM IPTG or (B) in the absence of IPTG.

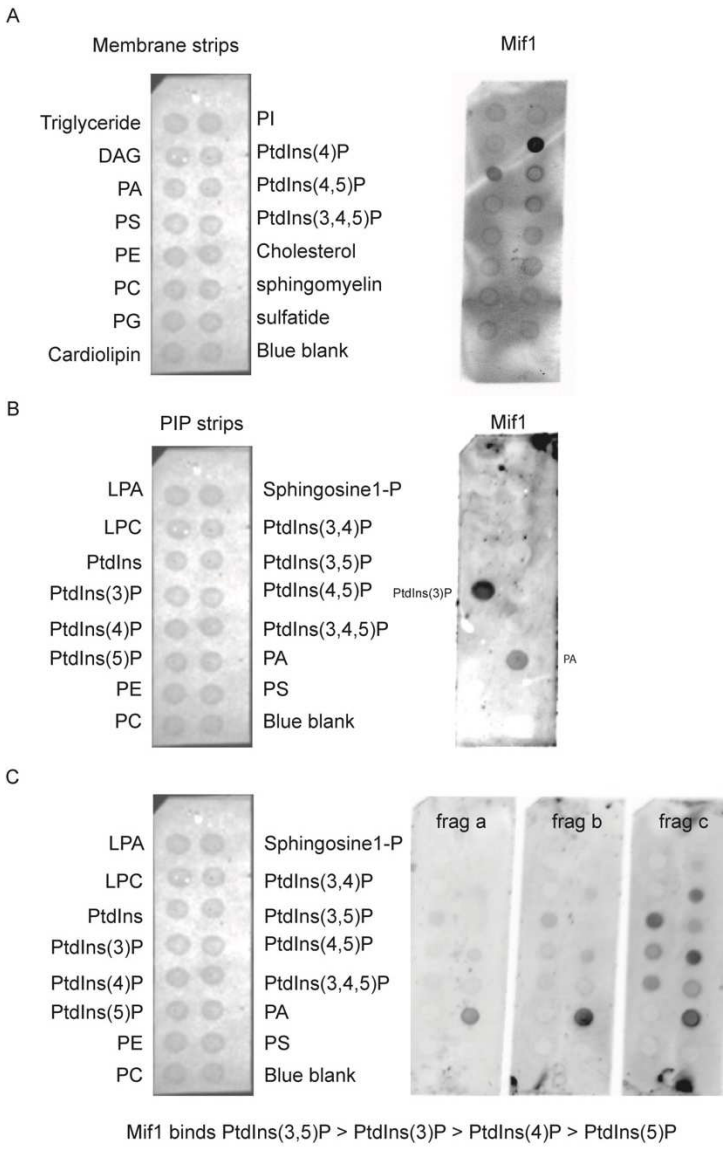

Figure 5.4. Mif1 binds specific phosphoinositide and phosphatidic acid membrane lipids. (A) Lipid spotted membrane with various membrane lipids. (B) Far western using purified Mif1 protein and Mif1 specific antibody shows binding to both PI3P and PA. (C) Lipid cleavage assay with purified Mif1 protein or chaperone (12605) protein, incubated for 1 hour with decanoic acid-PNPP substrate. Cleavage and PnPP (4-nitrophenyl phosphate) release occurs if acyl-ester linkage is hydrolyzed.

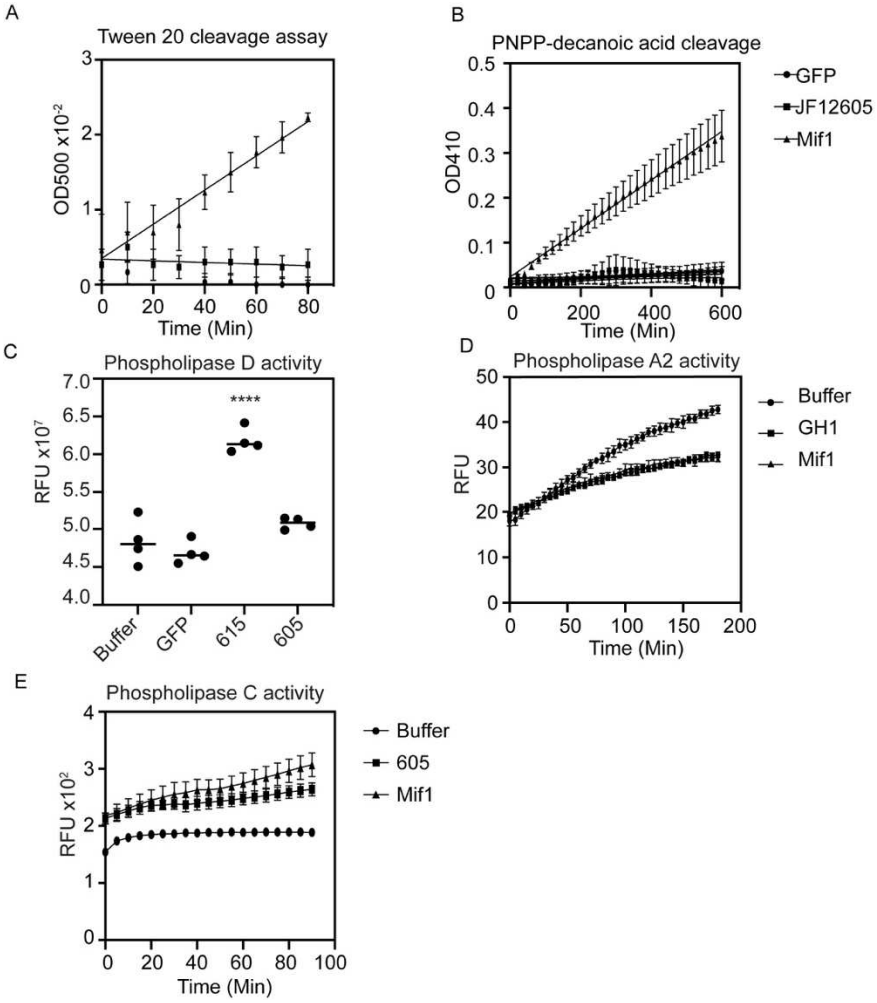

Figure 5.5. Mif1 possesses phospholipase A1 and D activity. Lipase assays were performed with purified recombinantly expressed protein. (A) Lipid cleavage assay with purified Mif1 protein or chaperone (12605) protein, or a GFP control protein incubated with Tween-20 in the presence of Ca^{2+} and liberated lauric acid was observed via turbidity. (B) Purified proteins incubated for 1 hour with decanoic acid-PNPP substrate. Cleavage and PnPP (4-nitrophenyl phosphate) release occurs if acyl-ester linkage is hydrolyzed. (C) PLD specific lipid cleavage assay with phosphatidylcholine substrate to assess enzymatic cleavage site of lipases by presence of choline release, 3hr endpoint assay. (D) Phospholipase A2 specific cleavage assay with Mif1, Buffer, or a control protein GH1. (E) Phospholipase C specific cleavage assay with Buffer, Mif1 or 605 control protein. Data are represented as the mean ± SD of n = 12 technical replicates across three independent biological replicates. Significance is indicated as a comparison between the two conditions indicated by the line above (****$p < 0.0001$).

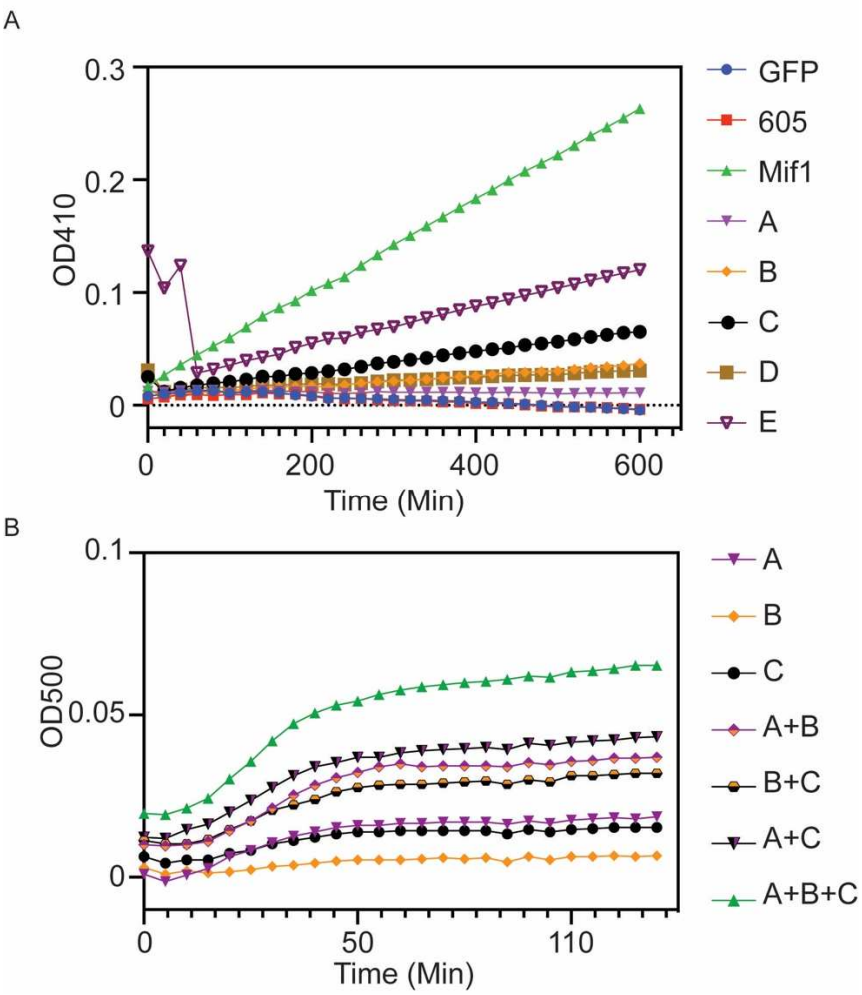

Figure 5.6. Mif1 fragment analysis for lipase activity. (A) Pnpp-decanoic acid lipase assay with purified proteins from BL21 plysE *E. coli.* The average of 4 technical replicates is shown. (B) tween-20 esterase assay of individually purified Mif1 fragments. The average of 3 technical replicates is shown.

Table 5.1. 3D-Blast hits using Alphafold2 predicted model of Mif1 (1-943aa).

Query Protein: Mif1, Search Database: PDB (29-May-10)

#	Protein	Length	Score	E-value	%Iden	%Gaps	Classification
1	2vqi:	542	199	2.00E-50	31.5	20.7	Transporter
2	1nqf:	554	196	1.00E-49	30.7	25.5	Transport protein
3	3m8d:	568	196	2.00E-49	32.6	24.5	Transport protein
4	1nqh:	543	191	3.00E-48	32.2	24.1	Transport protein
5	2gsk:	578	191	5.00E-48	30.6	26.3	Signaling protein/membrane protein
6	1nqe:	488	189	2.00E-47	34.4	23	Transport protein
7	1ujw:	507	188	4.00E-47	32	26.6	Transport protein/hydrolase
8	3m8b:	496	187	5.00E-47	34.3	24.6	Transport protein
9	1po3:	588	181	3.00E-45	30.8	24.3	Membrane protein
10	2vqi:	556	177	5.00E-44	30.9	24.5	Transport
11	2guf:	474	177	5.00E-44	34.2	24.5	Transport protein
12	1nqg:	605	177	7.00E-44	29.9	28.4	Transport protein
13	2ysu:	530	175	3.00E-43	32.1	30.8	Transport protein/hydrolase
14	2iah:	454	175	3.00E-43	34.4	25.1	Membrane protein
15	3efm:	466	169	1.00E-41	33.9	23.8	Membrane protein
16	1kmo:	597	168	3.00E-41	29.8	27.5	Membrane protein
17	3fhh:	603	167	7.00E-41	29.7	24	Membrane protein
18	1po3:	563	167	7.00E-41	30.4	23.1	Membrane protein
19	1kmp:	526	166	1.00E-40	32.9	24.9	Membrane protein
20	2b5m:	706	165	2.00E-40	26.9	23.2	DNA binding protein/ protein binding

Table S5.1. Search query and table of psiBLAST hits from full length Mif1 after 5 iterations.

SUBJECT	%ID	E-VALUE	SCORE	% POSITIVES
WP_039609812.1	100.000	0.0	697	100.00
WP_063366626.1	99.572	0.0	695	99.89
WP_235407130.1	78.075	0.0	681	88.56
WP_237137799.1	89.637	0.0	671	95.19
WP_063363969.1	89.316	0.0	670	94.98
WP_211036344.1	89.209	0.0	669	94.87
WP_063356378.1	77.837	0.0	669	88.22
WP_211013094.1	84.194	0.0	668	92.90
WP_065788920.1	79.037	0.0	667	88.24
WP_211033567.1	79.336	0.0	666	88.65
WP_023399347.1	84.086	0.0	664	93.23
WP_063383127.1	78.908	0.0	663	88.87
WP_063371891.1	78.908	0.0	663	88.76
WP_239426586.1	83.871	0.0	663	93.01
WP_142048640.1	77.730	0.0	661	88.22
WP_063875862.1	78.373	0.0	654	88.22
WP_063375575.1	78.266	0.0	654	88.22
WP_046356241.1	51.322	1.18e-160	507	70.37
WP_239789093.1	14.513	5.94e-121	410	30.40
WP_082170932.1	14.513	2.10e-120	408	30.30
WP_209126783.1	14.301	3.01e-120	408	30.40
WP_107759278.1	14.301	1.33e-119	406	30.40
WP_080762639.1	14.301	1.23e-118	403	30.30
WP_081943061.1	14.195	3.96e-118	402	30.08
NEP03102.1	17.874	1.08e-116	397	37.85
WP_196894410.1	17.474	2.91e-116	394	36.00
WP_103415941.1	14.603	9.80e-114	390	29.95

Table S5.1. Search query and table of psiblast hits from full length mif1 after 5 iterations. Continued.

SUBJECT	%ID	E-VALUE	Score	% Positives
WP_242746913.1	14.603	9.90e-114	390	29.95
WP_024105797.1	14.603	1.40e-113	390	29.95
MCB9235585.1	18.248	3.67e-113	384	35.56
WP_214453623.1	14.603	6.91e-113	388	29.95
WP_242815975.1	14.709	4.23e-112	385	30.16
WP_157722079.1	16.412	4.39e-111	379	33.23
ARU62990.1	16.412	1.74e-110	376	33.23
WP_094234930.1	15.164	7.60e-110	375	33.20
WP_132943549.1	16.197	6.35e-107	368	32.39
WP_201634173.1	14.490	6.24e-106	364	32.65
WP_146201013.1	14.963	8.87e-102	353	32.67
WP_094234938.1	15.081	3.87e-95	336	31.98
WP_038086002.1	14.345	7.59e-88	315	32.51
WP_110827158.1	16.921	1.55e-85	309	36.31
WP_161130893.1	14.286	1.40e-78	292	33.66
WP_161130893.1	16.690	1.01e-66	256	31.24
WP_082202648.1	14.286	4.80e-78	290	33.66
WP_082202648.1	16.405	1.10e-70	268	31.10
WP_016941234.1	14.481	1.85e-77	288	33.66
WP_016941234.1	16.120	2.30e-67	258	30.53
WP_100849495.1	14.481	2.37e-77	288	33.86
WP_100849495.1	16.833	2.70e-69	264	31.24
WP_121480134.1	14.090	2.86e-77	288	33.66
WP_121480134.1	16.690	2.13e-71	271	31.24
GGB88917.1	14.481	4.88e-77	287	33.86
GGB88917.1	16.833	6.32e-69	263	31.24

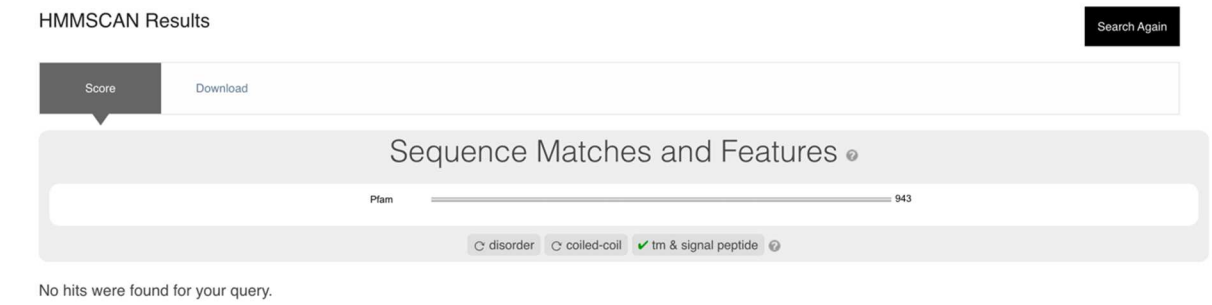

Figure S5.1. Mif1 does not share any homologous domains identified via HMMR search.

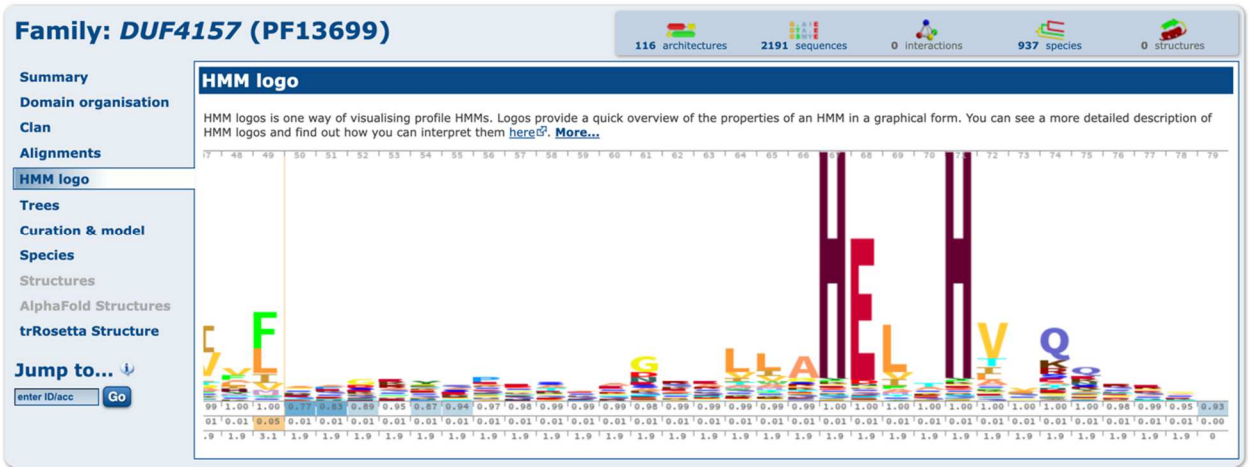

Figure S5.2. Identified domain from psiBLAST hits (DUF4157) shows conserved HExxH motif which is not found in Mif1.

TABLE S5.2. 3D-blast hits using Alphafold2 model of Mif1 fragments

QUERY PROTEIN: MIF1 1-943AA, SEARCH DATABASE: PDB (29-MAY-10)						
#	Protein	Length	Score	E-value	%Iden	%Gaps
1	2vqi:	542	199	2.00E-50	31.5	20.7
2	1nqf:	554	196	1.00E-49	30.7	25.5
3	3m8d:	568	196	2.00E-49	32.6	24.5
4	1nqh:	543	191	3.00E-48	32.2	24.1
5	2gsk:	578	191	5.00E-48	30.6	26.3
6	1nqe:	488	189	2.00E-47	34.4	23
7	1ujw:	507	188	4.00E-47	32	26.6
8	3m8b:	496	187	5.00E-47	34.3	24.6
9	1po3:	588	181	3.00E-45	30.8	24.3
10	2vqi:	556	177	5.00E-44	30.9	24.5
11	2guf:	474	177	5.00E-44	34.2	24.5
12	1nqg:	605	177	7.00E-44	29.9	28.4
13	2ysu:	530	175	3.00E-43	32.1	30.8
14	2iah:	454	175	3.00E-43	34.4	25.1
15	3efm:	466	169	1.00E-41	33.9	23.8
16	1kmo:	597	168	3.00E-41	29.8	27.5
17	3fhh:	603	167	7.00E-41	29.7	24
18	1po3:	563	167	7.00E-41	30.4	23.1
19	1kmp:	526	166	1.00E-40	32.9	24.9
20	2b5m:	706	165	2.00E-40	26.9	23.2
21	1xkw:	654	165	2.00E-40	28.9	31.7
22	3prx:	619	164	7.00E-40	29.9	26.2
23	1fep:	602	164	7.00E-40	31.6	29.6
24	2hdf:	498	161	3.00E-39	32.9	23.9
25	3i8e:	674	160	8.00E-39	27.6	26.7
26	3cu7:	647	160	1.00E-38	27.4	23.6
27	3e0c:	662	158	3.00E-38	27.6	21
28	3pvm:	767	158	3.00E-38	27.4	26.9
29	2w16:	610	158	4.00E-38	31.5	26.7
30	3ei2:	702	158	4.00E-38	26.6	25.9
31	1po0:	509	157	5.00E-38	32.2	25.9
32	2w76:	580	157	6.00E-38	30.2	26.9

TABLE S5.2. 3D-blast hits using Alphafold2 model of Mif1 fragments. Continued.

#	Protein	Length	Score	E-value	%Iden	%Gaps
33	2pn5:	469	157	8.00E-38	28.6	21.5
34	2hdi:	543	157	8.00E-38	31.7	28.5
35	3cu7:	647	157	8.00E-38	27.2	23.6
36	3prx:	632	156	2.00E-37	29.3	26.7
37	3njt:	374	156	2.00E-37	32.4	30.5
38	3b43:	602	155	2.00E-37	29.1	23.9
39	2fkj:	353	155	3.00E-37	36.3	32
40	3ei4:	702	154	4.00E-37	29.2	27.9
41	2w77:	455	154	5.00E-37	30.5	22.2
42	2o5p:	620	154	5.00E-37	29.7	29.2
43	2w6u:	638	154	7.00E-37	28.8	32.9
44	2w6u:	565	153	9.00E-37	29.9	25.1
45	2w6t:	639	153	9.00E-37	29.6	34.3
46	2w16:	518	153	9.00E-37	31.7	25.1
47	3ei4:	685	153	9.00E-37	28	27
48	2a74:	615	153	9.00E-37	28.6	21.1
49	3pvm:	763	153	9.00E-37	26.9	26.3
50	1pnz:	487	152	2.00E-36	31.8	26.9
51	2o5p:	615	152	2.00E-36	30.4	28
52	2w75:	619	151	3.00E-36	29.6	28.6
53	3ei1:	661	151	6.00E-36	25.6	25.4
54	3dmk:	681	149	1.00E-35	29.8	28
55	2w78:	638	149	2.00E-35	29.3	32.3
56	3kls:	627	149	2.00E-35	27.4	24.6
57	3cka:	325	149	2.00E-35	36.9	31.7
58	2qki:	620	148	3.00E-35	28.2	26
59	3g6j:	643	148	4.00E-35	28.5	26.4
60	3kvn:	491	148	5.00E-35	28.7	26.3
61	3kvn:	528	148	5.00E-35	28.2	29.2
62	2w78:	567	147	6.00E-35	30.7	27.9
63	2i07:	608	147	6.00E-35	28.8	27
64	1qfg:	630	147	6.00E-35	29.8	34.1
65	3kls:	628	147	8.00E-35	27.9	24.8
66	3ei3:	648	147	8.00E-35	25.5	25.3
67	1kit:	629	146	1.00E-34	28.8	27.2
68	1by3:	574	145	2.00E-34	27.9	30.1
69	2b5l:	666	145	2.00E-34	26.7	24.5

TABLE S5.2. 3D-blast hits using Alphafold2 model of Mif1 fragments. Continued.

#	Protein	Length	Score	E-value	%Iden	%Gaps
70	2w77:	573	145	3.00E-34	27.7	29.5
71	2hye:	728	145	3.00E-34	26.6	26.5
72	2grx:	508	145	3.00E-34	28.3	22.6
73	3emn:	305	145	3.00E-34	34.8	20.7
74	3ei4:	658	145	3.00E-34	26.6	28.6
75	3km9:	612	144	6.00E-34	27.5	25
76	2b39:	597	143	8.00E-34	25.8	21.4
77	2a74:	682	143	1.00E-33	28.3	25.2
78	1xkh:	578	143	1.00E-33	29.1	28.4
79	2b39:	599	143	1.00E-33	26.5	24.4
80	2x4m:	350	142	2.00E-33	32.6	25.4
81	2x4m:	368	142	2.00E-33	31	25
82	3cka:	345	142	2.00E-33	32.8	30.1
83	2qdz:	397	142	2.00E-33	31	24.9
84	2oy8:	313	141	3.00E-33	36.1	30.4
85	2w76:	648	141	5.00E-33	27.9	33.5
86	1a0s:	374	141	5.00E-33	32.1	28.9
87	1i78:	352	140	7.00E-33	33.8	25
88	3dmk:	682	140	1.00E-32	29.3	28.3
89	1oh2:	333	139	2.00E-32	32.7	26.1
90	1a0t:	333	139	2.00E-32	32.7	26.1
91	1a0s:	375	139	2.00E-32	33.1	29.3
92	3csn:	492	139	2.00E-32	31.9	27.2
93	2x4m:	349	138	3.00E-32	30.9	24.1
94	1vh4:	364	138	3.00E-32	28.3	22.5
95	3km9:	594	138	3.00E-32	28.5	29.8
96	3i89:	611	138	3.00E-32	27.5	21.9
97	2b5l:	623	138	3.00E-32	27	23.4
98	2w75:	592	138	3.00E-32	29.7	33.4
99	3dmk:	687	138	3.00E-32	30	29.5
100	1xkh:	570	138	4.00E-32	28.1	26

A) QUERY PROTEIN: MIF1 1-200AA SEARCH DATABASE: SCOP 1.75

#	Protein	Length	Score	E-value	%Iden	%Gaps
1	d2es4d1	167	115	2.00E-26	23.4	12
2	d2es4e1	145	109	8.00E-25	25.5	8.3

TABLE S5.2. 3D-blast hits using Alphafold2 model of mif1 fragments. Continued.

B) QUERY PROTEIN: MIF1 200-760AA SEARCH DATABASE: SCOP 1.75

#	Protein	Length	Score	E-value	%Iden	%Gaps
1	d2gufa1	567	194	8.00E-50	32.1	26.6
2	d1nqha_	562	189	4.00E-48	32	23.8
3	d2gska1	589	184	1.00E-46	31.9	26.5
4	d1nqea_	501	184	1.00E-46	31.3	25.9
5	d1nqga_	548	183	2.00E-46	30.8	24.8
6	d2ysua1	546	177	2.00E-44	30.4	27.8
7	d1po3a_	535	175	6.00E-44	30.1	27.9
8	d1ujwa_	471	171	1.00E-42	33.1	23.6
9	d1fepa_	570	171	1.00E-42	30.9	27.7
10	d1po3b_	525	171	1.00E-42	31.2	25.1
11	d1nqfa_	550	170	2.00E-42	30.5	25.3
12	d1kmoa_	326	166	2.00E-41	35.3	27.3
13	d1po0a_	536	166	3.00E-41	31.3	28.4
14	d1qkca_	664	162	3.00E-40	30	28.2
15	d2grxb1	407	162	4.00E-40	32.7	24.1
16	d2grxa1	411	161	7.00E-40	32.4	25.8
17	d1by5a_	605	161	1.00E-39	28.6	28.9
18	d1kmpa_	370	160	2.00E-39	31.9	25.7
19	d1pnza_	384	160	2.00E-39	31.8	25
20	d2fcpa_	447	151	7.00E-37	28.6	22.4

C) SEARCH RESULTS OF 3D-BLAST

QUERY PROTEIN: MIF1 760-943, SEARCH DATABASE: SCOP 1.75

#	Protein	Length	Score	E-value	%Iden	%Gaps
1	d2bkud1	178	113	8.00E-26	32	18
2	d1ya0a1	198	110	4.00E-25	30.8	20.2
3	d1ya0b1	196	106	9.00E-24	28.1	18.9
4	d2bpta1	174	103	4.00E-23	29.3	14.9
5	d1ib1b_	174	102	1.00E-22	25.9	16.7
6	d3ea5d1	178	101	3.00E-22	28.1	15.7
7	d2v7dc1	169	100	6.00E-22	25.4	14.8
8	d1oyza_	161	99.3	1.00E-21	32.3	22.4
9	d1ib1d_	176	98.9	1.00E-21	26.7	18.8
10	d2v7dd1	168	98.5	2.00E-21	25	13.7

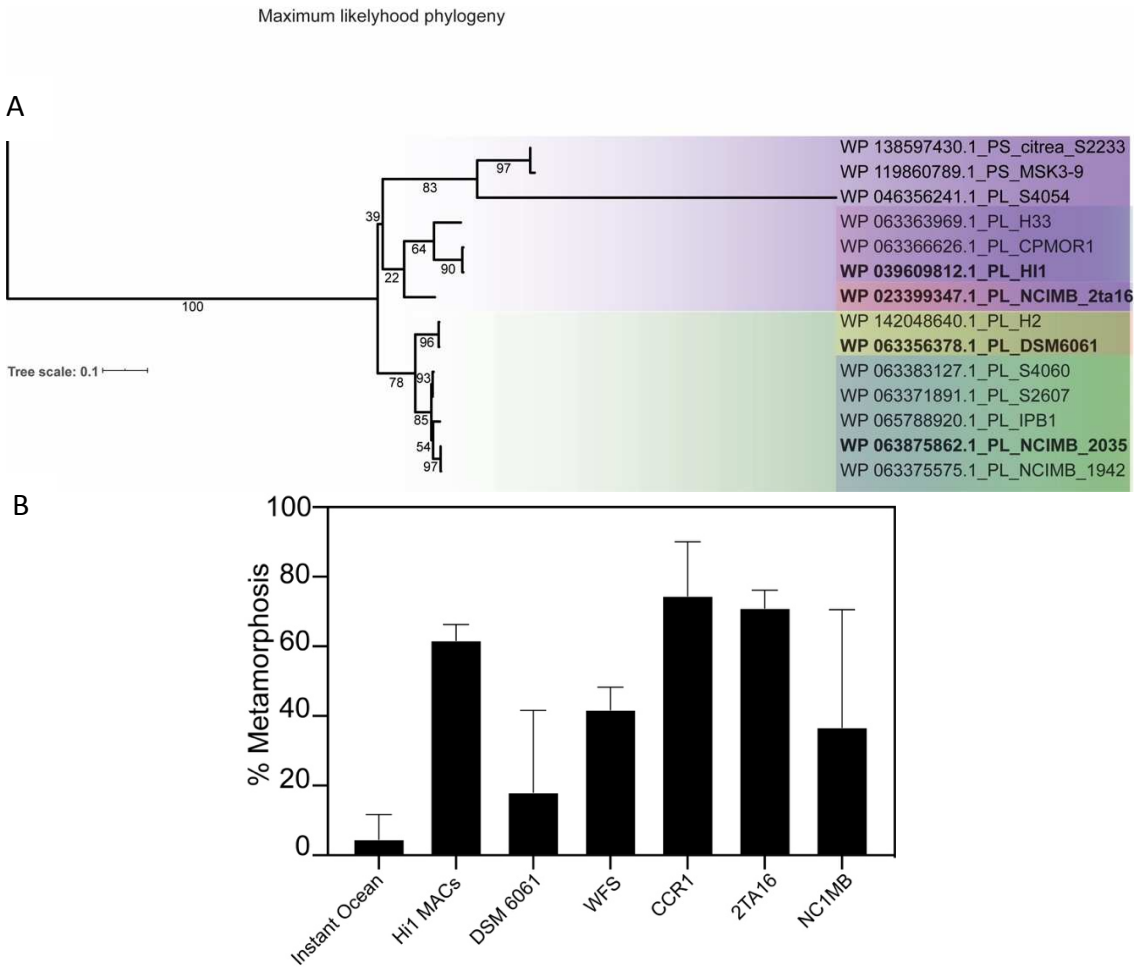

Figure S5.3. Related strains of bacteria with similar Mif1 homologues stimulate *Hydroides* metamorphosis (A) Maximum likelyhood tree showing the relatedness of Mif1 homologs in marine bacteria. (B) Metamorphosis assay of marine bacteria possessing a Mif1 homolog related to *P. Luteo*.

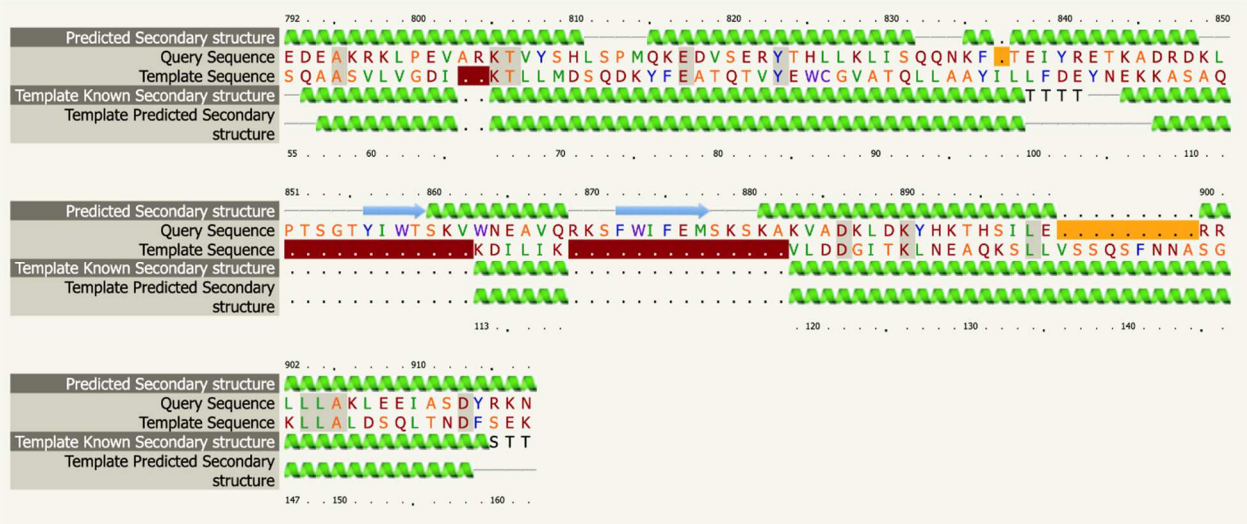

Figure S5.4. Alignment of Mif1 and *E. coli* hemolysin E. pore forming toxin via Phyre2.

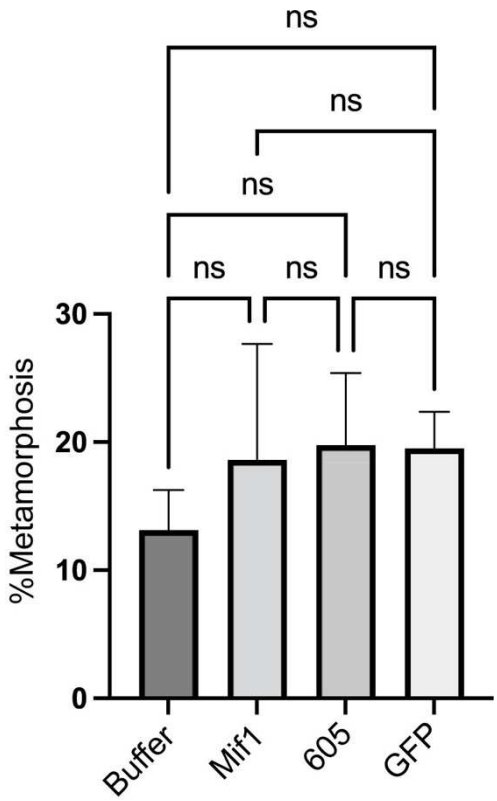

Figure S5.5. Metamorphosis of larvae is not affected by lipids produced during lipase assay. Metamorphosis assay of Hydroides with lipids isolated after incubation with purified recombinant protein.

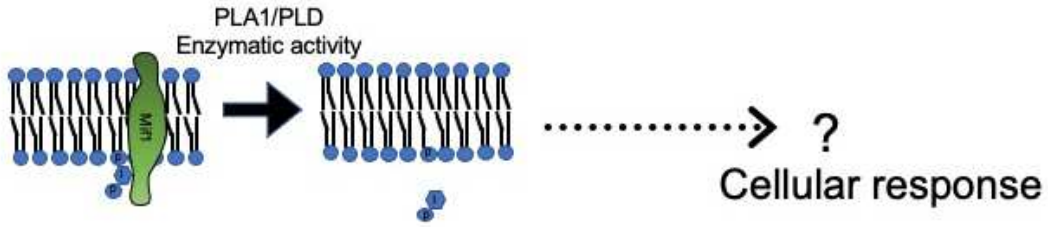

Figure S5.6. Mif1 binds PI(3)P and has PLA1/PLD Enzymatic activity.

Chapter 6

Future directions

6.1 MACs use in biotechnology

We aim to better understand the role of protein loading into the MACS complex. We have shown that Mif1 is required for the loading of Mif1 into the MACs complex and by better understanding how these proteins interact we can begin to hypothesize the requirements for proteins loaded into the MACs complex (Figure 6.1.). We hope that by determining the required sequence for protein loading that we could then direct any protein we desire into the complex for protein delivery by MACs.

Additionally, we have shown that MACs are able to target *Hydroides* cells, Mouse macrophages and insect SF9 cell lines. It is feasible to assume that MACs are able to some cells and not others. By determining the requirements for MACS to target specific cells we hope to understand the proteins that are directly interacting with the cellular surface (Figure 6.1.). Once we are able to determine the interacting proteins, we can then alter the sequence to a known binding sequence targeted to specific cells or receptors and use MACs in a targeted manner.

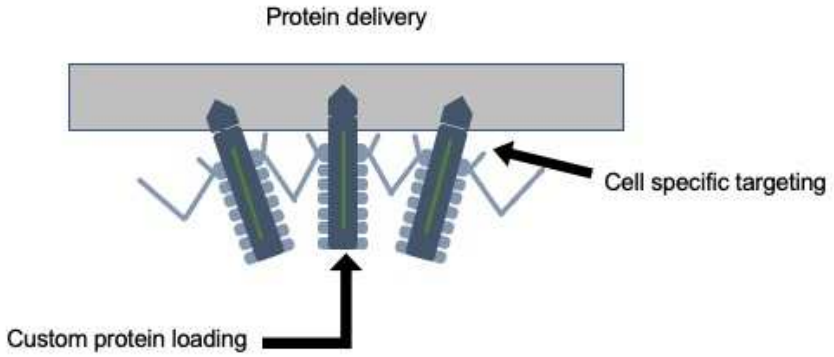

Figure 6.1. How to use MACs for biotechnology.